

The Study of d^8 Transition Metal Catalysts for Oxidative Arene Alkenylation

Weihaio Zhu
Taizhou, China

B.S. Applied Chemistry, Hangzhou Normal University, 2015

A Dissertation presented to the Graduate Faculty of the University of Virginia in
Candidacy for the Degree of Doctor of Philosophy

Department of Chemistry

University of Virginia
December 2020

ABSTRACT

ZHU, WEIHAO The Study of d^8 Transition Metal Catalysts for Oxidative Arene Alkenylation. (Under the direction of Professor T. Brent Gunnoe)

Alkyl and alkenyl arenes are important commodity chemicals that are produced on a large scale. Acid-catalyzed arene alkylation for the industrial production of alkyl and alkenyl arenes requires an energy intensive trans-alkylation process, which results from poly-alkylation due to the higher reactivity of alkylated arenes compared to starting arenes. In addition, acid-catalyzed methods have limitations that result from the reaction mechanism including exclusive selectivity for Markovnikov products for arene alkylation using α -olefins, inability to form alkenyl arenes in a single process starting with arenes and alkenes, and commonly observed slow reactivity with electron-deficient arenes. Transition metal-catalyzed aryl-carbon coupling reactions can be used to produce alkyl or alkenyl arenes. However, these C–C coupling reactions, which usually involve late transition metals such as Pd, often require activated aryl halide substrates and metal-containing trans-metalation reagents, and they typically generate halogenated by-products. An alternative method for the production of alkenyl arenes is transition metal-catalyzed oxidative arene alkenylation, which converts an arene, alkene and oxidant to an alkenyl arene. This dissertation is focused on development of oxidative arene alkenylation using late transition metal catalysts.

The Gunnoe group recently reported a diimine Rh(I) complex that serves as a catalyst precursor for the direct oxidative conversion of benzene and ethylene to styrene with over 800 turnover numbers and nearly quantitative yield relative to

air-recyclable Cu(II) oxidant. In an effort to determine the influence of the diimine ligand, a series of diimine ligated Rh(I) complexes was shown to yield statistically identical results in terms of activity and product selectivity in the catalytic benzene alkenylation. These ligated Rh complexes dissociate diimine ligands and are likely transformed into $[\text{Rh}(\mu\text{-OAc})(\eta^2\text{-C}_2\text{H}_4)]_2$ under catalytic conditions. In the absence of Cu(II) oxidants, $[\text{Rh}(\mu\text{-OAc})(\eta^2\text{-C}_2\text{H}_4)]_2$ undergoes thermolysis in benzene at 150 °C to form Rh(0) species. Furthermore, under the catalytic conditions with $\text{Cu}(\text{OAc})_2$, $[\text{Rh}(\mu\text{-OAc})(\eta^2\text{-C}_2\text{H}_4)]_2$ undergoes rapid decomposition to form catalytically inactive and insoluble Rh species. Thus, the observed induction period under some conditions is likely due to the formation of insoluble Rh (rapid) followed by re-dissolution of the Rh (slow). Using either $\text{Cu}(\text{OAc})_2$ treated to minimize particle size or more soluble Cu(II) oxidants such as copper(II) 2-ethylhexanoate $[\text{Cu}(\text{OHex})_2]$, the decomposition of $[\text{Rh}(\mu\text{-OAc})(\eta^2\text{-C}_2\text{H}_4)]_2$ to form insoluble rhodium species can be mitigated and the catalytically active Rh species maintained. In such cases, an induction period is not observed.

An oxidative conversion of unactivated arenes and simple alkenes to alkenyl arenes using unpurified air or O_2 as the sole oxidant has been developed. This method uses simple RhCl_3 as catalyst precursor and does not require metal-containing co-oxidants and additional ligands. Conditions to achieve > 1,000 turnovers of alkenyl benzene products has been demonstrated. The catalyst is selective for anti-Markovnikov (linear) 1-phenylpropylene products over Markovnikov (branched) 2-phenylpropylene products with linear:branched ratio in the range of 4-6:1. The

previously reported anaerobic benzene propenylation catalyzed by $[\text{Rh}(\mu\text{-OAc})(\eta^2\text{-C}_2\text{H}_4)_2]_2$ produces phenylpropylene products with ~8:1 ratio of linear 1-phenylpropylene products to branched 2-phenylpropylene when Cu(II) salts is used as the in situ oxidant. Based on kinetic studies, the different selectivities for catalytic reactions in the presence of Cu(II) (anaerobic catalysis) and absence of Cu(II) (using O_2 as the sole oxidant) are proposed to result from a change of rate-limiting steps from olefin insertion (under anaerobic conditions) to the reaction of Rh with O_2 after olefin insertion (under aerobic conditions).

An Ir(I) catalyst for arene alkenylation shows selectivity for linear 1-aryl propylene products using benzene and propylene. Conditions to accomplish 70:1 linear/branched ratio have been demonstrated. Compared to reported Rh-catalyzed arene alkenylation, the Ir-catalyzed process exhibits reduced reactivity and limited product yield relative to Cu(II) carboxylate oxidant.

ACKNOWLEDGEMENTS

It took me more than five years to reach the destination of this long journey. I have been fortunate enough to get assistance from a great many people along this journey. I would much like to express my heartfelt thanks to you all by writing this acknowledgement, although you deserve more than simple appreciation words here.

First, I would like to express my sincere gratitude to my advisor Brent Gunnoe. I get to know you in your inorganic chemistry, which is one of my favorite courses throughout my PhD education. To be frank, I was not interested in inorganic chemistry at the very beginning. However, you offered me such crystal clear and well-organized classes that I can have a good understanding of internal logic of inorganic chemistry and experience its charm. It is you that aroused my interest in this field. I am grateful that you accept me into your lab. I would say the best decision I made in the past five years is to join your lab and have you as my supervisor. Your enthusiasm for science and earnestness in academic study are inspiring. I also appreciate that you fully respect each student. Your patience and kindness will never be forgotten. Even if your schedule is always full, you are still willing to spare time listening to us and helping us with questions tirelessly. My appreciation also goes to Trecia and Leah. Thanks for hosting parties with fantastic food, ping pong games and billiards.

To Dr. Dean Harman, Dr. Lin Pu, Dr. Ian Harrison, and Dr. Bob Davis, thank you for agreeing to be my committee members, witnessing me through the marathon over the last 5 years and finally reading my thesis.

Special thanks to my advisors during my undergraduate and master education, Dr. Wanmei Li and Dr. Ken Hsu. I am grateful that you offer me the opportunities to learn experimental skills and perform research in your labs.

Dr. Brad, thanks for enlightening me the first glance of research. Dr. Junqi, thanks for mentoring me at the beginning of my career in the lab. I learned lots of useful techniques and knowledge under your instruction. Xiaofan, thanks for keeping forcing me to study hard before candidacy exams. I will not forget the LeBron James Jersey that you gave away to me as a gift! My thanks also go to Nichole for your valuable support both inside and outside the lab. I am also grateful to Dr. Shunyan for always giving me reliable suggestions. It really helps a lot! To Dr. Zhongwen, I am glad to have collaboration with you for my first paper. To Ke, thanks for eating Buffalo Wild Wings with me weekly. That's the infrequent relaxing time I have each week. To Fanji, thank you for having academic discussion in depth with me. I believe you will be a chemist with substantial achievements! Kaeleigh, thanks for all of the selfless things you do for the whole lab. To Hannah and Lucas, it was an absolute pleasure working with you and I'm grateful for your efforts and enthusiasm. I wish both of you much success in the future. Dr. Ana, Dr. Nathan, Dr. Ryan, and Dr. Bala, you are real assets for our lab. Dr. Mike, Dr. Ben, and Dr. Kathleen, you are talented scientists and I am glad we overlap in Gunnoe lab.

I have been lucky enough to work with some fantastic collaborators outside our lab. My sincere thanks go to Dr. Robert J. Davis, Dr. Bill Goddard, Dr. Sen Zhang, Lu, Charles and Chang. I appreciate your high-quality research work. I cannot nail down

my project and get my work published smoothly without your support. If I have the chance, I would be happy to work with you guys again in the future. To Diane, thanks for your efforts on characterizing crystals. I apologize that my crystal samples are in low-quality sometimes and caused some troubles to you. To Michael Birckhead, thanks for your kind works and greeting me in Chinese!

To my roommates Yuanming, Tao, Limin, Juncheng, Minghui, Yaodao, and Weixing, I can imagine my life would become a mess without your help. I know I may not be a good roommate, but thanks for putting up with my faults. It is my fortune to have you guys as my roommates. To Fang and Chang, I really enjoy the time playing basketball with you two. To Huiying, Jieqiong and Liuwang, we have experienced lots of hot pot parties and card games that I will remember for long. To Chaojie, Jiamin and Minyue, thanks for inviting me to your wonderful parties! I am really pleased to have a future road trip with two of you for celebration of graduation. See you then! Yulei, we have a lot of memories that I will treasure forever! I believe we will have more in the future!

Finally, I wish to show my gratitude to my family members. To my parents and grandparents, thank you for supporting, encouraging, understanding and trusting me no matter what. To my aunts and uncles, thanks for caring about me and treating me in the kindest way. Special thanks to my uncle, Tony Chen, you have been always my role model and my career in chemistry is significantly impacted by you. I am on the way chasing you although it is a long journey.

All the best to you all and those who are not mentioned so far but helped me

along the way.

TABLE OF CONTENTS

LIST OF SCHEMES.....	X
LIST OF FIGURES	XIV
LIST OF TABLES	XXIV
1 Introduction.....	1
1.1 Overview of Catalysis	1
1.2 Industrial Catalytic Processes.....	2
1.2.1 Overview	2
1.2.2 Industrial Examples of Organometallic Catalysts.....	3
1.2.3 Alkyl Arenes and Friedel-Crafts Catalysis	8
1.2.4 Alkenyl arenes and Current Industrial Processes.....	12
1.3 C–C Coupling Reactions via C–X Activation.....	13
1.4 C–C Coupling Reactions Based on C–H Activation	15
1.4.1 Mechanisms for C–H Activation	15
1.4.2 Transition Metal-Catalyzed Olefin Hydroarylation.....	17
1.4.3 Transition Metal-Catalyzed Arene Alkenylation	38
1.5 References	53
2 Mechanistic Studies of Styrene Production Catalyzed by Rh Complexes with Diimine Ligands.....	62
2.1 Introduction	62
2.2 Results and Discussion.....	69
2.2.1 Effect of Diimine Ligand Identity on Reactivity and Selectivity for Benzene Alkenylation	69
2.2.2 Stability of Diimine Ligated Rh Complexes toward Ethylene Pressure	73
2.2.3 Thermolysis of $[\text{Rh}(\eta^2\text{-C}_2\text{H}_4)_2(\mu\text{-OAc})]_2$ to form Rh(0) species	76
2.2.4 Removal of the Induction Period with Thermally Treated $\text{Cu}(\text{OAc})_2$	81
2.2.5 Removal of the Induction Period by the Addition of Excess $^{\text{Fl}}\text{DAB}$ Ligand	99
2.2.6 Initial Studies to Understand the Transformation of Rh	104
2.2.7 Experimental Comparison of Rh(I), Rh(II) and Rh(III) Catalyst Precursors.....	126
2.2.8 Characterization of Rh Resting State and Active Catalyst: experimental studies.....	127
2.2.9 Characterization of Rh Resting State and Active Catalyst: Computational Studies	139
2.3 Summary and Conclusions	143
2.4 Experimental Section	146
2.5 References	166
3 Rhodium-Catalyzed Arene Alkenylation Using Only Dioxygen as Oxidant.....	174

3.1	Introduction	174
3.2	Results and Discussion	180
3.3	Summary and Conclusions	202
3.4	Experimental Section	203
3.5	References	208
4	Catalytic Synthesis of Super Linear Alkenyl Arenes with a Simple Iridium Salt as Catalyst Precursor	216
4.1	Introduction	216
4.2	Results and Discussion	222
4.3	Conclusions	234
4.4	Experimental Section	235
4.5	References	239
5	Future outlook	242
5.1	Future Direction of Rh-Catalyzed Arene Alkenylation	242
5.2	Future Direction of Ir-Catalyzed Arene Alkenylation	244
5.3	Future Research Opportunities for Arene Alkenylation Using Other Metals 247	
5.4	References	247

LIST OF SCHEMES

Scheme 1.2.1. Catalytic Cycle for Wacker process.....	4
Scheme 1.2.2. Equations for Wacker process and overall balanced reaction (bottom).....	4
Scheme 1.2.3. Catalytic cycle for Co-catalyzed hydroformylation.....	6
Scheme 1.2.4. Catalytic Cycle for Monsanto acetic acid process	7
Scheme 1.2.5. Alkyl arenes and their derivatives.....	9
Scheme 1.2.6. Mechanism for acid catalyzed benzene alkylation.	9
Scheme 1.2.7. Current method for the industrial production of alkyl benzenes. .	10
Scheme 1.2.8. Product selectivity from acid catalyzed benzene alkylation using α -olefins	11
Scheme 1.2.9. Comparison of branched alkylbenzenes, linear alkylbenzenes and super linear alkyl benzenes.	12
Scheme 1.2.10. Current method for the synthesis of 1-aryl alkanes	12
Scheme 1.2.11. Current method for the industrial production of styrene.....	13
Scheme 1.3.1. Catalytic cycle for late transition metal catalyzed cross-coupling reactions	14
Scheme 1.4.1. Categories of transition metal-mediated C–H bond activation....	15
Scheme 1.4.2. Generic catalytic cycle for transition metal-catalyzed ethylene hydrophenylation.	18
Scheme 1.4.3. Anti-Markovnikov and Markovnikov products selectivity is dictated by the olefin insertion step (top) and, depending on details, the rates of subsequent reactions (e.g., under Curtin-Hammett conditions) (bottom).	19
Scheme 1.4.4. Explanations for distinct meta/para/ortho selectivity of acid-catalyzed arene alkylation and metal-catalyzed C–H activation.	20
Scheme 1.4.5. Ethylene hydrophenylation using [Ir(μ -acac-O,O,C ³)-(acac-O,O)-(acac-C ³)] ₂ as a catalyst precursor.....	21
Scheme 1.4.6. Proposed mechanism for ethylene hydrophenylation using [Ir(μ -acac-O,O,C ₃)-(acac-O,O)-(acac-C ₃)] ₂ as a catalyst precursor	23
Scheme 1.4.7. Ethylene hydrophenylation catalyzed by Ir(trop-O,O) ₂ Ph(Py).....	24
Scheme 1.4.8. Catalytic cycle for hydrophenylation of ethylene catalyzed by TpRu(L)(NCMe)Ph complexes and side reactions.....	25
Scheme 1.4.9. Correlation of Ru(III/II) redox potential of TpRu(L)(NCMe)(Ph) complexes with TON for ethylene hydrophenylation.....	27
Scheme 1.4.10. Hydrophenylation of ethylene catalyzed by [(HC(pz') ₃)Ru(P(OCH ₂) ₃ CEt)(NCMe)Ph][BAr' ₄] complex	27
Scheme 1.4.11. Structures of charge neutral Pt(II) catalysts with 2,2'-pyridyl-indolate ligands	28
Scheme 1.4.12. Structures of charge neutral (pyridyl)pyrrolide Pt(II) complexes	30
Scheme 1.4.13. Steric interaction between coordinated olefin and the pyrrole ring during the olefin insertion step. R= CH ₃ , C ₅ H ₁₁ , tBu, R'=H, CH ₃	31
Scheme 1.4.14. Proposed mechanisms for ethylbenzene, diethylbenzene and	

styrene formation using bipyridyl-supported Pt(II) complexes	32
Scheme 1.4.15. Proposed mechanisms for dialkylation products formation from Pt-catalyzed ethylene hydrophenylation.	33
Scheme 1.4.16. TOs and ratios of ethylbenzene to styrene from cationic Pt(II) catalyzed ethylene hydrophenylation (100 °C with 0.1 MPa of ethylene; EtPh:styrene ratios after 4 hours).....	34
Scheme 1.4.17. Mechanisms for transition metal-catalyzed benzene alkenylation with ethylene.	39
Scheme 1.4.18. Oxidative hydrophenylation of ethylene catalyzed by [(MeOTTM)Ru(P(OCH ₂) ₃ CEt)(NCMe)Ph][BAR' ₄].	41
Scheme 1.4.19. Benzene alkenylation with ethylene catalyzed by (^{F1} DAB)Rh(TFA)(η ² -C ₂ H ₄).....	42
Scheme 1.4.20. Proposed mechanism for benzene alkenylation using Rh(I) as a catalyst precursor	43
Scheme 1.4.21. Benzene alkenylation with propylene catalyzed by [Rh(μ-OAc)(η ² -C ₂ H ₄) ₂] ₂	44
Scheme 1.4.22. Comparison of Wacker process with styrene process.....	48
Scheme 1.4.23. Concept of using a "capping arene" ligand to protect Rh(I) against oxidation to Rh(III). Reprinted with permission from reference 102. Copyright 2019 American Chemical Society.	49
Scheme 1.4.24. (5-FP)Rh(TFA)(η ² -C ₂ H ₄) catalyzed benzene propenylation using Cu(OPiv) ₂ /air as oxidants under aerobic/anaerobic conditions.	50
Scheme 1.4.25. Metal-catalyzed aerobic benzene ethylation using O ₂ as the sole oxidant.....	51
Scheme 1.4.26. Proposed mechanism for metal-catalyzed aerobic styrene production using O ₂ as the sole oxidant.....	52
Scheme 2.1.1. Structures of (^{F1} DAB)Rh(TFA)(η ² -COE) and (^{F1} DAB)Rh(TFA)(η ² -C ₂ H ₄).....	64
Scheme 2.1.2. Catalytic benzene alkenylation by Rh(I) catalyst precursors. ...	67
Scheme 2.1.3. Proposed catalytic cycle for benzene alkenylation using Rh(I) as a catalyst precursor.	68
Scheme 2.2.1. General synthetic procedure for <i>in situ</i> generated catalysts from diimines and [Rh(μ-OAc)(η ² -C ₂ H ₄) ₂] ₂ . Complexes 3 and 6 have been isolated and fully characterized.	70
Scheme 2.2.2. Oxidative conversion of benzene and propylene to propenylbenzenes catalyzed by complexes 1-6 or [Rh(μ-OAc)(η ² -C ₂ H ₄) ₂] ₂	73
Scheme 2.2.3. Structures of three Rh catalyst precursors for Rh(I) dimer [Rh(μ-OAc)(η ² -C ₂ H ₄) ₂] ₂ (1), Rh(II) dimer [Rh(μ-OPiv) ₂ (HOPiv)] ₂ (2), and RhCl ₃ (3).	127
Scheme 2.2.4. Conversion of [Rh(μ-OAc)(η ² -C ₂ H ₄) ₂] ₂ to [Rh ^I (μ-OPiv) ₂ (η ² -C ₂ H ₄) ₂] ₂ (μ-Cu) (4) at room temperature and [Rh(μ-OPiv) ₂ (HOPiv)] ₂ (2) at 120 °C under 50 psig ethylene.....	129
Scheme 2.2.5. Conversion of [Rh(μ-OAc)(η ² -C ₂ H ₄) ₂] ₂ to solution A (containing	

[Rh(μ -OPiv) ₂ (HOPiv)] ₂	132
Scheme 2.2.6. Proposed pathway for conversion of [Rh ^I (μ -OPiv) ₂ (η^2 -C ₂ H ₄) ₂] ₂ (μ -Cu) (4) to [Rh(μ -OPiv) ₂ (HOPiv)] ₂ (2).	138
Scheme 2.2.7. B3LYP-D3 free energies at 423 K for (from left to right): [Rh ^{II} (μ -OAc) ₂ (HOAc)] ₂ (2), Rh ^I ₂ Cu ^{II} (μ -OAc) ₄ (η^2 -C ₂ H ₄) ₄ (4), [Rh ^I (μ -OAc)(η^2 -C ₂ H ₄) ₂] ₂ (1), Rh ^I (κ^2 -OAc)(η^2 -C ₂ H ₄) ₂ (5), Rh ^{II} (κ^2 -OAc) ₂ (6), and Rh ^{III} (κ^2 -OAc) ₃ (7). Stoichiometric amounts of Cu ^{II} (OAc) ₂ , Cu ^I (OAc), C ₂ H ₄ , and HOAc were added to maintain the same number of atoms. Similarly, monomer energies were doubled to be consistent with the dimers. The Cu ^I (OAc) was modeled as a neutral single molecule in (implicit) solution.....	140
Scheme 2.2.8. B3LYP-D3 free energy profile at 423 K for styrene formation from [Rh ^I (μ -OPiv) ₂ (η^2 -C ₂ H ₄) ₂] ₂ (μ -Cu) (4).	142
Scheme 2.4.1. ¹ H NMR spectrum of complex 6 (600 MHz, C ₆ D ₆).	165
Scheme 2.4.2. ¹³ C { ¹ H} NMR spectrum of complex 6 (151 MHz, C ₆ D ₆).	165
Scheme 3.1.1. Arene alkenylation consuming stoichiometric oxidants (A), ethylene (B), dioxygen in the presence (C) or absence (D) of co-oxidants.	176
Scheme 3.1.2. Arene alkenylation using O ₂ as the oxidant to produce alkenyl arene and water(depicted with benzene and ethylene).	177
Scheme 3.1.3. Metal-catalyzed arene alkenylation using only air or dioxygen as oxidant in the absence of co-oxidants.	178
Scheme 3.1.4. Examples of catalyst for aerobic benzene ethylation using dioxygen as the direct oxidant.	179
Scheme 3.1.5. (5-FP)Rh(TFA)(η^2 -C ₂ H ₄) catalyzed benzene propenylation using Cu(OPiv) ₂ /air as oxidants under aerobic/anaerobic conditions.	180
Scheme 3.2.1. Aerobic benzene alkenylation with ethylene in presence of α -methylstyrene	190
Scheme 3.2.2. Explanation for the increase of observed L/B ratio during the aerobic benzene alkenylation with propylene based on product reaction with hydrogen peroxide.	190
Scheme 3.2.3. Kinetic isotope experiment using two parallel reactions with C ₆ H ₆ versus C ₆ D ₆ . Each reaction was run in triplicate. The reactions were sampled every 4 h until 12 h. Each trial produces styrene at a constant rate within 12 hours (Figure S10). <i>k_H</i> and <i>k_D</i> values were determined using average initial rates (from 0 to 4 h) of three separate experiments. The reported error represents the propagated standard deviation of all values.....	195
Scheme 3.2.4. Proposed mechanism for aerobic styrene production using RhCl ₃ as a catalyst precursor in the presence of HOAc.....	197
Scheme 3.2.5. Comparison of mechanistic pathway (top) and reaction coordinate (bottom) of Rh-catalyzed benzene ethylation under aerobic and anaerobic conditions.....	199
Scheme 3.2.6. Possible explanation for different linear/branched product selectivity of aerobic and anaerobic Rh catalysis.	201

-
- Scheme 3.2.7.** Rh-catalyzed aerobic benzene alkenylation with styrene to produce trans-stilbene. Reaction conditions: 9 mL benzene, 1 mL acetic acid, 0.5 mmol styrene, 0.560 mM RhCl₃, 1 atm air, 170 °C. Yields, which were determined by GC, represent the average of three separate experiments based on the amount of styrene. The standard deviations given in parentheses are based on three independent experiments.202
- Scheme 3.2.8.** Rh-catalyzed aerobic alkenylation of toluene with 1-pentene. Reaction conditions: 9 mL toluene, 1 mL acetic acid, 2000 equivalent of 1-pentene relative to Rh, 0.112 mM RhCl₃, 1 atm air, 170 °C. Hydrogenation was achieved using 10% Pd/C under hydrogen atmosphere. The reaction was run in triplicate. The standard deviations given in parentheses are based on three independent experiments. The L:B ratio in the graphic is the ratio of anti-Markovnikov to Markovnikov products.....202
- Scheme 4.1.1.** Linear/branched product selectivity is controlled by the regioselectivity of the olefin insertion and/or the relative rates of subsequent reactions following insertion.....217
- Scheme 4.1.2.** Linear/branched selectivity of previously reported catalysts for propylene hydrophenylation.220
- Scheme 4.1.3.** Structure of Ni complex **h**.221
- Scheme 4.1.4.** Linear/branched selectivity of previously reported Rh(I) catalysts for oxidative propylene hydrophenylation.....221
- Scheme 4.2.1.** [Ir(μ-Cl)(COE)]₂-catalyzed alkenylation of toluene with 1-pentene. Reaction conditions: 10 mL toluene, 480 eq. Cu(OHex)₂ (relative to per Ir atom), 960 eq. HOHex (relative to per Ir atom), 0.0025 mol % [Ir(μ-Cl)(COE)]₂ (relative to toluene), 1000 eq. 1-pentene (relative to per Ir atom), 165 °C. Each data point represents the average of three separate experiments. Error bars represent the standard deviations based on a minimum of three independent experiments.....230
- Scheme 4.2.2.** Isomerization of α-methylstyrene in [Ir(μ-Cl)(COE)]₂-catalyzed benzene alkenylation with ethylene. Reaction conditions: 10 mL benzene, 50 eq. α-methylstyrene (relative to per Ir atom), 1200 eq. Cu(OHex)₂ (relative to per Ir atom), 4800 eq. HOHex (relative to per Ir atom), 0.0005 mol % [Ir(μ-Cl)(COE)]₂ (relative to benzene), 50 psig ethylene, 165 °C, 60 h. Each data point represents the average of three separate experiments. Error bars represent the standard deviations based on a minimum of three independent experiments.232
- Scheme 5.1.1.** Candidates of NHC-Rh complexes that will be prepared and probed for catalytic arene alkenylation.....244
- Scheme 5.2.1.** Examples of potential ligands to support Ir(I) metal.245
- Scheme 5.2.2.** Ligand sterics "above" or "below" the Ir square plane bias the orientation of the olefin and facilitate the formation of linear products.246

LIST OF FIGURES

- Figure 1.4.1.** Structure (left) and ORTEP (right) of (5-FP)Rh(TFA)(η^2 -C₂H₄) (hydrogen atoms omitted). ORTEP reprinted with permission from reference 102. Copyright 2019 American Chemical Society.46
- Figure 2.2.1.** ORTEPs of complexes **3** (left) and **6** (right) (50% probability). H atoms and solvent molecules are omitted for clarity. For the structure of complex **6**, only the major position for the disordered atom in the phenyl ring is shown. Selected bond lengths (Å): for complex **3**: Rh1-N1 1.957(5), Rh1-N2 1.964(5), Rh1-O3 2.061(5), Rh1-O1 2.066(4), O1-C1 1.259(8), O2-C1 1.232(7) C1-C2 1.524(9); for complex **6**: Rh1-N2 1.945(3), Rh1-N1 1.968(3), Rh1-O1 2.057(3), Rh1-O4 2.086(2), O1-C41 1.251(5), O2-C41 1.259(5), C41-C42 1.515(5). Selected bond angles (°): for complex **3**: N1-Rh1-N2 77.6(2), N2-Rh1-O3 95.4(2), N1-Rh1-O1 93.5(2), O3-Rh1-O1 91.6(2), N1-Rh1-O3 168.7(2) N2-Rh1-O1 166.17(19), O2-C1-O1 127.4(6), C1-O1-Rh1 126.7(4), C1-O2-Rh2 122.9(4); for complex **6**: N2-Rh1-N1 78.9(1), N1-Rh1-O1 95.9(1), N2-Rh1-O4 91.0(1), O1-Rh1-O4 92.9(1), N2-Rh1-O1 167.2(1), N1-Rh1-O4 168.59(12), O1-C41-O2 126.1(4), C41-O1-Rh1 124.7(3), C41-O2-Rh2 124.9(3).70
- Figure 2.2.2.** Plot of TOs versus time for styrene production catalyzed by complexes **1–6** or [Rh(μ -OAc)(η^2 -C₂H₄)₂]₂. Reaction conditions: 0.001 mol % of Rh (relative to benzene), 240 eq. of Cu(OAc)₂ (relative to Rh), 10 mL benzene, 40 psig ethylene, 150 °C. Each data point is the average of three separate experiments. Error bars represent the standard deviations based on a minimum of three independent experiments.....72
- Figure 2.2.3.** ¹H NMR spectra for conversion of complex **3** (A) and complex **6** (B) to [Rh(μ -OAc)(η^2 -C₂H₄)₂]₂ and ^{F1}DAB ligand in benzene-*d*₆ at room temperature under 10 psig ethylene.75
- Figure 2.2.4.** Photographs of NMR tubes containing [(^{F1}DAB)Rh(μ -OAc)]₂ and benzene-*d*₆ before/after being treatment with 10 psig of C₂H₄.76
- Figure 2.2.5.** ¹H NMR spectra for thermolysis of [Rh(μ -OAc)(η^2 -C₂H₄)₂]₂. The bottom spectrum is starting material, [Rh(μ -OAc)(η^2 -C₂H₄)₂]₂. The top spectrum is acquired after heating [Rh(μ -OAc)(η^2 -C₂H₄)₂]₂ at 150 °C for 15 minutes.....78
- Figure 2.2.6.** (A) Plot of [Rh(μ -OAc)(η^2 -C₂H₄)₂]₂ concentration versus time for decomposition in benzene-*d*₆ at different temperatures. Each data point is the average of three separate experiments. Error bars represent the standard deviation based on a minimum of three independent experiments. (B) Eyring plot for [Rh(μ -OAc)(η^2 -C₂H₄)₂]₂ decomposition. Reaction conditions: 0.2 mol % of [Rh(μ -OAc)(η^2 -C₂H₄)₂]₂ (relative to benzene), 0.5 mL benzene-*d*₆, 20 psig N₂, 90-120 °C.78
- Figure 2.2.7.** Comparison of kinetic plot for the decomposition of [Rh(μ -OAc)(η^2 -C₂H₄)₂]₂ in the absence of ethylene versus in the presence of 20 psig ethylene. Reaction conditions: 0.2 mol % of [Rh(μ -OAc)(η^2 -C₂H₄)₂]₂

(relative to benzene), 0.5 mL benzene-*d*₆, 20 psig nitrogen/ethylene, 90 °C. Each data point is the average of three separate experiments. Error bars represent the standard deviations based on a minimum of three independent experiments. 79

Figure 2.2.8. Comparison of kinetic plot for the decomposition of $[\text{Rh}(\mu\text{-OAc})(\eta^2\text{-C}_2\text{H}_4)_2]_2$ in C_6H_6 versus C_6D_6 (A), C_6H_6 versus C_6F_6 (B), and C_6H_6 versus *d*₁₀-*p*-xylene (C). Reaction condition: 0.0025g $[\text{Rh}(\mu\text{-OAc})(\eta^2\text{-C}_2\text{H}_4)_2]_2$, 0.5ml benzene/ C_6F_6 /*d*₁₀-*p*-xylene 20 psig N₂, 90 °C. Each data point is the average of three separate experiments. Error bars represent the standard deviations based on a minimum of three independent experiments. 80

Figure 2.2.9. TEM lattice analysis (left), TEM-EDS measurement (top right) and selected area diffraction analysis (bottom right) of Rh species from thermal decomposition of $[\text{Rh}(\mu\text{-OAc})(\eta^2\text{-C}_2\text{H}_4)_2]_2$ at 150 °C under 40 psig of ethylene in benzene in the absence of $\text{Cu}(\text{OAc})_2$ 81

Figure 2.2.10. Plot of TOs versus time for styrene production catalyzed by $[\text{Rh}(\mu\text{-OAc})(\eta^2\text{-C}_2\text{H}_4)_2]_2$ after heating $\text{Cu}(\text{OAc})_2$ (0.24 mol % relative to benzene) in benzene (10 mL) for 0 to 24 hours at 150 °C. Reaction conditions: 0.001 mol % of Rh (relative to benzene), 40 psig ethylene, 150 °C. Each data point is the average of three separate experiments. Error bars represent the standard deviations based on a minimum of three independent experiments. 82

Figure 2.2.11. Comparison of TOs vs time plots for styrene production catalyzed by $[\text{Rh}(\mu\text{-OAc})(\eta^2\text{-C}_2\text{H}_4)_2]_2$ using isolated solid versus solution phase of the reaction mixture obtained by heating $\text{Cu}(\text{OAc})_2$ (0.24 mol % relative to benzene) in benzene (10 mL) for 12 hours at 150 °C. Each data point is the average of three separate experiments. Error bars represent the standard deviations based on a minimum of three independent experiments. 84

Figure 2.2.12. Comparison of TOs vs time plots for styrene production catalyzed by $[\text{Rh}(\mu\text{-OAc})(\eta^2\text{-C}_2\text{H}_4)_2]_2$ after heating $\text{Cu}(\text{OAc})_2$ (48.8 mg) in benzene versus hexane (10 mL) for 12 hours at 150 °C. Each data point is the average of three separate experiments. Error bars represent the standard deviations based on a minimum of three independent experiments. 84

Figure 2.2.13. Powder XRD profile of $\text{Cu}(\text{OAc})_2$ solid under different conditions: (A) untreated copper(II) acetate anhydrous; (B) solid materials isolated from the reaction mixture obtained heating copper(II) acetate in 10 mL benzene at 150 °C for 12 h (activated $\text{Cu}(\text{OAc})_2$); (C) solid materials isolated from the reaction mixture obtained by heating copper(II) acetate in 10 mL benzene with 0.005 mol % of ^{F1}DAB ligand at 150 °C for 2 h. 86

Figure 2.2.14. FT-IR spectra of $\text{Cu}(\text{OAc})_2$ solid under different conditions: (A) copper(II) acetate monohydrate; (B) untreated copper(II) acetate anhydrous; (C) solid materials isolated from the reaction mixture obtained heating copper(II) acetate in 10 mL benzene at 150 °C for 12 h (activated $\text{Cu}(\text{OAc})_2$); (D) solid materials isolated from the reaction mixture obtained by heating

- copper(II) acetate in 10 mL benzene with 0.005 mol % F1 DAB ligand at 150 °C for 2 h.....87
- Figure 2.2.15.** Curves from Differential Scanning Calorimetry (DSC) and Glass Transition Temperature, (T_g) experiments using untreated $\text{Cu}(\text{OAc})_2$ (**A**) and activated $\text{Cu}(\text{OAc})_2$ (**B**).....88
- Figure 2.2.16.** Comparison of TOs vs time plots for styrene production catalyzed by $[\text{Rh}(\mu\text{-OAc})(\eta^2\text{-C}_2\text{H}_4)_2]_2$ using commercial $\text{Cu}(\text{OAc})_2$ versus $\text{Cu}(\text{OAc})_2$ dried under dynamic vacuum at 150 °C for 18 hours. Each data point is the average of three separate experiments. Error bars represent the standard deviations based on a minimum of three independent experiments.88
- Figure 2.2.17.** TEM lattice analysis (A-C) and selected area diffraction analysis (D and E) of solid species from heating $\text{Cu}(\text{OAc})_2$ in benzene at 150 °C for 12 h. Figures S11B and S11C are obtained by magnifying the area marked with red frame in Figures S11A and S11B, respectively. Cu(111) plane is observed in the lattice constant analysis. The lattice parameters for Cu(111), Cu(200) and Cu(220) are found to be 0.21 nm, 0.18 nm and 0.12 nm, respectively. These data are consistent with the formation of Cu nanoparticles.91
- Figure 2.2.18.** Plot of TOs versus time for styrene production catalyzed by $[\text{Rh}(\mu\text{-OAc})(\eta^2\text{-C}_2\text{H}_4)_2]_2$ using commercial $\text{Cu}(\text{OAc})_2$ with the addition of solid Cu species obtained after the standard catalytic reaction, and its comparison to the standard reaction.92
- Figure 2.2.19.** SEM images of commercial $\text{Cu}(\text{OAc})_2$ (A, B) and solid isolated by heating $\text{Cu}(\text{OAc})_2$ in benzene at 150 °C for 12 h (C, D). Figures 7B and 7D are obtained by magnifying the area marked with red frame in Figures 7A and 7C, respectively.94
- Figure 2.2.20.** N_2 adsorption isotherm linear plot for untreated $\text{Cu}(\text{OAc})_2$ (**A**) and activated $\text{Cu}(\text{OAc})_2$ (**B**). Plot A shows large hysteresis between adsorption and desorption, which indicates capillary condensation in meso and macropores, Hysteresis between adsorption and desorption is nearly eliminated in plot **B**.....95
- Figure 2.2.21.** Plots of TOs versus time for styrene production catalyzed by $[\text{Rh}(\mu\text{-OAc})(\eta^2\text{-C}_2\text{H}_4)_2]_2$ using ball-milled $\text{Cu}(\text{OAc})_2$ and thermally treated ground $\text{Cu}(\text{OAc})_2$ and its comparison to the standard reaction. Each data point is the average of three separate experiments. Error bars represent the standard deviations based on a minimum of three independent experiments.96
- Figure 2.2.22.** Plots of TOs versus time for styrene production catalyzed by $[\text{Rh}(\mu\text{-OAc})(\eta^2\text{-C}_2\text{H}_4)_2]_2$ with the addition of 0, 0.25, 0.5, 1 eq. (relative to Rh) of PPh_3 (**A**), $\text{P}(\text{OCH}_2)_3\text{CEt}$ (**B**) or 1,10-phenanthroline (**C**). Each data point is the average of three separate experiments. Error bars represent the standard deviations based on a minimum of three independent experiments.97
- Figure 2.2.23.** Plot of TOs versus time for styrene production catalyzed by $[\text{Rh}(\mu\text{-OAc})(\eta^2\text{-C}_2\text{H}_4)_2]_2$ using copper(II) 2-ethylhexanoate [$\text{Cu}(\text{OHex})_2$] as

- the oxidant. Each data point is the average of three separate experiments. Error bars represent the standard deviations based on a minimum of three independent experiments. 99
- Figure 2.2.24.** Plots of TOs versus time for styrene production catalyzed by $[\text{Rh}(\mu\text{-OAc})(\eta^2\text{-C}_2\text{H}_4)_2]_2$ with the addition of 0 to 20 eq. of $^{\text{Fl}}\text{DAB}$ ligand. Reaction conditions: 0.001 mol % of Rh (relative to benzene), 240 eq. of $\text{Cu}(\text{OAc})_2$ (relative to Rh), 10 mL benzene, 40 psig ethylene, 150 °C. Error bars represent the standard deviations based on a minimum of three independent experiments. 101
- Figure 2.2.25.** Plot of TOs versus time for styrene production catalyzed by $[\text{Rh}(\mu\text{-OAc})(\eta^2\text{-C}_2\text{H}_4)_2]_2$ using solid materials isolated from the reaction mixture obtained by heating copper(II) acetate in 10 mL benzene with 0.005 mol % $^{\text{Fl}}\text{DAB}$ at 150 °C for 2 h. Each data point is the average of three separate experiments. Error bars represent the standard deviations based on a minimum of three independent experiments..... 101
- Figure 2.2.26.** Comparison of TOs versus time plots for styrene production catalyzed by $[\text{Rh}(\mu\text{-OAc})(\eta^2\text{-C}_2\text{H}_4)_2]_2$ and $[(^{\text{Fl}}\text{DAB})\text{Rh}(\mu\text{-OAc})]_2$ (**3**). Reaction conditions: 0.005 mol % of Rh (relative to benzene), 240 eq. of $\text{Cu}(\text{OAc})_2$ (relative to Rh), 10 mL benzene, 15 psig ethylene, 150 °C. Error bars represent the standard deviations based on a minimum of three independent experiments. 103
- Figure 2.2.27.** Comparison of TOs versus time plots for styrene production using various loading of $[\text{Rh}(\mu\text{-OAc})(\eta^2\text{-C}_2\text{H}_4)_2]_2$ with the addition of 100 eq. of $^{\text{Fl}}\text{DAB}$ ligand. Reaction conditions: 0.001 or 0.0001 mol % of Rh (relative to benzene), 100 eq. of $^{\text{Fl}}\text{DAB}$ ligand (relative to Rh), 0.269 mmol $\text{Cu}(\text{OAc})_2$ (240 eq. relative to 0.001 mol % Rh, 2400 eq. relative to 0.0001 mol % Rh), 10 mL benzene, 40 psig ethylene, 150 °C. Each data point is the average of three separate experiments. Error bars represent the standard deviations based on a minimum of three independent experiments..... 104
- Figure 2.2.28.** Comparison of plots for TOs versus time for styrene production using solid materials versus soluble material isolated from the reaction mixture after 12 h (**A**) or 1 h (**B**) of the catalysis with 40 psig ethylene using $[\text{Rh}(\mu\text{-OAc})(\eta^2\text{-C}_2\text{H}_4)_2]_2$ [0.001 mol % of Rh (relative to benzene)] at 150 °C. TOs of styrene were obtained by subtracting TO at 0 h (if any) from the raw TO data. Error bars represent the standard deviations based on a minimum of three independent experiments. 107
- Figure 2.2.29.** X-ray photoelectron spectra (Rh 3d region) of (top) Rh metal foil and (bottom) silica-supported Rh metal nanoparticles. 109
- Figure 2.2.30.** X-ray photoelectron spectrum (region Rh 3d) of insoluble Rh species formed during the thermal decomposition of $[\text{Rh}(\mu\text{-OAc})(\eta^2\text{-C}_2\text{H}_4)_2]_2$ (0.001 mol % Rh relative to benzene) at 150 °C under 40 psig of ethylene in benzene in the absence of $\text{Cu}(\text{OAc})_2$ 109
- Figure 2.2.31.** X-ray photoelectron spectra (region Rh 3d) of recovered Rh species formed (**A** and **B**) after 1 h and 12 h of catalysis, respectively, with

- 40 psig ethylene and $[\text{Rh}(\mu\text{-OAc})(\eta^2\text{-C}_2\text{H}_4)_2]_2$ (0.001 mol % Rh relative to benzene) using **untreated** $\text{Cu}(\text{OAc})_2$ (240 eq. relative to Rh); **(C)** after 1 h of catalysis with 40 psig ethylene and $[\text{Rh}(\mu\text{-OAc})(\eta^2\text{-C}_2\text{H}_4)_2]_2$ (0.001 mol % Rh relative to benzene) using **activated** $\text{Cu}(\text{OAc})_2$ (240 eq. relative to Rh).
..... 111
- Figure 2.2.32.** X-ray photoelectron spectra (region Rh 3d) of $[\text{Rh}(\mu\text{-OAc})(\eta^2\text{-C}_2\text{H}_4)_2]_2$ **(A)**, $\text{Rh}_2(\text{OAc})_4$ **(B)** and $\text{RhCl}_3 \cdot x\text{H}_2\text{O}$ **(C)**..... 112
- Figure 2.2.33.** X-ray photoelectron spectrum (region Rh 3d) of recovered Rh species from the thermal decomposition of $[\text{Rh}(\mu\text{-OAc})(\eta^2\text{-C}_2\text{H}_4)_2]_2$ (0.001 mol % Rh relative to benzene) in benzene after 1 h in the presence of SiO_2 .
..... 113
- Figure 2.2.34.** TEM/STEM images and EDS analysis of recovered Rh species from the thermal decomposition of $[\text{Rh}(\mu\text{-OAc})(\eta^2\text{-C}_2\text{H}_4)_2]_2$ (0.001 mol % Rh relative to benzene) in benzene after 1 h in the presence of SiO_2 . **(A)** bright field TEM images of SiO_2 captured Rh species; **(B-D)** dark-field STEM images of SiO_2 captured Rh species; **(E)** EDS analysis of selected particle (circled in red on Figure 15C)..... 114
- Figure 2.2.35.** A STEM image of recovered Rh species formed after 1 h of catalysis with 40 psig ethylene and $[\text{Rh}(\mu\text{-OAc})(\eta^2\text{-C}_2\text{H}_4)_2]_2$ (0.001 mol % Rh relative to benzene) using untreated $\text{Cu}(\text{OAc})_2$ (240 eq. relative to Rh) (left) and EDS analysis of selected single particle circled in red on the left STEM image (right)..... 115
- Figure 2.2.36.** STEM-EDS maps of recovered Rh species formed after 1 h in the catalysis with 40 psig ethylene and $[\text{Rh}(\mu\text{-OAc})(\eta^2\text{-C}_2\text{H}_4)_2]_2$ (0.001 mol % Rh relative to benzene) using untreated $\text{Cu}(\text{OAc})_2$ (240 eq. relative to Rh). **(A)** overall dark-field STEM image; **(B)** EDS map of Rh; **(C)** EDS maps of Cu; **(D)** EDS maps of O. Rh, Cu and O are shown in yellow, orange and red, respectively. 116
- Figure 2.2.37.** Plots of TOs versus time for styrene production catalyzed by various loading of $[\text{Rh}(\mu\text{-OAc})(\eta^2\text{-C}_2\text{H}_4)_2]_2$ (0.001 mol % Rh, 0.005 mol % Rh, and 0.01 mol % Rh relative to benzene). Error bars represent the standard deviations based on a minimum of three independent experiments.
..... 117
- Figure 2.2.38.** Plots of TOs versus time for styrene production using the solution phase of the reaction mixture after 1 h of the catalysis with 40 psig ethylene using $[\text{Rh}(\mu\text{-OAc})(\eta^2\text{-C}_2\text{H}_4)_2]_2$ under the conditions where activated $\text{Cu}(\text{OAc})_2$ oxidant is used **(A)** or 5 eq. of $^{\text{Fl}}$ DAB ligand is added **(B)** and its comparison to the catalysis with 40 psig ethylene using $[\text{Rh}(\mu\text{-OAc})(\eta^2\text{-C}_2\text{H}_4)_2]_2$ with the use of activated $\text{Cu}(\text{OAc})_2$ **(a)** or addition of 5 eq. of $^{\text{Fl}}$ DAB ligand **(b)**. TO of styrene was obtained by subtracting TO at 0 h (if any) from the raw TO data. Error bars represent the standard deviations based on a minimum of three independent experiments..... 119
- Figure 2.2.39.** Plot of TOs versus time for styrene production catalyzed by $[\text{Rh}(\mu\text{-OAc})(\eta^2\text{-C}_2\text{H}_4)_2]_2$ at 125 °C after heating $\text{Cu}(\text{OAc})_2$ (0.24 mol %

relative to benzene) in benzene (10 mL) for 12 hours at 150 °C. Each data point is the average of three separate experiments. Error bars represent the standard deviations based on a minimum of three independent experiments.

..... 123

Figure 2.2.40. Plot of TOs versus time for styrene production using the reaction mixture obtained after 1 h of the standard catalytic reaction and activated $\text{Cu}(\text{OAc})_2$ solid. TO of styrene was obtained by subtracting TO at 0 h (if any) from the raw TO data. Each data point is the average of three separate experiments. Error bars represent the standard deviations based on a minimum of three independent experiments..... 124

Figure 2.2.41. Plot of TOs versus time for styrene production using the reaction mixture obtained after 1 h of the standard catalytic reaction and commercial $\text{Cu}(\text{OAc})_2$ with the addition of 5 eq. $^{\text{Fl}}$ DAB ligand. TO of styrene was obtained by subtracting TO at 0 h (if any) from the raw TO data. Each data point is the average of three separate experiments. Error bars represent the standard deviations based on a minimum of three independent experiments.

..... 124

Figure 2.2.42. Plot of TOs versus time for styrene production using commercial $\text{Cu}(\text{OAc})_2$ and the reaction mixture obtained by heating $[\text{Rh}(\mu\text{-OAc})(\eta^2\text{-C}_2\text{H}_4)_2]_2$ (0.001 mol % Rh relative to benzene) and 5 eq. of $^{\text{Fl}}$ DAB in benzene (10 mL) for 1 hour at 150 °C under 40 psig ethylene. Each data point is the average of three separate experiments. Error bars represent the standard deviations based on a minimum of three independent experiments. 125

Figure 2.2.43. Plot of TOs versus time for styrene production using activated $\text{Cu}(\text{OAc})_2$ and the reaction mixture obtained by heating $[\text{Rh}(\mu\text{-OAc})(\eta^2\text{-C}_2\text{H}_4)_2]_2$ (0.001 mol % Rh relative to benzene) in benzene (10 mL) for 1 hour at 150 °C under 40 psig ethylene. Each data point is the average of three separate experiments. Error bars represent the standard deviations based on a minimum of three independent experiments. 125

Figure 2.2.44. Comparison of TOs vs time for the conversion of benzene and ethylene to styrene using different molecular Rh catalyst precursors. Each data point is the average of at least three separate experiments. Error bars represent the standard deviations based on a minimum of three independent experiments. Reaction conditions: 0.001 mol % of Rh (relative to benzene), 480 eq. $\text{Cu}(\text{OPiv})_2$ (relative to Rh), 960 eq. HOPIV (relative to Rh), 10 mL benzene, 50 psig ethylene, 150 °C. 127

Figure 2.2.45. ^1H NMR spectra for conversion of $[\text{Rh}(\mu\text{-OAc})(\eta^2\text{-C}_2\text{H}_4)_2]_2$ to $[\text{Rh}^{\text{I}}(\mu\text{-OPiv})_2(\eta^2\text{-C}_2\text{H}_4)_2]_2(\mu\text{-Cu})$ (**4**) at room temperature and $[\text{Rh}(\mu\text{-OPiv})_2(\text{HOPIV})]_2$ (**2**) at 120 °C under 50 psig ethylene..... 130

Figure 2.2.46. ^1H NMR spectra for conversion of $[\text{Rh}(\mu\text{-OAc})(\eta^2\text{-C}_2\text{H}_4)_2]_2$ to $[\text{Rh}^{\text{I}}(\mu\text{-OPiv})_2(\eta^2\text{-C}_2\text{H}_4)_2]_2(\mu\text{-Cu})$ at room temperature and $[\text{Rh}(\mu\text{-OPiv})_2(\text{HOPIV})]_2$ at 120 °C in the absence of ethylene. 131

Figure 2.2.47. ORTEP of $[\text{Rh}(\mu\text{-OPiv})_2(\text{HOPIV})]_2$ (**2**) (50% probability). H atoms

and solvent molecules are omitted for clarity. Only the major position for the disordered atom is shown..... 131

Figure 2.2.48. Comparison of TOs vs time plots for the conversion of benzene and ethylene to styrene using $[\text{Rh}(\mu\text{-OPiv})_2(\text{HOPIv})]_2$ (**2**) and solution A. Each data point is the average of at least three separate experiments and error bars represent the standard deviations based on these independent experiments. Reaction conditions: 0.001 mol % of Rh (relative to benzene), 480 eq. $\text{Cu}(\text{OPiv})_2$ (relative to Rh), 960 eq. HOPIv (relative to Rh), 10 mL benzene, 50 psig ethylene, 150 °C..... 132

Figure 2.2.49. ORTEP of $[\text{Rh}^I(\mu\text{-OPiv})_2(\eta^2\text{-C}_2\text{H}_4)_2]_2(\mu\text{-Cu})$ (**4**) (50% probability). H atoms are omitted for clarity. Selected bond lengths (Å): Cu1-O2 1.948(3), Cu1-O3 1.949(3), Rh1-O4 2.078(3), Rh1-C1 2.112(4), Rh1-C2 2.118(3), Rh1-Cu1 3.0095(5), Rh1-O1 2.079(3), Rh1-C3 2.112(4), Rh1-C4 2.122(4), C1-C2 1.393(6), C3-C4 1.402(6). Selected bond angles (°): O4-Rh1-O1 87.78(11), C1-Rh1-C2 38.45(16), C1-Rh1-C3 88.43(18), C1-Rh1-C4 100.63(17), O4-Rh1-C1 160.42(14), O1-Rh1-C1 88.93(15), C3-Rh1-C4 38.66(16), O2'-Cu1-O3' 90.05(12), O2'-Cu1-O3 89.95(12), O1-C5-O2 125.9(3), O3-C10-O4 125.7(3). 133

Figure 2.2.50. ^1H NMR spectra for conversion of $[\text{Rh}^I(\mu\text{-OPiv})_2(\eta^2\text{-C}_2\text{H}_4)_2]_2(\mu\text{-Cu})$ (**4**) to $[\text{Rh}(\mu\text{-OPiv})_2(\text{HOPIv})]_2$ (**2**) at 120 °C after 12 hours..... 135

Figure 2.2.51. Comparison of TOs vs time plots for the conversion of benzene and ethylene to styrene using $[\text{Rh}(\mu\text{-OAc})(\eta^2\text{-C}_2\text{H}_4)_2]_2$ (**1**) and $[\text{Rh}^I(\mu\text{-OPiv})_2(\eta^2\text{-C}_2\text{H}_4)_2]_2(\mu\text{-Cu})$ (**4**). Each data point is the average of at least three separate experiments with error bars representing the standard deviations based on these independent experiments. Reaction conditions: 0.001 mol % of Rh (relative to benzene), 480 eq. $\text{Cu}(\text{OPiv})_2$ (relative to Rh), 960 eq. HOPIv (relative to Rh), 10 mL benzene 50 psig ethylene, 150 °C. 135

Figure 2.2.52. Kinetic plots and Eyring plot (E) for conversion of $[\text{Rh}^I(\mu\text{-OPiv})_2(\eta^2\text{-C}_2\text{H}_4)_2]_2(\mu\text{-Cu})$ (**4**) to $[\text{Rh}(\mu\text{-OPiv})_2(\text{HOPIv})]_2$ (**2**) at 21 °C (**A**), 45 °C (**B**), 50 °C (**C**), and 60 °C (**D**) under ethylene. Reaction conditions: 9.35 mM of $[\text{Rh}(\mu\text{-OAc})(\eta^2\text{-C}_2\text{H}_4)_2]_2$ as starting material, 0.3 mL benzene- d_6 , 24 eq. $\text{Cu}(\text{OPiv})_2$ (relative to Rh), 48 eq. HOPIv (relative to Rh), 50 psig ethylene. The rate of decay of **4** was determined based on the amount of complex **2** formed. Each data point is the average of three separate experiments and error bars represent the standard deviations based these independent experiments. 138

Figure 2.2.53. Kinetic plots for conversion of $[\text{Rh}^I(\mu\text{-OPiv})_2(\eta^2\text{-C}_2\text{H}_4)_2]_2(\mu\text{-Cu})$ (**4**) to $[\text{Rh}(\mu\text{-OPiv})_2(\text{HOPIv})]_2$ (**2**) at 45 °C (top) and 50 °C (bottom) in the absence of ethylene. Reaction conditions: 9.35 mM of $[\text{Rh}(\mu\text{-OAc})(\eta^2\text{-C}_2\text{H}_4)_2]_2$ as starting material, 0.3 mL benzene- d_6 , 24 eq. $\text{Cu}(\text{OPiv})_2$ (relative to Rh), 48 eq. HOPIv (relative to Rh). The rate of decay of **4** is determined based on the amount of complex **2** formed. Each data point is the average of three separate experiments and error bars represent

- the standard deviations based these independent experiments. 139
- Figure 3.2.1.** Comparison of TOs vs time for aerobic benzene alkenylation with ethylene in presence of acids. Reaction conditions: 10 mL of benzene, 0.112 mM RhCl₃, 70 psig ethylene, 1 atm air, 150 °C. Equivalents of acid or acetic anhydride are relative to RhCl₃. Each data point represents the average of three separate experiments. Error bars represent the standard deviations based on a minimum of three independent experiments. 184
- Figure 3.2.2.** Comparison of TOs vs time for aerobic benzene alkenylation using different volume ratios of benzene and acetic acid. Reaction conditions: 10 mL of a benzene/acetic acid solution, 0.112 mM RhCl₃, 70 psig ethylene, 1 atm air, 150 °C. Each data point represents the average of three separate experiments. Error bars represent the standard deviations based on a minimum of three independent experiments. 185
- Figure 3.2.3.** Comparison of TOs vs time for aerobic benzene alkenylation with ethylene catalyzed by [Rh(μ -OAc)(η^2 -C₂H₄)₂]₂ and RhCl₃. Reaction conditions: 5 mL benzene, 5 mL HOAc, 0.112 mM Rh, 70 psig ethylene, 1 atm air, 150 °C. Each data point represents the average of three separate experiments. Error bars represent the standard deviations based on a minimum of three independent experiments. 185
- Figure 3.2.4.** Comparison of TOs vs time for aerobic benzene alkenylation with ethylene in the absence or presence of additives. Reaction conditions: 5 mL C₆H₆, 5 mL HOAc, 0.112 mM RhCl₃, 70 psig ethylene, 1 atm air, 150 °C. Each data point represents the average of three separate experiments. Equivalents of additives are relative to RhCl₃. Error bars represent the standard deviations based on a minimum of three independent experiments. 186
- Figure 3.2.5.** Comparison of TOs vs time for aerobic benzene alkenylation with ethylene in the absence or presence of water. Reaction conditions: 5 mL benzene, 5 mL HOAc, 0.112 mM RhCl₃, 70 psig ethylene, 1 atm air, 150 °C. Each data point represents the average of three separate experiments. Error bars represent the standard deviations based on a minimum of three independent experiments. 186
- Figure 3.2.6.** Effect of reaction temperature on aerobic benzene alkenylation reaction. Reaction conditions: 5 mL C₆H₆, 5 mL HOAc, 0.112 mM RhCl₃, 1 atm air. Each data point represents the average of three separate experiments. Error bars represent the standard deviations based on a minimum of three independent experiments. 187
- Figure 3.2.7.** Plots of TOs of total products versus time (**A**) and L/B ratio versus time (**B**) for aerobic benzene alkenylation with propylene at 150 and 170 °C. Reaction conditions: 5 mL C₆H₆, 5 mL HOAc, 0.112 mM RhCl₃, 25 psig propylene, 1 atm air, 170 °C. Each data point represents the average of three separate experiments. Error bars represent the standard deviations based on a minimum of three independent experiments. 189
- Figure 3.2.8.** Plots of L/B ratio of 4 phenylpropylene products versus time under

catalytic conditions. Reaction conditions: 5 mL C₆H₆, 5 mL HOAc, 0.112 mM RhCl₃, 70 psig ethylene, 1 atm air, 23 eq. of allylbenzene, 9 eq. of α -methylstyrene, 3 eq. of cis- β -methylstyrene, 23 eq. of trans- β -methylstyrene, 170 °C. Each data point represents the average of three separate experiments. Error bars represent the standard deviations based on a minimum of three independent experiments..... 189

Figure 3.2.9. Comparison of TOs of styrene vs time for aerobic benzene alkenylation with ethylene using different volume ratios of benzene and acetic acid. Reaction conditions: 10 mL of a benzene/acetic acid solution, 0.022 mM RhCl₃, 70 psig ethylene, 1 atm air, 170 °C. Each data point represents the average of three separate experiments. Error bars represent the standard deviations based on a minimum of three independent experiments. 191

Figure 3.2.10. Comparison of TOs of benzaldehyde vs time for aerobic benzene alkenylation with ethylene using different volume ratios of benzene and acetic acid. Reaction conditions: 10 mL of a benzene/acetic acid solution, 5 mL HOAc, 0.112 mM RhCl₃, 70 psig ethylene, 1 atm air, 170 °C. Each data point represents the average of three separate experiments. Error bars represent the standard deviations based on a minimum of three independent experiments. To avoid the decay of internal standard hexamethylbenzene under aerobic conditions as the catalysis proceeds for long, hexamethylbenzene was not added at the beginning of the catalysis. Instead, external hexamethylbenzene was added while sampling 192

Figure 3.2.11. Log–log plots of observed rate constants (k_{obs}) versus (A) concentration of C₂H₄. Reaction conditions: 5 mL C₆H₆, 5 mL HOAc, 0.112 mM RhCl₃, 1 atm air, 170 °C. (B) k_{obs} versus concentration of RhCl₃. Reaction conditions: 5 mL C₆H₆, 5 mL HOAc, 70 psig C₂H₄, 1 atm air, 170 °C. (C) k_{obs} versus pressure of O₂. Reaction conditions: 5 mL C₆H₆, 5 mL HOAc, 70 psig C₂H₄, 0.112 mM RhCl₃, 150 °C. Each reaction was run in triplicate. The reactions were sampled every 4 h until 12 h. Each trial produces styrene at a constant rate within 12 hours (Figure S7-S9). Observed rate constants (k_{obs}) were extracted from the initial rate regime (from 0 to 4 h) of styrene TOs versus time plots (Figure S7-S9). The concentration of ethylene dissolved in benzene under various ethylene pressures at 170 °C was determined according to a reported method.⁸⁶ Each data point represents the average of three separate experiments. Error bars represent the standard deviations based on a minimum of three independent experiments..... 194

Figure 3.2.12. Plot of k_{obs} versus [C₂H₄]. Reaction conditions: 5 mL C₆H₆, 5 mL HOAc, 0.112 mM RhCl₃, 1 atm air, 170 °C. Each data point represents the average of three separate experiments. Error bars represent the standard deviations based on a minimum of three independent experiments. 195

Figure 3.2.13. Comparison of TOs vs time for aerobic benzene alkenylation with ethylene in acetic acid-*d*₄ and perprotio acetic acid. Reaction conditions: 5 mL benzene, 5 mL acetic acid-*d*₄ or perprotio acetic acid, 0.112 mM Rh, 70 psig ethylene, 1 atm air, 170 °C. Each data point represents the average of three

separate experiments. Error bars represent the standard deviations based on a minimum of three independent experiments..... 195

Figure 4.2.1. Results for $[\text{Ir}(\mu\text{-Cl})(\text{COE})_2]$ -catalyzed oxidative hydrophenylation of propylene using 1200 eq. $\text{Cu}(\text{OPiv})_2$ (relative to per Ir atom) and 4800 eq. HOPiv (relative to per Ir atom). Reaction conditions: 10 mL benzene, 0.0005 mol % $[\text{Ir}(\mu\text{-Cl})(\text{COE})_2]$ (relative to benzene), 30 psig propylene, 165 °C. The TOs are the average of a minimum of three experiments. Each data point represents the average of three separate experiments. Error bars represent the standard deviations based on a minimum of three independent experiments.227

Figure 4.2.2. Results for $[\text{Ir}(\mu\text{-Cl})(\text{COE})_2]$ -catalyzed oxidative hydrophenylation of propylene using 0.004 mol% of Ir (relative to benzene). Reaction conditions: 10 mL benzene, 1200 eq. $\text{Cu}(\text{OHex})_2$ (relative to per Ir atom), 2400 eq. HOHex (relative to per Ir atom), 0.002 mol % $[\text{Ir}(\mu\text{-Cl})(\text{COE})_2]$ (relative to benzene), 30 psig propylene, 165 °C. The TOs are the average of a minimum of three experiments. Each data point represents the average of three separate experiments. Error bars represent the standard deviations based on a minimum of three independent experiments.....228

Figure 4.2.3. Results for $[\text{Ir}(\mu\text{-Cl})(\text{COE})_2]$ -catalyzed oxidative hydrophenylation of propylene with in situ aerobic $\text{Cu}(\text{II})$ regeneration (two-stage copper recycling method). The reactor is charged with 1atm air and 70 psig of N_2 at every sampling point for regenerating $\text{Cu}(\text{II})$ oxidant at 120 °C, and then air was removed with a propylene purge and oxidative propylene hydroarylation was continued. Reaction conditions: 10 mL benzene, 240 eq. $\text{Cu}(\text{OHex})_2$ (relative to per Ir atom), 1200 eq. HOHex (relative to per Ir atom), 0.0005 mol % $[\text{Ir}(\mu\text{-Cl})(\text{COE})_2]$ (relative to benzene), 30 psig propylene, 165 °C. Each data point represents the average of three separate experiments. Error bars represent the standard deviations based on a minimum of three independent experiments.229

Figure 4.2.4. Plots of L/B ratio of 4 phenylpropylene products versus time under catalytic conditions. Reaction conditions: 10 mL C_6H_6 , $[\text{Ir}(\mu\text{-Cl})(\text{COE})_2]$ (0.001 mol% of Ir relative to benzene), 1200 equivalent of $\text{Cu}(\text{OHex})_2$ (relative to per Ir atom), 4800 equivalents of 2-ethyl hexanoic acid (relative to per Ir atom), 30 psig propylene, 1.5 eq. of allylbenzene, 2.5 eq. of α -methylstyrene, 15 eq. of cis- β -methylstyrene, 40 eq. of trans- β -methylstyrene, 165 °C. Each data point represents the average of three separate experiments. Error bars represent the standard deviations based on a minimum of three independent experiments.....233

LIST OF TABLES

Table 1.4.1. Comparison of L:B ratio for hydroarylation with α -olefins using cationic Pt(II) complexes.	36
Table 2.2.1. Comparison of oxidative coupling of benzene and propylene to propenylbenzene catalyzed by complexes 1–6 or $[\text{Rh}(\mu\text{-OAc})(\eta^2\text{-C}_2\text{H}_4)_2]_2^a$	73
Table 2.2.2. Effect of different Cu species for styrene production catalyzed by $[\text{Rh}(\mu\text{-OAc})(\eta^2\text{-C}_2\text{H}_4)_2]_2$. ^a TOs were obtained at 4 hrs.	88
Table 2.2.3. Formal oxidation states of Rh in and Rh 3d _{5/2} binding energy of Rh metal foil, $[\text{Rh}(\mu\text{-OAc})(\eta^2\text{-C}_2\text{H}_4)_2]_2$, Rh ₂ (OAc) ₄ and RhCl ₃ · xH ₂ O.....	112
Table 2.2.4. Comparison of amount of soluble Rh material at different time points in the catalysis with 40 psig ethylene (condition: 10 mL benzene, 0.001 mol % Rh complex (relative to benzene) and 240 eq. of Cu(II) (relative to Rh), 150 °C).....	122
Table 3.2.1. Optimization of the rhodium catalyzed aerobic benzene alkenylation using air as oxidant. ^a	182
Table 3.2.2. Product distributions for aerobic benzene alkenylation with ethylene under typical reaction conditions (1).	184
Table 3.2.3. Product distributions for aerobic benzene alkenylation with ethylene under typical reaction conditions (2).	192
Table 4.2.1. Results for Ir-catalyzed oxidative hydrophenylation of propylene under different conditions. The TOs are the average of a minimum of three experiments. Values in parentheses represent the standard deviations based on a minimum of three independent experiments. TOs are obtained by GC-FID.	223
Table 4.2.2. Results for $[\text{Ir}(\mu\text{-Cl})(\text{COE})]_2$ -catalyzed oxidative hydrophenylation of propylene under aerobic conditions using air as in situ terminal oxidant. The TOs are the average of a minimum of three experiments. Values in parentheses represent the standard deviations based on a minimum of three independent experiments. TOs are obtained by GC-FID.....	224
Table 4.2.3. Results for $[\text{Ir}(\mu\text{-Cl})(\text{COE})]_2$ -catalyzed oxidative hydrophenylation of propylene using 1200 eq. Cu(OHex) ₂ (relative to per Ir atom) and 4800 eq. HOHex (relative to per Ir atom). Reaction conditions: 10 mL benzene, 0.0005 mol % $[\text{Ir}(\mu\text{-Cl})(\text{COE})]_2$ (relative to benzene), 30 psig propylene, 165 °C. The TOs are the average of a minimum of three experiments. Values in parentheses represent the standard deviations based on a minimum of three independent experiments. TOs are obtained by GC-FID.....	225
Table 4.2.4. Isomerization of allyl benzene to cis- β -methylstyrene and trans- β -methylstyrene in $[\text{Ir}(\mu\text{-Cl})(\text{COE})]_2$ -catalyzed benzene alkenylation with ethylene. Reaction conditions: 10 mL benzene, 50 eq. allylbenzene (relative to per Ir atom), 1200 eq. Cu(OHex) ₂ (relative to per Ir atom), 4800 eq. HOHex (relative to per Ir atom), 0.0005 mol % $[\text{Ir}(\mu\text{-Cl})(\text{COE})]_2$	

(relative to benzene), 50 psig ethylene, 165 °C, 60 h. The equivalents are the average of a minimum of three experiments. Values in parentheses represent the standard deviations based on a minimum of three independent experiments. TOs are obtained by GC-FID.232

1 Introduction

1.1 Overview of Catalysis

Catalysis is the process of accelerating a chemical reaction by adding a substance which is called a catalyst. The catalyst is not consumed during the reaction and usually only a sub-stoichiometric amount of catalyst is needed to modify the reaction rate. A catalyst increases the rate of a reaction by providing an alternative mechanism with different transition states and lower activation energy than the reaction pathway without the catalyst. The catalyst usually operates by reacting with substances to form a new intermediate(s), which after reaction regenerates the original catalyst and releases product(s) to complete the catalytic cycle. The chemical industries rely heavily on catalysis because it enables highly efficient and selective production of chemicals in an energy-efficient manner. Catalysis contributes to approximately 35% of global GDP.¹

The completion of an entire catalytic cycle with the generation of desired products and recovery of the catalyst is called a turnover (TO). Turnover number (TON) is defined as the number of turnovers that a catalyst can mediate before the catalyst becomes inactivated. TON is an important term to indicate the longevity (or, stability) of the catalyst. Another classical term for quantifying catalytic processes is turnover frequency (TOF), which is the number of turnovers per unit time. TOF is used for representing the catalytic activity, but it is distinct from the classical reaction rate.²

Catalysis using organometallic compounds functions by coordinating substrates to the metallic complex, which leads to a new reaction pathway possessing low activation barrier as in other types of catalysis.³ The development of organometallic catalysis has had a significant impact on small-scale fine chemical synthesis as well as chemical industry.

1.2 Industrial Catalytic Processes

1.2.1 Overview

There are two categories of catalysts in chemical industry, homogeneous and heterogeneous catalysts, depending on whether catalysts react with substrates in the same phase. Homogeneous catalysts operate in the same phase as the substrates, typically in a solvent. Heterogeneous catalysts function in a different phase from the reactants. The majority of heterogeneous catalysts are solid phase catalysts that absorb liquid or gaseous substrates onto their surface. Only specific areas within the surface of heterogeneous catalysts have catalytic activity, called active sites. The reaction rate is dependent on the available active sites. Often, the active sites (usually atoms or crystal faces) are dispersed on another solid material to suppress atom agglomeration and enlarge surface area.

Heterogeneous catalysis offers some advantages compared to homogeneous catalysis such as more facile catalyst/product separation and ease of catalyst recycling.⁴ However, defining the nature of the active site of a heterogeneous catalyst is challenging, which limits the ability to tune catalyst activity and selectivity. Despite

this, heterogeneous catalysts play an important role in chemical industries. Approximately 90% of chemicals (by volume) are produced by heterogeneous catalysts.⁵ Industrial examples of heterogeneous catalysis include Haber–Bosch process, the Ostwald process, the Ziegler–Natta process, methane steam reforming and Fischer-Tropsch catalysis.

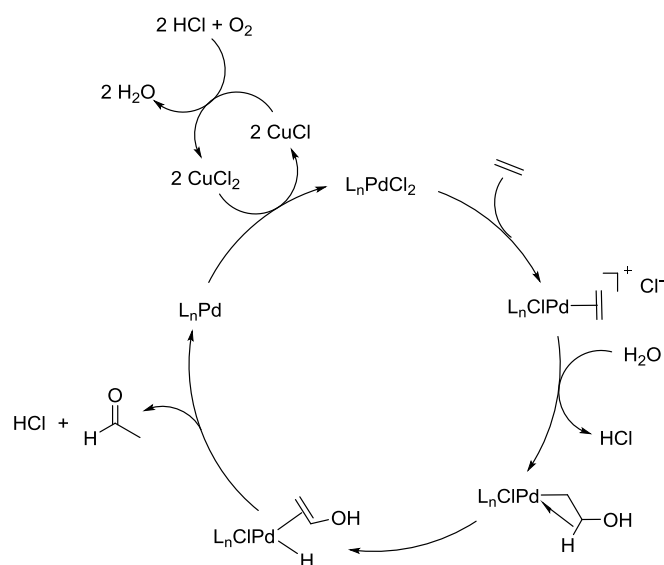
It is common that homogenous catalysts exhibit higher catalytic activity (under comparable conditions) and product selectivity than heterogeneous catalysts.^{6, 7} The techniques and strategies to study the mechanism of homogeneous catalysis and modify catalysts are well developed, which often allows catalysts design and optimization.⁸ While heterogeneous catalysts are responsible for the majority of the current Industrial processes, homogeneous organometallic catalysts are successfully utilized for several important commercialized processes. Some prominent examples are described below.

1.2.2 Industrial Examples of Organometallic Catalysts

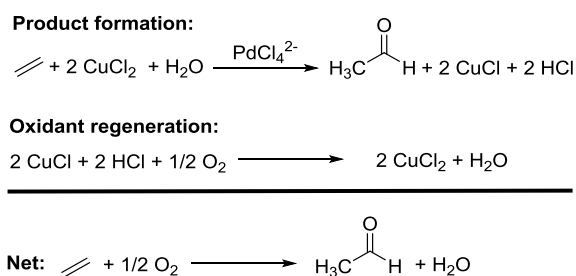
One of the widely-commercialized industrial processes using a molecular homogeneous organometallic catalyst is Wacker Process. This process is developed for the oxidation of ethylene to produce acetaldehyde using PdCl_4^{2-} as the catalyst and CuCl_2 as the *in situ* oxidant. Wacker Process was first studied in the 1950s and was applied on an industrial scale in 1960.⁹ The proposed mechanism is depicted in Scheme 1.2.1.¹⁰ The reaction begins with coordination of the alkene to palladium. Then, nucleophilic attack of H_2O on the coordinated alkene and subsequent β -hydride

elimination takes place to afford an enol complex. Release of HCl and acetaldehyde after rearrangement of enol produces palladium(0), which is then reoxidized to Pd(II) using 2 equivalents of CuCl₂. The resulting CuCl is then reoxidized to CuCl₂ with O₂ and the HCl produced from the reaction. Aerobic regeneration of Cu(II) yields an overall conversion of ethylene and molecular O₂ to acetaldehyde (Scheme 1.2.2).

In the Wacker process, Cu(II) oxidant is regenerated either *in situ* using *purified* O₂ by introducing ethylene and O₂ into a single reactor concurrently (one-stage process) or in a separate reactor using air (two-stage process).¹¹ The two-stage process requires additional oxidation reactor whereas the one-stage process requires the use of purified O₂. Therefore, the two processes are cost-competitive with one another.¹¹



Scheme 1.2.1. Catalytic Cycle for Wacker process.

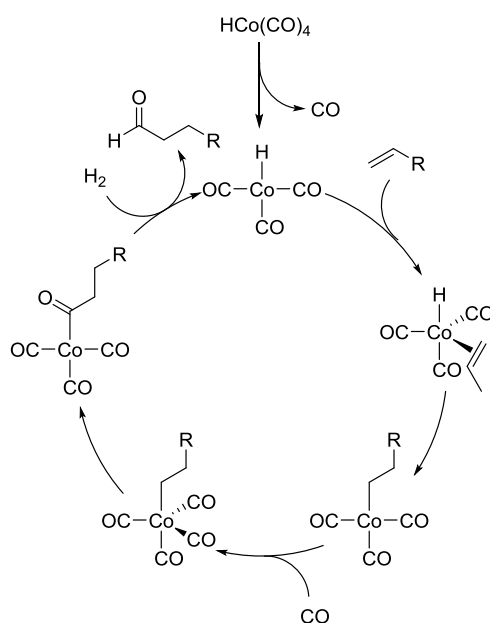


Scheme 1.2.2. Equations for Wacker process and overall balanced reaction (bottom).

Olefin hydroformylation is one of the important achievements of current industrial chemistry. This process produces aldehydes via addition of CO and H₂ (synthesis gas) to an alkene in the presence, typically, of homogeneous Rh or Co catalysts. In 1938, Otto Roelen first discovered the hydroformylation process using HCo(CO)₄ as the catalyst.¹² The mechanism of Co-catalyzed hydroformylation was elucidated by Heck and Breslow (Scheme 1.2.3).¹³ The process is initiated with dissociation of CO from HCo(CO)₄ to afford the 16-electron square planar intermediate HCo(CO)₃. Subsequent olefin coordination and insertion into the Co–H bond gives RCH₂CH₂Co(CO)₄ intermediate where R is derived from the olefin. Binding of another equivalent of CO and migratory insertion of CO into the Co-alkyl bond gives the {RCH₂CH₂C(O)}Co(CO)₃. Oxidative addition of dihydrogen and reductive elimination releases aldehyde product and regenerates the active HCo(CO)₃ catalyst. Large industrial hydroformylation processes based on cobalt catalysts have been developed by BASF, ExxonMobil and Shell.^{14, 15}

Although cobalt catalysts are broadly applied for olefin hydroformylation due to their low cost, they usually exhibit low catalytic activity. In addition, cobalt catalysts exhibit moderate selectivity toward desired linear aldehyde products when they are used for the hydroformylation of α -olefins such as propene.¹⁶ The development of highly active rhodium-based catalysts overcame the drawbacks of cobalt catalysts. Currently, most commercial hydroformylation processes are based on rhodium.¹⁷ Typically, Rh catalysts are 100-1000 more active than Co catalysts.^{18, 19} Therefore, Rh-based hydroformylation is more economical although the expense of Rh metal is

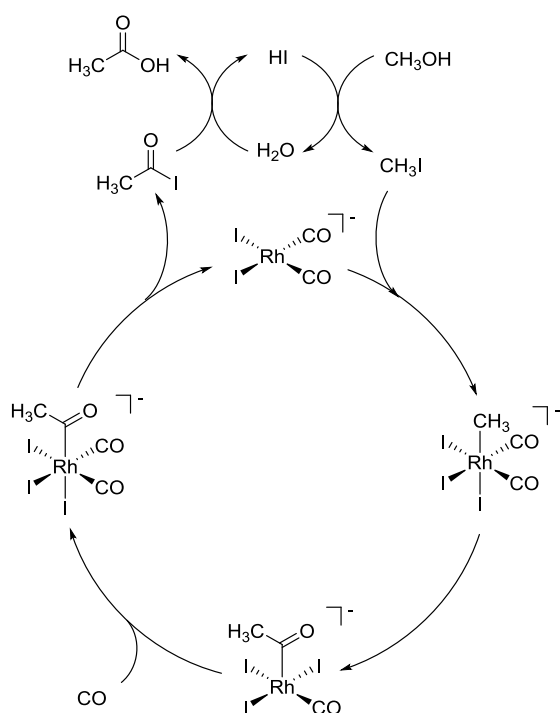
higher than Co. Given the large difference in the price of Rh and Co, it is perhaps surprising that Rh processes can compete. But, methods for efficient recycling of Rh have been developed. Therefore, the expense of Rh represents an initial capital investment, that is readily amortized, rather than an ongoing operating expense.



Scheme 1.2.3. Catalytic cycle for Co-catalyzed hydroformylation.

Another industrial process using an organometallic catalyst is the Monsanto acetic acid process. This process converts methanol, which can be produced from synthesis gas (a fuel gas mixture containing CO and H_2), and carbon monoxide to afford acetic acid in the presence of a Rh(I) pre-catalyst and methyl iodide. This process was first developed by the Monsanto Company in late 1960s.^{20, 21} This process can achieve $> 99\%$ selectivity based on methanol and operates under mild conditions (at 30–60 atm pressure and 150–200 °C).^{20, 21} The mechanism of the Monsanto process involves two catalytic cycles (Scheme 1.2.4).²² The first catalytic cycle starts with the oxidative addition of methyl iodide to $[\text{Rh}(\text{CO})_2\text{I}_2]^-$ to form $[\text{Rh}(\text{I})_3(\text{CO})_2(\text{Me})]^-$. Migratory insertion of carbon monoxide into the Rh–Me bond

and subsequent coordination of another equivalent of carbon monoxide affords an acetyl complex $[\{\text{CH}_3\text{C}(\text{O})\}\text{Rh}(\text{CO})_2\text{I}_3]^-$. The final step is reductive elimination to form acetyl iodide and regenerate the Rh catalyst. In the second catalytic cycle, acetyl iodide is hydrolyzed to form acetic acid product and HI. HI can then react with MeOH to form MeI which is involved in the oxidative addition step in the first cycle.



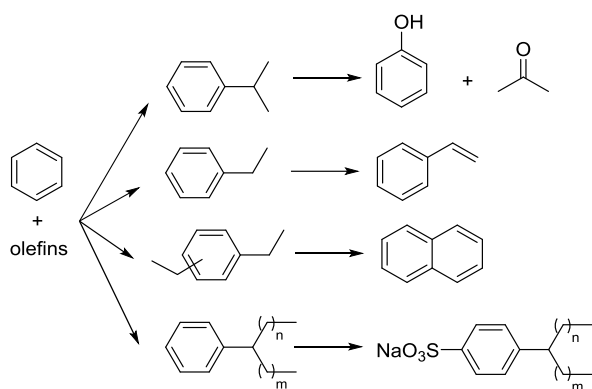
Scheme 1.2.4. Catalytic Cycle for Monsanto acetic acid process

In the late 1990s, British Petroleum (BP) Chemicals developed the Cativa Process as an alternative for the Monsanto process.²¹ The Cativa process uses an iridium-containing catalyst, and its mechanism is similar to the Monsanto process. The initial challenge of the Cativa process is that the Ir catalysts had slower reaction rates than Rh catalysts. Mechanistic studies revealed an inverse dependence on ionic iodide concentration and high reaction rates should be practicable at low iodide concentrations.²³ Therefore, to improve Ir catalyst reactivity, ruthenium additives

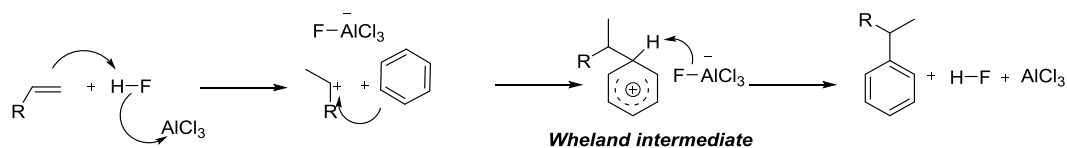
were introduced as promoters to assist in removing iodide and enable the catalysis to proceed at low iodide concentrations.²³ The iridium-based Cativa process requires less water compared to the rhodium-based Monsanto process, which reduces the number of drying columns and inhibits formation of undesired by-products through suppression of the water gas shift reaction.²¹

1.2.3 Alkyl Arenes and Friedel-Crafts Catalysis

Alkyl arenes are used as precursors for a range of products, including plastics, elastomers, pharmaceuticals and fine chemicals (Scheme 1.2.5).²⁴⁻²⁷ For example, ethylbenzene is produced on a scale of ~40 million tons annually.²⁸ More than 98% of ethylbenzene is converted to styrene, the raw material for making polystyrene plastic.²⁹⁻³¹ Another important alkyl benzene, cumene, serves as a precursor for the synthesis of phenol and acetone, which are widely-used industrial chemicals.³² In industry, alkyl arenes are produced on a large scale from benzene and olefin using acid-based catalysis for arene alkylation such as Brønsted acid-based or zeolite-based catalysts.^{24-27, 31, 33, 34} The mechanism for representative Friedel-Crafts alkylation of benzene catalyzed by HF and AlCl₃ is shown in Scheme 1.2.6. HF reacts with AlCl₃ to liberate a proton for addition to the alkene to generate an electrophilic carbocation intermediate that undergoes electrophilic attack to benzene to form a Wheland intermediate. Finally, deprotonation of the Wheland intermediate with the conjugate base produces alkyl benzene and regenerates the catalyst.



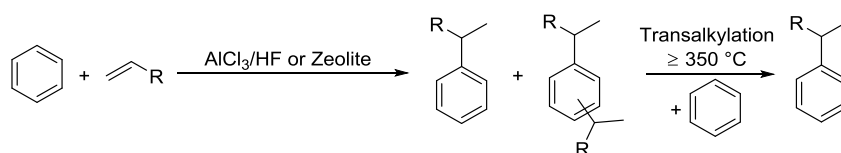
Scheme 1.2.5. Alkyl arenes and their derivatives.



Scheme 1.2.6. Mechanism for acid catalyzed benzene alkylation.

The drawbacks of Friedel-Crafts catalysis include: 1) incorporation of corrosive and environmentally harmful acids (e.g. HCl or HF), 2) required neutralization of product mixtures, which results in decomposition of AlCl_3 and the stoichiometric generation of generation of halogenated waste. Therefore, the inability to recycle the catalyst, production of substantial halogenated waste and requirement of corrosion resistant reactors increases the expense of this process.^{29, 33} In order to overcome some of the deficiencies of traditional Friedel-Crafts catalysis, heterogeneous catalysts, zeolites, have been developed since the 1980s.³³ Zeolites are microporous aluminosilicate minerals that function as acid.^{25, 35} The overall acidity of zeolites can be modulated by adjusting aluminum content.³⁵ Zeolites can maintains activity for up to 3 years without catalyst regeneration.³³ Another advantage of zeolite catalyst compared to the Friedel-Crafts catalysis is the absence of salt waste.

Although zeolite catalysts improved certain aspects of conventional Friedel-Crafts catalysts, they do not represent a fundamental change in the mechanism of alkylation. These acid-catalyzed methods for arene alkylation have limitations that are inherent to the mechanism. For example, given that the reaction operates via electrophilic aromatic substitution, the alkylated arene is more electron-rich and, thus, is more reactive than starting arene, which results in the production of undesired polyalkylated arenes.³⁶ Therefore, additional distillation and an energy-consuming trans-alkylation process are needed in industry to increase the yield of monoalkylated product (Scheme 1.2.7).^{31, 33, 34} Shape- and size-selective zeolite catalysts are able to reduce the production of polyalkylated benzenes by tuning their pore sizes to bias regioselectivity toward monoalkyl benzenes production.²⁵ However, the transalkylation step is not avoided.^{25, 29}

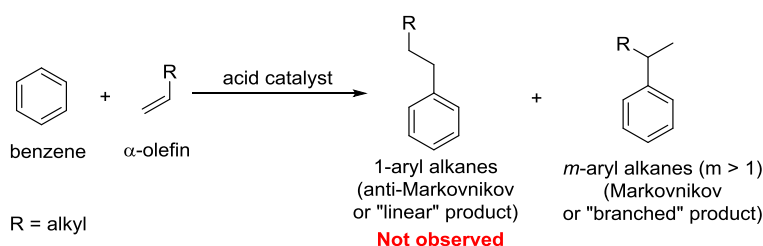


Scheme 1.2.7. Current method for the industrial production of alkyl benzenes.

Acid-catalyzed arene alkylation is limited by its reaction scope. This process is not effective for electron-deficient arenes.³⁶ For example, chlorobenzene reacts approximately 10-fold more slowly than benzene and nitrobenzene is inert toward acid-catalyzed alkylation.^{37, 38}

Another disadvantage of acid-catalyzed arene alkylation includes the inability to produce straight-chain 1-aryl alkanes (i.e., anti-Markovnikov products or linear products) when using α -olefins (Scheme 1.2.8). This is due to the formation of more

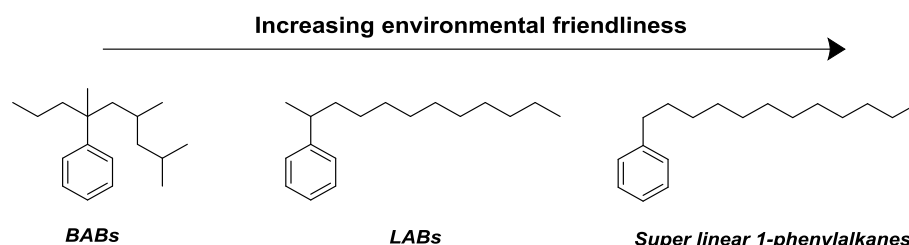
stable secondary versus primary carbocation intermediate, which results in exclusive formation of Markovnikov products or branched products, *m*-aryl alkanes ($m > 1$).²⁵



Scheme 1.2.8. Product selectivity from acid catalyzed benzene alkylation using α -olefins

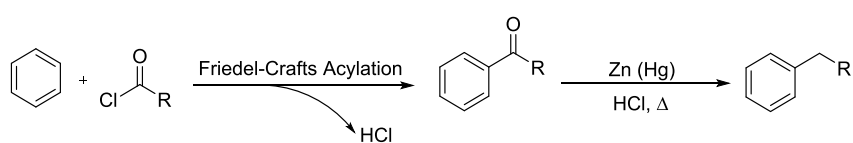
Long chain alkylbenzenes are produced via acid-catalyzed arene alkylation for subsequent sulfonation to make alkylbenzene sulfonates (Scheme 1.2.5), which widely-used starting materials for surfactants. Branched alkylbenzene sulfonates (BASs), which are made from branched alkylbenzenes (BABs, Scheme 1.2.9), were first used as the active components in detergents. However, due to its highly branched alkyl chain, BASs are difficult to biodegrade and caused pollution of lakes and streams.^{39, 40} In the 1960s, linear alkylbenzene sulfonates (LASs) were introduced to supplant BASs. LASs are produced from linear alkylbenzenes (LABs, Scheme 1.2.9) and are typically consist of 2- and 3-phenyl substituted alkyl chains. Compared to the highly branched BABs, LABs are more readily biodegraded.^{39, 40} Current methods for the large-scale production of LABs involve acid-catalyzed benzene alkylation with linear long chain monoalkenes (*e.g.* dodecene). However, these acid-catalyzed reactions are not able to produce 1-phenylalkanes, which our group has called "super linear alkyl benzenes" (SLABs) to differentiate them from LABs (Scheme 1.2.9). Since they cannot be produced with existing catalyst technologies, 1-phenylalkanes

are potential new precursors for soaps and detergents as well as other applications (e.g., deep oil recovery) that could offer improved biodegradability, increased deterative power and enhanced thermal stability.⁴¹



Scheme 1.2.9. Comparison of branched alkylbenzenes, linear alkylbenzenes and super linear alkyl benzenes.

Currently, the preparation of 1-aryl alkanes involves Friedel-Crafts acylation followed by a Clemmensen reduction (Scheme 1.2.10), which is not viable for large-scale production due to the relatively high expense of the substrates. Therefore, the development of processes for the synthesis of 1-phenylalkanes or, more generally, 1-aryl alkanes, that operate by a different mechanism offers potential benefits and opportunities.

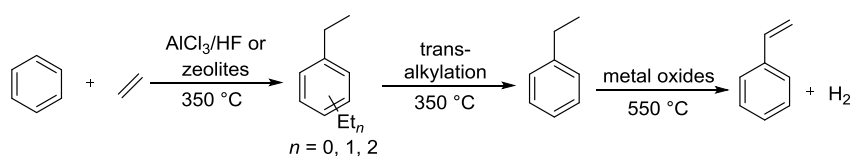


Scheme 1.2.10. Current method for the synthesis of 1-aryl alkanes

1.2.4 Alkenyl arenes and Current Industrial Processes

Alkenyl arenes are important commodity chemicals and are produced on a large scale worldwide.²⁴⁻²⁷ Generally, acid-based catalytic processes generate saturated alkyl arene products and cannot be used to directly synthesize alkenyl arenes. For example, styrene was produced globally on a scale of ~38 million tons in 2018.^{28, 31, 33,}

³⁴ The current method for the industrial production of styrene involves 1) Friedel-Crafts or zeolite-catalyzed benzene ethylation to generate ethylbenzene and polyethylbenzenes; 2) Transalkylation to convert poly-ethylbenzene products and benzene to ethylbenzene; and 3) Dehydrogenation of ethylbenzene to form styrene (Scheme 1.2.11).^{29, 33, 34} The dehydrogenation reaction is reversible and highly endothermic. This process usually proceeds at high temperature (up to 600 °C) by flowing ethylbenzene steam over an iron(III) oxide catalyst.⁴² After the dehydrogenation process, distillation is needed to separate styrene from ethylbenzene since high conversions are not possible. Since the difference in boiling points between the styrene (145 °C) and ethylbenzene (136 °C) is small under ambient pressure, multiple distillation columns are required. Therefore, styrene production method requires multiple steps and consumes substantial energy.

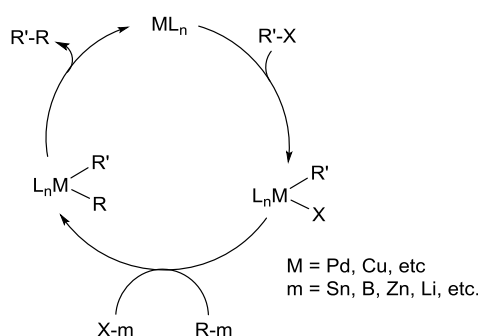


Scheme 1.2.11. Current method for the industrial production of styrene

1.3 C–C Coupling Reactions via C–X Activation

Catalysts that mediate the formation of C–C bonds are of substantial value in both largescale commodity and fine chemical processes. Transition metal-mediated Heck, Stille, Suzuki, Negishi and related cross-coupling reactions are widely studied and used methods to construct new C–C bonds.⁴³⁻⁵² The transformations usually involve the reaction of an organometallic reagent R–M (R = organic fragment, M = main group metal in most cases) with an organic electrophile R'–X (R' = organic fragment,

X = halogen in most cases) in the presence of a late transition metal catalyst to achieve a C–C bond formation and the product R-R'. The proposed generic reaction mechanism for this type of reaction is shown in Scheme 1.3.1. The oxidative addition of an organic electrophile R'-X to L_nM yields $L_nMX(R')$, followed by a transmetallation step to transfer R fragment from organometallic reagent to $L_nMX(R')$ with the formation of $L_nM(R)(R')$. Finally, reductive elimination of the two organic ligands R and R' takes place to regenerate the catalyst and give the coupling product. Cross-coupling reactions have been used in numerous synthetic applications ranging from polymers to pharmaceuticals.^{53, 54}



Scheme 1.3.1. Catalytic cycle for late transition metal catalyzed cross-coupling reactions

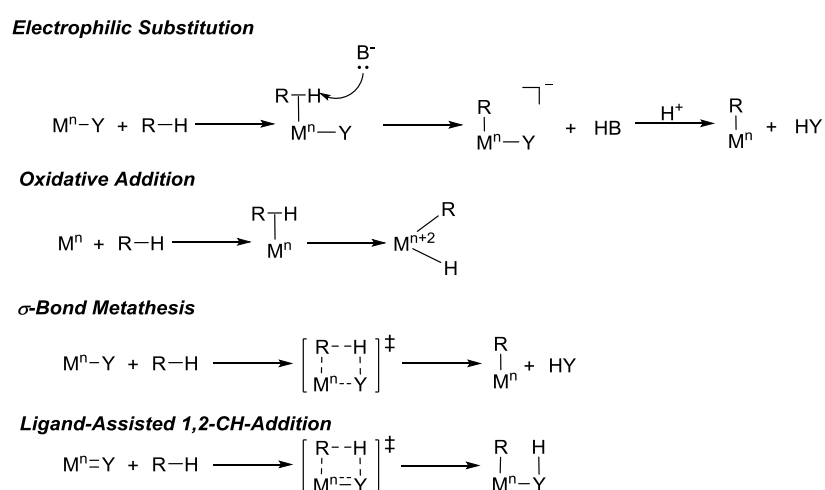
The classic cross coupling reactions typically require the use of “activated” aryl halides or pseudohalides (such as triflate) as aromatic substrates, which leads to the generation of stoichiometric amounts of halogenated byproducts. In addition, most variations of these coupling reactions incorporate a stoichiometric amount of a second organometallic reagent. While high-value and low-volume commercial processes have made use of these cross coupling catalytic processes, the commercialization of these reactions on a large scale has been hindered by the high cost of the halogenated

aromatic starting compounds, the generation of halogenated waste, the stoichiometric use of metal-containing reagents, and noble metal catalysts.

1.4 C–C Coupling Reactions Based on C–H Activation

1.4.1 Mechanisms for C–H Activation

The incorporation of two-electron cleavage of C–H bonds into C–C coupling reactions circumvent some of the deficiencies of C–C coupling reactions via C–X bond activation. However, direct activation of strong C–H bonds is challenging due to the large bond dissociation energies and the non-polar nature of most C–H bonds. But, transition metal-mediated C–H bond activation has been developed and incorporated into catalytic hydrocarbon functionalization reactions. Different from traditional one-electron homolytic cleavage of C–H bonds, transition metals often selectively activate stronger C–H bonds over weaker ones via even-electron reactions. There are four general categories of C–H activation mechanisms (Scheme 1.4.1):



Scheme 1.4.1. Categories of transition metal-mediated C–H bond activation.

Electrophilic substitution is a common category of metal-mediated C–H bond activation. A C–H bond initially coordinates to an electrophilic metal center (Scheme 1.4.1). Then, the resulting C–H bond, with enhanced acidity due to metal-coordination, is deprotonated by an internal or external base to form a new M–C bond.⁵⁵ The Shilov catalytic system for methane partial oxidation to methanol using $[\text{PtCl}_4]^{2-}$ catalyst is a representative example of this method.⁵⁶

C–H activation via oxidative addition is usually achieved by low-valent and electron-rich transition metal complexes. The metal center inserts into the C–H by contributing two *d* electrons to form M–C and M–H bonds (Scheme 1.4.1).⁵⁷ Overall, the metal center is formally oxidized by two electrons.

The σ -bond metathesis reaction proceeds through a concerted process in which M–C and C–H bonds are cleaved and formed in a single step. A hydrogen atom is transferred from a C–H bond to a ligand on the metal center, which forms a new M–C bond and ligand–H species (Scheme 1.4.1). A four-centered/four-electron transition state is proposed (Scheme 1.4.1).^{58,59} Since there is no net change of metal oxidation state during C–H activation by σ -bond metathesis, the mechanism is accessible for complexes of high-valent early transition metals with d^0 configurations such as Lu(III) and Zr(IV) complexes.⁵⁸

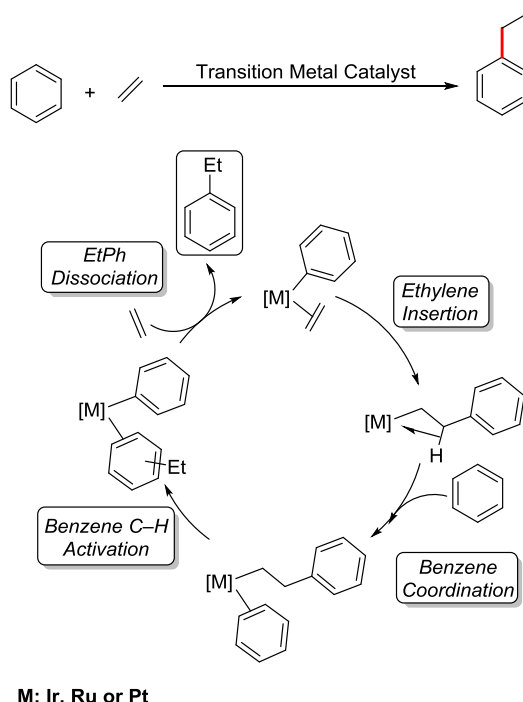
Another mechanism for C–H activation is 1,2-addition of C–H bonds across metal–heteroatom bonds. Coordination of a C–H bond to a M–X (e.g., X = O, OR, NR or NHR) complex polarizes the C–H bond (Scheme 1.4.1). The acidic C–H bond is then deprotonated by the basic ligand X with the formation of M–XH and a new M–C

bond (Scheme 1.4.1). This mechanism can be viewed as internal electrophilic substitution, since the base is a ligand in the inner coordination sphere of the metal.⁶⁰ The 1,2-CH-addition of hydrocarbons across d^0 early transition metal, and d^6 and d^8 later transition metal have been reported.^{57, 61}

1.4.2 Transition Metal-Catalyzed Olefin Hydroarylation

1.4.2.1 Overview

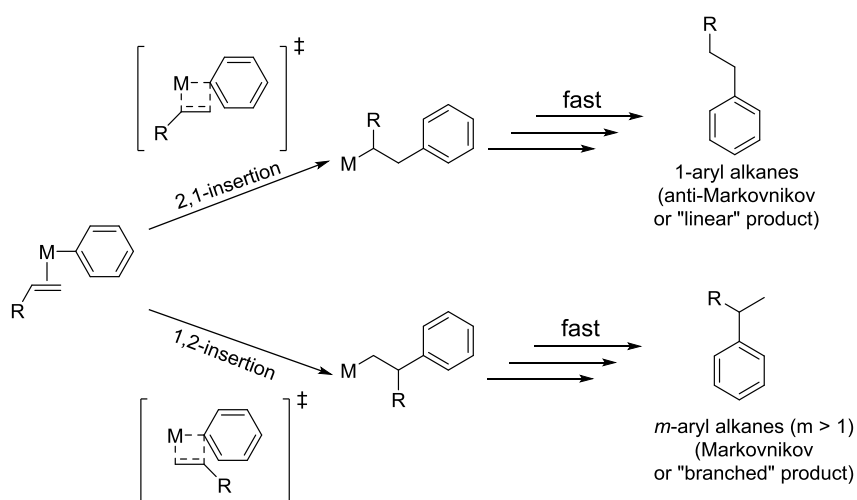
Transition metal-mediated arene alkylation using simple unactivated olefins and unfunctionalized arene substrates that function by a mechanism incorporating arene C–H activation and olefin insertion provides possible advantages over the traditional acid-based catalysis and as well as C–C cross coupling reactions via C–X bond activation. A generalized reaction pathway for arene alkylation is shown in Scheme 1.4.2, and potential advantages include: a) possible selective production of super linear 1-aryl alkane by circumventing carbocationic intermediates, b) potential tolerance of electron-deficient arenes, c) new regioselectivity for alkylation of substituted arenes due to sterically controlled metal-mediated C–H activation mechanism, and d) possible inhibition of polyalkylation since monoalkyl arene products can potentially have similar or decreased reactivity to arene substrates.



Scheme 1.4.2. Generic catalytic cycle for transition metal-catalyzed ethylene hydrophenylation.

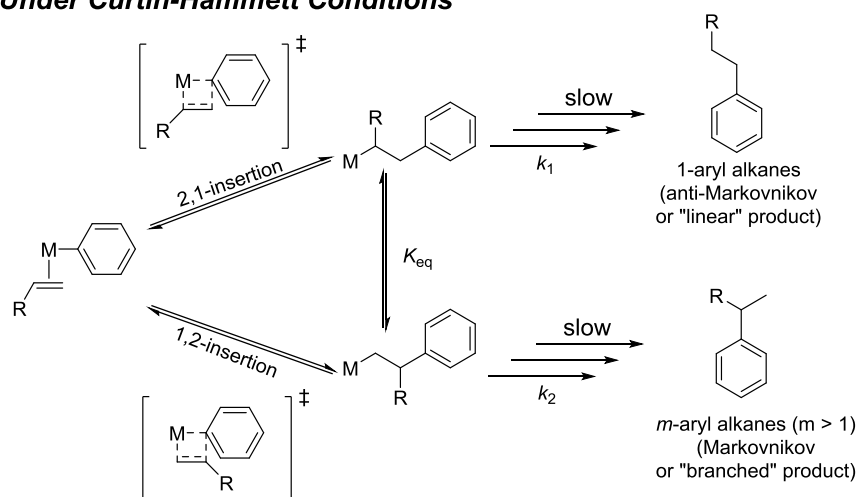
Olefin hydroarylation catalyzed by molecular Ir,⁶²⁻⁶⁷ Ru⁶⁸⁻⁷⁵ or Pt⁷⁶⁻⁸⁴ complexes has been demonstrated for benzene alkylation. The Ir and Ru transition metal catalysts can produce 1-aryl alkanes (i.e., anti-Markovnikov addition product) from α -olefins and arenes. The selectivity between anti-Markovnikov (herein, called linear) and Markovnikov (herein, called branched) products is determined by the mode of olefin insertion and, under Curtin–Hammett conditions, the equilibrium between insertion products and relative rates of product formation after olefin insertion step (Scheme 1.4.3). For example, if the olefin insertion is an irreversible step or rate-limiting step, the linear:branched selectivity is controlled by the relative rate of 2,1-insertion versus 1,2-insertion. In contrast, if the olefin insertion is reversible and the rate of interconversion between two metal-alkyl intermediates formed after olefin insertion is much faster than following steps (i.e., Curtin-Hammett kinetic conditions), the

product ratio is dictated by the equilibrium constant K_{eq} between two insertion products and the rate constants (k_1 and k_2) for the subsequent reactions. In contrast, traditional acid-mediated catalysis exclusively produces m -aryl alkanes ($m \geq 2$, i.e., the Markovnikov addition products).



Anti-Markovnikov and Markovnikov products selectivity is dictated by the olefin insertion step

Under Curtin-Hammett Conditions



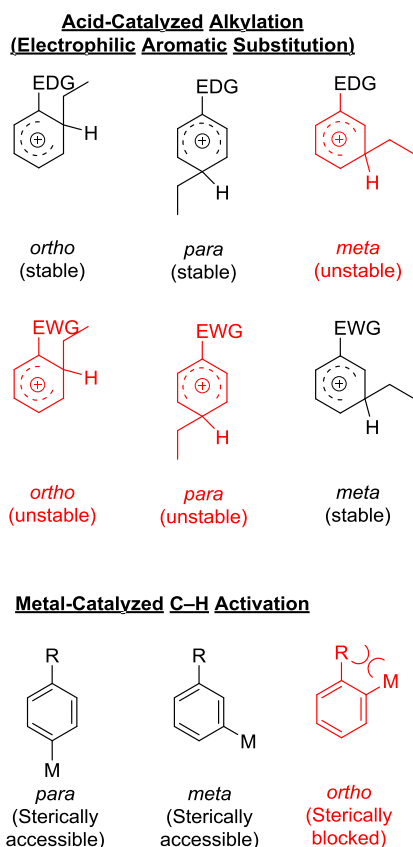
Anti-Markovnikov and Markovnikov products selectivity is dictated by the rates of reactions after olefin insertion

Scheme 1.4.3. Anti-Markovnikov and Markovnikov products selectivity is dictated by the olefin insertion step (top) and, depending on details, the rates of subsequent

reactions (e.g., under Curtin-Hammett conditions) (bottom).

Product distributions from Ir, Ru or Pt-catalyzed olefin hydroarylation using substituted benzenes demonstrate that the functionalization occurs at the sterically more accessible *meta*- and *para*- positions over the *ortho*- position (Scheme 1.4.4).³⁷

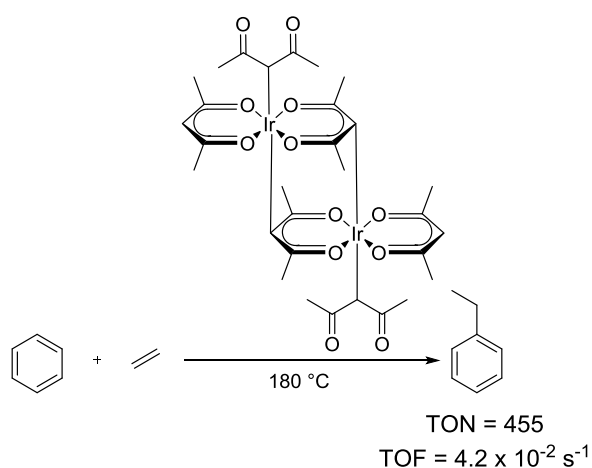
³⁸ In contrast, due to the electrophilic aromatic substitution mechanism, Friedel–Crafts catalysis with electron-rich arenes show selectivity for *ortho*- and *para*- alkylated products, and catalysis with electron-deficient arenes is selective for *meta* products (Scheme 1.4.4).



Scheme 1.4.4. Explanations for distinct *meta/para/ortho* selectivity of acid-catalyzed arene alkylation and metal-catalyzed C–H activation.

1.4.2.2 Iridium(III) Catalysts

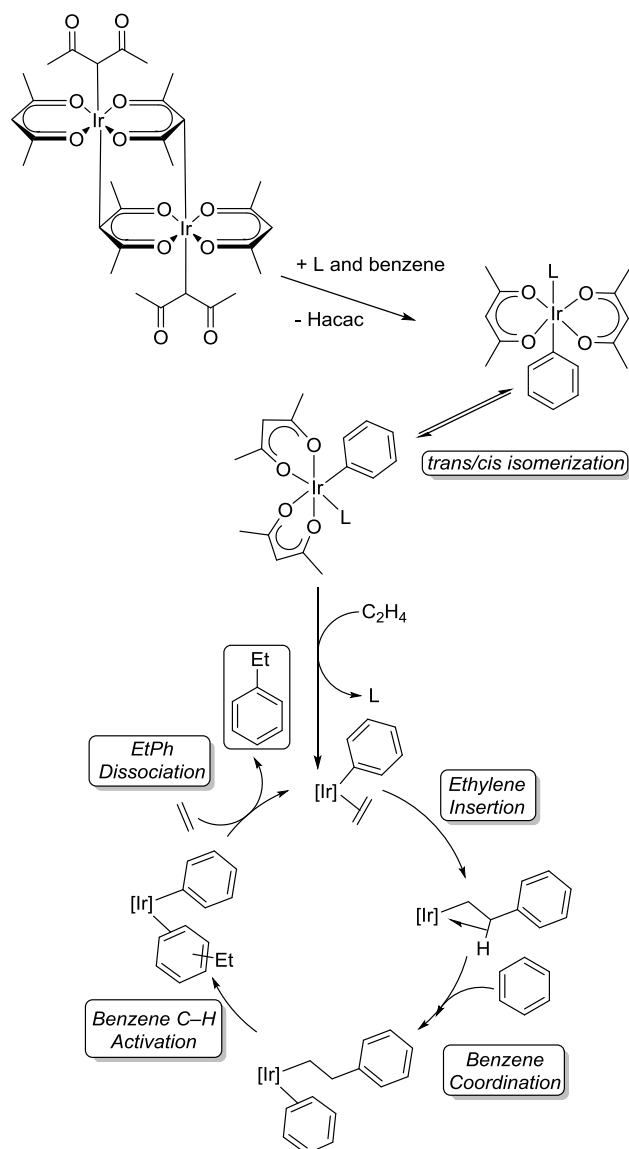
Periana, Goddard and coworkers reported the conversion of olefin and benzene to alkyl benzene catalyzed by Ir^{III}(acac)₂ complexes (acac = acetylacetonate) (Scheme 2).⁶²⁻⁶⁶ Initial studies showed that ethylene hydrophenylation using [Ir(μ-acac-O,O,C³)-(acac-O,O)-(acac-C³)₂] as the catalyst precursor at 180 °C affords 455 TONs after 3 hours with a TOF of 4.2 x 10⁻² s⁻¹ (Scheme 1.4.5).⁶² The binuclear Ir^{III}(acac)₂ catalyst selectively produces linear 1-aryl propane with ~1.6:1 ratio of linear to branched products when propylene and benzene are reactants. Benzene alkylation with 1-hexene gave 1-aryl hexane and 2-aryl hexane with 2.2:1 L/B ratio and no 3-aryl hexane was observed. Reaction with ethylene in toluene gave an *ortho:meta:para* (*o:m:p*) ratio of 0:63:37. The L/B and *o:m:p* selectivity of the Ir catalyst indicates the production of alkyl benzenes proceeds through a non-acidic pathway.



Scheme 1.4.5. Ethylene hydrophenylation using [Ir(μ-acac-O,O,C³)-(acac-O,O)-(acac-C³)₂] as a catalyst precursor.

The active catalyst is proposed to be a mononuclear 16-electron Ir(acac-O,O)₂Ph(L)

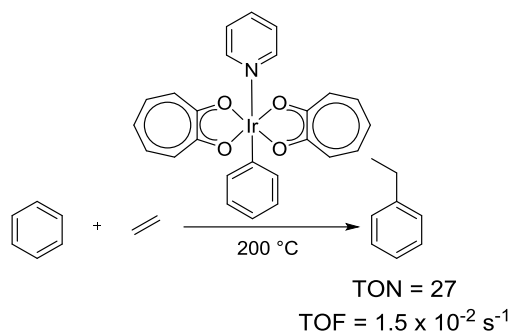
(L = acac, H₂O or pyridine) species, which is formed by break-up of the binuclear [Ir(μ -acac-O,O,C³)-(acac-O,O)-(acac-C³)]₂ and subsequent benzene C–H activation.⁶³ The complex *trans*-(acac-O,O)₂Ir(Ph)(pyridine) was detected by NMR analysis of crude reaction mixtures and independently synthesized.⁶³ Based on experimental studies and computational calculations, a plausible mechanistic pathway was proposed (Scheme 1.4.6).^{63, 65, 66} The catalyst precursor, *trans*-(acac-O,O)₂Ir(Ph)(L), undergoes *trans* to *cis* isomerization (orientation of Ph and L) to form *cis*-(acac-O,O)₂Ir(Ph)(L). Subsequently, the olefin substitutes for L and inserts into the iridium phenyl bond. The final step is C–H bond activation of benzene through a oxidative hydrogen migration transition state to regenerate *cis*-(acac-O,O)₂Ir(Ph)(L) intermediate with the liberation of alkyl benzene products. Computational studies suggest that olefin insertion is the rate-determining step with H^\ddagger calculated to be 25.2 kcal/mol at 0 K.⁶⁶



Scheme 1.4.6. Proposed mechanism for ethylene hydrophenylation using $[\text{Ir}(\mu\text{-acac-O,O,C}_3\text{)}(\text{acac-O,O})(\text{acac-C}_3)]_2$ as a catalyst precursor

In addition to $\text{Ir}(\text{acac-O,O})_2\text{Ph(L)}$, $\text{Ir}(\text{trop-O,O})_2\text{Ph(Py)}$ ($\text{trop-O,O} = \kappa^2\text{-O,O-tropolonato}$, $\text{py} = \text{pyridine}$) serves as an active catalyst for hydrophenylation of ethylene and propylene.⁶⁷ Relative to acac-O,O ligand, the trop-O,O ligand is less electron donating and possesses a smaller bite angle (five-membered chelate ring size vs. six-membered chelate ring size for acac). The reaction with propylene in benzene using $\text{Ir}(\text{trop-O,O})_2\text{Ph(Py)}$ ($\text{Py} = \text{pyridine}$) complex produces *n*-propylbenzene and

isopropylbenzene in 61:39 ratio, showing anti-Markovnikov regioselectivity that is nearly identical to the acac Ir complex. The catalysis with ethylene resulted in 27 TONs of ethylbenzene after 30 min, corresponding to an apparent TOF of $1.5 \times 10^{-2} \text{ s}^{-1}$ at $200 \text{ }^\circ\text{C}$ (Scheme 1.4.7). The Ir(trop-O,O)₂Ph(Py) complex has lower catalytic olefin hydrophenylation rate but higher benzene C–H activation rate than the acac-O,O analogue. Calculations predict that Ir(trop-O,O)₂Ph(Py) has higher activation barrier for rate-limiting olefin insertion than the acac-O,O system.⁶⁷

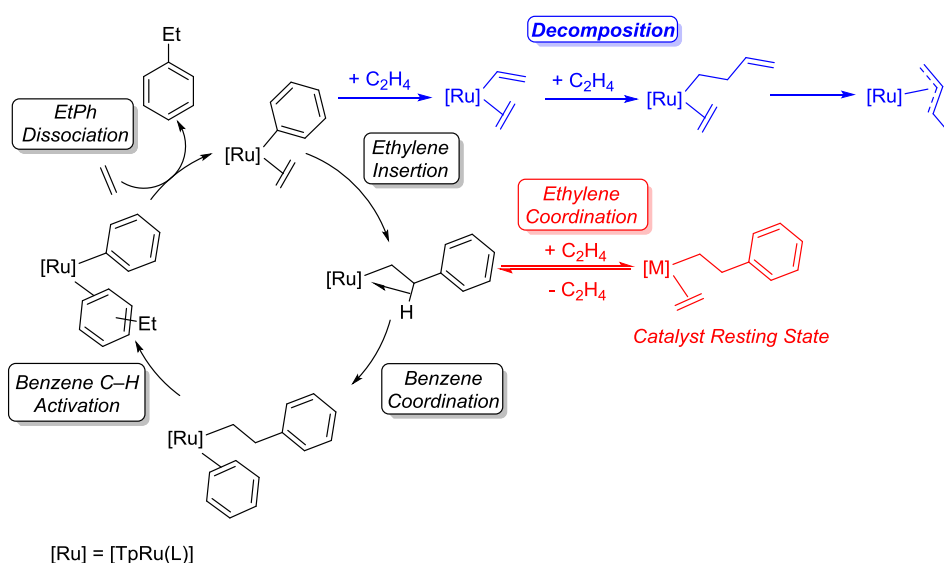


Scheme 1.4.7. Ethylene hydrophenylation catalyzed by Ir(trop-O,O)₂Ph(Py).

1.4.2.3 Ruthenium(II) Catalysts

The Gunnoe group has reported a series of ruthenium complexes, TpRu(L)(NCMe)Ph (Tp = hydridotris(pyrazolyl)borate, L = CO, PMe₃, P(OCH₂)₃CEt, P(pyr)₃, P(OCH₂)₂(OCCH₃); pyr = *N*-pyrrolyl) as catalysts for olefin hydroarylation.^{68-73, 85} The proposed catalytic cycle for all TpRu(L)(NCMe)Ph catalysts in Scheme 1.4.8 includes: 1) substitution of a labile acetonitrile ligand with ethylene, 2) ethylene insertion into the Ru–Ph bond to form Ru(CH₂CH₂Ph) species, 3) benzene coordination and C–H activation to produce Ru–Ph intermediate with coordinated ethylbenzene, and 4) displacement of ethylbenzene with ethylene to

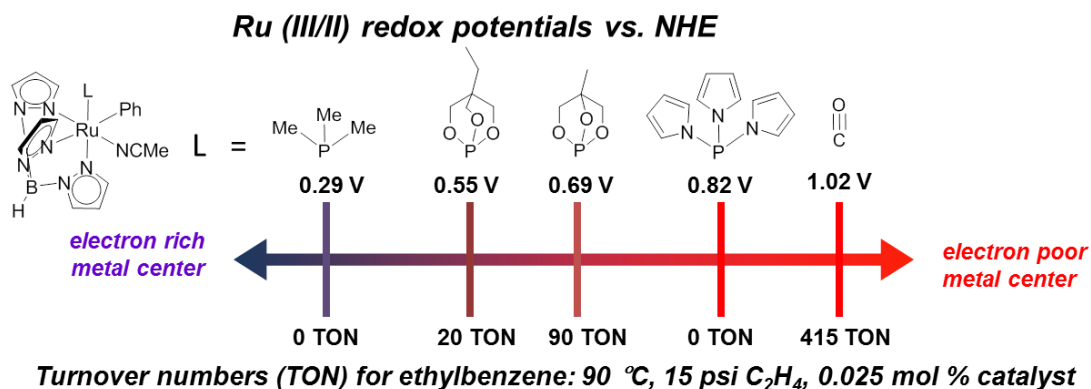
regenerate the catalyst.⁷⁵ The proposed catalyst resting states are $\text{TpRu(L)(CH}_2\text{CH}_2\text{Ph)(}\eta^2\text{-C}_2\text{H}_4\text{)}$, which need to liberate ethylene before re-entering the catalytic cycle (Scheme 1.4.8).⁷⁵ Catalytic hydrophenylation of ethylene using TpRu(CO)(NCMe)Ph in a 1:1 molar mixture of C_6H_6 and C_6D_6 reveals an intermolecular kinetic isotope effect of $k_{\text{H}}/k_{\text{D}} = 2.1(1)$, consistent with a rate-limiting benzene C–H activation step.⁶⁹ All TpRu(L)(NCMe)Ph catalysts show an inverse dependence of the rate of catalysis on ethylene concentration, which is in agreement with ethylene removing the active catalyst from the catalytic cycle to form the proposed catalyst resting states.⁷⁵



Scheme 1.4.8. Catalytic cycle for hydrophenylation of ethylene catalyzed by TpRu(L)(NCMe)Ph complexes and side reactions

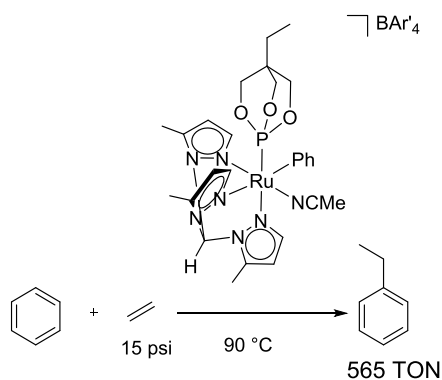
Reversible Ru(III/II) potentials from cyclic voltammetry were used to estimate the relative electron density for the series of TpRu(L)(NCMe)Ph complexes. These data allowed us to determine the impact of metal electron density on stoichiometric benzene C–H(D) activation, catalyst activity and catalyst longevity. The relative electron densities of the TpRu(L)(NCMe)Ph complexes are $\text{PMe}_3 > \text{P(OCH}_2\text{)}_3\text{CEt} >$

$\text{P}(\text{OCH}_2)_2(\text{OCCH}_3) > \text{P}(\text{pyr})_3 > \text{CO}$ (Scheme 1.4.9).⁷⁵ For stoichiometric reactions of $\text{TpRu}(\text{L})(\text{NCMe})\text{Ph}$ and C_6D_6 to produce $\text{TpRu}(\text{L})(\text{NCMe})\text{Ph-}d_5$ and $\text{C}_6\text{H}_5\text{D}$, increased donor ability of L leads to more rapid C–D activation of C_6D_6 .⁷⁵ In contrast with the trend for C–D activation rate, for catalytic ethylene hydroarylation, less electron-rich $\text{TpRu}(\text{CO})(\text{NCMe})\text{Ph}$ complexes show higher TOFs and TONs (Scheme 1.4.9).⁷⁵ Based on the experimental and computational data, more electron-rich Ru complexes have a larger activation barrier for olefin insertion. Meanwhile, an off-cycle ethylene C–H activation pathway becomes more competitive as L becomes more electron-donating. Ethylene C–H activation by $\text{TpRu}(\text{L})(\text{Ph})(\eta^2\text{-C}_2\text{H}_4)$ eventually results in the irreversible decomposition to inactive $\text{TpRu}(\text{L})(\eta^3\text{-C}_3\text{H}_4\text{Me})$ complexes as observed by ^1H NMR spectroscopy (Scheme 1.4.8). Therefore, less electron-rich Ru(II) metal centers enhance catalyst performance by suppressing the catalyst deactivation pathway. $\text{TpRu}[\text{P}(\text{pyr})_3](\text{NCMe})\text{Ph}$ possesses moderate Ru(III/II) potentials. However, olefin hydroarylation using $\text{TpRu}[\text{P}(\text{pyr})_3](\text{NCMe})\text{Ph}$ is inactive likely due to the steric bulk of the $\text{P}(\text{pyr})_3$ ligand, which suppresses olefin coordination and insertion.⁷⁰ $\text{P}(\text{pyr})_3$ possesses the largest cone angle (145 °) among the other ligands (CO 95 °, PMe_3 118 °, $\text{P}(\text{OCH}_2)_3\text{CEt}$ 101 °).⁷⁰



Scheme 1.4.9. Correlation of Ru(III/II) redox potential of TpRu(L)(NCMe)(Ph) complexes with TON for ethylene hydrophenylation

Given the observation that less electron-donating L enhances catalyst longevity, the more electron-deficient cationic $[(HC(pz')_3)Ru(P(OCH_2)_3CEt)(NCMe)Ph][BAR'_4]$ $[HC(pz')_3 = \text{tris}(3,5\text{-dimethylpyrazolyl})\text{methane}, \quad BAR'_4 = \text{tetrakis}[3,5\text{-bis}(\text{trifluoro-methyl})\text{phenyl borate}]$ complex was prepared as catalyst precursor for ethylene hydroarylation, and it gives 565 TONs of ethylbenzene formation at 90 °C with 15 psi of ethylene after 131 h (Scheme 1.4.10).⁷⁴ $[(HC(pz')_3)Ru(P(OCH_2)_3CEt)(NCMe)Ph][BAR'_4]$ shows increased thermal stability compared to the other TpRu(L)(NCMe)Ph complexes, which allows catalytic hydrophenylation of ethylene to proceed up to 175 °C. At 175 °C, a TOF of $2.1 \times 10^{-2} \text{ s}^{-1}$ is achieved, which is the highest reaction rate among the TpRu(L)(NCMe)Ph and related complexes.⁷⁴



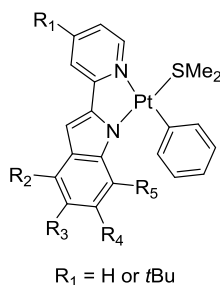
Scheme 1.4.10. Hydrophenylation of ethylene catalyzed by $[(HC(pz')_3)Ru(P(OCH_2)_3CEt)(NCMe)Ph][BAR'_4]$ complex

Hydrophenylation with propylene using TpRu(CO)(NCMe)Ph afforded 14 TOs of branched cumene and linear *n*-propylbenzene products with a 1:1.6 L/B ratio.⁶⁸ The formation of linear products is indicative of a non-Friedel-Crafts arene alkylation

pathway.

1.4.2.4 Platinum(II) Catalysts

Tilley and co-workers demonstrated that a series of charge neutral square planar Pt complexes with 2,2'-pyridyl-indolate ligands (Scheme 1.4.11) catalyze hydroarylation of ethylene with TOs in the range of 3-25 after 24 h at 100 °C.⁷⁸ In the presence of 1 atm propylene, these Pt complexes form branched cumene with 1:1.4-3.2 linear/branched ratio at 100 °C after 24 h.⁷⁸ Reaction with ethylene in toluene using one of the Pt complexes, (tBuPyInd)PtPh(SMe₂), [tBuPyInd = (2-(4-(tert-butyl)pyridin-2-yl)-1H-indole)] revealed a 98% selectivity for *meta* and *para* products over *ortho* product.⁷⁸ Both the fact that anti-Markovnikov product is produced and that *meta* and *para* functionalized products are favored indicate that the catalysis proceeds through a metal-mediated C–H bond activation pathway rather than acid-catalyzed mechanism. In addition, hydrophenylation of ethylene in the presence of Hg(0) did not inhibit product formation, suggesting that Pt nanoparticles are not the catalytically active species.⁷⁸



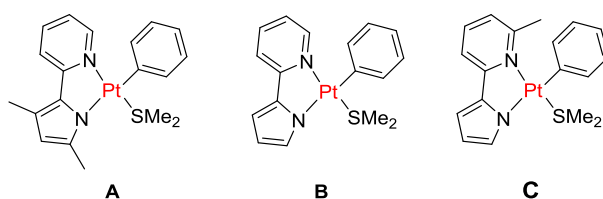
Scheme 1.4.11. Structures of charge neutral Pt(II) catalysts with 2,2'-pyridyl-indolate ligands

Goldberg and coworkers developed a series of charge neutral (pyridyl)pyrrolide

Pt(II) complexes that catalyze the hydroarylation of ethylene and α -olefins.⁷⁷ For example, hydrophenylation of ethylene using neutral Pt(II) complexes (dmpp)PtMe₃ and (dmpp)Pt(SMe₂)Ph (dmpp=3,5-dimethyl-2-(2-pyridyl)pyrrolide) resulted in 26 and 36 TONs of ethylbenzene at 100 °C, respectively. With propylene, (dmpp)PtMe₃ and (dmpp)Pt(SMe₂)Ph catalysts afford 8 and 18 TONs of propyl benzene products, respectively. These two neutral (pyridyl)pyrrolide supported Pt(II) complexes are both selective for cumene over *n*-propylbenzene with ~1:6 L/B ratio. The complexes (dmpp)PtMe₃ and (dmpp)Pt(SMe₂)Ph show selectivity toward *meta*- and *para*-alkylated products. Toluene ethylation with (dmpp)PtMe₃ and (dmpp)Pt(SMe₂)Ph as the catalyst precursors afforded an *o*:*m+p* ratio of 7:93 and 6:94, respectively. Deuterium-labeling studies for the hydroarylation of ethylene for the (dmpp)Pt(SMe₂)Ph system indicate that an intramolecular C–H activation of the arene ring occurs during the catalytic cycle, followed by alkyl C–H reductive elimination.

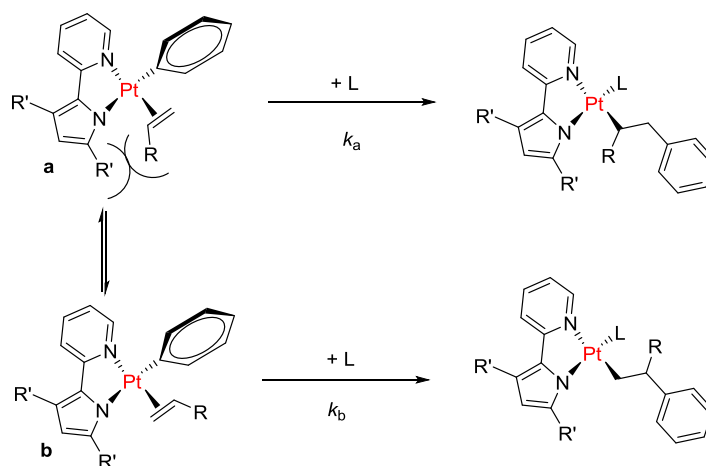
The Goldberg group then studied variations of the substituents on the (pyridyl)pyrrolide ligands allow effective tuning of the selectivity to anti-Markovnikov alkylarene production as well as the competitive vinyl arene production.⁷⁶ A series of Pt(II) complexes (Scheme 1.4.12) were synthesized as pre-catalysts for the conversion of olefins and benzene to alkyl arenes. Removing the methyl groups on the pyrrolide portion of the ligand resulted in substantial changes in the linear/branched products selectivity. The complex **A** showed strong propensity for the Markovnikov product in hydroarylation of different α -olefins (L/B ratio of 15:85 for propylene hydroarylation, 16:83 for 1-hexene, 15:48 for neohexene). In

contrast, using complex **B**, under the same reaction conditions, the linear and branched products were formed in a 48:52 ratio for propylene hydroarylation, 57:43 ratio for 1-hexene hydroarylation, and 85:5 for neohexene hydroarylation. This result represents a significant increase in the anti-Markovnikov selectivity. Notably, the methyl group from the pyridyl portion (complex **C**) changed the major product of the propylene reaction from alkylarene to α -methyl styrene.



Scheme 1.4.12. Structures of charge neutral (pyridyl)pyrrolide Pt(II) complexes

Scheme 1.4.13 shows two possible olefin insertion modes. For catalyst **A**, it was proposed that rotamer **a** is favored over rotamer **b** due to the steric interaction between a methyl group at the fifth position of the pyrrole ring and alkyl chain of the olefin. The methyl group also has an impact on the relative insertion barriers. In other words, the value of k_a/k_b is decreased because of the methyl group of the pyrrole ring. Those two effects led to the significant difference in Markovnikov/anti-Markovnikov selectivity between catalyst **A** and **B**. When catalyst **C** was used, β -hydride elimination is kinetically favored over intramolecular arene C–H activation since the methyl group in the sixth position on the pyridyl ring blocks approach of the arene. In this case, the product of β -hydride elimination, α -methyl styrene, was formed over alkyl arenes.

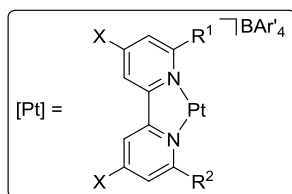


Scheme 1.4.13. Steric interaction between coordinated olefin and the pyrrole ring during the olefin insertion step. R= CH₃, C₅H₁₁, tBu, R'=H, CH₃.

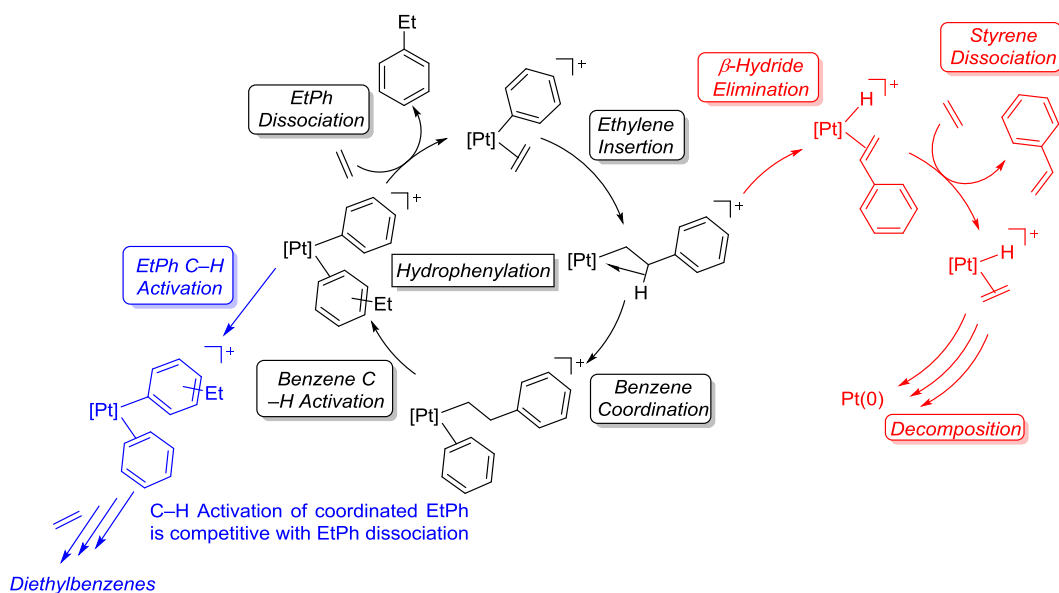
Our group reported that the formally cationic Pt(II) complex [(^tbpy)Pt(Ph)(THF)][BAR'₄] (**1**) (^tbpy = 4,4'-di-tert-butyl-2,2'-bipyridine, Ar' = 3,5-bis(trifluoromethyl)phenyl) serves as a catalyst precursor for olefin hydroarylation.⁸⁴ Our studies include:

1) The reaction at 120 °C with 0.03 MPa of ethylene (4.2 mmol) for 4 hours resulted in the production of ~119 TO of ethylbenzene, diethylbenzenes, and styrene, corresponding to an 89% yield. A TOF of $7.1 \times 10^{-3} \text{ s}^{-1}$ for ethylbenzene production is reached with 0.1 MPa of ethylene pressure at 120 °C after 4 hours.

2) Based on experimental and computational results, a plausible mechanism for the conversion of benzene and ethylene to ethylbenzene using [(^tbpy)Pt(Ph)(THF)][BAR'₄] was proposed (Scheme 1.4.14). The labile coordinated THF is substituted by ethylene, followed by olefin insertion into the Pt–phenyl bond to generate [(^tbpy)Pt(CH₂CH₂Ph)]⁺. Subsequent benzene coordination and C–H activation yields coordinated ethylbenzene. The final step is the substitution of coordinated ethylbenzene with ethylene to regenerate the catalyst.



Less electron donating 4,4' substituents ($X = \text{NO}_2, \text{Br}, \text{CO}_2\text{Et}$) or sterically bulky 6,6' substituents ($R^1 = R^2 = \text{CH}_3$) increased propensity of styrene dissociation

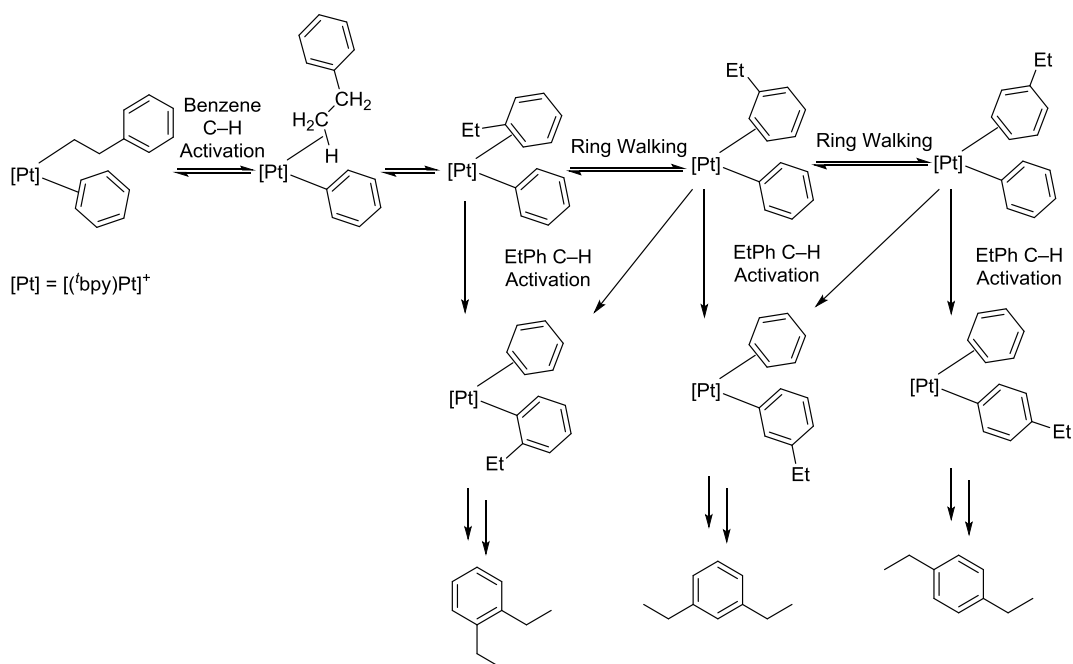


Scheme 1.4.14. Proposed mechanisms for ethylbenzene, diethylbenzene and styrene formation using bipyridyl-supported Pt(II) complexes

3) The $[(^t\text{bpy})\text{Pt}(\text{Ph})(\text{THF})][\text{BAR}'_4]$ catalyst produces substantial quantities of diethylbenzenes that account for approximately 20% of the total alkyl arene products. In contrast with Friedel–Crafts catalysis, using the cationic Pt complex shows a faster rate of ethylbenzene production from benzene than diethylbenzene formation from ethylbenzene. It is hypothesized that relatively slow dissociation of ethylbenzene from Pt(II) provides an opportunity for a more competitive second C–H activation, which leads to the production of diethylbenzene (Scheme 1.4.14). Computational studies suggest that for $[(\text{bpy})\text{Pt}(\text{CH}_2\text{CH}_2\text{Ph})]^+$ (bpy = 2,2'-bipyridine), the energetics of ethylbenzene dissociation and a second C–H activation are of a similar magnitude.

4) Using $[(^t\text{bpy})\text{Pt}(\text{Ph})(\text{THF})]^+$, the conversion of benzene and ethylene to

diethylbenzene shows a *ortho:meta:para* products ratio of 1.0:2.6:1.6, whereas the formation of diethylbenzenes from *free* ethylbenzene and ethylene shows an increased *o:m:p* ratio of 1.0:34.8:24.0.⁸⁶ We proposed distinct pathways for diethylbenzene formation from benzene/ethylene and ethylbenzene/ethylene to explain the different *m+p/o* selectivity.⁸⁶ For the formation of diethylbenzenes from ethylene and benzene, before C–H activation of the coordinated ethylbenzene, the ring walking process requires Pt(II) interact with the *ortho* carbon (Scheme 1.4.15), thus providing access to the *ortho* C–H bond. In contrast, for the reaction of free ethylbenzene, ethylbenzene likely directly coordinates to Pt(II) via an η^2 -C,C mode before C–H activation, which likely favors η^2 -2,3 and/or η^2 -3,4 to avoid steric interactions with the methyl group.

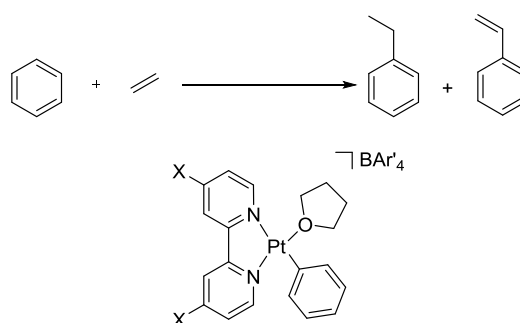


Scheme 1.4.15. Proposed mechanisms for dialkylation products formation from Pt-catalyzed ethylene hydrophenylation.

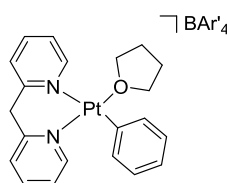
5) Monitoring the catalysis by ^1H NMR spectroscopy reveals that the only observable species during the catalysis is $[(bpy)Pt(CH_2CH_2Ph)(\eta^2-C_2H_4)]^+$, which is likely the off-cycle catalyst resting state. Catalyst activity decreases with increasing

ethylene concentration, indicating that ethylene can coordinate to $[(^t\text{bpy})\text{Pt}(\text{CH}_2\text{CH}_2\text{Ph})]^+$ intermediate to form the resting state, which removes Pt from the catalytic cycle and slows down the reaction (Scheme 1.4.14).

In a follow up study, the influence of 4,4'-substituents of the bipyridyl ligand on the catalytic hydroarylation of olefins was investigated for the series of complexes **1-6** (Scheme 1.4.16).⁸² Based on the studies, the following points are emphasized:



	X = OMe (1)	X = <i>t</i>Bu (2)	X = H (3)
TOs of EtPh and styrene	104	84	127
EtPh : Styrene	29.6	26.2	21.5
	X = Br (4)	X = CO₂Et (5)	X = NO₂ (6)
TOs of EtPh and styrene	15	64	1
EtPh : Styrene	0.6	5.3	0.1



TOs of EtPh and styrene	469
EtPh : Styrene	138

Scheme 1.4.16. TOs and ratios of ethylbenzene to styrene from cationic Pt(II) catalyzed ethylene hydrophenylation (100 °C with 0.1 MPa of ethylene; EtPh:styrene ratios after 4 hours).

1) Pt complexes with electron-withdrawing 4,4'-substituents (complexes **4-5**) are less catalytically reactive than Pt complexes with electron-donating groups

(complexes **1-3**) after 4 hours with no signs of catalyst deactivation. This is likely due to the more facile oxidative addition of benzene C–H bond as electron density of metal center is increased.

2) Olefin hydroarylation catalyzed by Pt complexes **1-6** results in ethylbenzene and styrene production. The formation of styrene likely occurs via β -hydride elimination from $[(^x\text{bpy})\text{Pt}(\text{CH}_2\text{CH}_2\text{Ph})]^+$ (Scheme 1.4.14). Simulations indicate that the ΔG^\ddagger of β -hydride elimination from $[(^t\text{bpy})\text{Pt}(\text{CH}_2\text{CH}_2\text{Ph})]^+$ is low (5.0 kcal/mol), and the lack of substantial styrene production may result from the unfavorable energetics for the styrene dissociation step. Our studies reveals that more donating 4,4'-substituents lead to an increase in the ratio of ethylbenzene to styrene (Scheme 1.4.16). A possible rationalization for the trend is that increasing the Pt electron density might suppress the styrene dissociation by strengthening metal-to-olefin π -backbonding. Also, if the net dissociation of the styrene incorporates an associative ligand exchange with ethylene, more strongly electron-donating ligands could inhibit ethylene coordination, and hence, styrene dissociation (Scheme 1.4.14).

3) Complexes that possess more donating ^xbpy ligands (**1-3**) give higher TONs for total ethylbenzene and styrene products whereas complexes with less donating ^xbpy ligands (**4-6**) have lower TONs (Scheme 1.4.16). One possible rationalization for this trend is that the unstable Pt(II)–H intermediates, formed during styrene production process, are more readily formed in the catalysis by **4-6** and are more prone to decomposition (Scheme 1.4.14).

In addition to the electronic modification on dipyriddy ligands, we designed

$[(\text{dpm})\text{Pt}(\text{Ph})(\text{THF})][\text{BAr}'_4]$ (dpm = 2,2'-dipyridylmethane) complex for catalytic olefin hydroarylation by introducing a methylene spacers between two pyridyl rings.⁸¹ The complex $[(\text{dpm})\text{Pt}(\text{Ph})(\text{THF})][\text{BAr}'_4]$ produces ethylbenzene and styrene in an approximate 138:1 ratio at 100 °C, which is a significantly higher ratio than that for $[(\text{t}^{\text{bpy}})\text{Pt}(\text{Ph})(\text{THF})][\text{BAr}'_4]$ (~8:1) (Scheme 1.4.16). Catalytic conversion of benzene and ethylene to ethylbenzene using $[(\text{dpm})\text{Pt}(\text{Ph})(\text{THF})][\text{BAr}'_4]$ gives a TON of 469, which is more long-lived than that of $[(\text{t}^{\text{bpy}})\text{Pt}(\text{Ph})(\text{THF})][\text{BAr}'_4]$ (TON of 84) under identical conditions (Scheme 1.4.16). We speculate that the increased stability of $[(\text{dpm})\text{Pt}(\text{Ph})(\text{THF})][\text{BAr}'_4]$ compared to $[(\text{t}^{\text{bpy}})\text{Pt}(\text{Ph})(\text{THF})][\text{BAr}'_4]$ is due to less facile associative displacement of styrene by ethylene for the dpm-Pt catalyst and thus a reduced predilection for styrene production accompanied by formation of unstable Pt-H, which leads to catalyst decomposition.

Generally, hydroarylation with α -olefins using Pt(II) complexes exhibits selectivity toward Markovnikov branched products.⁸³ Propylene (0.1 MPa) hydroarylation using complexes **1-6** revealed that bipyridyl ligands with less-donating 4,4'-substituents increase selectivity toward branched cumene over linear *n*-propylbenzene (Table 1.4.1).⁸³ Surprisingly, the structural differences between dpm and tbpy ligands did not have a significant impact on L:B ratio (Table 1.4.1).⁸³

Table 1.4.1. Comparison of L:B ratio for hydroarylation with α -olefins using cationic Pt(II) complexes.

Complex	α -Olefin	L:B ratio
---------	------------------	-----------

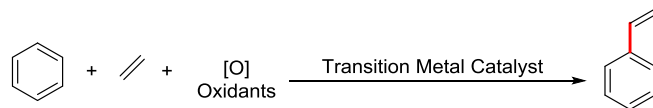
[(^t bpy)Pt(Ph)(THF)][BAr' ₄](1)	propylene	1:2.9
	1-pentene	~1:3
[(^{OMe} bpy)Pt(Ph)(THF)][BAr' ₄](2)	propylene	1:2.9
[(^H bpy)Pt(Ph)(THF)][BAr' ₄](3)	propylene	1:3.2
[(^{Br} bpy)Pt(Ph)(THF)][BAr' ₄](4)	propylene	1:3.8
[(^{COOEt} bpy)Pt(Ph)(THF)][BAr' ₄](5)	propylene	1:3.7
[(^{NO₂} bpy)Pt(Ph)(THF)][BAr' ₄](6)	propylene	1:4.6
[(dpm)Pt(Ph)(THF)][BAr' ₄](7)	propylene	1:4.4
	1-pentene	~1:3

Computational studies of hydroarylation of propylene catalyzed by complexes **1**, **4** and **6** suggest that Curtin–Hammett conditions is responsible for the linear/branched selectivity for the Pt(II) catalyzed propylene hydroarylation.⁸³ That is, the product selectivity for catalysts **1**, **4** and **6** is not determined by the kinetic selectivity of the olefin insertion step but by the equilibrium between the insertion products and the relative rates of subsequent rate-limiting C–H activation. The calculated transition state of benzene C–H activation leading to branched product is lower than that leading to linear product. Reducing the donor ability of the bpy ligands increases the selectivity for branched products by increasing the C–H activation transition state energy differences between pathways leading to linear and branched alkyl arene ($\Delta\Delta G^\ddagger$). This is consistent with experimental trends in linear/branched ratios as a function of electron donor ability of the bpy ligands.

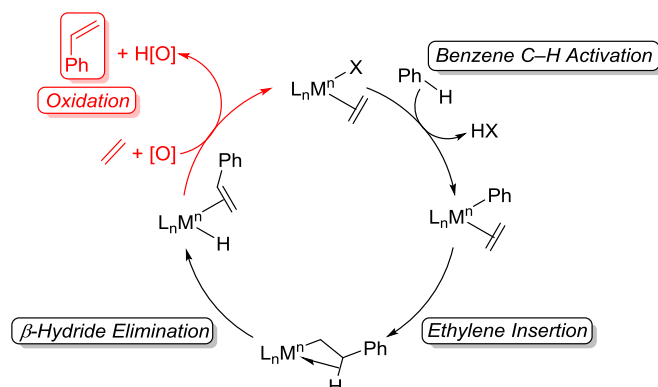
1.4.3 Transition Metal-Catalyzed Arene Alkenylation

1.4.3.1 Overview

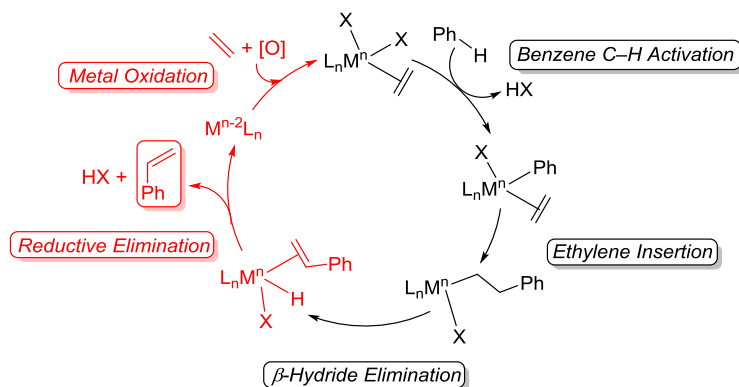
Transition metal-catalyzed arene alkenylation to convert unactivated olefins and arene substrates to alkenyl arenes in the presence of oxidant is another possible alternative to traditional acid-based catalysis and cross-coupling reactions via C–X activation. Such transition metal-catalyzed processes usually incorporate C–H activation of the arene, olefin insertion into metal–aryl bonds followed by a β -hydride elimination step to form metal-hydride species and alkenyl arenes. The conversion of the resulting M–H intermediate to active catalyst typically has two operative pathways. One proceeds via direct oxidation of M–H without a change in the oxidation state of the metal (mechanism I, Scheme 1.4.17), whereas the other involves an initial reductive elimination to reduce metal and subsequent re-oxidation of metal to regenerate catalyst (mechanism II, Scheme 1.4.17). Metal-catalyzed arene alkenylation shares common advantages with metal-catalyzed arene alkylation due to their similar mechanism and overcomes the deficiencies of acid catalysis. In addition, arene alkenylation offers a direct and single-step route for production of unsaturated vinyl arenes, which requires multiple steps using current industrial methods.



Mechanism I:



Mechanism II:



[O]: Ag(I), Cu(II), O₂, C₂H₄, (NH₄)₂S₂O₈, V₂O₅, benzoquinone, polyoxometalates, PhCO₃tBu, ...

M: Rh, Pd, Ru, ...

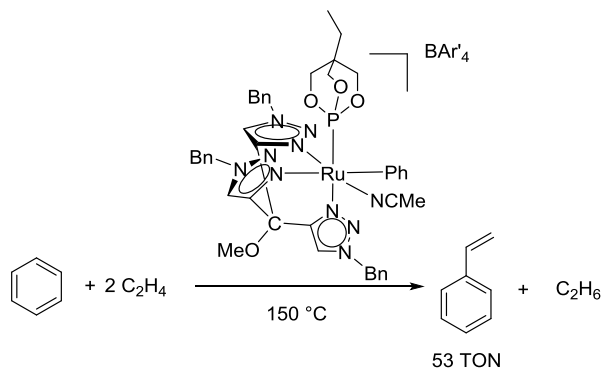
X = carboxylate

Scheme 1.4.17. Mechanisms for transition metal-catalyzed benzene alkenylation with ethylene.

1.4.3.2 Anaerobic Catalysis Using Stoichiometric Oxidants

Examples of Pd and Rh catalyzed arene alkenylation under anaerobic conditions by consuming stoichiometric oxidants such as (NH₄)₂S₂O₈,⁸⁷ AgOAc,⁸⁸ V₂O₅,⁸⁹ PhCO₃tBu⁹⁰ or copper(II) carboxylates⁹¹⁻⁹⁶ have been reported. Among these reactions, benzene alkenylation with ethylene or simple α -olefins to form corresponding alkenyl benzenes has been rarely demonstrated. Possibly the first example was reported by Fujiwara and co-workers using Pd(OAc)₂ as a catalyst for

benzene ethenylation to produce styrene in the absence of additional oxidants.⁹⁷ However, this initial report did not include catalytic turnovers with respect to Pd(OAc)₂ (4% yield of styrene based on the Pd catalyst was reported), and it produced a significant amount of undesired stilbene product (16% yield based on the Pd catalyst). Periana and coworkers reported a Rh(III) catalyst that gives 24 TOs of styrene, corresponding to 36% yield relative to Cu(II) oxidant.⁹⁶ Tanaka and coworkers disclosed a Rh(I) catalyst that produces 3 TOs of styrene under irradiation along with 4 TOs of biphenyl products.⁹⁸ Hong and coworkers reported that Rh₄(CO)₁₂ catalyzes the conversion of benzene, ethylene and CO to form 472 TOs of styrene and 809 TOs of 3-pentanone.⁹⁹ This reaction is not carbon-economical since it consumes 2 equivalents of ethylene and one equivalent of CO to generate undesired 3-pentanone. Recently, We disclosed a cationic Ru(II) complex [(MeOTTM)Ru(P(OCH₂)₃CEt)(NCMe)Ph][BAr'₄] (MeOTMM = 4,4',4''-(methoxymethanetriyl)-tris(1-benzyl-1H-1,2,3-triazole)] that catalyzes the oxidative hydrophenylation of ethylene to produce 53 TOs of styrene with ethylene serving as the oxidant (Scheme 1.4.18).¹⁰⁰ The use of ethylene as oxidant is interesting since the reduced ethane could be returned to a cracker to produce more ethylene. In general, these catalysts are limited by low selectivity, low yield and low TONs.

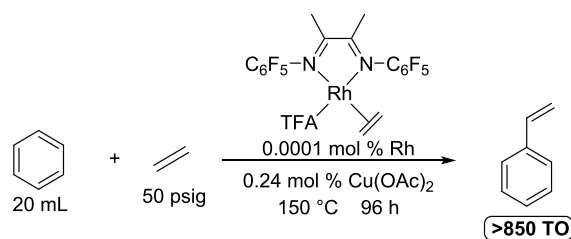


Scheme 1.4.18. Oxidative hydrophenylation of ethylene catalyzed by [(MeOTTM)Ru(P(OCH₂)₃CEt)(NCMe)Ph][BAR'₄].

Previous studies suggest that the activation barrier for olefin insertion into Pt(II) aryl bonds might be higher for overall charge-neutral complexes than for cationic complexes.⁸³ Therefore, we anticipated that activation barriers for ethylene insertion into Rh(I)–Ph bonds of charge-neutral Rh(I) complexes might be higher than those of cationic Pt(II) complexes. Thus, for Rh(I) complexes, we considered that use of electron-withdrawing diimine ligands might facilitate the olefin insertion step. In addition, we had reported that the Rh(I) complex (^{F1}DAB)Rh(TFA)(η²-COE) [^{F1}DAB = *N,N'*-bis(pentafluorophenyl)-2,3-dimethyl-1,4-diaza-1,3-butadiene; TFA = trifluoroacetate; COE = cyclooctene] is a catalyst precursor for arene H/D exchange in trifluoroacetic acid.¹⁰¹ Thus, we considered that Rh(I) supported by the fluorinated ^{F1}DAB ligand might catalyze arene alkylation or alkenylation.

We initially demonstrated that (^{F1}DAB)Rh(TFA)(η²-C₂H₄) serves as a catalyst precursor for the selective production of styrene from benzene and ethylene in the presence of Cu(II) salts.¹⁰² At 150 °C with 25 psig ethylene, near-quantitative yield (> 95% yield) of styrene, based on Cu(II) as limiting reagent, was obtained when 60 to 240 equivalents (relative to Rh catalyst) of Cu(OAc)₂ and 0.001 mol % of

(^{Fl}DAB)Rh(TFA)(η^2 -C₂H₄) were used (assuming 2 equivalents of CuX₂ are consumed per equivalent of styrene, maximum TOs with y equivalents of CuX₂ is y/2). Reactions with both soluble [copper(II) 2-ethylhexanoate (Cu(OHex)₂) and copper(II) pivalate (Cu(OPiv)₂)] and insoluble [copper(II) acetate (Cu(OAc)₂)] Cu(II) salts reach over 90% yield relative to Cu(II) oxidant. For catalysis using 0.0001 mol % of (^{Fl}DAB)Rh(TFA)(η^2 -C₂H₄) and 2400 equivalents of Cu(OAc)₂, the catalyst remained active after 96 hours and afforded ~850 TONs (Scheme 1.4.19).

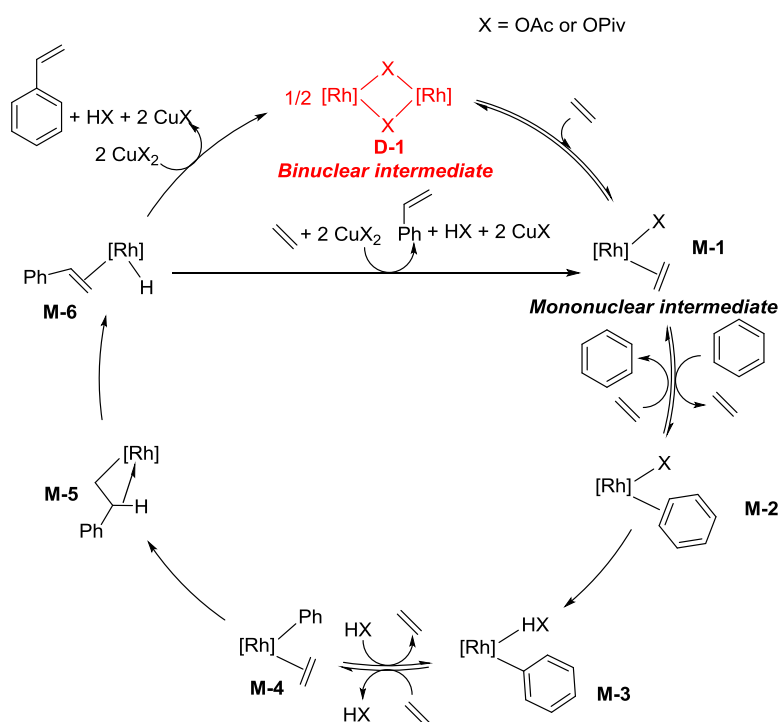


Scheme 1.4.19. Benzene alkenylation with ethylene catalyzed by (^{Fl}DAB)Rh(TFA)(η^2 -C₂H₄)

Kinetic studies of Rh catalyzed benzene alkenylation were performed in the presence of ethylene (79 mM to 237 mM) using (^{Fl}DAB)Rh(η^2 -C₂H₄)(OAc) catalyst precursor (0.056 to 0.23 mM) and soluble Cu(OPiv)₂ (13 mM to 54 mM) in order to maintain a homogeneous reaction solution during the catalysis.¹⁰³ A first-order dependence on ethylene concentration using 79 mM to 237 mM of ethylene was observed. The reaction rate displays a near zero-order dependence on Cu(OPiv)₂, which suggests that the involvement of Cu(II) occurs after the rate-limiting step. The rate dependence on Rh concentration is approximately half-order at 7.9 mM C₂H₄ and near first-order at 17.5 mM C₂H₄. In addition, the order in Rh is 0.83(1) at 130 °C and 0.64(1) at 160 °C. Ethylene concentration and temperature influences the order in Rh,

suggesting the possibility of divergent catalytic pathways (see below).

Based on mechanistic studies, our proposed catalytic cycle involves: 1) benzene coordination to Rh complexes and subsequent benzene C–H activation via CMD pathway using an acetate ligand, 2) ethylene coordination and insertion into the Rh–Ph bond, 3) β -hydride elimination from the resulting Rh–CH₂CH₂Ph intermediate, and 4) styrene dissociation and oxidation of Rh–H intermediate with CuX₂ to regenerate the catalyst (Scheme 1.4.20).¹⁰³

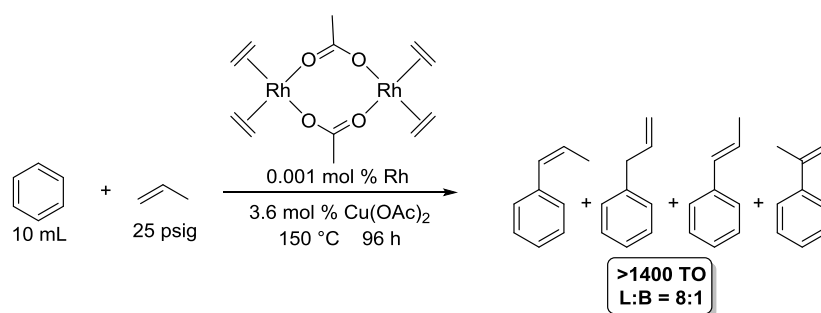


Scheme 1.4.20. Proposed mechanism for benzene alkenylation using Rh(I) as a catalyst precursor

Based on the kinetic studies, two competing pathways whose contributions vary with ethylene concentration and temperature were proposed (Scheme 11).¹⁰³ At low ethylene concentration, the Rh–H intermediate **M-6** releases styrene and reacts with Cu(II) oxidant to generate a binuclear Rh intermediate **D-1**, which would result in

half-order kinetics in Rh. At high ethylene concentration, styrene is exchanged with ethylene and the Rh–H intermediate **M-6** reacts with the oxidant to form a monomeric Rh intermediate **M-1**, which would give rise to first-order kinetics with respect to Rh.

We also reported that arene alkenylation using Rh(I) catalyst precursors and α -olefins produces anti-Markovnikov addition products. Using $[\text{Rh}(\mu\text{-OAc})(\eta^2\text{-C}_2\text{H}_4)_2]_2$ (0.001 mol% relative to benzene) as the catalyst precursor and $\text{Cu}(\text{OAc})_2$ (240 equivalents relative to Rh) as the oxidant, the anaerobic reaction of benzene with 25 psig of propylene at 150 °C affords propenyl benzene products with a L/B ratio of 8:1 after 48 h. Catalysis using 0.001 mol% of $[\text{Rh}(\mu\text{-OAc})(\eta^2\text{-C}_2\text{H}_4)_2]_2$ with 3600 equivalents of $\text{Cu}(\text{OPiv})_2$ after 96 h afforded 1474(3) TOs of alkenylated products, corresponding to an overall 82% yield based on Cu(II) as limiting reagent (Scheme 1.4.21).



Scheme 1.4.21. Benzene alkenylation with propylene catalyzed by $[\text{Rh}(\mu\text{-OAc})(\eta^2\text{-C}_2\text{H}_4)_2]_2$.

Catalysis using other olefins was probed {10 mL of benzene, 0.01 mol % $[\text{Rh}(\mu\text{-OAc})(\eta^2\text{-C}_2\text{H}_4)_2]_2$ (relative to benzene), 2000 equivalents of olefin (relative to Rh) or 25 psig for gaseous olefins, and 240 equivalents of $\text{Cu}(\text{OAc})_2$ (relative to Rh)}. For neohexene and isobutylene, only the linear products were produced with 30(8)

TOs and 100(2) TOs after 72 h, respectively. Catalysis with 1-pentene afforded quantitative yield relative to oxidant and an ~8:1 ratio of linear (*n*-pentylbenzene) to branched (2-pentylbenzene) products after hydrogenation.¹⁰⁴ Catalysis starting with 2-pentene produces 22(4) TOs of *n*-pentylbenzene, 48(6) TOs of 2-pentylbenzene and 27(5) TOs of 3-pentylbenzene after hydrogenation. Given that approximately 1% of 1-pentene is observed during the catalysis with 2-pentene, the linear and branched pentylbenzene product distribution indicates that the catalysis with 1-pentene is approximately 30 times more rapid than with 2-pentene.

For arene propenylation using $[\text{Rh}(\mu\text{-OAc})(\eta^2\text{-C}_2\text{H}_4)_2]_2$, the rates of reaction with electron-deficient arenes are similar to the rates of reaction with electron-rich arenes. This contrasts acid-based catalysis, for which less effective catalysis for electron-deficient arenes is generally observed.^{26, 37, 38, 105} Also, olefin hydrophenylation using AlCl_3 shows selectivity toward *ortho*- and *para*-alkylated products due to the electrophilic aromatic substitution mechanism. In contrast, arene alkenylation with propylene and mono-substituted arenes using $[\text{Rh}(\mu\text{-OAc})(\eta^2\text{-C}_2\text{H}_4)_2]_2$ favors the *meta* and *para* positions. This is likely due to the more sterically hindered *ortho* position of mono-substituted benzene than *meta* and *para* positions, which leads to less accessible *ortho*-C–H bond activation. Toluene propenylation with $[\text{Rh}(\mu\text{-OAc})(\eta^2\text{-C}_2\text{H}_4)_2]_2$ as the catalyst precursor afforded 86(17) TOs (72% yield) of alkenyl toluene with an *o:m:p* ratio of 1:8.9:9.3. The reaction of chlorobenzene and propylene using $[\text{Rh}(\mu\text{-OAc})(\eta^2\text{-C}_2\text{H}_4)_2]_2$ gave 116(3) TOs (97% yield) of alkenylated chlorobenzene with an *o:m:p* ratio of 1:11:7 after 72 h.

Recently, we reported that (5-FP)Rh(TFA)(η^2 -C₂H₄) (5-FP = 1,2-bis(*N*-7-azaindolyl)benzene; TFA = trifluoroacetate) can catalyze anti-Markovnikov benzene propenylation (Figure 1.4.1).¹⁰⁶ The reaction with 30 psig of propylene at 150 °C using Cu(OPiv)₂ in the presence of HOPiv (480 equiv relative to Rh) after 0.5 h affords 86 TOs of propenyl benzene products with a L:B ratio of ~11:1. At 80 °C, the L:B ratio increases to 18:1 accompanied by decreased catalytic activity. A 79% yield of alkenyl benzene was reached after 10 h using a large amount of Cu(OPiv)₂ (2400 equiv relative to Rh) for the catalysis with propylene, indicating a long-lived process.

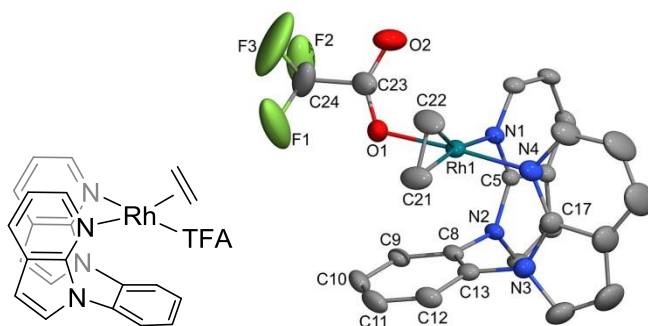


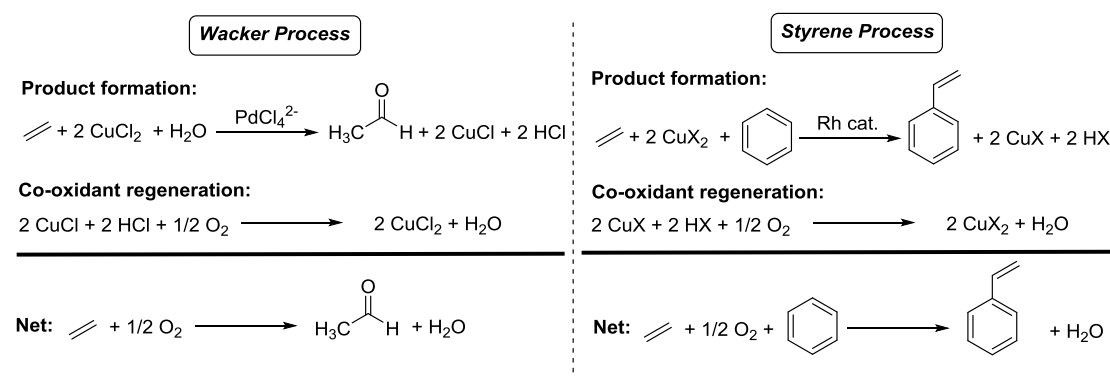
Figure 1.4.1. Structure (left) and ORTEP (right) of (5-FP)Rh(TFA)(η^2 -C₂H₄) (hydrogen atoms omitted). ORTEP reprinted with permission from reference 102. Copyright 2019 American Chemical Society.

1.4.3.3 Aerobic Catalysis with Co-oxidants

While the above listed reactions represent important advancements, the use of O₂ as the ultimate oxidant is ideal since it is inexpensive (especially when the source is unpurified air) and the only waste is water. The Matsumoto and Fujiwara groups demonstrated Pd and Rh catalyzed aerobic benzene ethenylation to form styrene in which the Cu(II) or Ag(I) is present as the co-oxidant and is regenerated *in situ* using air or O₂.^{97, 107, 108} However, the aerobic reaction developed by the Fujiwara group

provides less than 1 TON of styrene (59% yield of styrene based on the catalyst) when Pd(OAc)₂ was used as the catalyst and AgOAc was used as the co-oxidant.⁸⁶ Matsumoto and coworkers reported that Pd(OAc)₂ yields 39 TOs of styrene and 44 TOs of undesired vinyl acetate byproduct using Cu(OAc)₂/O₂ as the oxidant at 180 °C.¹⁰⁸ They also demonstrated that a series of Rh(III) complexes catalyze benzene ethenylation with styrene TOs in the range of 14-39 under the identical conditions.¹⁰⁸ However, significant production of vinylacetate (4-13 TOs) was also observed. Subsequently, We reported conditions for the formation of styrene from benzene and ethylene catalyzed by Pd(OAc)₂ using copper pivalate (Cu(OPiv)₂) in the presence of purified O₂ yields 2410 TOs of styrene with > 85% selectivity.¹⁰⁹ The keys to increase selectivity for styrene are applying low ethylene pressure (20 psig) to reduce the production of undesired vinyl pivalate and high reaction temperature (180 °C) to facilitate the conversion of vinyl pivalate and benzene to styrene.¹⁰⁹ During the aerobic arene alkenylation using Cu(II) as the co-oxidant, reduced CuX and HX (X = carboxylate) can be recycled with air to generate CuX₂ and H₂O. Therefore, these Rh and Pd catalyzed arene alkenylation reactions have the potential to use catalytic amounts of Cu(II). Aerobic regeneration of Cu(II) would yield an overall conversion of arene, olefin and O₂ to alkenyl arene and water (Scheme 1.4.22). The overall process is akin to the commercialized Wacker-Hoechst process for ethylene oxidation in which the CuCl₂ oxidant is regenerated either *in situ* by O₂ or *ex situ* in a separate reactor by air (Scheme 1.4.22).^{10, 27} Examples of aerobic benzene alkenylation using benzoquinone¹¹⁰ or polyoxometalates¹¹¹⁻¹¹³ as the co-oxidant were also reported.

However, the alkene substrate scope is restricted to electron-deficient acrylates. Ishii and co-workers reported Pd(OAc)₂-catalyzed aerobic benzene alkenylation with ethylene using heteropoly acids/air as the oxidant affords 100 TO of styrene and along with a substantial amount of stilbene by-product (67 TO) at 120 °C.¹¹³

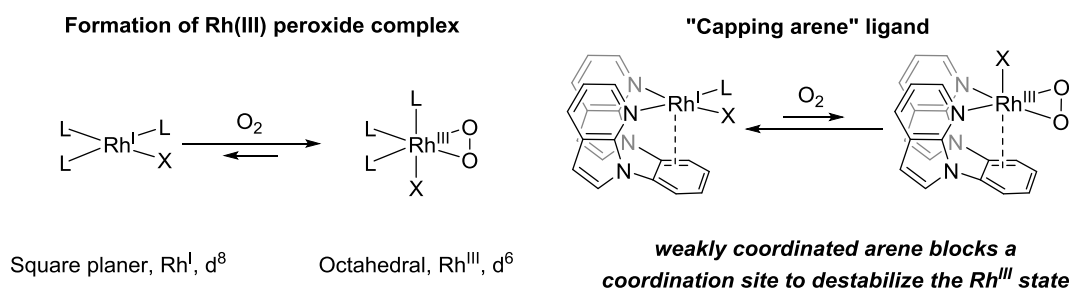


Scheme 1.4.22. Comparison of Wacker process with styrene process

We recently demonstrated that under optimized conditions (5-FP)Rh(TFA)(η^2 -C₂H₄) can catalyze aerobic benzene alkenylation in the presence of Cu(OPiv)₂ with air as the *in situ* oxidant.¹⁰⁶ We speculated that Rh(I) catalysts undergo aerobic deactivation to catalytically inactive Rh(III) peroxide complexes in the presence of O₂.¹¹⁴⁻¹¹⁶ Oxidation from Rh(I) to Rh(III) generally involves conversion of square planar complexes to six-coordinate octahedral complexes (Scheme 1.4.23). We hypothesized that a nitrogen based "capping arene" ligand, such as 5-FP, could be employed to block one of the coordination sites of the Rh center and prevent the coordination of a sixth donating ligand to the metal during oxidation from Rh(I) to Rh(III). Hence, we expected that this structure would destabilize octahedral Rh(III) peroxide intermediates and protect Rh catalysts against oxidative degradation

or inhibition of the catalysis using air or O₂ as the *in situ* oxidant (Scheme 1.4.23).¹⁰⁶

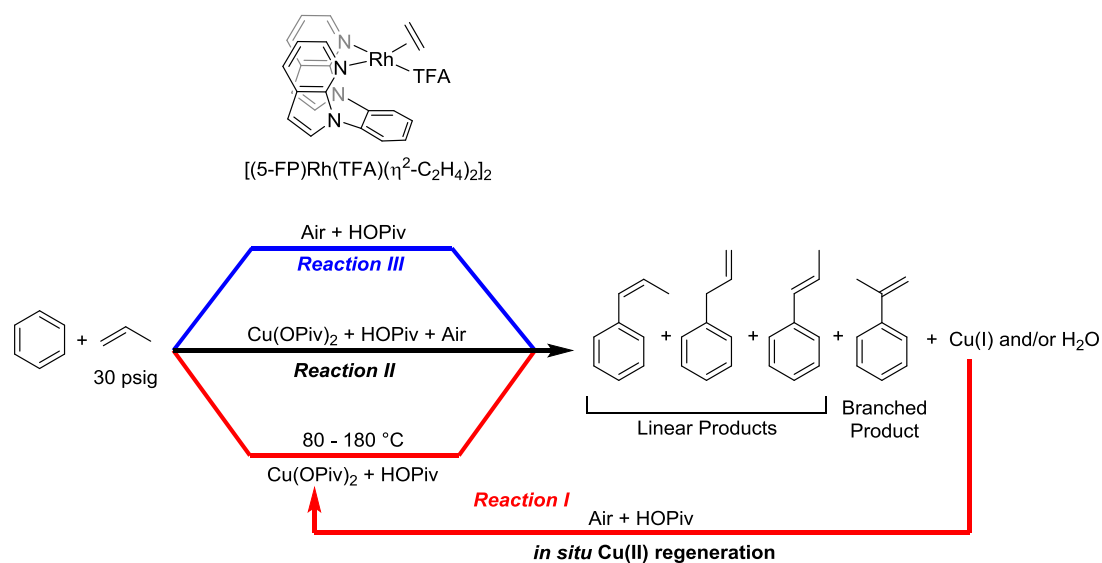
117-119



Scheme 1.4.23. Concept of using a "capping arene" ligand to protect Rh(I) against oxidation to Rh(III). Reprinted with permission from reference 102. Copyright 2019 American Chemical Society.

Benzene propenylation with *in situ* aerobic Cu(II) regeneration was performed using (5-FP)Rh(TFA)(η^2 -C₂H₄) with benzene, propylene (30 psig), Cu(OPiv)₂ (240 equivalents) and HOPiv at 150 °C (Reaction I, Scheme 1.4.24). After all of the Cu(II) oxidant is consumed, Cu(OPiv)₂ was regenerated *in situ* by heating the reaction mixture under air at 120 °C for 10 mins followed by propylene purge to remove air. Catalytic activity continues after 10 air recycling steps with ~800 TOs.¹⁰⁶ We also studied oxidative propylene hydrophenylation under aerobic conditions using air as *in situ* oxidant (Reaction II, Scheme 1.4.24, performing catalysis in the presence of air and Cu(II)). Catalysis using 0.001 mol% (5-FP)Rh(TFA)(η^2 -C₂H₄), 240 eq. Cu(OPiv)₂ and 2400 eq. HOPiv under 30 of psig propylene and 1 atm air at 150 °C yielded over 1200 TOs after 48 hours.¹⁰⁶ The L:B ratio increases from 6:1 to 8:1 as catalysis proceeds, which is likely attributed to an undefined side reaction with α -methylstyrene that occurs in the presence of O₂. We reduced the catalyst loading to 0.0001 mol% and demonstrated that > 13,000 TOs are achieved after 336 hours at

150 °C with no evidence of catalyst deactivation.¹⁰⁶

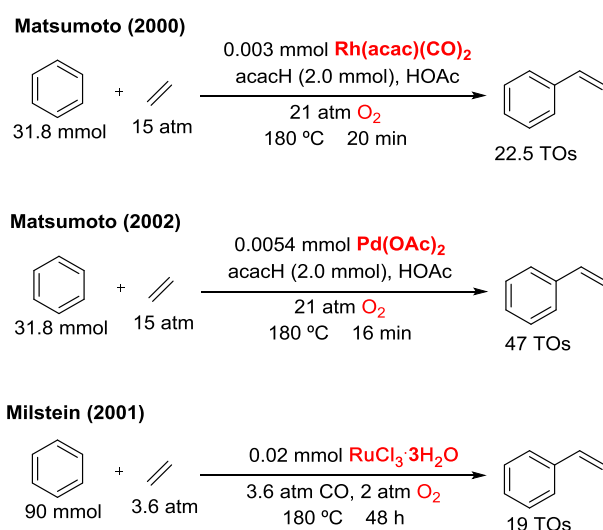


Scheme 1.4.24. (5-FP)Rh(TFA)($\eta^2\text{-C}_2\text{H}_4$) catalyzed benzene propenylation using Cu(OPiv)₂/air as oxidants under aerobic/anaerobic conditions.

1.4.3.4 Aerobic Catalysis Using Air/O₂ as the Sole Oxidant

Unfortunately, the limited stability of the Cu(II) carboxylate co-oxidant gives rise to the formation of side products (*e.g.*, phenyl carboxylate) that results from its thermal degradation. To eliminate the requirement of using co-oxidants, Pd and Ru catalyzed arene alkenylation using electron-deficient acrylates as alkene source with O₂ as the direct oxidant were developed.¹²⁰⁻¹²³ Some of these reported reactions require the use of directing groups.^{120, 122} Only a few examples exist for aerobic styrene production from benzene and ethylene in the absence co-oxidant. Shue and coworkers demonstrated that Pd(OAc)₂ can catalyze benzene ethenylation under O₂ to yield 6 TOs of styrene at 80 °C.¹²⁴ Matsumoto and coworkers reported Pd and Rh catalysts with the addition of acetylacetone affords 47 and 23 TOs of styrene under

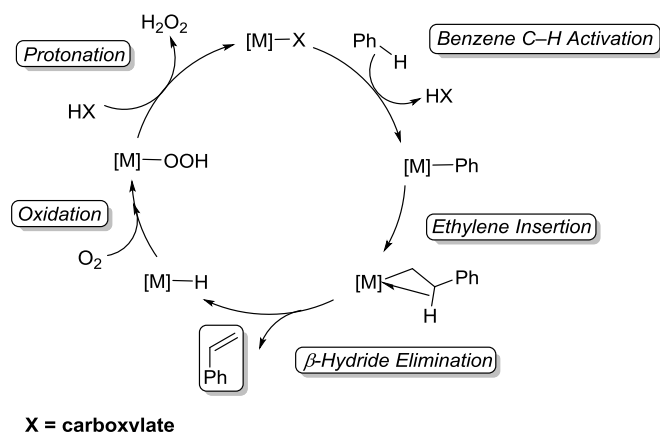
1.55 MPa of ethylene and 2.10 MPa of purified O_2 at 180 °C, respectively (Scheme 1.4.25).^{107, 108} Moreover, Milstein and coworkers reported a Ru(II) catalyst that yields 19 TOs under 2 atm O_2 pressure and 3.6 atm of carbon monoxide (Scheme 1.4.25).¹²⁵ These reactions give low TOs and require harsh conditions including high pressure of pure O_2 and use of carbon monoxide. We recently reported that (5-FP)Rh(TFA)(η^2 -C₂H₄) catalyzes benzene propenylation using unpurified air (1 atm) as the sole oxidant in the absence of Cu(II) to afford > 500 TOs after 240 h with L:B ratio of ~5 (Reaction III, Scheme 1.4.24).



Scheme 1.4.25. Metal-catalyzed aerobic benzene ethylation using O_2 as the sole oxidant

A generic catalytic cycle for metal-catalyzed aerobic styrene production is depicted in Scheme 1.4.26. First, a M-Ph species is generated via benzene C-H activation and one equivalent HX (X = carboxylate) is released. Thereafter, ethylene migratory insertion into the M-Ph bond followed by β -hydride elimination delivers styrene and a M-H intermediate. Next, O_2 inserts into M-H to form the metal hydroperoxide complex. Protonation of M-OOH regenerates the catalytically active

M–X intermediate and releases hydrogen peroxide.



Scheme 1.4.26. Proposed mechanism for metal-catalyzed aerobic styrene production using O₂ as the sole oxidant.

The aim of this dissertation is to discuss the development of d^8 transition metal catalysts for oxidative arene alkenylation. The work discussed herein includes: 1) a detailed experimental mechanistic study regarding the catalytic oxidative vinylation of benzene to form styrene using several diimine-ligated Rh(I) catalyst precursors, including a rationale for observed induction periods, 2) Development and mechanistic study of the ligand-free Rh-catalyzed oxidative conversion of unactivated arenes and alkenes to alkenyl arenes using unpurified air or purified O₂ as the only oxidant in the absence of co-oxidants.

Studies of catalytic benzene alkenylation using different diimine ligated Rh(I) acetate complexes and Cu(OAc)₂ as the oxidant revealed statistically identical results in terms of activity and product selectivity. Under ethylene pressure, two representative diimine ligated rhodium(I) acetate complexes were demonstrated to exchange the diimine ligand with ethylene rapidly to form [Rh(μ-OAc)(η²-C₂H₄)₂]₂ and free diimine. Thus, it was concluded that diimine ligands are not likely

coordinated to the active Rh catalysts under catalytic conditions. At 150 °C under catalytic conditions using commercial $\text{Cu}(\text{OAc})_2$ as the oxidant, $[\text{Rh}(\mu\text{-OAc})(\eta^2\text{-C}_2\text{H}_4)_2]_2$ undergoes rapid decomposition to form catalytically inactive and insoluble Rh species, followed by gradual dissolution of the insoluble Rh to form the soluble Rh, which is active for styrene production. The induction period is a result of the insoluble Rh leaching back into solution to form the soluble active catalyst. The Rh decomposition process can be suppressed and the catalytically active Rh species maintained by using soluble Cu(II) oxidants or $\text{Cu}(\text{OAc})_2$ that has been preheated. In such cases, an induction period is not observed.

We report the oxidative conversion of unactivated arenes and alkenes to alkenyl arenes using unpurified air or purified dioxygen as the only oxidant. This method uses RhCl_3 salt as the catalyst precursor and avoids the use of co-oxidants such as Cu(II). The use of dioxygen as the in situ oxidant gives water as the only by-product of the alkenylation reaction. Conditions to achieve > 1000 turnovers of alkenyl benzene products have been developed. Compared to the Rh catalysis using Cu(II) oxidants, the aerobic reactions give decreased reaction rate and reduced anti-Markovnikov/Markovnikov selectivity when using α -olefins. Mechanistic studies indicate that the reduced L/B selectivity relative to the anaerobic Rh catalysis using Cu(II) oxidants is likely a result of Curtin–Hammett conditions.

1.5 References

1. Ma, Z.; Zaera, F. Heterogeneous Catalysis by Metals in *Encyclopedia of Inorganic Chemistry*; John Wiley & Sons, Ltd: New York, 2006.

-
2. Kozuch, S.; Martin, J. M. L. "Turning over" Definitions in Catalytic Cycles. *ACS Catal.* **2012**, *2*, 2787-2794.
 3. Murzin, D.; Salmi, T., Chapter 2 - Catalysis. In *Catalytic Kinetics*, Murzin, D.; Salmi, T., Eds. Elsevier Science: Amsterdam, 2005; pp 27-72.
 4. Deutschmann, O.; Knözinger, H.; Kochloefl, K.; Turek, T. Heterogeneous Catalysis and Solid Catalysts in *Ullmann's Encyclopedia of Industrial Chemistry*; Wiley-VCH Verlag GmbH & Co. KGaA: 2000.
 5. Rothenberg, G. *Catalysis : Concepts and Green Applications*; Wiley-VCH Verlag GmbH & Co. KGaA: Weinheim, Germany, 2008.
 6. Dijkstra, H. P.; van Klink, G. P. M.; van Koten, G. The Use of Ultra- and Nanofiltration Techniques in Homogeneous Catalyst Recycling. *Acc. Chem. Res.* **2002**, *35*, 798-810.
 7. Cole-Hamilton, D. J. Homogeneous Catalysis--New Approaches to Catalyst Separation, Recovery, and Recycling. *Science* **2003**, *299*, 1702.
 8. Van Leeuwen, P. W. *Homogeneous Catalysis: Understanding the Art*; Springer Science & Business Media: 2006.
 9. Jira, R. Acetaldehyde from Ethylene—a Retrospective on the Discovery of the Wacker Process. *Angew. Chem. Int. Ed.* **2009**, *48*, 9034-9037.
 10. Keith, J. A.; Henry, P. M. The Mechanism of the Wacker Reaction: A Tale of Two Hydroxypalladations. *Angew. Chem. Int. Ed.* **2009**, *48*, 9038-9049.
 11. Eckert, M.; Fleischmann, G.; Jira, R.; Bolt, H. M.; Golka, K. Acetaldehyde in *Ullmann's Encyclopedia of Industrial Chemistry*; Wiley-VCH Verlag GmbH & Co. KGaA: 2000.
 12. Cornils, B.; Herrmann, W. A.; Rasch, M. Otto Roelen, Pioneer in Industrial Homogeneous Catalysis. *Angew. Chem. Int. Ed.* **1994**, *33*, 2144-2163.
 13. Heck, R. F.; Breslow, D. S. The Reaction of Cobalt Hydrotetracarbonyl with Olefins. *J. Am. Chem. Soc.* **1961**, *83*, 4023-4027.
 14. Dümbgen, G.; Neubauer, D. Großtechnische Herstellung Von Oxo-Alkoholen Aus Propylen in Der Basf. *Chem. Ing. Tech.* **1969**, *41*, 974-980.
 15. Cornils, B.; Herrmann, W. A.; Wong, C.-H.; Zanthoff, H. W. Catalysis from a to z: A Concise Encyclopedia, 2408 Seiten, Verlag Wiley-Vch Verlag GmbH & Co. KgaA; 2012.
 16. Bianchi, M.; Piacenti, F.; Frediani, P.; Matteoli, U. Hydroformylation of Deuterated Olefins in the Presence of Cobalt Catalysts: II. Experiments at Low Pressure of Carbon Monoxide. *J. Organomet. Chem.* **1977**, *137*, 361-365.
 17. Hartwig, J. F. Organotransition Metal Chemistry, from Bonding to Catalysis. University Science Books: New York; 2009; Vol. 753, pp 757-578.
 18. Osborn, J. A.; Wilkinson, G.; Young, J. F. Mild Hydroformylation of Olefins Using Rhodium Catalysts. *Chem. Commun. (London)* **1965**, 17-17.
 19. Evans, D.; Osborn, J. A.; Wilkinson, G. Hydroformylation of Alkenes by Use of Rhodium Complex Catalysts. *J. Chem. Soc. A* **1968**, 3133-3142.
 20. Chenier, P. J. *Survey of Industrial Chemistry*; 2nd Ed.; Wiley Vch: New York; 1992.
 21. Sunley, G. J.; Watson, D. J. High Productivity Methanol Carbonylation Catalysis

-
- Using Iridium: The Cativa™ Process for the Manufacture of Acetic Acid. *Catal. Today* **2000**, *58*, 293-307.
22. Forster, D. Mechanistic Pathways in the Catalytic Carbonylation of Methanol by Rhodium and Iridium Complexes. In *Adv. Organomet. Chem.*, Stone, F. G. A.; West, R., Eds. Academic Press; 1979; Vol. 17, pp 255-267.
23. Jones, J. H. The Cativa™ Process for the Manufacture of Acetic Acid: Iridium Catalyst Improves Productivity in an Established Industrial Process. *Platinum Metals Rev.* **2000**, *44*, 94-105.
24. Olah, G. A.; Molnár, Á. *Hydrocarbon Chemistry*; Wiley-Interscience: Hoboken: NJ, 2003; pp 283.
25. Perego, C.; Pollesel, P. Advances in Aromatics Processing Using Zeolite Catalysts. *Advances in Nanoporous Materials*; Elsevier: 2010; Vol. 1, pp 97-149.
26. Chen, S. S. *Kirk-Othmer Encyclopedia of Chemical Technology*; John Wiley & Sons, Inc.: Hoboken: NJ, 2000; pp 325-357.
27. Wittcoff, H. A.; Reuben, B. G.; Plotkin, J. S. Chemicals and Polymers from Ethylene. In *Industrial Organic Chemicals*; John Wiley & Sons, Inc.: Hoboken: NJ, 2004; pp 100-166.
28. Garside, M. *Guide to the Business of Chemistry - 2019*; American Chemistry Council: 2019.
29. Gerzeliev, I. M.; Khadzhiev, S. N.; Sakharova, I. E. Ethylbenzene Synthesis and Benzene Transalkylation with Diethylbenzenes on Zeolite Catalysts. *Pet. Chem.* **2011**, *51*, 39-48.
30. Perego, C.; Ingallina, P. Combining Alkylation and Transalkylation for Alkylaromatic Production. *Green Chemistry* **2004**, *6*, 274-279.
31. Čejka, J.; Wichterlová, B. Acid-Catalyzed Synthesis of Mono- and Dialkyl Benzenes over Zeolites: Active Sites, Zeolite Topology, and Reaction Mechanisms. *Cat. Rev.* **2002**, *44*, 375-421.
32. Weber, M.; Kleine-Boymann, M. Phenol in *Ullmann's Encyclopedia of Industrial Chemistry*; Wiley-VCH Verlag GmbH & Co. KGaA: 2000.
33. Perego, C.; Ingallina, P. Recent Advances in the Industrial Alkylation of Aromatics: New Catalysts and New Processes. *Catal. Today* **2002**, *73*, 3-22.
34. Perego, C.; Ingallina, P. Combining Alkylation and Transalkylation for Alkylaromatic Production. *Green Chem.* **2004**, *6*, 274-279.
35. Marcilly, C. Superacids and Bases of Interest in Catalysis. In *Acido-Basic Catalysis* Editions Technip: Paris; 2006; Vol. 1, pp 57-130.
36. Caro, J.; Noack, M.; Ernst, S. Chapter 1 - Zeolite Membranes – Status and Prospective. In *Advances in Nanoporous Materials*; Elsevier: 2010; Vol. 1, pp 1-96.
37. Olah, G. A.; Kuhn, S. J.; Hardie, B. A. Aromatic Substitution. XVII.1 Ferric Chloride and Aluminum Chloride Catalyzed Chlorination of Benzene, Alkylbenzenes, and Halobenzenes. *J. Am. Chem. Soc.* **1964**, *86*, 1055-1060.
38. Olah, G. A.; Kuhn, S. J.; Flood, S. H.; Hardie, B. A. Aromatic Substitution. Xv.1 Ferric Chloride Catalyzed Bromination of Halobenzenes in Nitromethane Solution. *J. Am. Chem. Soc.* **1964**, *86*, 1044-1046.
39. de Almeida, J. L. G.; Dufaux, M.; Taarit, Y. B.; Naccache, C. Linear

-
- Alkylbenzene. *J. Am. Oil Chem. Soc.* **1994**, *71*, 675-694.
40. Kocal, J. A.; Vora, B. V.; Imai, T. Production of Linear Alkylbenzenes. *Appl. Catal., A* **2001**, *221*, 295-301.
41. Baumgartner, F. N. Relation of Molecular Structure to Detergency of Some Alkylbenzene Sulfonates. *Ind. Eng. Chem.* **1954**, *46*, 1349-1352.
42. Lee, E. H. Iron Oxide Catalysts for Dehydrogenation of Ethylbenzene in the Presence of Steam. *Cat. Rev.* **1974**, *8*, 285-305.
43. Negishi, E.-i.; Anastasia, L. Palladium-Catalyzed Alkynylation. *Chem. Rev.* **2003**, *103*, 1979-2018.
44. Stille, J. K. The Palladium-Catalyzed Cross-Coupling Reactions of Organotin Reagents with Organic Electrophiles. *Angew. Chem. Int. Ed.* **1986**, *25*, 508-524.
45. Stanforth, S. P. Catalytic Cross-Coupling Reactions in Biaryl Synthesis. *Tetrahedron* **1998**, *54*, 263-303.
46. Hassan, J.; Sévignon, M.; Gozzi, C.; Schulz, E.; Lemaire, M. Aryl–Aryl Bond Formation One Century after the Discovery of the Ullmann Reaction. *Chem. Rev.* **2002**, *102*, 1359.
47. Beletskaya, I. P.; Cheprakov, A. V. The Heck Reaction as a Sharpening Stone of Palladium Catalysis. *Chem. Rev.* **2000**, *100*, 3009-3066.
48. Suzuki, A. Organoborates in New Synthetic Reactions. *Acc. Chem. Res.* **1982**, *15*, 178-184.
49. Maaliki, C.; Thiery, E.; Thibonnet, J. Emergence of Copper-Mediated Formation of C–C Bonds. *Eur. J. Org. Chem.* **2017**, *2017*, 209-228.
50. Varun, B. V.; Dhineshkumar, J.; Bettadapur, K. R.; Siddaraju, Y.; Alagiri, K.; Prabhu, K. R. Recent Advancements in Dehydrogenative Cross Coupling Reactions for C–C Bond Formation. *Tetrahedron Lett.* **2017**, *58*, 803-824.
51. Zhang, Y.-F.; Shi, Z.-J. Upgrading Cross-Coupling Reactions for Biaryl Syntheses. *Acc. Chem. Res.* **2019**, *52*, 161-169.
52. Biffis, A.; Centomo, P.; Del Zotto, A.; Zecca, M. Pd Metal Catalysts for Cross-Couplings and Related Reactions in the 21st Century: A Critical Review. *Chem. Rev.* **2018**, *118*, 2249-2295.
53. King, A. O.; Yasuda, N. Palladium-Catalyzed Cross-Coupling Reactions in the Synthesis of Pharmaceuticals. *Organometallics in Process Chemistry. Topics in Organometallic Chemistry*; Heidelberg: Springer; 2004; pp 205-245.
54. Hartwig, J. F. *Organotransition Metal Chemistry, from Bonding to Catalysis*; University Science Books: New York; 2010.
55. Labinger, J. A.; Bercaw, J. E. Understanding and Exploiting C–H Bond Activation. *Nature* **2002**, *417*, 507-514.
56. Gol'dshleger, N. F.; Tyabin, M. B.; Shilov, A. E.; Shteinman, A. A. Activation of Saturated Hydrocarbons. Deuterium-Hydrogen Exchange in Solutions of Transition Metal Complexes. *Zh. Fiz. Khim.* **1969**, *43*, 2174-2175.
57. Webb, J. R.; Burgess, S. A.; Cundari, T. R.; Gunnoe, T. B. Activation of Carbon–Hydrogen Bonds and Dihydrogen by 1,2-Ch-Addition across Metal–Heteroatom Bonds. *Dalton Trans.* **2013**, *42*, 16646-16665.
58. Waterman, R. Σ -Bond Metathesis: A 30-Year Retrospective. *Organometallics*

2013, 32, 7249-7263.

59. Thompson, M. E.; Baxter, S. M.; Bulls, A. R.; Burger, B. J.; Nolan, M. C.; Santarsiero, B. D.; Schaefer, W. P.; Bercaw, J. E. .Sigma.-Bond Metathesis for Carbon-Hydrogen Bonds of Hydrocarbons and Sc-R (R = H, Alkyl, Aryl) Bonds of Permethylscandocene Derivatives. Evidence for Noninvolvement of The .Pi. System in Electrophilic Activation of Aromatic and Vinylic C-H Bonds. *J. Am. Chem. Soc.* **1987**, *109*, 203-219.

60. Oxgaard, J.; Tenn, W. J.; Nielsen, R. J.; Periana, R. A.; Goddard, W. A. Mechanistic Analysis of Iridium Heteroatom C-H Activation: Evidence for an Internal Electrophilic Substitution Mechanism. *Organometallics* **2007**, *26*, 1565-1567.

61. Wolczanski, P. T. Activation of Carbon-Hydrogen Bonds Via 1,2-Rh-Addition/-Elimination to Early Transition Metal Imides. *Organometallics* **2018**, *37*, 505-516.

62. Matsumoto, T.; Taube, D. J.; Periana, R. A.; Taube, H.; Yoshida, H. Anti-Markovnikov Olefin Arylation Catalyzed by an Iridium Complex. *J. Am. Chem. Soc.* **2000**, *122*, 7414-7415.

63. Periana, R. A.; Liu, X. Y.; Bhalla, G. Novel Bis-Acac-O, O-Ir (III) Catalyst for Anti-Markovnikov, Hydroarylation of Olefins Operates by Arene C-H Activation. *Chem. Commun.* **2002**, 3000-3001.

64. Bhalla, G.; Liu, X. Y.; Oxgaard, J.; Goddard, W. A.; Periana, R. A. Synthesis, Structure, and Reactivity of O-Donor Ir(III) Complexes: C-H Activation Studies with Benzene. *J. Am. Chem. Soc.* **2005**, *127*, 11372-11389.

65. Bhalla, G.; Bischof, S. M.; Ganesh, S. K.; Liu, X. Y.; Jones, C. J.; Borzenko, A.; Tenn, W. J.; Ess, D. H.; Hashiguchi, B. G.; Lokare, K. S.; Leung, C. H.; Oxgaard, J.; Goddard, W. A.; Periana, R. A. Mechanism of Efficient Anti-Markovnikov Olefin Hydroarylation Catalyzed by Homogeneous Ir(III) Complexes. *Green Chem.* **2011**, *13*, 69-81.

66. Oxgaard, J.; Muller, R. P.; Goddard, W. A.; Periana, R. A. Mechanism of Homogeneous Ir(III) Catalyzed Regioselective Arylation of Olefins. *J. Am. Chem. Soc.* **2004**, *126*, 352-363.

67. Bhalla, G.; Oxgaard, J.; Goddard, W. A.; Periana, R. A. Anti-Markovnikov Hydroarylation of Unactivated Olefins Catalyzed by a Bis-Tropolonato Iridium(III) Organometallic Complex. *Organometallics* **2005**, *24*, 3229-3232.

68. Lail, M.; Arrowood, B. N.; Gunnoe, T. B. Addition of Arenes to Ethylene and Propene Catalyzed by Ruthenium. *J. Am. Chem. Soc.* **2003**, *125*, 7506-7507.

69. Lail, M.; Bell, C. M.; Conner, D.; Cundari, T. R.; Gunnoe, T. B.; Petersen, J. L. Experimental and Computational Studies of Ruthenium(II)-Catalyzed Addition of Arene C-H Bonds to Olefins. *Organometallics* **2004**, *23*, 5007-5020.

70. Foley, N. A.; Lail, M.; Gunnoe, T. B.; Cundari, T. R.; Boyle, P. D.; Petersen, J. L. Combined Experimental and Computational Study of $\text{TpRu}\{\text{P}(\text{pyr})_3\}(\text{NCMe})\text{Me}$ (pyr = N-pyrrolyl): Inter- and Intramolecular Activation of C-H Bonds and the Impact of Sterics on Catalytic Hydroarylation of Olefins. *Organometallics* **2007**, *26*, 5507-5516.

71. Foley, N. A.; Lail, M.; Lee, J. P.; Gunnoe, T. B.; Cundari, T. R.; Petersen,

-
- J. L. Comparative Reactivity of Tpru(L)(Ncme)Ph (L = Co or Pme₃): Impact of Ancillary Ligand L on Activation of Carbon-Hydrogen Bonds Including Catalytic Hydroarylation and Hydrovinylation/Oligomerization of Ethylene. *J. Am. Chem. Soc.* **2007**, *129*, 6765–6781.
72. Foley, N. A.; Ke, Z.; Gunnoe, T. B.; Cundari, T. R.; Petersen, J. L. Aromatic C–H Activation and Catalytic Hydrophenylation of Ethylene by Tpru{P(Och₂)₃cet}(Ncme)Ph. *Organometallics* **2008**, *27*, 3007-3017.
73. Joslin, E. E.; McMullin, C. L.; Gunnoe, T. B.; Cundari, T. R.; Sabat, M.; Myers, W. H. Catalytic Hydroarylation of Ethylene Using TpRu(L)(NCMe)Ph (L = 2,6,7-Trioxa-1-phosphabicyclo[2,2,1]heptane): Comparison to TpRu(L')(NCMe)Ph Systems (L' = CO, PMe₃, P(pyr)₃, or P(OCH₂)₃CEt). *Organometallics* **2012**, *31*, 6851-6860.
74. Burgess, S. A.; Joslin, E. E.; Gunnoe, T. B.; Cundari, T. R.; Sabat, M.; Myers, W. H. Hydrophenylation of Ethylene Using a Cationic Ru(II) Catalyst: Comparison to a Neutral Ru(II) Catalyst. *Chem. Sci.* **2014**, *5*, 4355-4366.
75. Foley, N. A.; Lee, J. P.; Ke, Z.; Gunnoe, T. B.; Cundari, T. R. Ru(II) Catalysts Supported by Hydridotris(pyrazolyl)borate for the Hydroarylation of Olefins: Reaction Scope, Mechanistic Studies, and Guides for the Development of Improved Catalysts. *Acc. Chem. Res.* **2009**, *42*, 585-597.
76. Clement, M. L.; Grice, K. A.; Luedtke, A. T.; Kaminsky, W.; Goldberg, K. I. Platinum(II) Olefin Hydroarylation Catalysts: Tuning Selectivity for the Anti-Markovnikov Product. *Chem. - Eur. J.* **2014**, *20*, 17287-17291.
77. Luedtke, A. T.; Goldberg, K. I. Intermolecular Hydroarylation of Unactivated Olefins Catalyzed by Homogeneous Platinum Complexes. *Angew. Chem., Int. Ed.* **2008**, *47*, 7694-7696.
78. Suslick, B. A.; Liberman-Martin, A. L.; Wambach, T. C.; Tilley, T. D. Olefin Hydroarylation Catalyzed by (Pyridyl-Indolate)Pt(II) Complexes: Catalytic Efficiencies and Mechanistic Aspects. *ACS Catal.* **2017**, *7*, 4313-4322.
79. McKeown, B. A.; Foley, N. A.; Lee, J. P.; Gunnoe, T. B. Hydroarylation of Unactivated Olefins Catalyzed by Platinum(II) Complexes. *Organometallics* **2008**, *27*, 4031-4033.
80. McKeown, B. A.; Gonzalez, H. E.; Friedfeld, M. R.; Brosnahan, A. M.; Gunnoe, T. B.; Cundari, T. R.; Sabat, M. Platinum(II)-Catalyzed Ethylene Hydrophenylation: Switching Selectivity between Alkyl- and Vinylbenzene Production. *Organometallics* **2013**, *32*, 2857-2865.
81. McKeown, B. A.; Gonzalez, H. E.; Gunnoe, T. B.; Cundari, T. R.; Sabat, M. Pt^{II}-Catalyzed Ethylene Hydrophenylation: Influence of Dipyridyl Chelate Ring Size on Catalyst Activity and Longevity. *ACS Catal.* **2013**, *3*, 1165-1171.
82. McKeown, B. A.; Gonzalez, H. E.; Michaelos, T.; Gunnoe, T. B.; Cundari, T. R.; Crabtree, R. H.; Sabat, M. Control of Olefin Hydroarylation Catalysis Via a Sterically and Electronically Flexible Platinum(II) Catalyst Scaffold. *Organometallics* **2013**, *32*, 3903-3913.
83. McKeown, B. A.; Prince, B. M.; Ramiro, Z.; Gunnoe, T. B.; Cundari, T. R. Pt^{II}-Catalyzed Hydrophenylation of α -Olefins: Variation of Linear/Branched Products

-
- as a Function of Ligand Donor Ability. *ACS Catal.* **2014**, *4*, 1607-1615.
84. McKeown, B. A.; Gonzalez, H. E.; Friedfeld, M. R.; Gunnoe, T. B.; Cundari, T. R.; Sabat, M. Mechanistic Studies of Ethylene Hydrophenylation Catalyzed by Bipyridyl Pt(II) Complexes. *J. Am. Chem. Soc.* **2011**, *133*, 19131-19152.
85. Foley, N. A.; Lee, J. P.; Ke, Z.; Gunnoe, T. B.; Cundari, T. R. Ru (II) Catalysts Supported by Hydridotris(Pyrazolyl)Borate for the Hydroarylation of Olefins: Reaction Scope, Mechanistic Studies, and Guides for the Development of Improved Catalysts. *Acc. Chem. Res.* **2009**, *42*, 585.
86. McKeown, B. A.; Gonzalez, H. E.; Friedfeld, M. R.; Gunnoe, T. B.; Cundari, T. R.; Sabat, M. Mechanistic Studies of Ethylene Hydrophenylation Catalyzed by Bipyridyl Pt(II) Mocomplexes. *J Am Chem Soc* **2011**, *133*, 19131-19152.
87. She, Z.; Shi, Y.; Huang, Y.; Cheng, Y.; Song, F.; You, J. Versatile Palladium-Catalyzed C–H Olefination of (Hetero)Arenes at Room Temperature. *Chem. Commun.* **2014**, *50*, 13914-13916.
88. Wang, P.; Verma, P.; Xia, G.; Shi, J.; Qiao, J. X.; Tao, S.; Cheng, P. T. W.; Poss, M. A.; Farmer, M. E.; Yeung, K.-S.; Yu, J.-Q. Ligand-Accelerated Non-Directed C–H Functionalization of Arenes. *Nature* **2017**, *551*, 489-493.
89. Vora, H. U.; Silvestri, A. P.; Engelin, C. J.; Yu, J.-Q. Rhodium(II)-Catalyzed Nondirected Oxidative Alkenylation of Arenes: Arene Loading at One Equivalent. *Angew. Chem. Int. Ed.* **2014**, *53*, 2683-2686.
90. Kubota, A.; Emmert, M. H.; Sanford, M. S. Pyridine Ligands as Promoters in PdII/O-Catalyzed C–H Olefination Reactions. *Org. Lett.* **2012**, *14*, 1760-1763.
91. Agasti, S.; Dey, A.; Maiti, D. Traceless Directing Group Mediated Branched Selective Alkenylation of Unbiased Arenes. *Chem. Commun.* **2016**, *52*, 12191-12194.
92. Ying, C.-H.; Yan, S.-B.; Duan, W.-L. 2-Hydroxy-1,10-Phenanthroline Vs 1,10-Phenanthroline: Significant Ligand Acceleration Effects in the Palladium-Catalyzed Oxidative Heck Reaction of Arenes. *Org. Lett.* **2014**, *16*, 500-503.
93. Liebov, N. S.; Zhu, W.; Chen, J.; Webster-Gardiner, M. S.; Schinski, W. L.; Gunnoe, T. B. Rhodium-Catalyzed Alkenylation of Toluene Using 1-Pentene: Regioselectivity to Generate Precursors for Bicyclic Compounds. *Organometallics* **2019**, *38*, 3860-3870.
94. Ghosh, K.; Mihara, G.; Nishii, Y.; Miura, M. Nondirected C-H Alkenylation of Arenes with Alkenes under Rhodium Catalysis. *Chem. Lett.* **2018**, *48*, 148-151.
95. Patureau, F. W.; Nimphius, C.; Glorius, F. Rh Catalyzed C–H Activation and Oxidative Olefination without Chelate Assistance: On the Reactivity of Bromoarenes. *Org. Lett.* **2011**, *13*, 6346-6349.
96. Taube, D.; Periana, R.; Matsumoto, T. Oxidative Coupling of Olefins and Aromatics Using a Rhodium Catalyst and a Copper(II) Redox Agent. U.S. Patent 6127590A, 2000.
97. Fujiwara, Y.; Moritani, I.; Danno, S.; Asano, R.; Teranishi, S. Aromatic Substitution of Olefins. Vi. Arylation of Olefins with Palladium(II) Acetate. *J. Am. Chem. Soc.* **1969**, *91*, 7166-7169.
98. Sasaki, K.; Sakakura, T.; Tokunaga, Y.; Wada, K.; Tanaka, M. C=C Double

Bond Insertion in Catalytic C–H Activation. Dehydrogenative Cross Coupling of Arenes with Olefins. *Chem. Lett.* **1988**, *17*, 685-688.

99. Hong, P.; Yamazaki, H. Rhodium Carbonyl-Catalyzed Activation of Carbon-Hydrogen Bonds for Application in Organic Synthesis.: V. Phenylation of Olefins with Benzenes. *J. Mol. Catal.* **1984**, *26*, 297-311.

100. Jia, X.; Gary, J. B.; Gu, S.; Cundari, T. R.; Gunnoe, T. B. Oxidative Hydrophenylation of Ethylene Using a Cationic Ru(II) Catalyst: Styrene Production with Ethylene as the Oxidant. *Isr. J. Chem.* **2017**, *57*, 1037-1046.

101. Webster-Gardiner, M. S.; Fu, R.; Fortman, G. C.; Nielsen, R. J.; Gunnoe, T. B.; Goddard III, W. A. Arene C–H Activation Using Rh(I) Catalysts Supported by Bidentate Nitrogen Chelates. *Catal. Sci. Technol.* **2015**, *5*, 96-100.

102. Vaughan, B. A.; Webster-Gardiner, M. S.; Cundari, T. R.; Gunnoe, T. B. A Rhodium Catalyst for Single-Step Styrene Production from Benzene and Ethylene. *Science* **2015**, *348*, 421-424.

103. Vaughan, B. A.; Khani, S. K.; Gary, J. B.; Kammert, J. D.; Webster-Gardiner, M. S.; McKeown, B. A.; Davis, R. J.; Cundari, T. R.; Gunnoe, T. B. Mechanistic Studies of Single-Step Styrene Production Using a Rhodium(I) Catalyst. *J. Am. Chem. Soc.* **2017**, *139*, 1485-1498.

104. Webster-Gardiner, M. S.; Chen, J.; Vaughan, B. A.; McKeown, B. A.; Schinski, W.; Gunnoe, T. B. Catalytic Synthesis of “Super” Linear Alkenyl Arenes Using an Easily Prepared Rh(I) Catalyst. *J. Am. Chem. Soc.* **2017**, *139*, 5474-5480.

105. Röper, M.; Gehrler, E.; Narbeshuber, T.; Siegel, W. In *Ullmann's Encyclopedia of Industrial Chemistry*; Wiley-VCH Verlag GmbH & Co. KGaA: Weinheim, Germany, 2000.

106. Chen, J.; Nielsen, R. J.; Goddard, W. A.; McKeown, B. A.; Dickie, D. A.; Gunnoe, T. B. Catalytic Synthesis of Superlinear Alkenyl Arenes Using a Rh(I) Catalyst Supported by a “Capping Arene” Ligand: Access to Aerobic Catalysis. *J. Am. Chem. Soc.* **2018**, *140*, 17007-17018.

107. Matsumoto, T.; Yoshida, H. Oxidative Arylation of Ethylene with Benzene to Produce Styrene. *Chem. Lett.* **2000**, *29*, 1064-1065.

108. Matsumoto, T.; Periana, R. A.; Taube, D. J.; Yoshida, H. Direct Synthesis of Styrene by Rhodium-Catalyzed Oxidative Arylation of Ethylene with Benzene. *J. Catal.* **2002**, *206*, 272-280.

109. Jia, X.; Foley, A. M.; Liu, C.; Vaughan, B. A.; McKeown, B. A.; Zhang, S.; Gunnoe, T. B. Styrene Production from Benzene and Ethylene Catalyzed by Palladium(II): Enhancement of Selectivity toward Styrene Via Temperature-Dependent Vinyl Ester Consumption. *Organometallics* **2019**, *38*, 3532-3541.

110. Babu, B. P.; Meng, X.; Bäckvall, J.-E. Aerobic Oxidative Coupling of Arenes and Olefins through a Biomimetic Approach. *Chem. Eur. J.* **2013**, *19*, 4140-4145.

111. Obora, Y.; Ishii, Y. Pd(II)/Hpmov-Catalyzed Direct Oxidative Coupling Reaction of Benzenes with Olefins. *Molecules* **2010**, *15*, 1487-1500.

112. Yokota, T.; Tani, M.; Sakaguchi, S.; Ishii, Y. Direct Coupling of Benzene with Olefin Catalyzed by Pd(OAc)₂ Combined with Heteropolyoxometalate under

-
- Dioxygen. *J. Am. Chem. Soc.* **2003**, *125*, 1476-1477.
113. Yamada, T.; Sakakura, A.; Sakaguchi, S.; Obora, Y.; Ishii, Y. Oxidative Arylation of Ethylene with Benzene Catalyzed by Pd(Oac)₂/Heteropoly Acid/O₂ System. *New J. Chem.* **2008**, *32*, 738-742.
114. Vilella-Arribas, L.; García-Melchor, M.; Balcells, D.; Lledós, A.; López, J. A.; Sancho, S.; Villarroya, B. E.; del Río, M. P.; Ciriano, M. A.; Tejel, C. Rhodium Complexes Promoting C–O Bond Formation in Reactions with Oxygen: The Role of Superoxo Species. *Chem. Eur. J.* **2017**, *23*, 5232-5243.
115. Ahijado, M.; Braun, T.; Noveski, D.; Kocher, N.; Neumann, B.; Stalke, D.; Stammer, H.-G. Rhodium-Mediated Formation of Peroxides from Dioxygen: Isolation of Hydroperoxo, Silylperoxo, and Methylperoxo Intermediates. *Angew. Chem. Int. Ed.* **2005**, *44*, 6947-6951.
116. Praetorius, J. M.; Allen, D. P.; Wang, R.; Webb, J. D.; Grein, F.; Kennepohl, P.; Crudden, C. M. N-Heterocyclic Carbene Complexes of Rh: Reaction with Dioxygen without Oxidation. *J. Am. Chem. Soc.* **2008**, *130*, 3724-3725.
117. Fu, R.; O'Reilly, M. E.; Nielsen, R. J.; Goddard III, W. A.; Gunnoe, T. B. Rhodium Bis(Quinolinyl)Benzene Complexes for Methane Activation and Functionalization. *Chem. Eur. J.* **2015**, *21*, 1286-1293.
118. O'Reilly, M. E.; Johnson, S. I.; Nielsen, R. J.; Goddard, W. A.; Gunnoe, T. B. Transition-Metal-Mediated Nucleophilic Aromatic Substitution with Acids. *Organometallics* **2016**, *35*, 2053-2056.
119. O'Reilly, M. E.; Fu, R.; Nielsen, R. J.; Sabat, M.; Goddard, W. A.; Gunnoe, T. B. Long-Range C–H Bond Activation by RhIII-Carboxylates. *J. Am. Chem. Soc.* **2014**, *136*, 14690-14693.
120. Bechtoldt, A.; Tirler, C.; Raghuvanshi, K.; Warratz, S.; Kornhaas, C.; Ackermann, L. Ruthenium Oxidase Catalysis for Site-Selective C–H Alkenylations with Ambient O₂ as the Sole Oxidant. *Angew. Chem. Int. Ed.* **2016**, *55*, 264-267.
121. Zhang, Y.-H.; Shi, B.-F.; Yu, J.-Q. Pd(II)-Catalyzed Olefination of Electron-Deficient Arenes Using 2,6-Dialkylpyridine Ligands. *J. Am. Chem. Soc.* **2009**, *131*, 5072-5074.
122. Gandeepan, P.; Cheng, C.-H. Allylic Carbon–Carbon Double Bond Directed Pd-Catalyzed Oxidative Ortho-Olefination of Arenes. *J. Am. Chem. Soc.* **2012**, *134*, 5738-5741.
123. Dams, M.; De Vos, D. E.; Celen, S.; Jacobs, P. A. Toward Waste-Free Production of Heck Products with a Catalytic Palladium System under Oxygen. *Angew. Chem. Int. Ed.* **2003**, *42*, 3512-3515.
124. Shue, R. S. Catalytic Coupling of Aromatics and Olefins by Homogeneous Palladium(II) Compounds under Oxygen. *J. Chem. Soc. D* **1971**, 1510-1511.
125. Weissman, H.; Song, X.; Milstein, D. Ru-Catalyzed Oxidative Coupling of Arenes with Olefins Using O₂. *J. Am. Chem. Soc.* **2001**, *123*, 337-338.

2 Mechanistic Studies of Styrene Production

Catalyzed by Rh Complexes with Diimine Ligands

This chapter is adapted from “Mechanistic Studies of Single-Step Styrene Production Catalyzed by Rh Complexes with Diimine Ligands: An Evaluation of the Role of Ligands and Induction Period. Zhu, W.; Luo, Z.; Chen, J.; Liu, C.; Yang, L.; Dickie, D. A.; Liu, N.; Zhang, S.; Davis, R. J.; Gunnoe, T. B. *ACS Catal.* **2019**, *9*, 7457-7475.” Copyright 2019 American Chemical Society. As highlighted below, parts of this work were performed in collaboration with Davis group, Sen group at the University of Virginia and Goddard group at the California Institute of Technology.

2.1 Introduction

Alkyl and alkenyl arenes serve as an important raw material for plastics, elastomers, pharmaceuticals, and fine chemicals.¹⁻⁵ Alkyl and alkenyl arenes are currently produced by initial acid-catalyzed arene alkylation.^{1-2, 5-8} For example, the current method for the industrial production of styrene involves Friedel-Crafts or zeolite-catalyzed benzene ethylation using ethylene to generate ethylbenzene that is subsequently dehydrogenated.⁹ This method requires multiple steps, including a trans-alkylation reaction that converts poly-ethylbenzene products and benzene to ethylbenzene, and it consumes substantial energy.^{6-8, 10-11} The transition metal-mediated Heck reaction is able to accomplish arene alkenylation, but it usually incorporates an aryl halide or pseudohalide and a second organometallic reagent, which leads to the generation of a stoichiometric amount of metal-containing

byproduct as well as halogenated byproducts.¹²⁻¹⁵

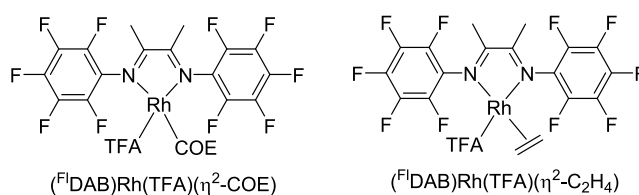
Transition metal-catalyzed arene alkenylation that proceeds by arene C–H activation and olefin insertion offers possible advantages over acid-catalyzed processes. Potential advantages include: a) single-step alkenylation via β -hydride elimination, b) selective production of linear 1-aryl alkene, c) conversions of electron-deficient arenes, d) complementary regioselectivity for substituted arenes, and e) inhibition of polyalkylation. Although a variety of transition metal catalysts have been designed to achieve the net addition of an aromatic C–H bond across olefinic C=C bonds (*i.e.*, olefin hydroarylation) to synthesize alkyl aromatics,¹⁶⁻³⁸ examples of the direct conversion of benzene (or related arenes such as toluene or xylenes) and unfunctionalized olefins to alkenyl arenes are relatively rare.^{24, 39-48} Reported catalysts are generally based on rhodium, ruthenium, platinum or palladium. Despite the success of these catalysts, room for improvement remains. Catalyst longevity is limited.^{19, 49-50} For example, our studies of Pt(II) catalysts demonstrate the ability to control the selectivity for styrene versus ethylbenzene formation. However, for catalysts that are selective for styrene formation, we are unable to develop conditions to prevent decomposition via the formation of Pt(s).²⁴ Also, Ru, Ir, and Pt catalysts show limited selectivity for 1-aryl alkane products in the conversion of unactivated arenes and α -olefins.^{16-17, 32-34, 26} Furthermore, these reported Ru, Ir, and Pt catalysts for arene alkylation produced undesired polyalkylated arene products.^{16-17,}

32-34, 26

Rh is known to activate aromatic C–H bonds as well as mediate olefin insertion.

We speculated that the reduction of Rh(I) to Rh(0) might be less thermodynamically favorable relative to the reduction of Pt(II) to Pt(0). Hong and coworkers reported that the catalyst precursor $\text{Rh}_4(\text{CO})_{12}$ produces 472 TONs of styrene from benzene and ethylene under CO pressure, but selectivity is an issue as 809 TOs of 3-pentanone are formed.³⁹ Periana and coworkers reported a Rh(III) catalyst that gives 24 TOs of styrene {36% yield relative to Cu(II)}.⁴⁰ Tanaka and coworkers disclosed a Rh(I) catalyst that produces 3 TOs of styrene under irradiation along with 4 TOs of biphenyl.⁴⁴ In general, these catalysts are limited by low selectivity, low yield, low TONs, and/or the use of non-air-recyclable oxidants.

Previous studies suggest that the activation barrier for olefin insertion into Pt(II) aryl bonds may be higher for charge-neutral complexes than for cationic complexes.²⁶ And, we anticipated that activation barriers for ethylene insertion into Rh(I)–Ph bonds of Rh(I) complexes might be higher than those of cationic Pt(II) complexes. Thus, we first considered that electron-withdrawing diimine ligands might facilitate olefin insertion. In addition, we had reported that the Rh(I) complex $(^{\text{Fl}}\text{DAB})\text{Rh}(\text{TFA})(\eta^2\text{-COE})$ ($^{\text{Fl}}\text{DAB}$ = N,N'-bis(pentafluorophenyl)-2,3-dimethyl-1,4-diaza-1,3-butadiene; TFA = trifluoroacetate; COE = cyclooctene, Scheme 2.1.1) is a catalyst precursor for arene H/D exchange in trifluoroacetic acid.⁵¹



Scheme 2.1.1. Structures of $(^{\text{Fl}}\text{DAB})\text{Rh}(\text{TFA})(\eta^2\text{-COE})$ and

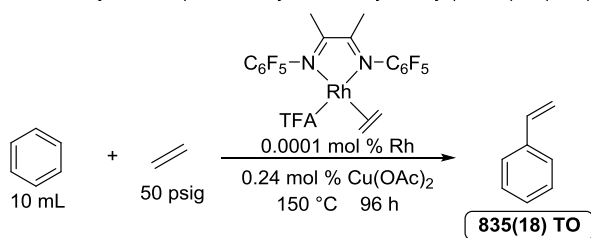
$(^{\text{Fl}}\text{DAB})\text{Rh}(\text{TFA})(\eta^2\text{-C}_2\text{H}_4)$.

Previously, our group reported a Rh(I) complex, $(^{\text{Fl}}\text{DAB})\text{Rh}(\text{TFA})(\eta^2\text{-C}_2\text{H}_4)$ ($^{\text{Fl}}\text{DAB} = N,N'$ -bis(pentafluorophenyl)-2,3-dimethyl-1,4-diaza-1,3-butadiene; TFA = trifluoroacetate), that serves as a catalyst precursor for the direct oxidative conversion of benzene and ethylene to styrene with over 800 turnover numbers (TONs) and quantitative yield relative to the air-recyclable Cu(II) oxidant (Scheme 2.1.2).⁵¹⁻⁵² We also reported that the simple Rh(I) salt, $[\text{Rh}(\mu\text{-OAc})(\eta^2\text{-C}_2\text{H}_4)_2]_2$, can catalyze the oxidative reaction of α -olefins and arenes to produce alkenyl arenes using $\text{Cu}(\text{OAc})_2$ as the oxidant with up to 10:1 linear:branched product ratio and >1470 total catalytic turnovers (TOs; Scheme 2.1.2).⁵³ Recently, we reported that an air-stable Rh catalyst, $(5\text{-FP})\text{Rh}(\text{TFA})(\eta^2\text{-C}_2\text{H}_4)$ (TFA = trifluoroacetate, 5-FP = 1,2-bis(*N*-7-azaindolyl)benzene), can catalyze aerobic oxidative arene alkenylation to selectively produce linear alkenyl arenes with *in situ* air as the terminal oxidant.⁵⁴ Previous mechanistic studies of styrene production using $(^{\text{Fl}}\text{DAB})\text{Rh}(\text{TFA})(\eta^2\text{-C}_2\text{H}_4)$ as a catalyst precursor revealed complicated kinetics including observation of an induction period under some conditions.⁵² Microscopy and filtration experiments after the induction period suggested that Rh nanoparticles are not likely responsible for the observed catalytic arene alkenylation. Based on mechanistic studies, the proposed catalytic cycle is initiated by Rh-mediated activation of the C–H bond of benzene by a Rh–carboxylate complex to yield a Rh–Ph intermediate, rate-limiting olefin insertion into a Rh–Ph bond to produce a Rh–CH₂CH₂Ph intermediate, and β -hydride elimination. the resulting Rh–H intermediates react with Cu(II) to regenerate the

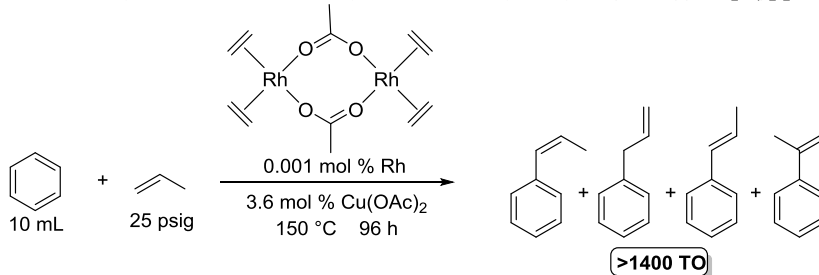
active catalyst (Scheme 2.1.3). The kinetic studies suggest two divergent and competing pathways whose contributions vary with $[C_2H_4]$ (Scheme 2.1.3). At low ethylene concentration, the pathway that proceeds through a binuclear Rh intermediate **D-1** would give rise to half-order kinetics with respect to Rh. At high ethylene concentration, the pathway that proceeds through monomeric Rh intermediates **M-1** would give rise to first-order kinetics with respect to Rh. Despite detailed previous studies, the exact identities of actual molecular catalyst and intermediates involved in the cycle are challenging to determine and remain under study.

Previous work:

a) Benzene vinylation to produce styrene catalyzed by $(^t\text{DAB})\text{Rh}(\text{TFA})(\eta^2\text{-C}_2\text{H}_4)_2$

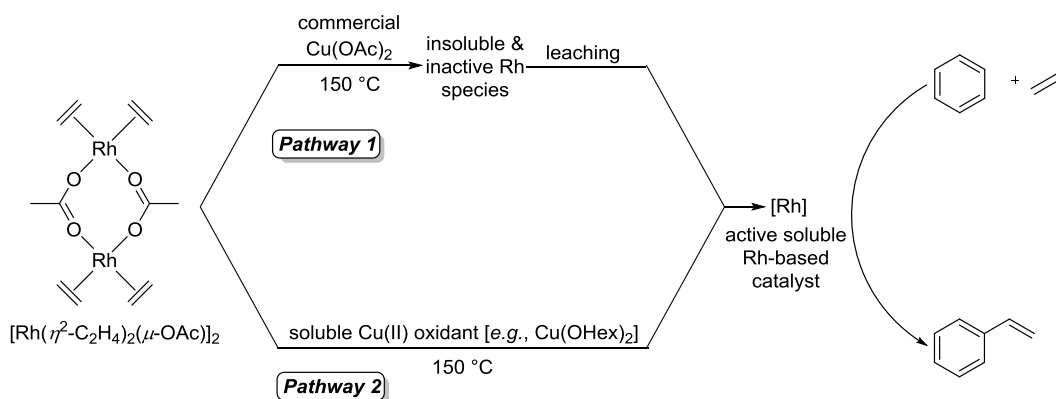
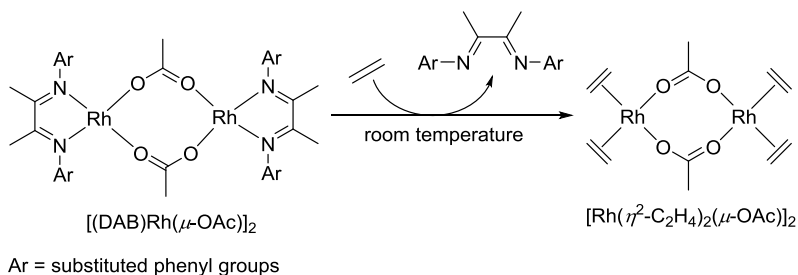


b) Benzene alkenylation to produce propenyl benzenes catalyzed by $[\text{Rh}(\mu\text{-OAc})(\eta^2\text{-C}_2\text{H}_4)_2]_2$

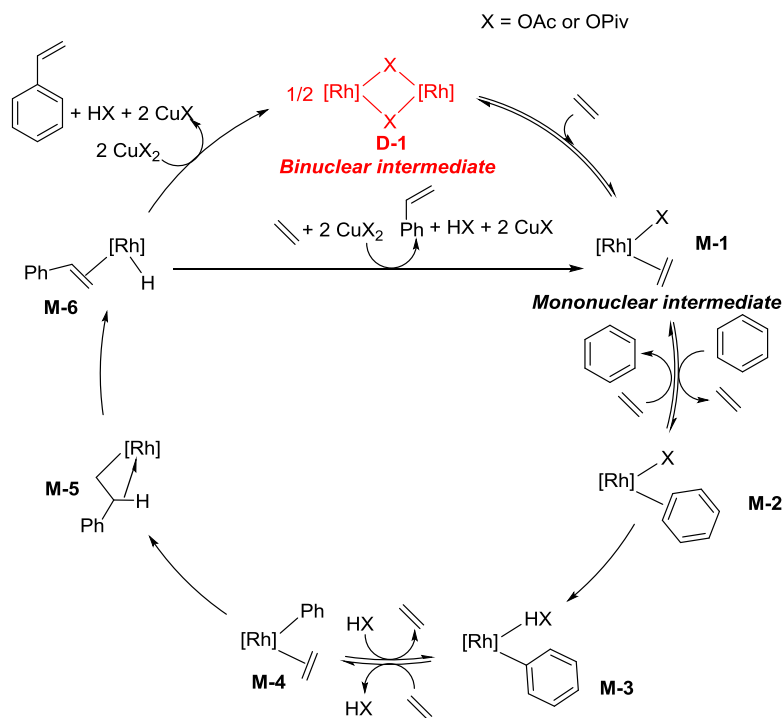


This work:

c) Mechanistic studies of styrene production process catalyzed by $[(\text{DAB})\text{Rh}(\mu\text{-OAc})]_2$ system



Scheme 2.1.2. Catalytic benzene alkenylation by Rh(I) catalyst precursors.



Scheme 2.1.3. Proposed catalytic cycle for benzene alkenylation using Rh(I) as a catalyst precursor.

We report new findings regarding the catalytic oxidative vinylation of benzene to form styrene using several diimine-ligated rhodium acetate catalyst precursors (Scheme 2.1.2). We have revealed that in the presence of ethylene, two representative diimine-based rhodium acetate complexes readily dissociate the diimine ligand and generate $[\text{Rh}(\mu\text{-OAc})(\eta^2\text{-C}_2\text{H}_4)_2]_2$. Under the catalytic conditions with commercial $\text{Cu}(\text{OAc})_2$, $[\text{Rh}(\mu\text{-OAc})(\eta^2\text{-C}_2\text{H}_4)_2]_2$ undergoes rapid decomposition to form catalytically inactive and insoluble Rh species, from which soluble molecular Rh species gradually leach back into solution to form the soluble active catalyst. The process of Rh decomposition and re-dissolution is proposed to give rise to the observed induction period. Using either $\text{Cu}(\text{OAc})_2$ treated to decrease particle size, either by heating or ball milling (herein, referred to as activated $\text{Cu}(\text{OAc})_2$), or more soluble Cu(II) oxidants such as copper(II) 2-ethylhexanoate $[\text{Cu}(\text{OHex})_2]$, the

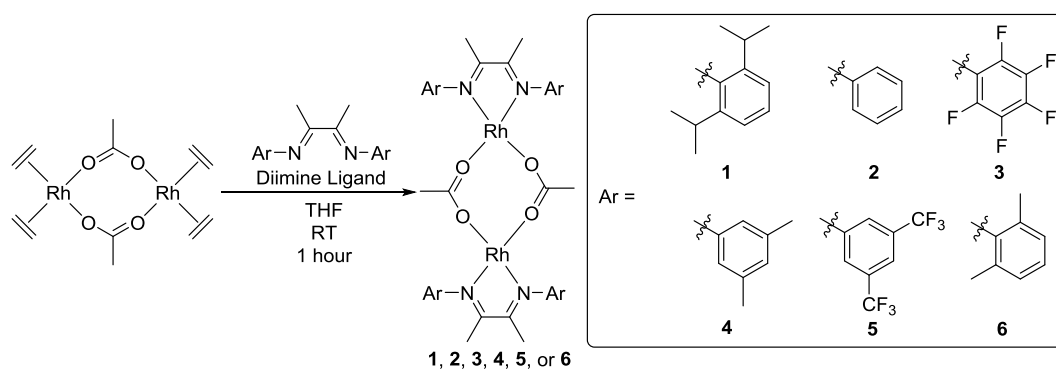
decomposition of $[\text{Rh}(\mu\text{-OAc})(\eta^2\text{-C}_2\text{H}_4)_2]_2$ to form insoluble rhodium species can be mitigated, and the induction period is not observed. It is now well-established that some catalytic processes using molecular Rh,⁵⁵⁻⁵⁷ Pd,⁵⁸⁻⁶⁰ Ir,⁶¹⁻⁶³ Ru⁶⁴⁻⁶⁵, or Fe⁶⁶⁻⁶⁸ precursors occur through decomposition to form reduced nanoparticles, which serve as the actual catalysts. However, we are unaware of a previous example of an induction period attributed to degradation of molecular species to form an insoluble but inactive material followed by re-dissolution to provide the active and soluble catalyst. When using $[\text{Rh}(\mu\text{-OAc})(\eta^2\text{-C}_2\text{H}_4)_2]_2$ as the catalyst precursor and $\text{Cu}(\text{OPiv})_2$ as the soluble Cu(II) oxidant, the trimetallic complex $[\text{Rh}^{\text{I}}(\mu\text{-OPiv})_2(\eta^2\text{-C}_2\text{H}_4)_2]_2(\mu\text{-Cu})$ is identified as the catalyst resting state.

2.2 Results and Discussion

2.2.1 Effect of Diimine Ligand Identity on Reactivity and Selectivity for Benzene Alkenylation

Following the success of $(^{\text{Fl}}\text{DAB})\text{Rh}(\text{TFA}/\text{OAc})(\text{C}_2\text{H}_4)$ and $[\text{Rh}(\mu\text{-OAc})(\eta^2\text{-C}_2\text{H}_4)_2]_2$ complexes as catalyst precursors,⁵¹⁻⁵² a series of new rhodium (I) acetate complexes (**1-6**) supported by different diimine ligands with varied electronic and steric properties (Scheme 2.2.1) were synthesized and probed them for catalytic benzene alkenylation. The new *N*-supported Rh complexes were not isolated, but instead were utilized for catalysis after *in situ* generation by reaction of $[\text{Rh}(\mu\text{-OAc})(\eta^2\text{-C}_2\text{H}_4)_2]_2$ with the diimine proligands in THF for 30 minutes at room temperature followed by removal of THF solvent. In order to test the viability of the

synthetic procedure, the structures of two representative *in situ* generated diimine rhodium complexes (**3** and **6**) have been confirmed by X-ray diffraction (Figure 1.4.1), multi-nuclear NMR spectroscopy and elemental analysis. As depicted in Figure 1.4.1, both complexes **3** and **6** possess dimeric structures, which are commonly observed in Rh(I) complexes.⁶⁹⁻⁷² The N–Rh–N bond angles of complexes **3** and **6** are compressed from the ideal 90° bond angles of a four-coordinate square planar structure to less than 80°, which are typical for Rh(I) diimine complexes.⁷³⁻⁷⁴ The N–Rh–N and O–Rh–O bond angles are larger for complex **6** than complex **3**.



Scheme 2.2.1. General synthetic procedure for *in situ* generated catalysts from diimines and $[\text{Rh}(\mu\text{-OAc})(\eta^2\text{-C}_2\text{H}_4)_2]_2$. Complexes **3** and **6** have been isolated and fully characterized.

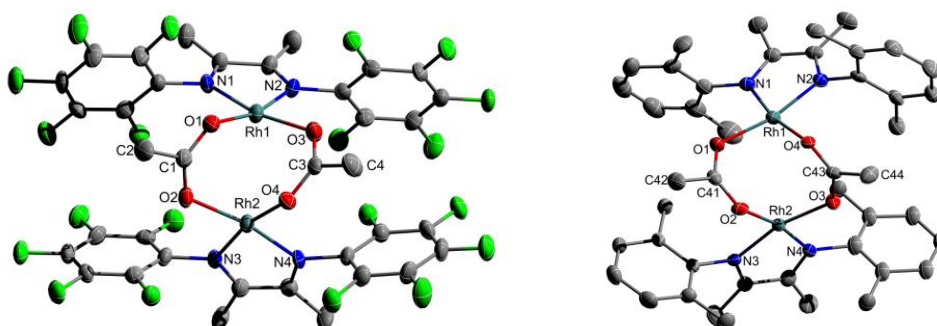


Figure 2.2.1. ORTEPs of complexes **3** (left) and **6** (right) (50% probability). H atoms and solvent molecules are omitted for clarity. For the structure of complex **6**, only the major position for the disordered atom in the phenyl ring is shown. Selected bond lengths (Å): for complex **3**: Rh1–N1 1.957(5), Rh1–N2 1.964(5), Rh1–O3 2.061(5), Rh1–O1 2.066(4), O1–C1 1.259(8), O2–C1 1.232(7), C1–C2 1.524(9); for complex **6**:

Rh1-N2 1.945(3), Rh1-N1 1.968(3), Rh1-O1 2.057(3), Rh1-O4 2.086(2), O1-C41 1.251(5), O2-C41 1.259(5), C41-C42 1.515(5). Selected bond angles (°): for complex **3**: N1-Rh1-N2 77.6(2), N2-Rh1-O3 95.4(2), N1-Rh1-O1 93.5(2), O3-Rh1-O1 91.6(2), N1-Rh1-O3 168.7(2) N2-Rh1-O1 166.17(19), O2-C1-O1 127.4(6), C1-O1-Rh1 126.7(4), C1-O2-Rh2 122.9(4); for complex **6**: N2-Rh1-N1 78.9(1), N1-Rh1-O1 95.9(1), N2-Rh1-O4 91.0(1), O1-Rh1-O4 92.9(1), N2-Rh1-O1 167.2(1), N1-Rh1-O4 168.59(12), O1-C41-O2 126.1(4), C41-O1-Rh1 124.7(3), C41-O2-Rh2 124.9(3).

We first evaluated the reactivity of diimine ligated Rh complexes and $[\text{Rh}(\mu\text{-OAc})(\eta^2\text{-C}_2\text{H}_4)_2]_2$ for the single-step production of styrene from benzene and 40 psig ethylene (Figure 2.2.2). All reactions were performed under a standard set of conditions (10 mL benzene, 0.001 mol % Rh complex (relative to benzene) and 240 equiv. of $\text{Cu}(\text{OAc})_2$ (relative to the catalyst), 150 °C). As shown in Figure 2, overlap of the turnovers (TOs) versus time plots for all of the diimine-based Rh(I) catalyst precursors indicates that variation of the diimine ligand has a negligible effect on catalytic reactivity. The reactions with ethylene using diimine rhodium complexes show pronounced induction periods. Although the catalysis using diimine ligated Rh(I) catalyst precursors exhibit a shorter induction period compared with the catalysis using $[\text{Rh}(\mu\text{-OAc})(\eta^2\text{-C}_2\text{H}_4)_2]_2$, the reaction using Rh(I) complexes with diimine ligands show a statistically identical apparent turnover frequency (TOF) after the induction period ($2.8 \times 10^{-3} \text{ s}^{-1}$) to $[\text{Rh}(\mu\text{-OAc})(\eta^2\text{-C}_2\text{H}_4)_2]_2$ (each TOF was calculated from the linear portion of TO versus time plots, which are typically observed between 8 h and 12 h). We label these apparent TOFs due to the unknown amount of Rh that is convert to active catalyst. We also probed linear:branched selectivity for alkenylation of benzene with the α -olefin propylene. The catalytic conversion of benzene, propylene and $\text{Cu}(\text{OAc})_2$ by diimine-based Rh(I) catalyst precursors and

[Rh(μ -OAc)(η^2 -C₂H₄)₂]₂ to propenyl benzenes was tested (Scheme 2.2.2). At 25 psig of propylene, all of the diimine Rh(I) catalyst precursors and [Rh(μ -OAc)(η^2 -C₂H₄)₂]₂ selectively produce linear straight-chain alkenyl arenes (the anti-Markovnikov product) with statistically identical 8:1 linear:branched ratios after 48 hours (Scheme 2.2.2 and Table 2.2.1). The L:B ratio is determined based on the ratio of *n*-propylbenzene to cumene that would result from hydrogenations of the alkenyl products (*i.e.*, the ratio of allylbenzene and β -methylstyrenes to α -methylstyrene). Thus, the identity of diimine ligand has no demonstrable effect on linear:branched selectivity. Taken together, these results suggest that the diimine ligand is not likely coordinated to the active Rh catalyst.

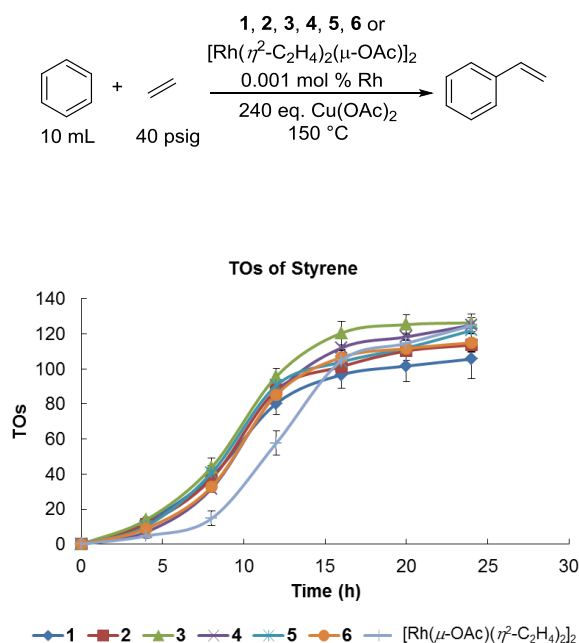
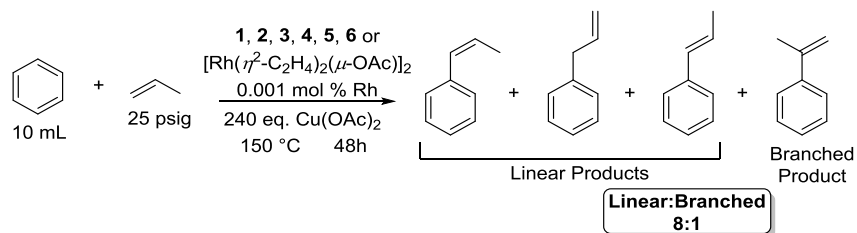


Figure 2.2.2. Plot of TOs versus time for styrene production catalyzed by complexes 1–6 or [Rh(μ -OAc)(η^2 -C₂H₄)₂]₂. Reaction conditions: 0.001 mol % of Rh (relative to benzene), 240 eq. of Cu(OAc)₂ (relative to Rh), 10 mL benzene, 40 psig ethylene, 150 °C. Each data point is the average of three separate experiments. Error bars represent the standard deviations based on a minimum of three independent experiments.



Scheme 2.2.2. Oxidative conversion of benzene and propylene to propenylbenzenes catalyzed by complexes **1–6** or $[\text{Rh}(\eta^2\text{-C}_2\text{H}_4)_2(\mu\text{-OAc})_2]$.

Table 2.2.1. Comparison of oxidative coupling of benzene and propylene to propenylbenzene catalyzed by complexes **1–6** or $[\text{Rh}(\mu\text{-OAc})(\eta^2\text{-C}_2\text{H}_4)_2]_2^{\text{a}}$

Complex	Total TOs of propenyl benzenes	L:B
1	49(7)	8:1
2	53(3)	8:1
3	54(5)	8:1
4	52(3)	8:1
5	53(8)	8:1
6	56(7)	8:1
$[\text{Rh}(\mu\text{-OAc})(\eta^2\text{-C}_2\text{H}_4)_2]_2$	57(4)	8:1
$[\text{Rh}(\mu\text{-OAc})(\eta^2\text{-C}_2\text{H}_4)_2]_2^{\text{b}}$	60(9)	9:1
$[\text{Rh}(\mu\text{-OAc})(\eta^2\text{-C}_2\text{H}_4)_2]_2^{\text{c}}$	50(4)	8:1

^a Unless otherwise noted, conditions are 0.001 mol % Rh relative to benzene, 25 psig propylene, 150 °C, 48 h, 240 eq. of $\text{Cu}(\text{OAc})_2$ relative to Rh. Each TO data is the average of three separate experiments. Standard deviations are calculated based on a minimum of three independent experiments. ^b $\text{Cu}(\text{OAc})_2$ was heated in 10 ml benzene for 12 h at 150 °C prior to the catalysis. ^c 5 eq. of ^{Fl}DAB ligand was introduced to the reaction solution before the catalysis.

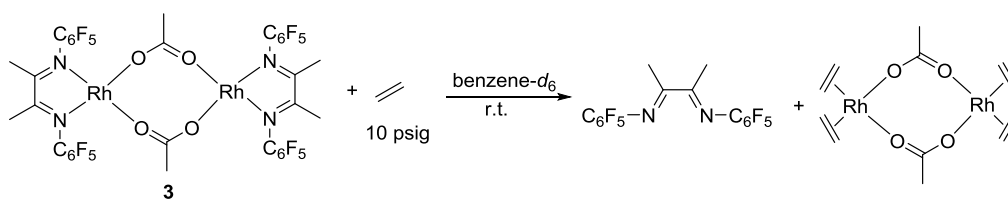
2.2.2 Stability of Diimine Ligated Rh Complexes toward Ethylene

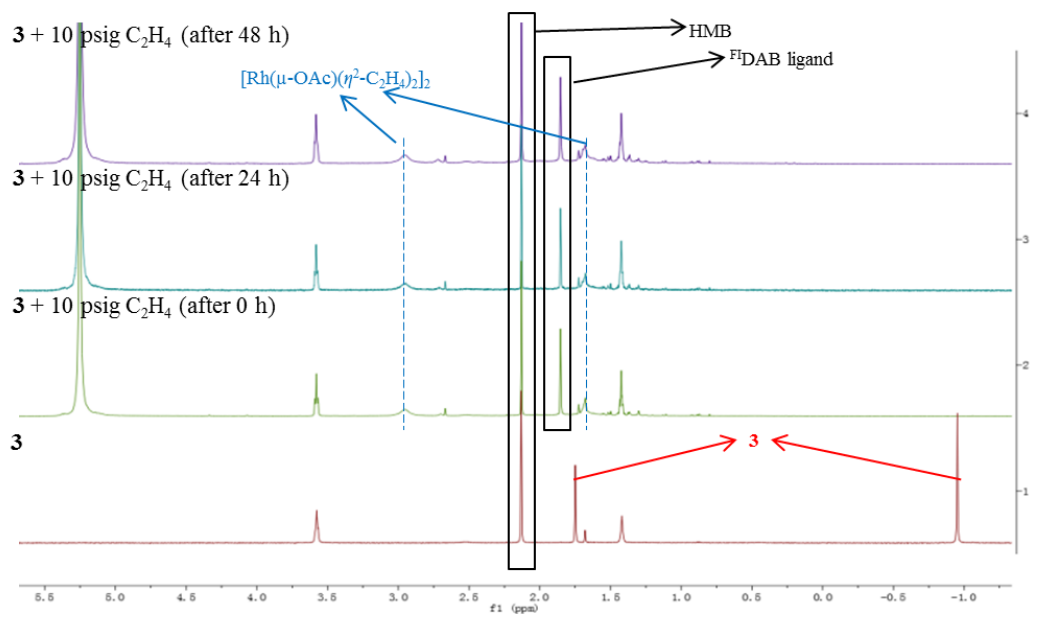
Pressure

Given that no significant ligand effects on reactivity and selectivity are observed in the catalysis with ethylene and propylene, the diimine ligated Rh complexes **1–6** and $[\text{Rh}(\mu\text{-OAc})(\eta^2\text{-C}_2\text{H}_4)_2]_2$ are likely converted to the same active Rh species under catalytic conditions. To test this hypothesis, we monitored the transformation of

complexes **3** and **6** under ethylene pressure by *in situ* ^1H NMR spectroscopy. $\text{Cu}(\text{OAc})_2$ was not used in these experiments as its paramagnetic properties result in broadened NMR spectra. As observed by ^1H NMR spectroscopy (Figure 2.2.3), approximately 10 minutes after being treated with 10 psig of ethylene at room temperature, approximately 90% of $[(^{\text{F1}}\text{DAB})\text{Rh}(\mu\text{-OAc})]_2$ (**3**) in benzene- d_6 was converted to $[\text{Rh}(\mu\text{-OAc})(\eta^2\text{-C}_2\text{H}_4)_2]_2$ accompanied by dissociation of the diimine ligand. The observations by ^1H NMR spectroscopy are consistent with the solution changing from purple $\{[(^{\text{F1}}\text{DAB})\text{Rh}(\mu\text{-OAc})]_2\}$ to yellow $\{[\text{Rh}(\mu\text{-OAc})(\eta^2\text{-C}_2\text{H}_4)_2]_2\}$ immediately following the addition of ethylene to the vessel (Figure 2.2.4). Likewise, the addition of 10 psig of ethylene to a benzene solution of complex **6** results in the same observation by ^1H NMR spectroscopy (Figure 2.2.3). Thus, in a standard catalytic reaction for all complexes **1-6**, we believe that diimine dissociation occurs prior to catalysis.

(A)





(B)

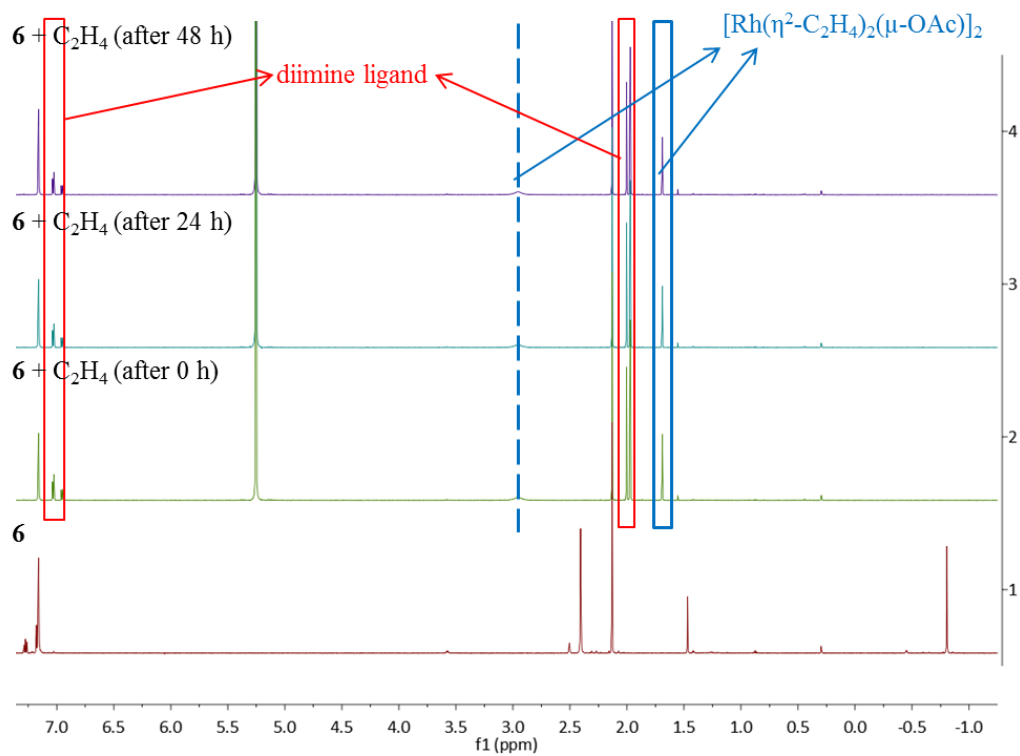
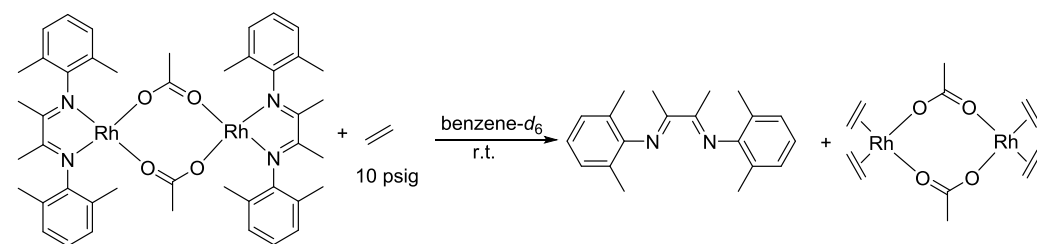
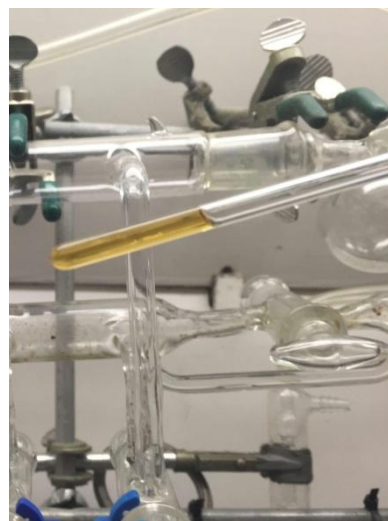


Figure 2.2.3. ¹H NMR spectra for conversion of complex **3** (A) and complex **6** (B) to [Rh(μ-OAc)(η²-C₂H₄)₂]₂ and ^{FI}DAB ligand in benzene-*d*₆ at room temperature under

10 psig ethylene.



Before treatment with C₂H₄



After treatment with C₂H₄

Figure 2.2.4. Photographs of NMR tubes containing $[(^{19}\text{F})\text{DAB}]\text{Rh}(\mu\text{-OAc})_2$ and benzene-*d*₆ before/after being treatment with 10 psig of C₂H₄.

2.2.3 Thermolysis of $[\text{Rh}(\eta^2\text{-C}_2\text{H}_4)_2(\mu\text{-OAc})_2]$ to form Rh(0) species

Junqi Chen in the Gunnoe lab studied thermal decomposition of $[\text{Rh}(\mu\text{-OAc})(\eta^2\text{-C}_2\text{H}_4)_2]_2$, 0.0057 mmol of $[\text{Rh}(\mu\text{-OAc})(\eta^2\text{-C}_2\text{H}_4)_2]_2$ was dissolved in 0.5 mL of benzene-*d*₆ in a J-Young pressure NMR tube. The J-Young tube was heated at 150 °C for 15 min, and a black solid and Rh mirror were observed. These observations are consistent with rapid reduction to elemental Rh (see next paragraph for discussion of analysis of the black solid). In addition, free HOAc and ethylene were observed by ¹H NMR spectroscopy (Figure 2.2.5). Kinetic studies were performed at 90, 100, 110 and 120 °C. The kinetic plots show a first order decay of $[\text{Rh}(\mu\text{-OAc})(\eta^2\text{-C}_2\text{H}_4)_2]_2$ (Figure 2.2.6). An Eyring plot was constructed using the

first-order rate constants from four different temperatures (Figure 2.2.6), and the ΔH^\ddagger and ΔS^\ddagger were calculated to be 28(1) kcal/mol and -1(6) cal/(mol K) respectively. The standard deviation for the ΔS^\ddagger value is too large to conclude if the actual ΔS^\ddagger is positive or negative. Additionally, when 20 psig of ethylene were added, the decomposition of $[\text{Rh}(\mu\text{-OAc})(\eta^2\text{-C}_2\text{H}_4)_2]_2$ is much slower than in the absence of added ethylene (Figure 2.2.7). Thus, the dissociation of ethylene is likely involved in the pathway for decomposition of $[\text{Rh}(\mu\text{-OAc})(\eta^2\text{-C}_2\text{H}_4)_2]_2$. In addition, the effect of the solvent was investigated. Benzene- d_6 , protio-benzene, C_6F_6 and p -xylene- d_{10} were compared. The Rh complex shows similar decomposition rates in each of the four solvents (Figure 2.2.8), indicating that the solvent is likely not involved directly in the decomposition reaction.

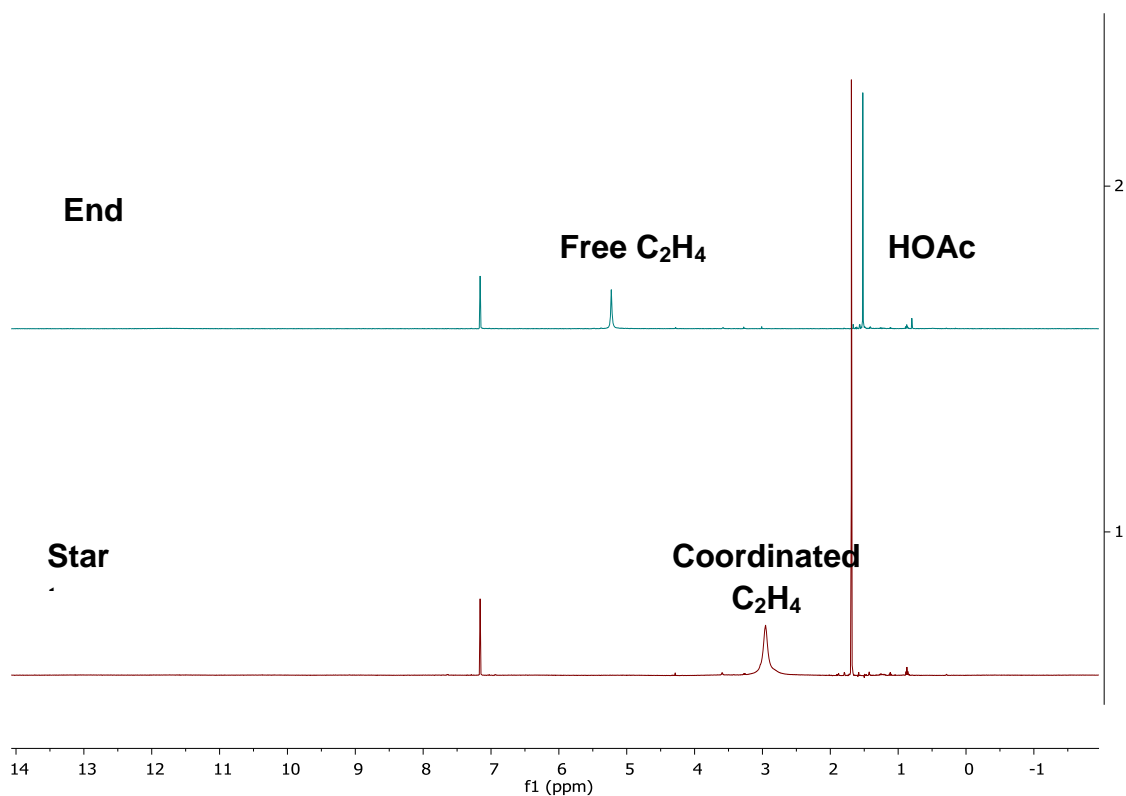


Figure 2.2.5. ^1H NMR spectra for thermolysis of $[\text{Rh}(\mu\text{-OAc})(\eta^2\text{-C}_2\text{H}_4)_2]_2$. The bottom spectrum is starting material, $[\text{Rh}(\mu\text{-OAc})(\eta^2\text{-C}_2\text{H}_4)_2]_2$. The top spectrum is acquired after heating $[\text{Rh}(\mu\text{-OAc})(\eta^2\text{-C}_2\text{H}_4)_2]_2$ at 150 °C for 15 minutes.

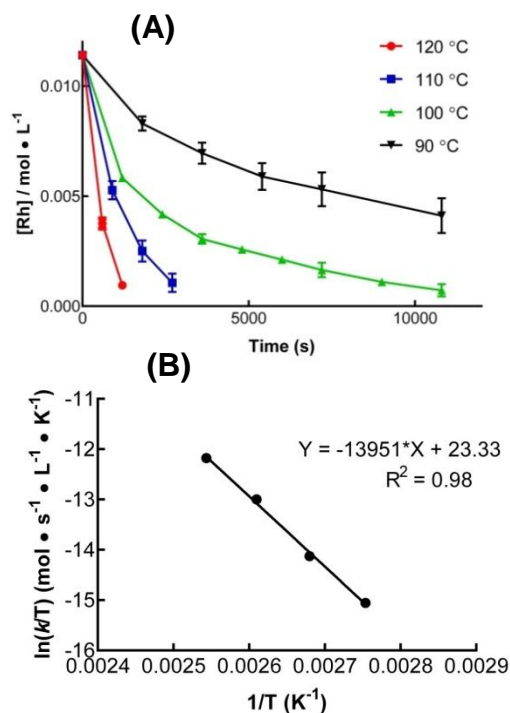


Figure 2.2.6. (A) Plot of $[\text{Rh}(\mu\text{-OAc})(\eta^2\text{-C}_2\text{H}_4)_2]_2$ concentration versus time for decomposition in benzene- d_6 at different temperatures. Each data point is the average of three separate experiments. Error bars represent the standard deviation based on a minimum of three independent experiments. (B) Eyring plot for $[\text{Rh}(\mu\text{-OAc})(\eta^2\text{-C}_2\text{H}_4)_2]_2$ decomposition. Reaction conditions: 0.2 mol % of $[\text{Rh}(\mu\text{-OAc})(\eta^2\text{-C}_2\text{H}_4)_2]_2$ (relative to benzene), 0.5 mL benzene- d_6 , 20 psig N_2 , 90-120 °C.

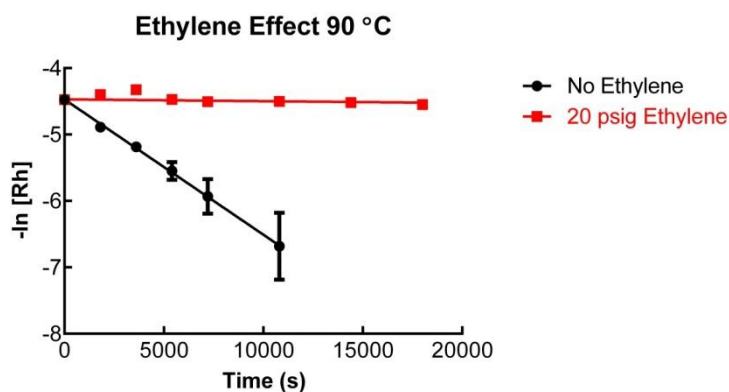


Figure 2.2.7. Comparison of kinetic plot for the decomposition of $[\text{Rh}(\mu\text{-OAc})(\eta^2\text{-C}_2\text{H}_4)_2]_2$ in the absence of ethylene versus in the presence of 20 psig ethylene. Reaction conditions: 0.2 mol % of $[\text{Rh}(\mu\text{-OAc})(\eta^2\text{-C}_2\text{H}_4)_2]_2$ (relative to benzene), 0.5 mL benzene- d_6 , 20 psig nitrogen/ethylene, 90 °C. Each data point is the average of three separate experiments. Error bars represent the standard deviations based on a minimum of three independent experiments.

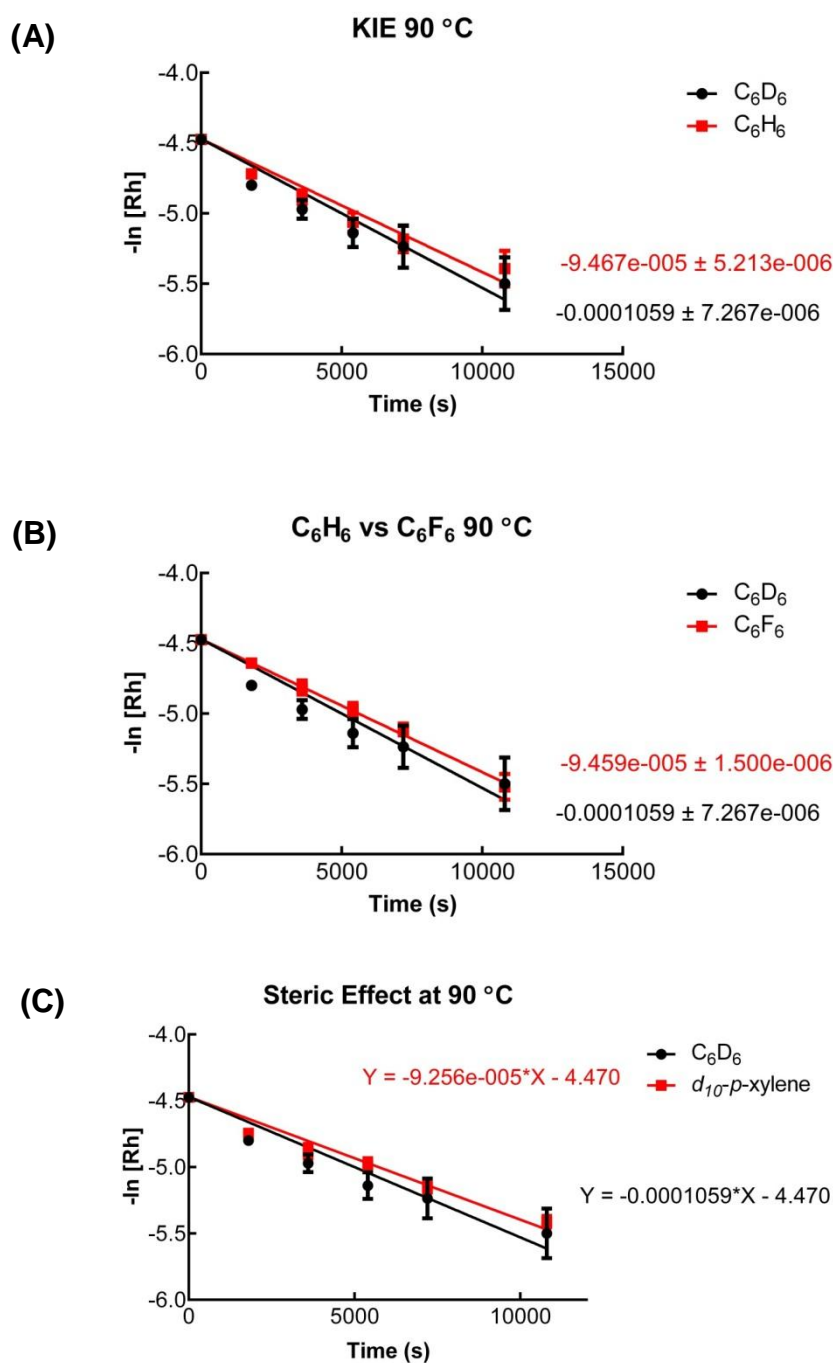


Figure 2.2.8. Comparison of kinetic plot for the decomposition of $[\text{Rh}(\mu\text{-OAc})(\eta^2\text{-C}_2\text{H}_4)_2]_2$ in C_6H_6 versus C_6D_6 (A), C_6H_6 versus C_6F_6 (B), and C_6H_6 versus $d_{10}\text{-}p\text{-xylene}$ (C). Reaction condition: 0.0025g $[\text{Rh}(\mu\text{-OAc})(\eta^2\text{-C}_2\text{H}_4)_2]_2$, 0.5ml benzene/ C_6F_6 / $d_{10}\text{-}p\text{-xylene}$ 20 psig N_2 , 90 °C. Each data point is the average of three separate experiments. Error bars represent the standard deviations based on a minimum of three independent experiments.

Zhongwen Luo in the Gunnoe lab characterized the black precipitate formed during the thermolysis of $[\text{Rh}(\mu\text{-OAc})(\eta^2\text{-C}_2\text{H}_4)_2]_2$ in the absence of $\text{Cu}(\text{OAc})_2$ by transmission electron microscopy (TEM). A 10 mL benzene solution of $[\text{Rh}(\mu\text{-OAc})(\eta^2\text{-C}_2\text{H}_4)_2]_2$ (0.001 mol % Rh) under 40 psig of ethylene was heated to 150 °C for 1 hour. The resulting mixture was centrifuged and the supernatant was decanted to isolate the black solid. Lattice parameter analysis, TEM-EDS measurement and selected area diffraction were used to characterize the black solid (Figure 2.2.9). These data confirm that Rh nanoparticles are formed during the thermal decomposition. Rh(111) and Rh(200) planes are observed in the lattice constant analysis. The lattice parameters for Rh(111), Rh(200) and Rh(220) are found to be 0.22 nm, 0.19 nm and 0.13 nm, respectively. Also, broad beam TEM-EDS measurement is consistent with the formation of Rh nanoparticles. In selected area diffraction measurement of the particles, three common planes of Rh nanoparticles, Rh(111), Rh(200) and Rh(220) were found.

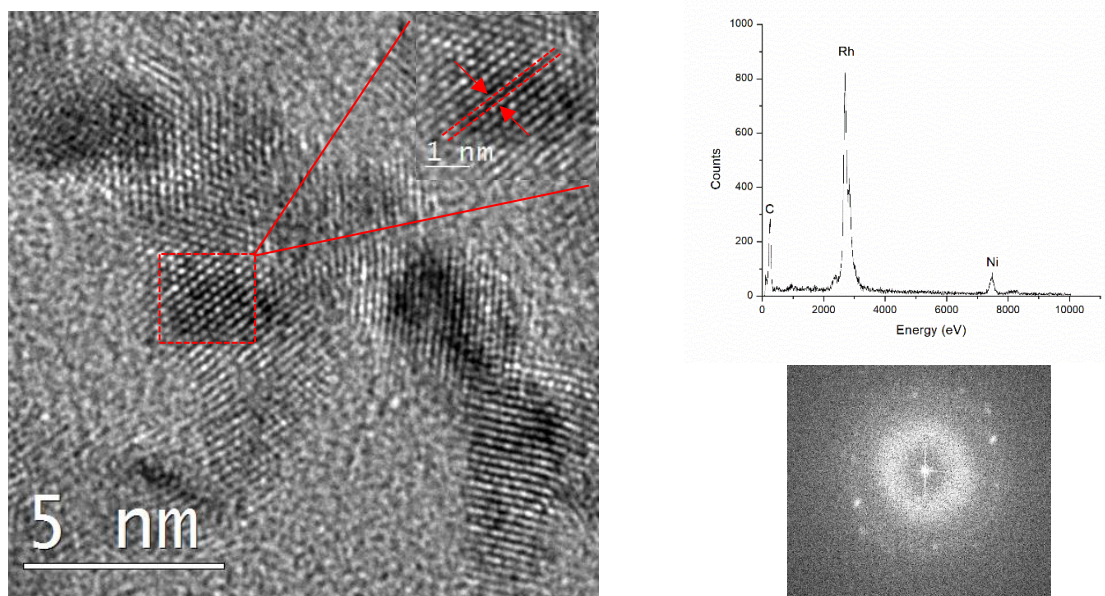


Figure 2.2.9. TEM lattice analysis (left), TEM-EDS measurement (top right) and selected area diffraction analysis (bottom right) of Rh species from thermal decomposition of $[\text{Rh}(\mu\text{-OAc})(\eta^2\text{-C}_2\text{H}_4)_2]_2$ at 150 °C under 40 psig of ethylene in benzene in the absence of $\text{Cu}(\text{OAc})_2$.

Taken together, our experimental data indicate that the reductive decomposition of $[\text{Rh}(\mu\text{-OAc})(\eta^2\text{-C}_2\text{H}_4)_2]_2$ to form Rh(s) likely involves dissociation of ethylene and subsequent ethylene C–H activation to form a Rh-vinyl intermediate and acetic acid. Beyond these steps, our data do not allow additional elucidation about the details of the formation of Rh(s), but the similar rates of reductive decomposition in different arene solvents suggests that the solvent is not likely the reducing agent.

2.2.4 Removal of the Induction Period with Thermally Treated

$\text{Cu}(\text{OAc})_2$

As shown in Figure 2.2.10, for catalysis at 150 °C using $\text{Cu}(\text{OAc})_2$ as the oxidant there is a pronounced induction period. We have discovered that this induction

period is not observed in the catalysis when $\text{Cu}(\text{OAc})_2$ is heated prior to the catalysis. Here, $\text{Cu}(\text{OAc})_2$ (48.8 mg) is heated in benzene (10 mL) for 12 hours at 150 °C with subsequent introduction of $[\text{Rh}(\mu\text{-OAc})(\eta^2\text{-C}_2\text{H}_4)_2]_2$ using the standard catalytic conditions (Figure 2.2.10). For the reaction using preheated $\text{Cu}(\text{OAc})_2$, the apparent TOF ($2.8 \times 10^{-3} \text{ s}^{-1}$) calculated after 8 h is statistically identical to that of the catalysis after the induction period without preheating $\text{Cu}(\text{OAc})_2$. Additionally, catalysis using propylene with the same preheating treatment shows a statistically identical linear:branched ratio as compared to that observed under standard conditions (Table 2.2.1). These results indicate the same catalytically active species is likely formed in the catalytic reaction with or without preheating $\text{Cu}(\text{OAc})_2$.

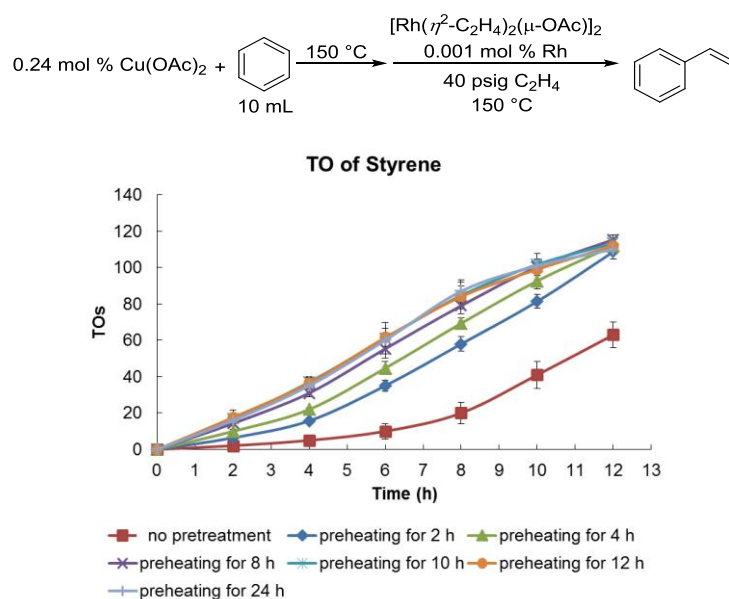


Figure 2.2.10. Plot of TOs versus time for styrene production catalyzed by $[\text{Rh}(\mu\text{-OAc})(\eta^2\text{-C}_2\text{H}_4)_2]_2$ after heating $\text{Cu}(\text{OAc})_2$ (0.24 mol % relative to benzene) in benzene (10 mL) for 0 to 24 hours at 150 °C. Reaction conditions: 0.001 mol % of Rh (relative to benzene), 40 psig ethylene, 150 °C. Each data point is the average of three separate experiments. Error bars represent the standard deviations based on a minimum of three independent experiments.

Having observed the removal of the induction period after preheating $\text{Cu}(\text{OAc})_2$ at $150\text{ }^\circ\text{C}$ for 12 h, we probed intermediate heating times for $\text{Cu}(\text{OAc})_2$ pretreatment from 2 h to 10 h. The induction period is reduced as the $\text{Cu}(\text{OAc})_2$ heating time is increased (Figure 2.2.10). Again, regardless of length of induction period the apparent TOFs (calculated from 6 h to 8 h when maximum apparent TOFs are achieved after the induction period) are nearly identical (Figure 2.2.10). The catalytic reactivity was not affected by increasing preheating time beyond 12 h of preheating (Figure 2.2.10).

We isolated solid materials by filtration from the mixture of $\text{Cu}(\text{OAc})_2$ in benzene after heating for 12 h (Figure 2.2.11). The isolated solid $\text{Cu}(\text{OAc})_2$ was used as the oxidant for standard catalytic reactions, and the induction period was not observed (Figure 2.2.11). Herein, we refer to the $\text{Cu}(\text{OAc})_2$ solid which was treated to enable the removal of the induction period, either by heating or ball milling (see below), in the catalysis as activated $\text{Cu}(\text{OAc})_2$. When the filtrate after heating $\text{Cu}(\text{OAc})_2$ at $150\text{ }^\circ\text{C}$ for 12 h was added to $[\text{Rh}(\mu\text{-OAc})(\eta^2\text{-C}_2\text{H}_4)_2]_2$ along with untreated $\text{Cu}(\text{OAc})_2$ and subjected to the standard catalytic conditions, there was a pronounced induction period (Figure 2.2.11). These results are consistent with some transformation of the solid $\text{Cu}(\text{OAc})_2$ rather than generation of a soluble material that might reduce/remove the induction period. Catalysis using $\text{Cu}(\text{OAc})_2$ solid isolated upon heating in hexanes (10 mL) for 12 hours at $150\text{ }^\circ\text{C}$ does not reveal a significant induction period, which implies benzene is not needed to make the activated $\text{Cu}(\text{OAc})_2$ (Figure 2.2.12).

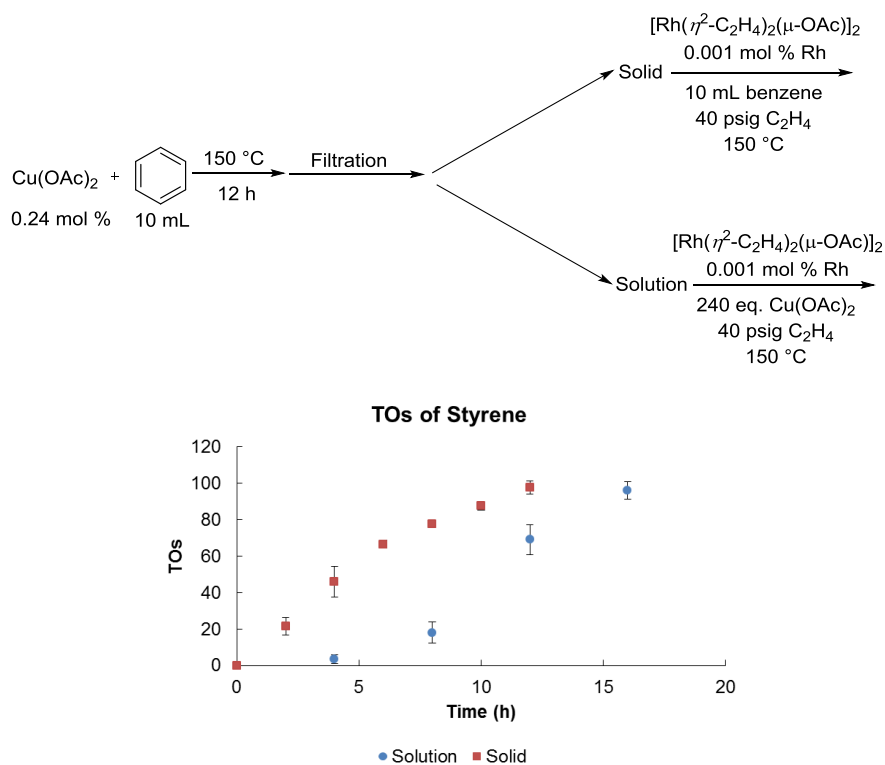


Figure 2.2.11. Comparison of TOs vs time plots for styrene production catalyzed by $[\text{Rh}(\mu\text{-OAc})(\eta^2\text{-C}_2\text{H}_4)_2]_2$ using isolated solid versus solution phase of the reaction mixture obtained by heating $\text{Cu}(\text{OAc})_2$ (0.24 mol % relative to benzene) in benzene (10 mL) for 12 hours at 150 $^\circ\text{C}$. Each data point is the average of three separate experiments. Error bars represent the standard deviations based on a minimum of three independent experiments.

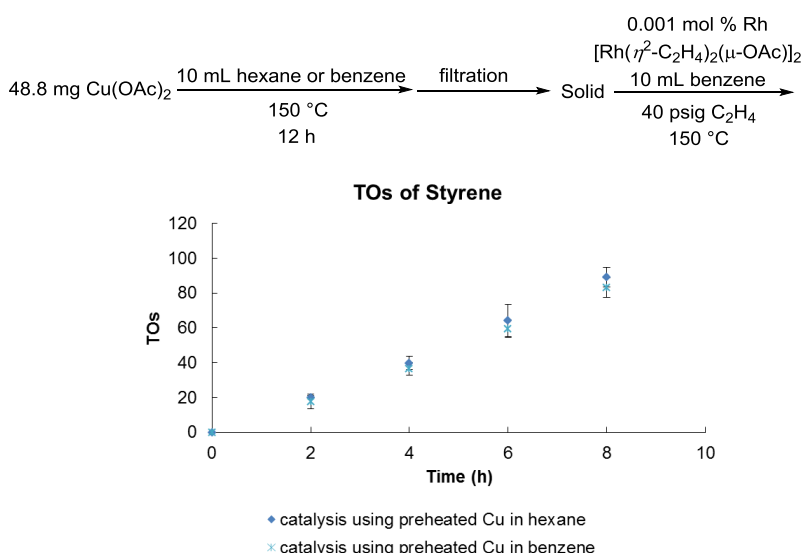


Figure 2.2.12. Comparison of TOs vs time plots for styrene production catalyzed by $[\text{Rh}(\mu\text{-OAc})(\eta^2\text{-C}_2\text{H}_4)_2]_2$ after heating $\text{Cu}(\text{OAc})_2$ (48.8 mg) in benzene versus hexane (10 mL) for 12 hours at 150 $^\circ\text{C}$. Each data point is the average of three separate experiments. Error bars represent the standard deviations based on a minimum of

three independent experiments.

Powder X-ray diffraction (XRD) and IR spectroscopy of the activated $\text{Cu}(\text{OAc})_2$ (*i.e.*, $\text{Cu}(\text{OAc})_2$ solid isolated after heating in benzene for 12 h) suggests negligible decomposition (Figure 2.2.13 and Figure 2.2.14). Additionally, comparative thermogravimetric analysis (TGA) performed by Zhongwen Luo in our lab and IR analysis of commercial anhydrous $\text{Cu}(\text{OAc})_2$ and copper(II) acetate hydrate provides evidence that the original anhydrous $\text{Cu}(\text{OAc})_2$ sample is not contaminated by copper(II) acetate hydrate (Figure 2.2.14 and Figure 2.2.15). Thus, the thermal treatment of the commercial anhydrous $\text{Cu}(\text{OAc})_2$ is not likely decreasing the water content. Additionally, the induction period is observed in the reaction using anhydrous $\text{Cu}(\text{OAc})_2$ prepared under dynamic vacuum at 150 °C for 18 hours (Figure 2.2.16). Thus, it is unlikely that the induction period is due to the presence of water in the $\text{Cu}(\text{OAc})_2$. Catalysis using untreated $\text{Cu}(\text{OAc})_2$ with HOAc or other Cu species such as CuO, Cu_2O , $\text{Cu}(\text{OAc})$, or Cu powder, which might be formed during thermal treatment of $\text{Cu}(\text{OAc})_2$,⁵³⁻⁵⁶ shows low turnovers of styrene at 2 or 4 h (Table 2.2.2). Thus, it is unlikely that these various Cu species are facilitating the generation of the actual Rh catalytic species or serving as co-catalyst.

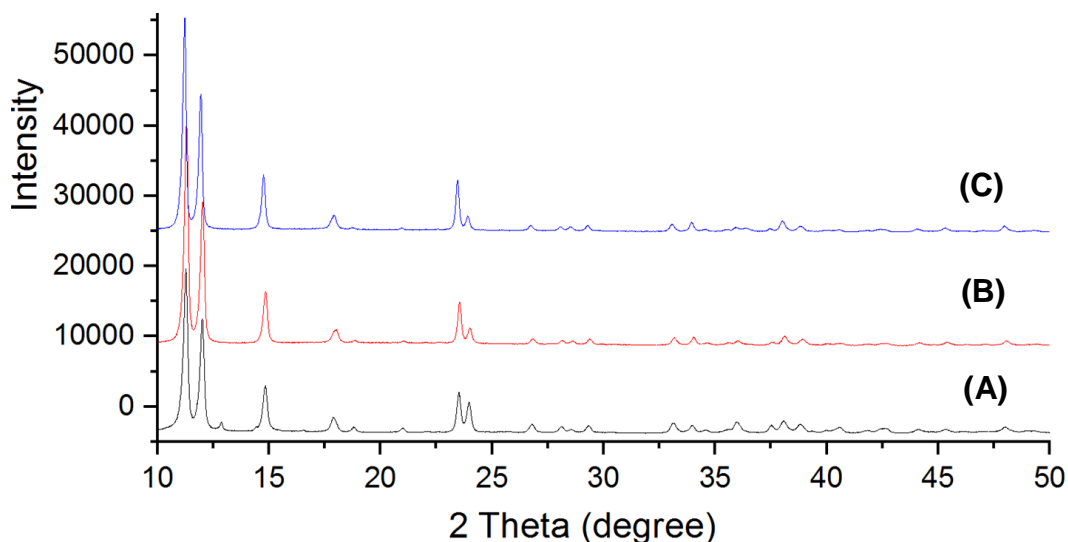
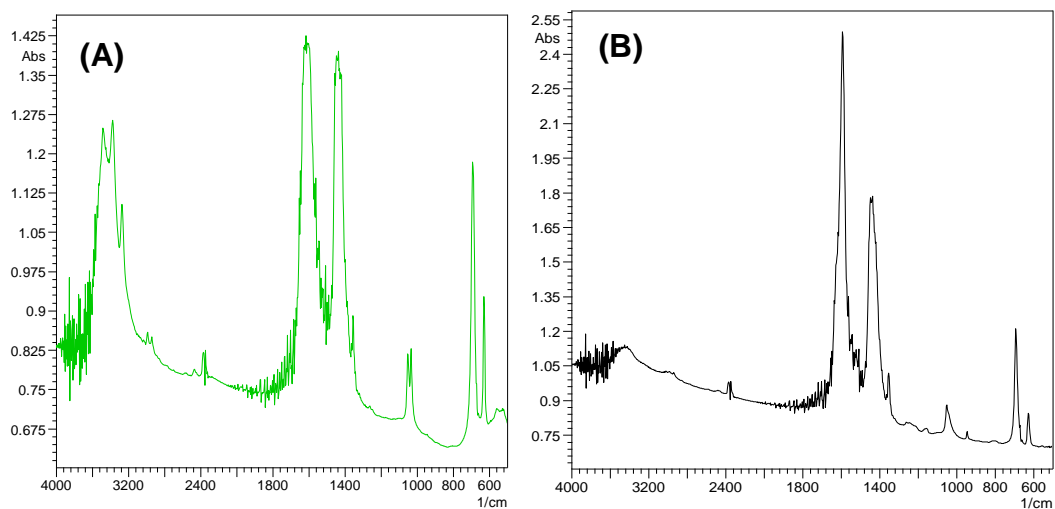


Figure 2.2.13. Powder XRD profile of $\text{Cu}(\text{OAc})_2$ solid under different conditions: (A) untreated copper(II) acetate anhydrous; (B) solid materials isolated from the reaction mixture obtained heating copper(II) acetate in 10 mL benzene at 150 °C for 12 h (activated $\text{Cu}(\text{OAc})_2$); (C) solid materials isolated from the reaction mixture obtained by heating copper(II) acetate in 10 mL benzene with 0.005 mol % of $^{\text{F1}}$ DAB ligand at 150 °C for 2 h.



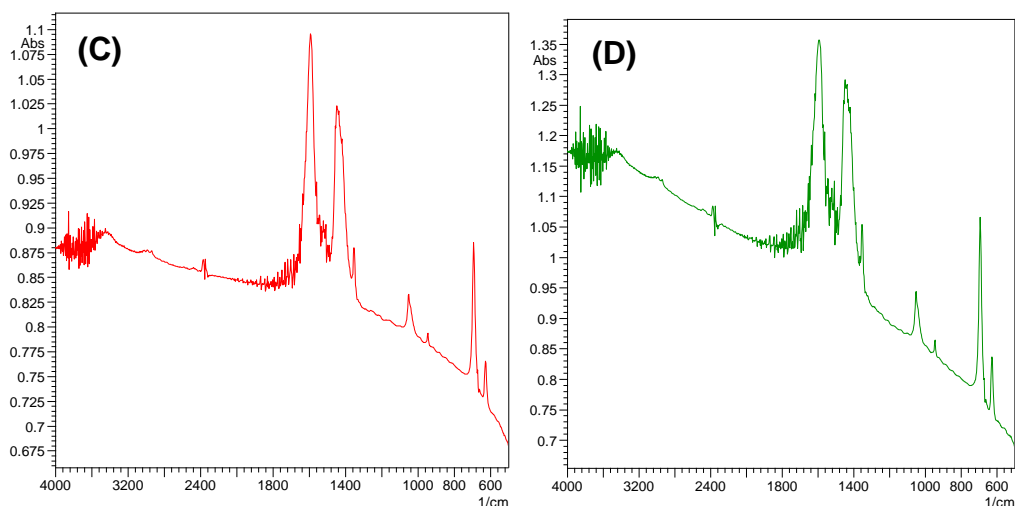
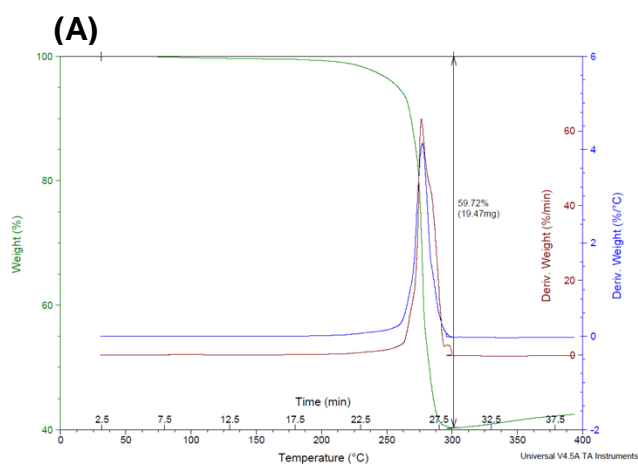


Figure 2.2.14. FT-IR spectra of $\text{Cu}(\text{OAc})_2$ solid under different conditions: (A) copper(II) acetate monohydrate; (B) untreated copper(II) acetate anhydrous; (C) solid materials isolated from the reaction mixture obtained heating copper(II) acetate in 10 mL benzene at 150 °C for 12 h (activated $\text{Cu}(\text{OAc})_2$); (D) solid materials isolated from the reaction mixture obtained by heating copper(II) acetate in 10 mL benzene with 0.005 mol % $\text{F}^{\text{I}}\text{DAB}$ ligand at 150 °C for 2 h.



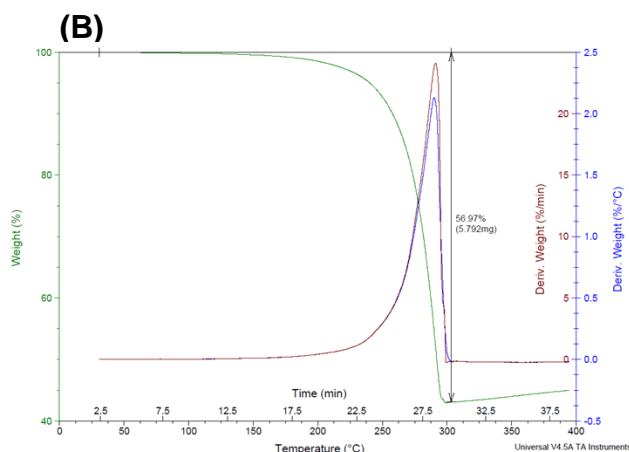
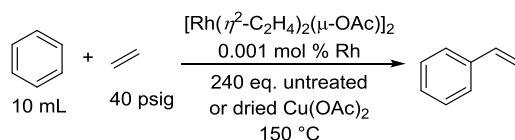


Figure 2.2.15. Curves from Differential Scanning Calorimetry (DSC) and Glass Transition Temperature, (T_g) experiments using untreated $\text{Cu}(\text{OAc})_2$ (A) and activated $\text{Cu}(\text{OAc})_2$ (B).



TOs of Styrene

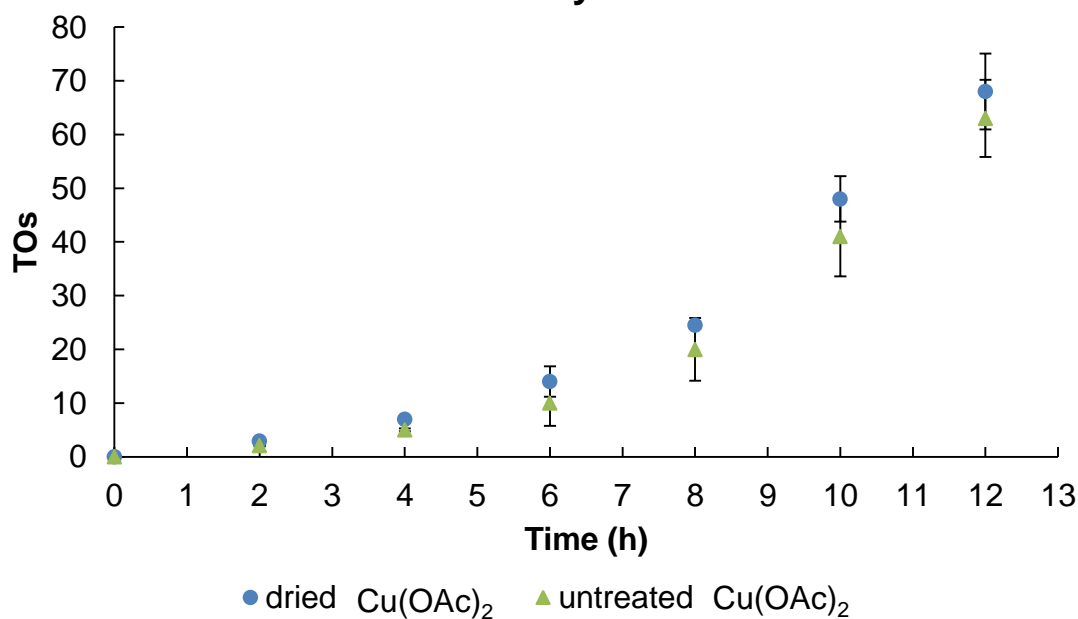
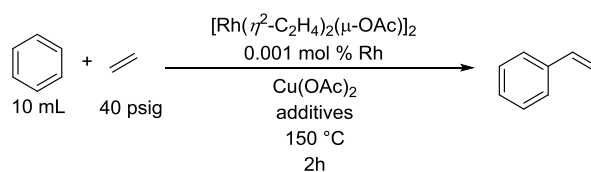


Figure 2.2.16. Comparison of TOs vs time plots for styrene production catalyzed by $[\text{Rh}(\mu\text{-OAc})(\eta^2\text{-C}_2\text{H}_4)_2]_2$ using commercial $\text{Cu}(\text{OAc})_2$ versus $\text{Cu}(\text{OAc})_2$ dried under dynamic vacuum at $150\text{ } ^\circ\text{C}$ for 18 hours. Each data point is the average of three separate experiments. Error bars represent the standard deviations based on a minimum of three independent experiments.

Table 2.2.2. Effect of different Cu species for styrene production catalyzed by

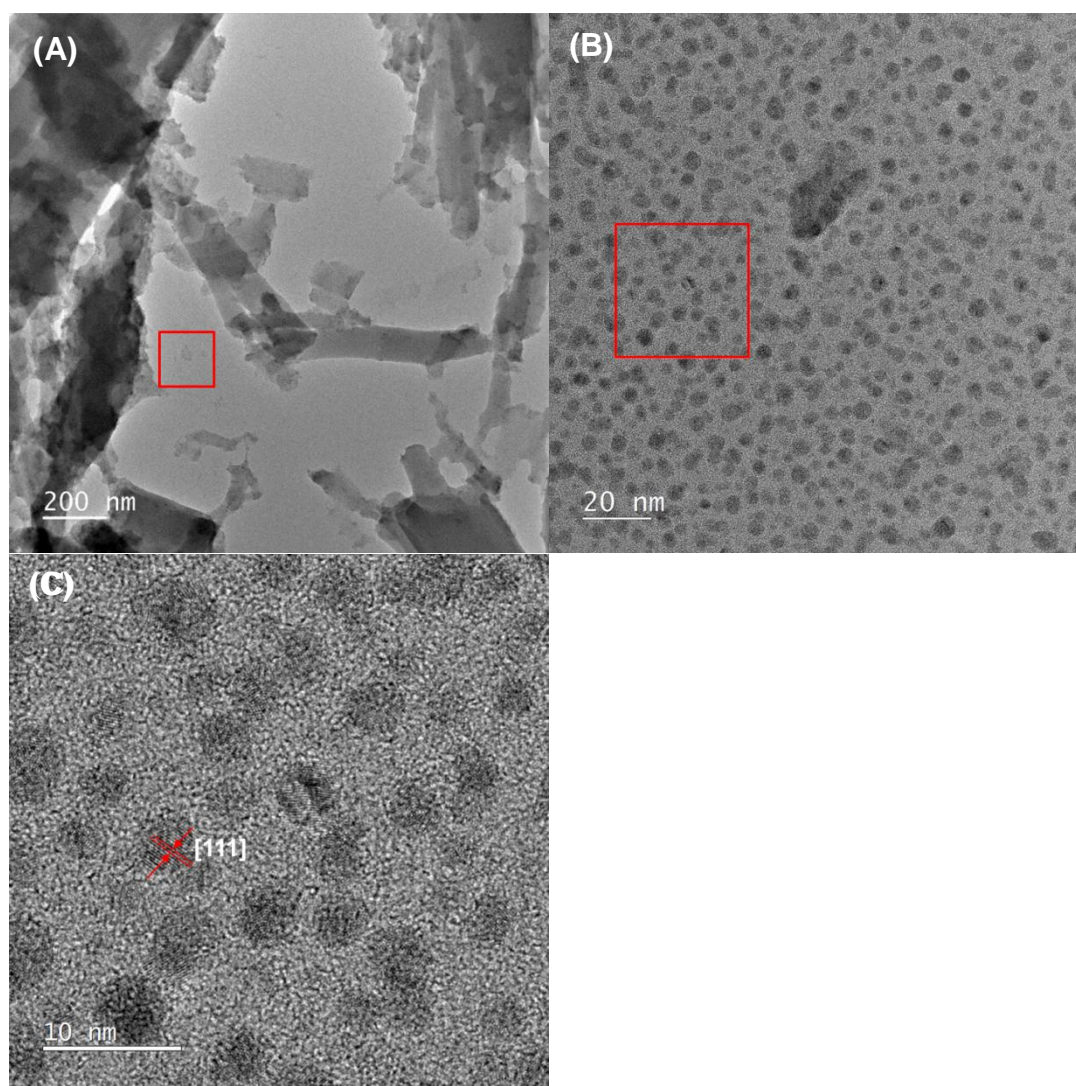
$[\text{Rh}(\mu\text{-OAc})(\eta^2\text{-C}_2\text{H}_4)_2]_2$.^a TOs were obtained at 4 hrs.



Loading of commercial Cu(OAc) ₂	Additives	TOs at 2 hrs
240 eq.	55 eq. Cu ₂ (I)O	2(0.9)
240 eq.	55 eq. Cu(II)O	2(0.5)
230 eq.	10 eq. Cu(I)OAc	4(1.7)
240 eq.	240 eq. Cu(I)OAc	5(0.7)
190 eq.	50 eq. Cu(I)OAc	4(0.9)
240 eq.	20 eq. HOAc	4(1.4)
240 eq.	240 eq. HOAc	11(2) ^a
220 eq.	20 eq. Cu(OAc) + 10 eq. HOAc	5(1.4)
200 eq.	40 eq. Cu(OAc) + 20 eq. HOAc	5(1.9)
240 eq. preheated Cu(OAc) ₂		18(4)

Zhongwen Luo in our lab observed the formation of Cu-based nanoparticles by TEM analysis after heating Cu(OAc)₂ in benzene for 12 h (Figure 2.2.17). To determine if these Cu-based nanoparticles play a role in the induction period, we performed the standard reaction using commercial Cu(OAc)₂ until it reached

completion. At this stage, the resulting reaction mixture is expected to contain a variety of decomposed Cu species including the Cu-based nanoparticles and Cu(OAc) without Cu(OAc)₂. Then the mixture was charged with fresh [Rh(μ -OAc)(η^2 -C₂H₄)₂]₂ and commercial untreated Cu(OAc)₂, and the mixture was subjected to the standard catalytic conditions. The TOs versus time plot shows an induction period and overlaps well with that of a standard catalytic reaction using commercial Cu(OAc)₂, suggesting the decomposed Cu species do not contribute to the removal of the induction period (Figure 2.2.18).



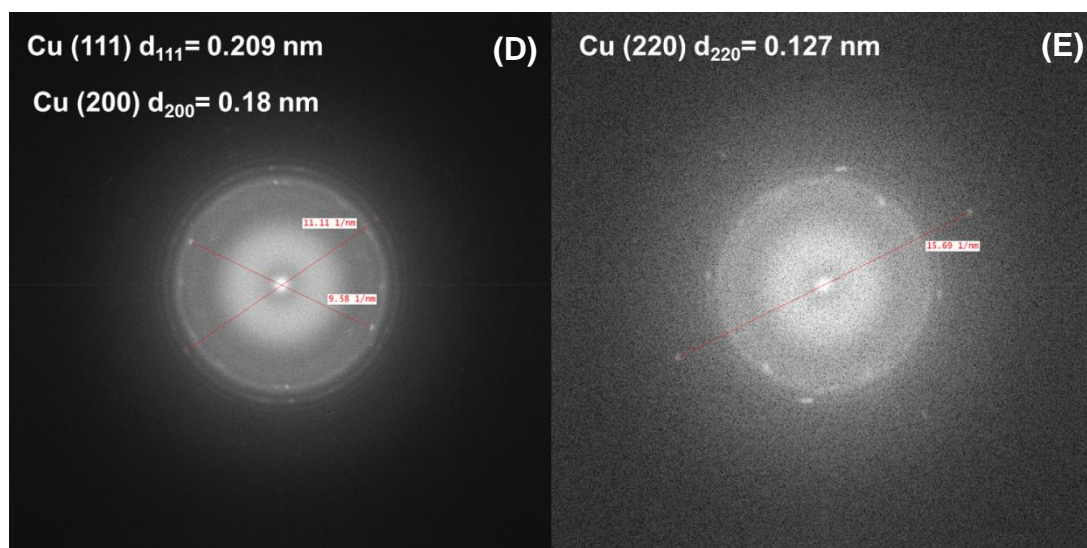
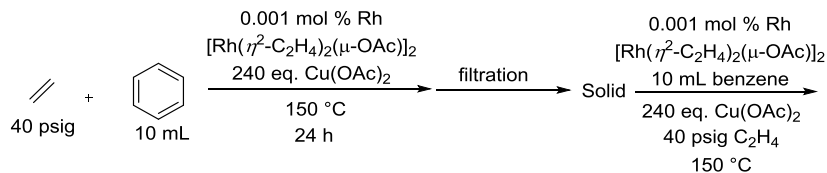


Figure 2.2.17. TEM lattice analysis (A-C) and selected area diffraction analysis (D and E) of solid species from heating $\text{Cu}(\text{OAc})_2$ in benzene at $150\text{ }^\circ\text{C}$ for 12 h. Figures S11B and S11C are obtained by magnifying the area marked with red frame in Figures S11A and S11B, respectively. Cu(111) plane is observed in the lattice constant analysis. The lattice parameters for Cu(111), Cu(200) and Cu(220) are found to be 0.21 nm, 0.18 nm and 0.12 nm, respectively. These data are consistent with the formation of Cu nanoparticles.



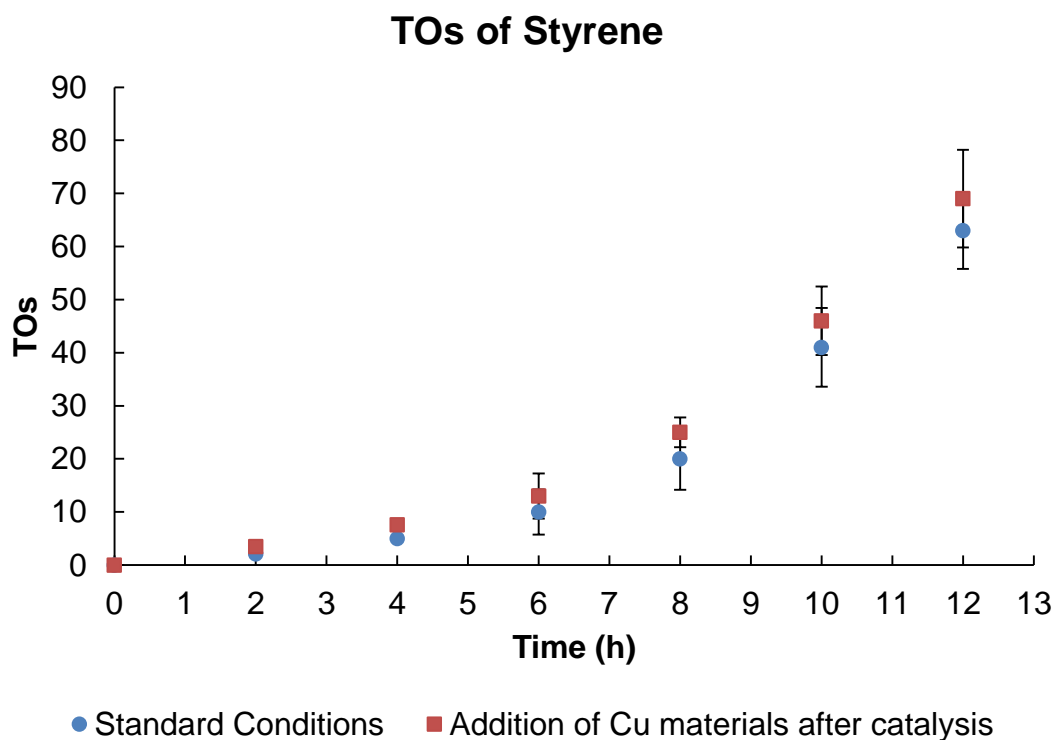


Figure 2.2.18. Plot of TOs versus time for styrene production catalyzed by $[\text{Rh}(\mu\text{-OAc})(\eta^2\text{-C}_2\text{H}_4)_2]_2$ using commercial $\text{Cu}(\text{OAc})_2$ with the addition of solid Cu species obtained after the standard catalytic reaction, and its comparison to the standard reaction.

Given the absence of evidence that chemical changes based on thermal treatment of $\text{Cu}(\text{OAc})_2$ give rise to removal of the induction period, we evaluated possible physical changes. A saturated $\text{Cu}(\text{OAc})_2$ mixture in benzene was prepared by adding a large excess of $\text{Cu}(\text{OAc})_2$ in benzene. UV-vis spectroscopy of the resulting solution exhibited no absorption signal when scanning the wavelength range from 300 to 800 nm at 25 °C. This suggests the $\text{Cu}(\text{OAc})_2$ is insoluble in benzene at room temperature. We preheated the $\text{Cu}(\text{OAc})_2$ in benzene at 150 °C for 12 hours, and the resulting $\text{Cu}(\text{OAc})_2$ /benzene mixture was decanted after centrifuging to remove insoluble materials. The isolated filtrate showed no UV-vis absorption peaks within the 300–800 nm range, indicating that the thermally treated $\text{Cu}(\text{OAc})_2$ is also insoluble in

benzene at room temperature.

Maes and co-workers reported that controlling the structure (shape and size of the particles) of cesium carbonate base, which is almost completely insoluble in the reaction solvent toluene, can significantly increase the rate of aryl halide amination with a rate-limiting deprotonation step involved in the catalytic cycle.⁷⁵ Collaborating with Chang Liu in the Sen group, we studied the morphology of $\text{Cu}(\text{OAc})_2$ solid materials under different conditions by using scanning electron microscopy (SEM) analysis. By comparing corresponding SEM images, although both samples showed irregularly shaped particles with a broad size distribution, we discovered that the solid materials isolated after heating $\text{Cu}(\text{OAc})_2$ in benzene at 150 °C for 12 h possessed smaller particles than the untreated commercial $\text{Cu}(\text{OAc})_2$ (Figure 2.2.19). Yang Lu in the Davis group probed the specific surface area of both thermally treated and untreated commercial $\text{Cu}(\text{OAc})_2$ using N_2 physisorption. However, the difference in the BET surface area between the commercial $\text{Cu}(\text{OAc})_2$ (8.2 m^2/g) and the activated $\text{Cu}(\text{OAc})_2$ (9.8 m^2/g) is not significant. Notably, the particle size of commercial $\text{Cu}(\text{OAc})_2$ observed in the SEM images is considerably larger than that estimated from the BET surface area assuming spherical morphology. These results along with N_2 adsorption isotherm indicate that the thermally treated $\text{Cu}(\text{OAc})_2$ consists of small particles whereas the commercial $\text{Cu}(\text{OAc})_2$ mainly possesses large aggregates.

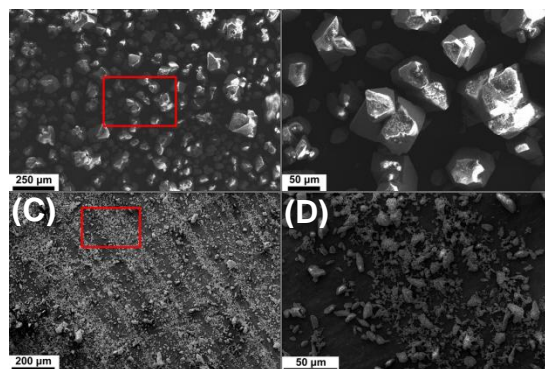
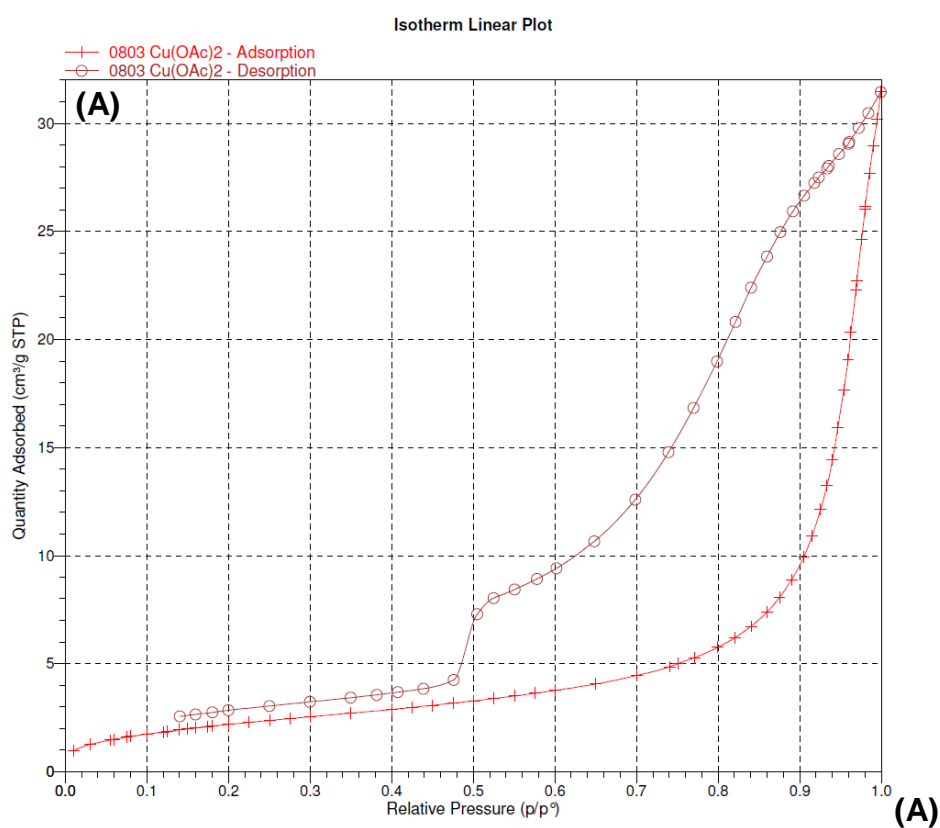


Figure 2.2.19. SEM images of commercial Cu(OAc)₂ (A, B) and solid isolated by heating Cu(OAc)₂ in benzene at 150 °C for 12 h (C, D). Figures 7B and 7D are obtained by magnifying the area marked with red frame in Figures 7A and 7C, respectively.



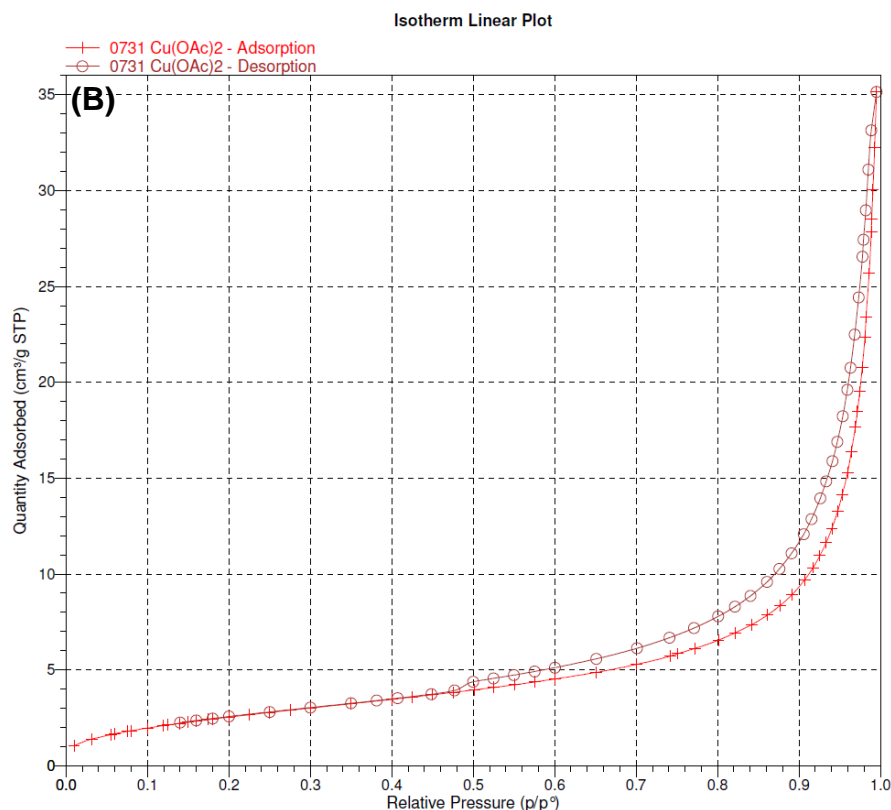
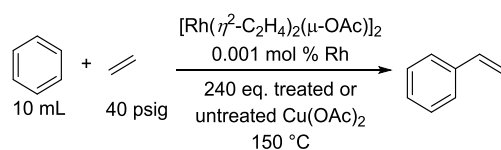


Figure 2.2.20. N₂ adsorption isotherm linear plot for untreated Cu(OAc)₂ (A) and activated Cu(OAc)₂ (B). Plot A shows large hysteresis between adsorption and desorption, which indicates capillary condensation in meso and macropores, Hysteresis between adsorption and desorption is nearly eliminated in plot B.

Catalytic styrene production using Cu(OAc)₂ ground by a ball mill reveals a shortened induction period (Figure 2.2.21). Notably, heating ground Cu(OAc)₂ in benzene for 4 h at 150 °C prior to the catalysis resulted in the complete removal of the induction period in the catalysis (Figure 2.2.21). In contrast, preheating commercial Cu(OAc)₂ for the same amount of time (4 h) does not remove the induction period. These results support the hypothesis that reducing the size of Cu(OAc)₂ particles removes or reduces the induction period.



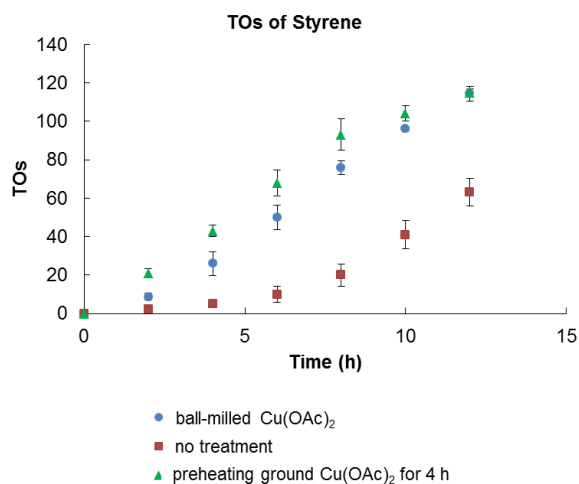


Figure 2.2.21. Plots of TOs versus time for styrene production catalyzed by $[\text{Rh}(\mu\text{-OAc})(\eta^2\text{-C}_2\text{H}_4)_2]_2$ using ball-milled $\text{Cu}(\text{OAc})_2$ and thermally treated ground $\text{Cu}(\text{OAc})_2$ and its comparison to the standard reaction. Each data point is the average of three separate experiments. Error bars represent the standard deviations based on a minimum of three independent experiments.

We performed catalyst fractional poisoning tests for catalysis with activated $\text{Cu}(\text{OAc})_2$ using PPh_3 , $\text{P}(\text{OCH}_2)_3\text{CEt}$ or 1,10-phenanthroline as poisoning reagents. As detailed in the Experimental Section, the catalytic activities were tested as a function of the addition of 0.25, 0.5, 1.0 equivalents (per equivalent of Rh) of poisoning reagents and compared to the reaction without addition of the poison. The addition of PPh_3 or $\text{P}(\text{OCH}_2)_3\text{CEt}$ leads to a slight reduction of reaction rate whereas the addition of 1,10-phenanthroline significantly slows the catalytic reaction. The key result from the poisoning tests is that ≤ 1 equivalent (per equivalent of Rh) of each poisoning reagent does not completely poison the catalyst, providing evidence against the formation of Rh nanoparticles as the active catalyst for the benzene alkenylation (Figure 2.2.22).

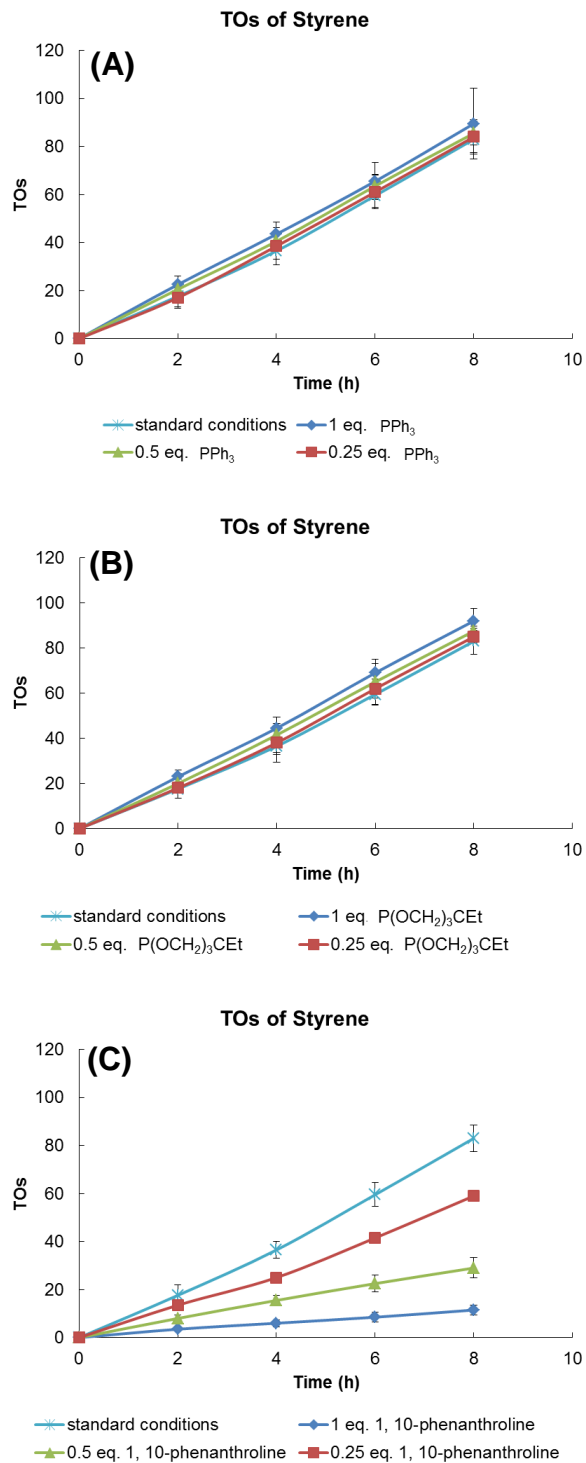
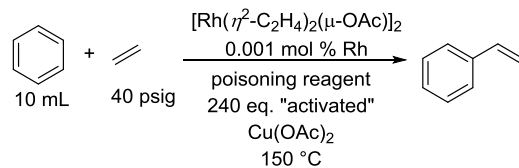


Figure 2.2.22. Plots of TOs versus time for styrene production catalyzed by $[\text{Rh}(\mu\text{-OAc})(\eta^2\text{-C}_2\text{H}_4)_2]_2$ with the addition of 0, 0.25, 0.5, 1 eq. (relative to Rh) of

PPh₃ (**A**), P(OCH₂)₃CEt (**B**) or 1,10-phenanthroline (**C**). Each data point is the average of three separate experiments. Error bars represent the standard deviations based on a minimum of three independent experiments.

Two possible rationalizations for the effect of activated Cu(OAc)₂ on the induction period are: (1) the Rh catalyzed arene alkenylation is a homogeneous process or (2) the Cu(II) oxidation step is a heterogeneous reaction. We believe that Cu(OAc)₂ becomes much more soluble in benzene as temperature increases from room temperature to 150 °C. Based on our previously proposed mechanism, at the reaction temperature (150 °C) soluble Cu(OAc)₂ can react with a Rh–H intermediate to regenerate a catalytically active Rh–OAc complex and complete the catalytic cycle.⁵⁰ We speculate that the activated Cu(OAc)₂ with a smaller particle size can dissolve in benzene more rapidly at the reaction temperature (150 °C) more rapidly than the untreated Cu(OAc)₂ that contains larger solid aggregates. This leads to the removal of the induction period since Rh intermediate(s) react with Cu(OAc)₂ more rapidly than they undergo reductive decomposition. We cannot entirely rule out the possibility of the generation of amorphous Cu(OAc)₂ after preheating Cu(OAc)₂ in organic solvent. The amorphous Cu(OAc)₂ can dissolve in benzene at 150 °C more rapidly than untreated Cu(OAc)₂. However, we do not have evidence for the formation of the amorphous Cu(OAc)₂ since it is unobservable by powder-XRD and IR spectroscopy. Activated Cu(OAc)₂ containing smaller particles is more "accessible" in a heterogeneous reaction and thus reacts faster with Rh intermediates than untreated Cu(OAc)₂.

In addition to the catalysis with ethylene using activated Cu(OAc)₂, we have also

performed the catalytic conversion of benzene and ethylene to styrene using 360 equiv. of copper(II) 2-ethylhexanoate ($\text{Cu}(\text{OHex})_2$) as the oxidant. $\text{Cu}(\text{OHex})_2$ is more soluble in benzene than $\text{Cu}(\text{OAc})_2$. Using $\text{Cu}(\text{OHex})_2$ as the oxidant, no apparent induction period was observed (Figure 2.2.23).

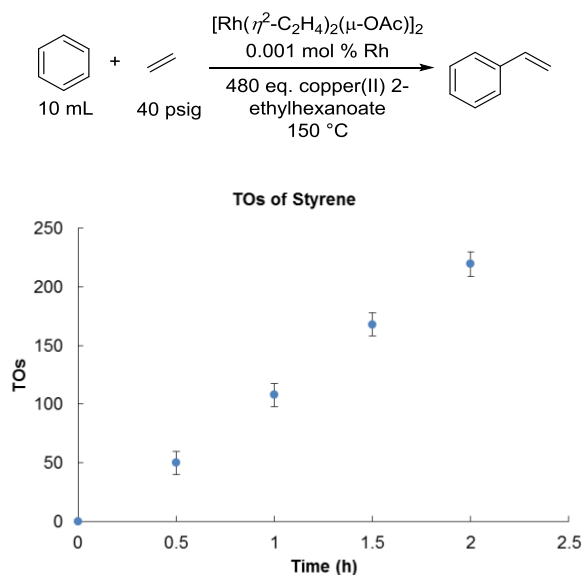


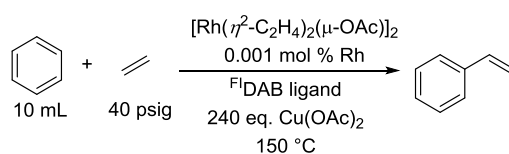
Figure 2.2.23. Plot of TOs versus time for styrene production catalyzed by $[\text{Rh}(\mu\text{-OAc})(\eta^2\text{-C}_2\text{H}_4)_2]_2$ using copper(II) 2-ethylhexanoate $[\text{Cu}(\text{OHex})_2]$ as the oxidant. Each data point is the average of three separate experiments. Error bars represent the standard deviations based on a minimum of three independent experiments.

2.2.5 Removal of the Induction Period by the Addition of Excess

$^{\text{Fl}}$ DAB Ligand

We performed the standard reaction using 240 equiv. of untreated $\text{Cu}(\text{OAc})_2$ with the addition of 1 to 20 equiv. of $^{\text{Fl}}$ DAB ligand (relative to the quantity of Rh) at the start of the reaction (Figure 2.2.24). When excess $^{\text{Fl}}$ DAB ligand is added, no pronounced induction period is observed. Notably, the introduction of additional

ligand does not impact the rate of the catalysis with ethylene. Also, in the catalytic conversion of benzene and propylene to propenylbenzenes, the addition of 5 equiv. of diimine ligand does not influence the linear:branched product ratio (Table 2.2.1). These results indicate the catalytic processes likely share the same active Rh catalyst. Monitoring the transformation of $[(^{\text{F1}}\text{DAB})\text{Rh}(\mu\text{-OAc})]_2$ under ethylene pressure at room temperature in the presence of 10 equiv. of diimine (relative to Rh) by *in situ* ^1H NMR spectroscopy revealed that approximately 90% of $[(^{\text{F1}}\text{DAB})\text{Rh}(\mu\text{-OAc})]_2$ is converted to $[\text{Rh}(\mu\text{-OAc})(\eta^2\text{-C}_2\text{H}_4)_2]_2$ 10 minutes after being treated with 10 psig of ethylene (Figure 2.2.3). This indicates that under the catalytic condition where a large excess of the diimine ligand is present, diimine ligand dissociation from $[(^{\text{F1}}\text{DAB})\text{Rh}(\mu\text{-OAc})]_2$ is not inhibited and the catalyst precursor is likely $[\text{Rh}(\mu\text{-OAc})(\eta^2\text{-C}_2\text{H}_4)_2]_2$. After heating commercial $\text{Cu}(\text{OAc})_2$ in benzene in the presence of $^{\text{F1}}\text{DAB}$ ligand (a 48:1 $\text{Cu}(\text{OAc})_2$ to $^{\text{F1}}\text{DAB}$ ratio was used) at 150 °C for 2 hours, the resulting mixture was filtered to isolate the solid Cu materials. Catalysis using the isolated solid as the oxidant reveals no apparent induction period (Figure 2.2.25). Powder-XRD and IR spectroscopy of the isolated $\text{Cu}(\text{OAc})_2$ (before use in catalysis) shows similar features to $\text{Cu}(\text{OAc})_2$ obtained by heating $\text{Cu}(\text{OAc})_2$ in benzene at 150 °C for 12 h (Figure 2.2.13 and Figure 2.2.14). This implies that the $^{\text{F1}}\text{DAB}$ ligand likely facilitates the conversion of commercial $\text{Cu}(\text{OAc})_2$ to activated $\text{Cu}(\text{OAc})_2$ through interaction of the diimine with $\text{Cu}(\text{OAc})_2$.



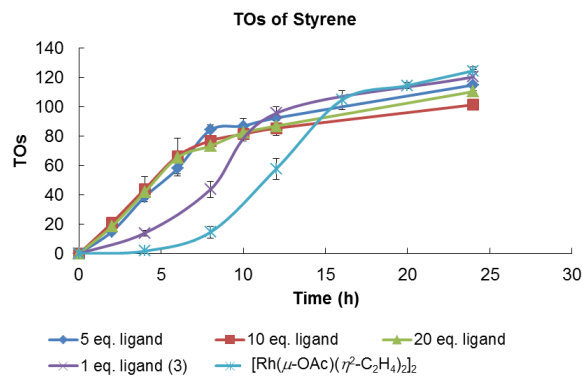


Figure 2.2.24. Plots of TOs versus time for styrene production catalyzed by $[\text{Rh}(\mu\text{-OAc})(\eta^2\text{-C}_2\text{H}_4)_2]_2$ with the addition of 0 to 20 eq. of F^1DAB ligand. Reaction conditions: 0.001 mol % of Rh (relative to benzene), 240 eq. of $\text{Cu}(\text{OAc})_2$ (relative to Rh), 10 mL benzene, 40 psig ethylene, 150 °C. Error bars represent the standard deviations based on a minimum of three independent experiments.

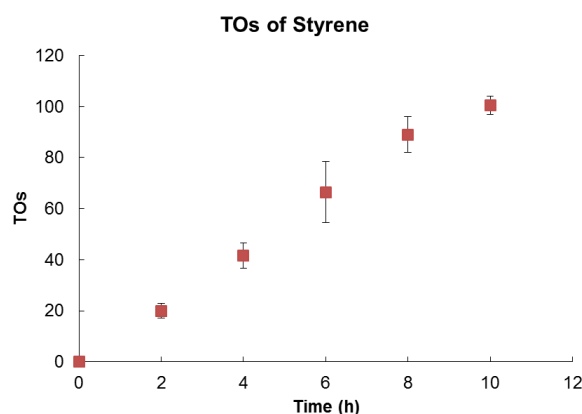
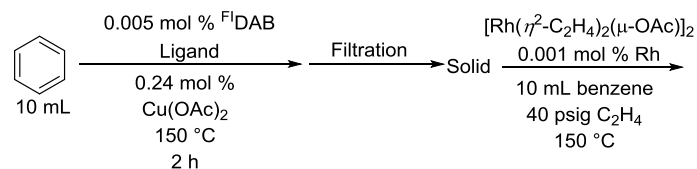


Figure 2.2.25. Plot of TOs versus time for styrene production catalyzed by $[\text{Rh}(\mu\text{-OAc})(\eta^2\text{-C}_2\text{H}_4)_2]_2$ using solid materials isolated from the reaction mixture obtained by heating copper(II) acetate in 10 mL benzene with 0.005 mol % F^1DAB at 150 °C for 2 h. Each data point is the average of three separate experiments. Error bars represent the standard deviations based on a minimum of three independent experiments.

As shown in Figure 2.2.2, catalysis using the diimine ligated Rh(I) catalyst precursor exhibits a reduced induction period compared with the catalysis using

$[\text{Rh}(\mu\text{-OAc})(\eta^2\text{-C}_2\text{H}_4)_2]_2$. This is likely due to dissociation of the diimine ligand from the diimine Rh(I) complex followed by diimine interaction with $\text{Cu}(\text{OAc})_2$ to facilitate the $\text{Cu}(\text{OAc})_2$ activation process. To test this hypothesis, we have compared TO versus time plots for catalysis with five-fold Rh loading (0.005 mol %) of $[\text{Rh}(\mu\text{-OAc})(\eta^2\text{-C}_2\text{H}_4)_2]_2$ and $[(^{\text{Fl}}\text{DAB})\text{Rh}(\mu\text{-OAc})]_2$ (**3**) under the standard catalytic conditions. The reaction using $[\text{Rh}(\mu\text{-OAc})(\eta^2\text{-C}_2\text{H}_4)_2]_2$ shows an apparent induction period while the catalysis using $^{\text{Fl}}\text{DAB}$ ligated Rh complex does not (Figure 2.2.26). This result is consistent with the aforementioned assumption that the dissociated diimine ligand from $[(^{\text{Fl}}\text{DAB})\text{Rh}(\mu\text{-OAc})]_2$ helps activate $\text{Cu}(\text{OAc})_2$ and thus removes the induction period. The addition of 100 equiv. of $^{\text{Fl}}\text{DAB}$ compound (relative to the quantity of Rh) also shows no induction period, but the rate of catalysis is suppressed using 0.269 mmol of $\text{Cu}(\text{OAc})_2$ (240 equiv. relative to Rh) and $[\text{Rh}(\mu\text{-OAc})(\eta^2\text{-C}_2\text{H}_4)_2]_2$ containing 0.001 mol % Rh. In contrast, adding 100 equiv. of $^{\text{Fl}}\text{DAB}$ does not have significant effects on the apparent TOF (calculated after 8 h) of the catalysis using 0.0001 mol % Rh and 0.269 mmol of $\text{Cu}(\text{OAc})_2$ (2400 equiv. relative to Rh) compared to that obtained in the standard catalytic run with no induction period observed (Figure 2.2.27). These results demonstrate that the addition of a large excess of $^{\text{Fl}}\text{DAB}$ compound seemingly inhibits catalysis by its interaction with $\text{Cu}(\text{OAc})_2$ instead of Rh species. This also implies that the activation of $\text{Cu}(\text{OAc})_2$ is likely due to reversible coordination of diimine ligand to $\text{Cu}(\text{OAc})_2$. Analogous (diimine) $\text{Cu}(\text{Cl})_2$ complexes have also been reported.^{76,77} Thus, the formation of activated $\text{Cu}(\text{OAc})_2$ facilitated by diimine might be due to reversible

coordination with $\text{Cu}(\text{OAc})_2$ to generate a transient $(^{\text{FI}}\text{DAB})\text{Cu}(\text{OAc})_2$ adduct, and the dynamic equilibrium between soluble $(^{\text{FI}}\text{DAB})\text{Cu}(\text{OAc})_2$ and insoluble $\text{Cu}(\text{OAc})_2$ solid leads to the activation of the $\text{Cu}(\text{OAc})_2$. $\text{Cu}(\text{OAc})_2$ is present in large excess relative to the diimine, thus complete conversion of $\text{Cu}(\text{OAc})_2$ to $(^{\text{FI}}\text{DAB})\text{Cu}(\text{OAc})_2$ is not possible.

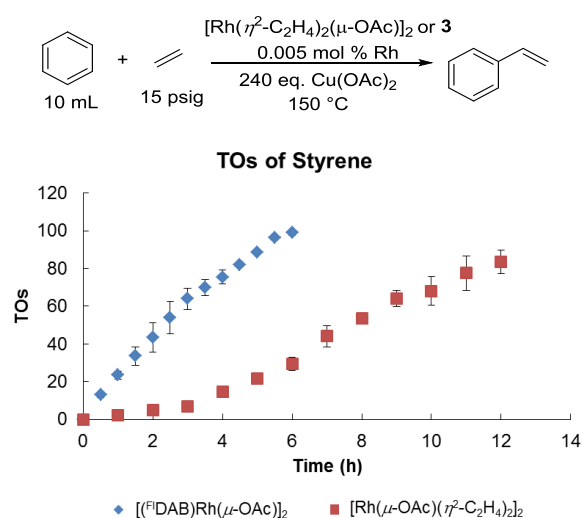


Figure 2.2.26. Comparison of TOs versus time plots for styrene production catalyzed by $[\text{Rh}(\mu\text{-OAc})(\eta^2\text{-C}_2\text{H}_4)_2]_2$ and $[(^{\text{FI}}\text{DAB})\text{Rh}(\mu\text{-OAc})_2]$ (**3**). Reaction conditions: 0.005 mol % of Rh (relative to benzene), 240 eq. of $\text{Cu}(\text{OAc})_2$ (relative to Rh), 10 mL benzene, 15 psig ethylene, 150 °C. Error bars represent the standard deviations based on a minimum of three independent experiments.

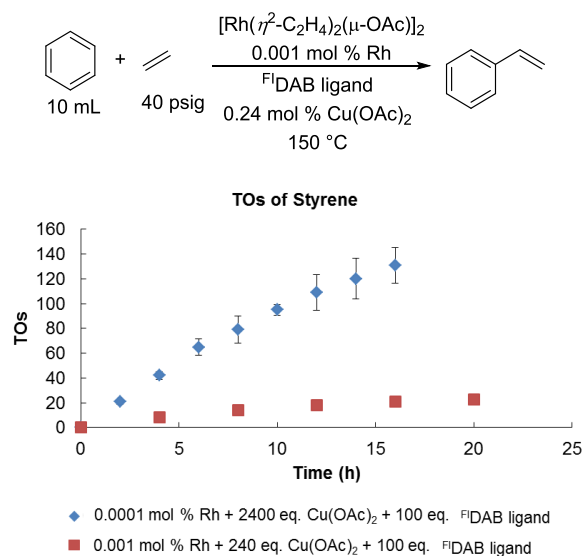


Figure 2.2.27. Comparison of TOs versus time plots for styrene production using various loading of $[\text{Rh}(\mu\text{-OAc})(\eta^2\text{-C}_2\text{H}_4)_2]_2$ with the addition of 100 eq. of $^{\text{Fl}}\text{DAB}$ ligand. Reaction conditions: 0.001 or 0.0001 mol % of Rh (relative to benzene), 100 eq. of $^{\text{Fl}}\text{DAB}$ ligand (relative to Rh), 0.269 mmol $\text{Cu}(\text{OAc})_2$ (240 eq. relative to 0.001 mol % Rh, 2400 eq. relative to 0.0001 mol % Rh), 10 mL benzene, 40 psig ethylene, 150 °C. Each data point is the average of three separate experiments. Error bars represent the standard deviations based on a minimum of three independent experiments.

2.2.6 Initial Studies to Understand the Transformation of Rh

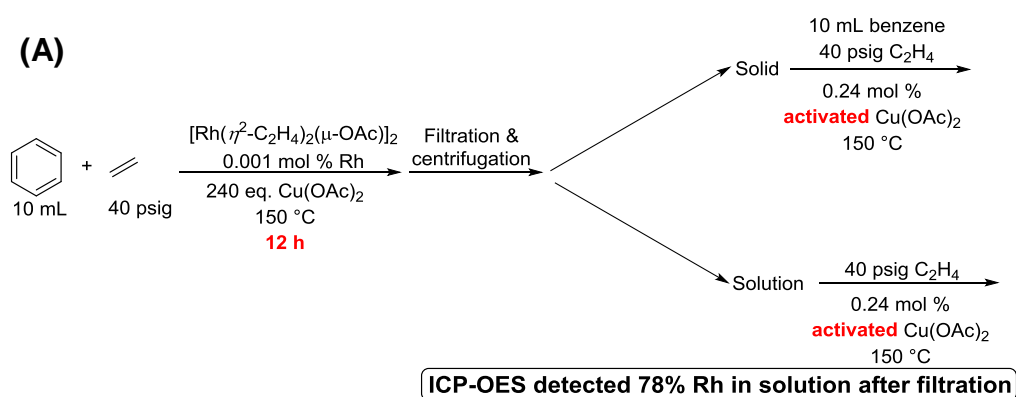
To understand the nature of the induction period and how Rh evolves, we probed the reactivity of our Rh catalyst in solid and solution phases of reaction mixtures separately both during and after the induction period of the catalysis with ethylene, benzene and $[\text{Rh}(\mu\text{-OAc})(\eta^2\text{-C}_2\text{H}_4)_2]_2$. In one case, a reaction was performed with untreated $\text{Cu}(\text{OAc})_2$ under the standard conditions for 12 h (after the induction period). The reaction mixture was then filtered, and the filtrate was centrifuged in order to separate any remaining insoluble solid that passed through the filter. The insoluble materials collected from the filtration and centrifugation were combined. The solid material and the supernatant were then separately subjected to the same catalytic conditions (*i.e.*, 0.269 mmol activated $\text{Cu}(\text{OAc})_2$ (240 equiv. relative to 0.001 mol % Rh), 40 psig ethylene, 150 °C) to compare their catalytic activity for styrene production (Figure 2.2.28). The reaction using the supernatant achieved 90% yield of styrene after 12 h whereas the reaction using the solid material only produced 7% yield of styrene after 12 h. This suggests that after the induction period, the active Rh catalyst is soluble. This experiment is consistent with hypothesis of the active catalyst being a soluble molecular species. This result is also in agreement with the

aforementioned catalyst fractional poisoning tests (see above). Notably, in the catalysis using the supernatant, the TO versus time plot of the catalysis is linear without an induction period (Figure 2.2.28) with no evidence of a second induction period (*e.g.*, formation of Rh nanoparticle catalysts from molecular Rh). Also the catalysis with the supernatant showed a ~25% loss of reactivity relative to the catalysis with $[\text{Rh}(\mu\text{-OAc})(\eta^2\text{-C}_2\text{H}_4)_2]_2$ and activated $\text{Cu}(\text{OAc})_2$ according to the comparison of apparent TOF calculated after 8 h [$2.1 \times 10^{-3} \text{ s}^{-1}$ (note: this apparent TOF is based on total starting amount of Rh) versus $2.8 \times 10^{-3} \text{ s}^{-1}$]. In contrast, catalysis using the insoluble material separated from the reaction mixture reveals an induction period.

Next, we performed a catalytic reaction with untreated $\text{Cu}(\text{OAc})_2$ and stopped the after 1 h (during the induction period). The sample preparation was performed as described immediately above to separate the insoluble and soluble materials. Using untreated $\text{Cu}(\text{OAc})_2$ as the oxidant, the catalysis with the isolated solid materials gave 96 TOs of styrene after 20 h while the soluble materials did not produce styrene after 20 h (Figure 2.2.28). These results suggest that during the induction period most of the Rh is insoluble. It is also germane that the reaction using the solid materials shows an induction period and nearly identical apparent TOF following the induction period (calculated from 12 to 16 h) as was observed in the standard reaction using $[\text{Rh}(\mu\text{-OAc})(\eta^2\text{-C}_2\text{H}_4)_2]_2$ and untreated $\text{Cu}(\text{OAc})_2$.

We used ICP-OES analysis to determine the amount of Rh in the reaction solution during and after the induction period. We performed standard catalytic reactions with

[Rh(μ -OAc)(η^2 -C₂H₄)₂]₂ and untreated Cu(OAc)₂ and stopped the reaction after 1 h (during the induction period) or after 12 h (after the induction period). The soluble materials were then collected by filtration and centrifugation/decantation the reaction mixture. Analysis of the soluble materials at 1 h by ICP-OES reveals <1% of Rh relative to the total amount of starting Rh, which is in agreement with the negligible reactivity of the isolated soluble materials mentioned above (Figure 2.2.28). However, 78% of starting Rh is found in the solution phase at the 12 h time point, which is consistent with ~25% loss of reactivity of the isolated solution phase described above (Figure 2.2.28). These results indicate that most Rh materials are insoluble during the induction period, but after the induction period and during catalysis, most Rh is converted to soluble materials.



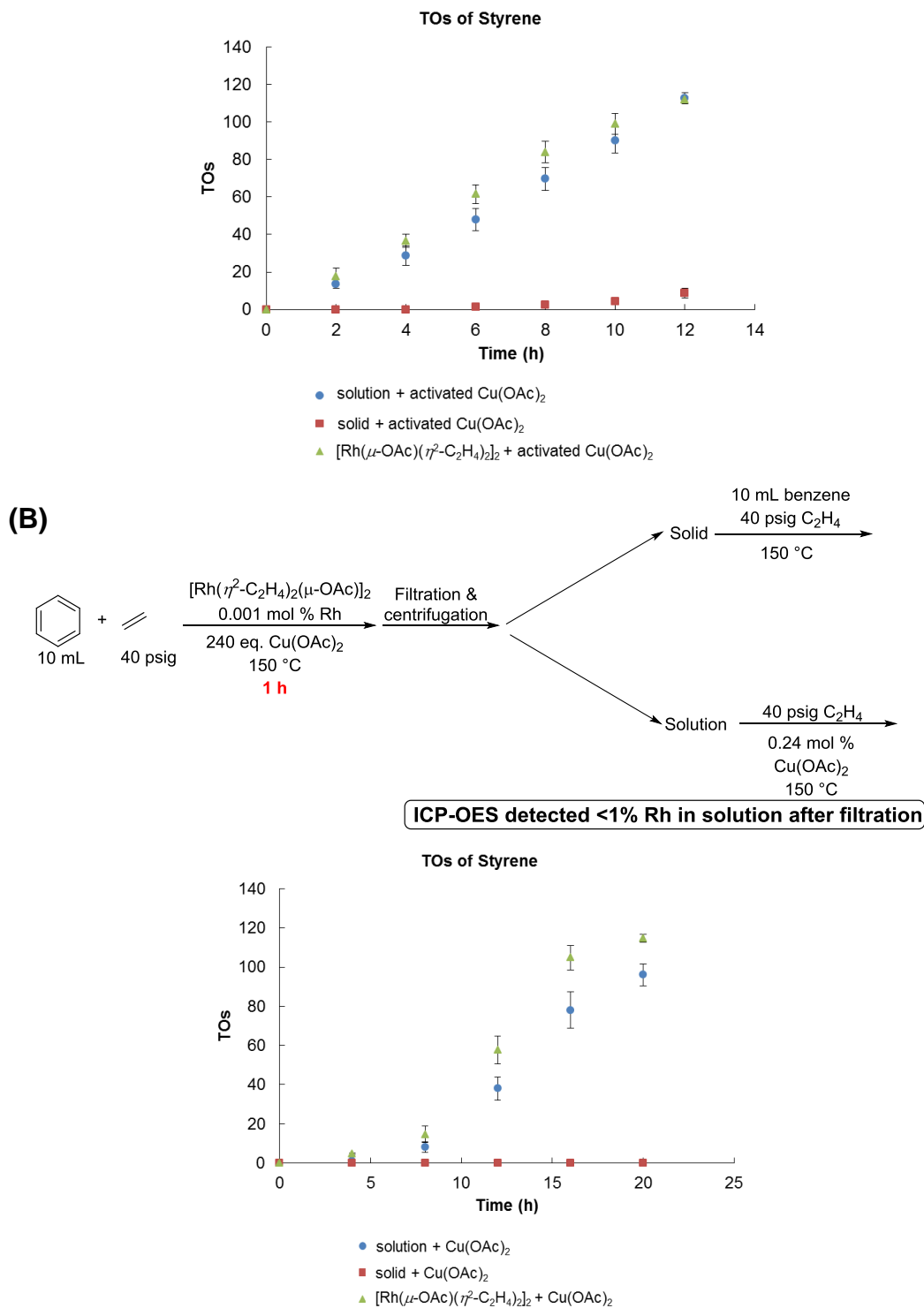
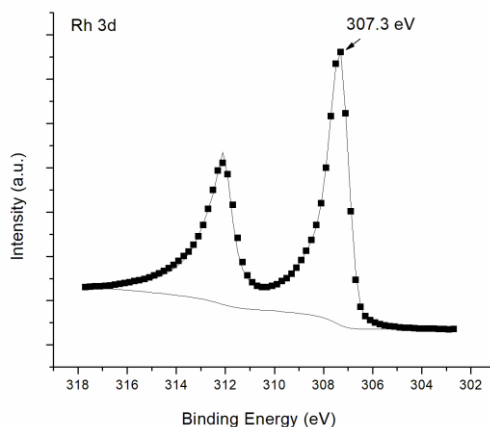


Figure 2.2.28. Comparison of plots for TOs versus time for styrene production using solid materials versus soluble material isolated from the reaction mixture after 12 h (A) or 1 h (B) of the catalysis with 40 psig ethylene using $[\text{Rh}(\mu\text{-OAc})(\eta^2\text{-C}_2\text{H}_4)_2]_2$ [0.001 mol % of Rh (relative to benzene)] at 150 °C. TOs of styrene were obtained by subtracting TO at 0 h (if any) from the raw TO data. Error bars represent the standard deviations based on a minimum of three independent experiments.

Based on these results, along with the observation that $[\text{Rh}(\mu\text{-OAc})(\eta^2\text{-C}_2\text{H}_4)_2]_2$ undergoes rapid thermal decomposition to form Rh nanoparticles in the absence of Cu(II), we propose that at 150 °C under catalytic conditions with untreated $\text{Cu}(\text{OAc})_2$, $[\text{Rh}(\mu\text{-OAc})(\eta^2\text{-C}_2\text{H}_4)_2]_2$ thermally decomposes to catalytically inactive and insoluble Rh material.

Next, we sought evidence for reduction of $[\text{Rh}(\mu\text{-OAc})(\eta^2\text{-C}_2\text{H}_4)_2]_2$ in the presence of untreated $\text{Cu}(\text{OAc})_2$. Collaborating with Zhongwen Luo in our lab, we studied the evolution of Rh species during the catalysis using X-ray photoelectron spectroscopy (XPS). To evaluate the binding energy of Rh(0), we obtained the photoemission spectrum of Rh metal foil and silica-supported Rh nanoparticles. As shown in Figure 2.2.29, the $3d_{5/2}$ binding energy for Rh(0) was measured to be 307.3 eV.



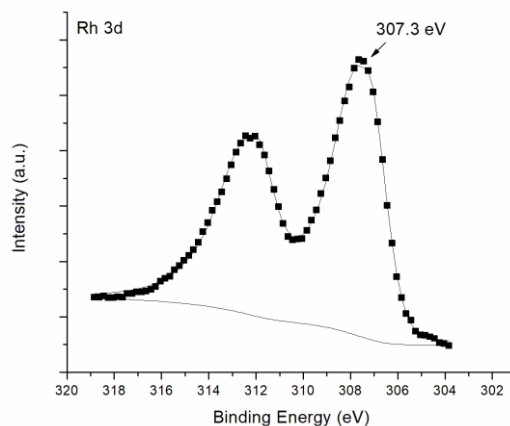


Figure 2.2.29. X-ray photoelectron spectra (Rh 3d region) of (top) Rh metal foil and (bottom) silica-supported Rh metal nanoparticles.

Using XPS, we then examined the black precipitate formed during the thermal decomposition of $[\text{Rh}(\mu\text{-OAc})(\eta^2\text{-C}_2\text{H}_4)_2]_2$ in benzene in the absence of $\text{Cu}(\text{OAc})_2$. The Rh $3d_{5/2}$ binding energy of the Rh species in the precipitate is 307.3 eV (Figure 2.2.30), as was observed for Rh foil. Thus, we conclude that $[\text{Rh}(\mu\text{-OAc})(\eta^2\text{-C}_2\text{H}_4)_2]_2$ decomposes to Rh(0) species upon heating in benzene in the absence of $\text{Cu}(\text{OAc})_2$, which is consistent with results from TEM studies that confirm the presence of Rh(0) nanoparticles.

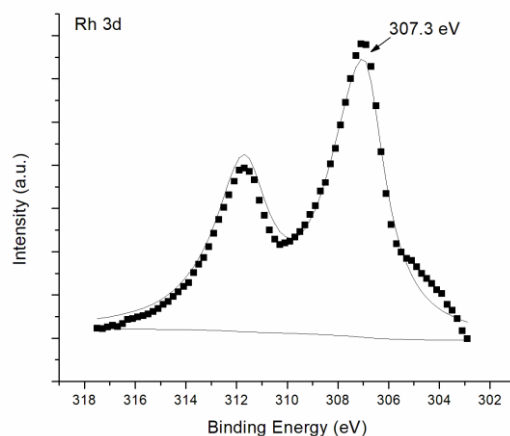


Figure 2.2.30. X-ray photoelectron spectrum (region Rh 3d) of insoluble Rh species formed during the thermal decomposition of $[\text{Rh}(\mu\text{-OAc})(\eta^2\text{-C}_2\text{H}_4)_2]_2$ (0.001 mol % Rh relative to benzene) at 150 °C under 40 psig of ethylene in benzene in the absence

of Cu(OAc)₂.

Subsequently, we examined the recovered Rh species after 1 h (during the induction period) and 12 h (after the induction period) in the catalysis with ethylene and [Rh(μ -OAc)(η^2 -C₂H₄)₂]₂ using 240 equiv. of untreated Cu(OAc)₂ (Figure 2.2.31). XPS data revealed Rh 3d_{5/2} binding energies of 309.2 eV and 308.9 eV after 1h and 12 h, respectively (Figure 2.2.31). Using activated Cu(OAc)₂ and analyzing the Rh material after 1 h reveals a Rh 3d_{5/2} binding energy of 308.9 eV (Figure 2.2.31). From these data, we conclude that the catalyst resting state has a Rh 3d_{5/2} binding energy of 308.9 eV. We also acquired XPS data for three well-defined molecular Rh complexes with different formal oxidation states of Rh, [Rh(μ -OAc)(η^2 -C₂H₄)₂]₂ (308.0 eV), Rh₂(OAc)₄ (308.7 eV), and RhCl₃ \times H₂O (309.6 eV) (Figure 2.2.31 and Table S3). Figure 2.2.31 indicate that the recovered soluble catalytic active Rh species showed a Rh 3d_{5/2} binding energy at 308.9 eV, which is most consistent with XPS data of the well-defined Rh(II) complex Rh₂(OAc)₄. Although caution is needed when interpreting the XPS data, since different types of ligands may result in differences in observed binding energy, analysis of the XPS data are consistent with a Rh(II) catalyst resting state.

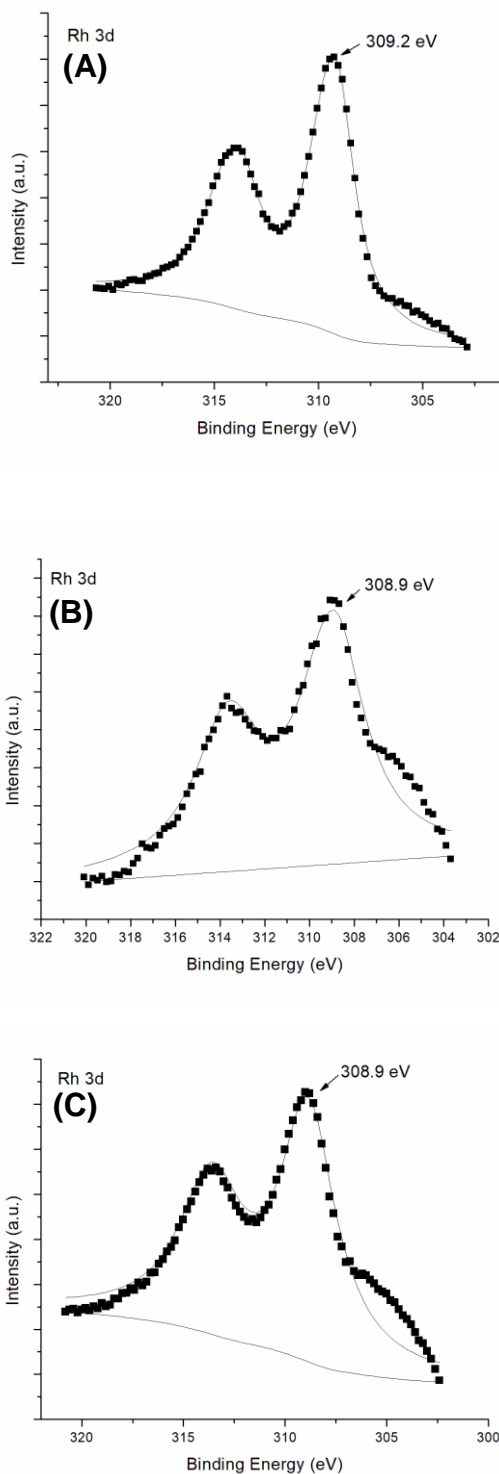


Figure 2.2.31. X-ray photoelectron spectra (region Rh 3d) of recovered Rh species formed (A and B) after 1 h and 12 h of catalysis, respectively, with 40 psig ethylene and $[\text{Rh}(\mu\text{-OAc})(\eta^2\text{-C}_2\text{H}_4)_2]_2$ (0.001 mol % Rh relative to benzene) using **untreated** $\text{Cu}(\text{OAc})_2$ (240 eq. relative to Rh); (C) after 1 h of catalysis with 40 psig ethylene and $[\text{Rh}(\mu\text{-OAc})(\eta^2\text{-C}_2\text{H}_4)_2]_2$ (0.001 mol % Rh relative to benzene) using **activated** $\text{Cu}(\text{OAc})_2$ (240 eq. relative to Rh).

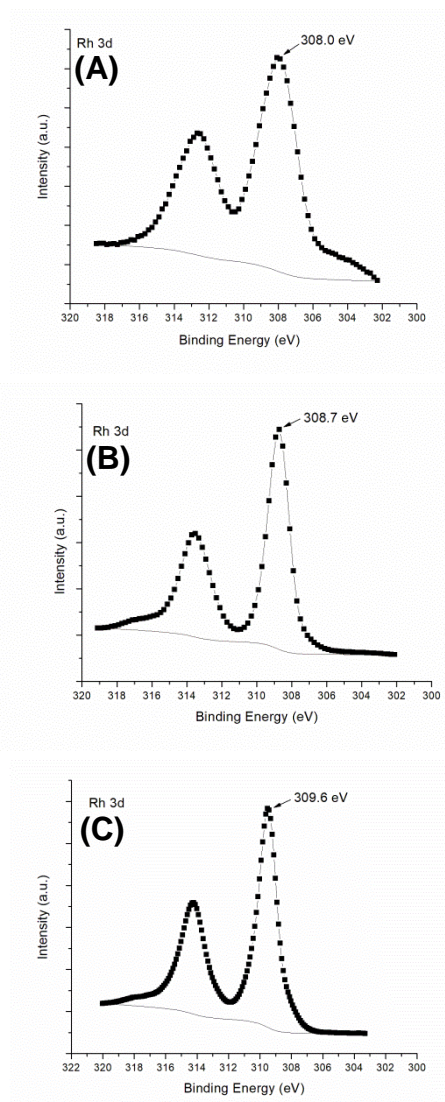


Figure 2.2.32. X-ray photoelectron spectra (region Rh 3d) of $[\text{Rh}(\mu\text{-OAc})(\eta^2\text{-C}_2\text{H}_4)_2]_2$ (A), $\text{Rh}_2(\text{OAc})_4$ (B) and $\text{RhCl}_3 \cdot x\text{H}_2\text{O}$ (C).

Table 2.2.3. Formal oxidation states of Rh in and Rh $3d_{5/2}$ binding energy of Rh metal foil, $[\text{Rh}(\mu\text{-OAc})(\eta^2\text{-C}_2\text{H}_4)_2]_2$, $\text{Rh}_2(\text{OAc})_4$ and $\text{RhCl}_3 \cdot x\text{H}_2\text{O}$

Complex	Formal oxidation state of Rh	Rh $3d_{5/2}$ binding energy
Rh metal foil	0	307.3 eV
$[\text{Rh}(\mu\text{-OAc})(\eta^2\text{-C}_2\text{H}_4)_2]_2$	+1	308.0 eV
$\text{Rh}_2(\text{OAc})_4$	+2	308.7 eV
$\text{RhCl}_3 \cdot x\text{H}_2\text{O}$	+3	309.6 eV

In a control experiment, $[\text{Rh}(\mu\text{-OAc})(\eta^2\text{-C}_2\text{H}_4)_2]_2$ was heated together with mesoporous SiO_2 in benzene at 150 °C for 1 h in an attempt to capture the reduced Rh species on the SiO_2 support. The non-volatile materials from this thermolysis reaction

were analyzed by XPS and TEM-EDS. A $3d_{5/2}$ peak at 307.0 eV was observed by XPS, similar to metallic Rh (Figure 2.2.33). Indeed, TEM/EDS and lattice constant analysis confirmed that Rh(0) nanoparticles were captured by SiO_2 (Figure 2.2.34). These results verified that our sample recovery method enabled us to observe Rh(0) nanoparticles if they were formed during the catalytic reaction.

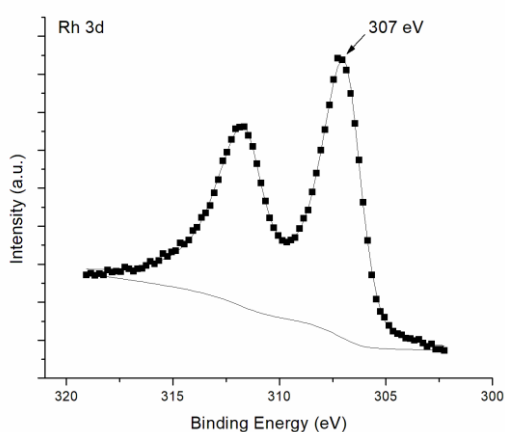
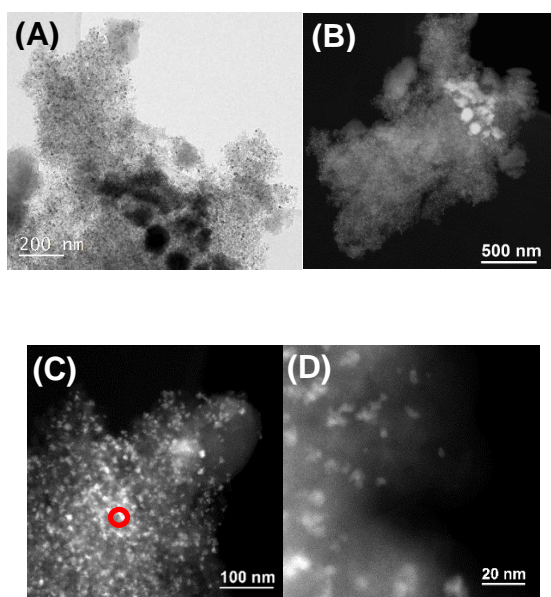


Figure 2.2.33. X-ray photoelectron spectrum (region Rh 3d) of recovered Rh species from the thermal decomposition of $[\text{Rh}(\mu\text{-OAc})(\eta^2\text{-C}_2\text{H}_4)_2]_2$ (0.001 mol % Rh relative to benzene) in benzene after 1 h in the presence of SiO_2 .



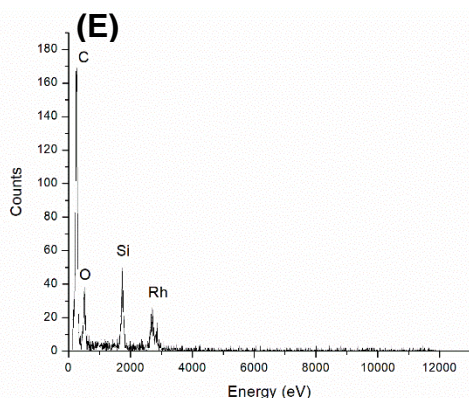


Figure 2.2.34. TEM/STEM images and EDS analysis of recovered Rh species from the thermal decomposition of $[\text{Rh}(\mu\text{-OAc})(\eta^2\text{-C}_2\text{H}_4)_2]_2$ (0.001 mol % Rh relative to benzene) in benzene after 1 h in the presence of SiO_2 . (A) bright field TEM images of SiO_2 captured Rh species; (B-D) dark-field STEM images of SiO_2 captured Rh species; (E) EDS analysis of selected particle (circled in red on Figure 15C).

Zhongwen Luo in our lab characterized the recovered Rh species formed after 1 h of catalysis using untreated $\text{Cu}(\text{OAc})_2$ by scanning transmission electron microscopy (STEM). The STEM-EDS analysis of non-volatile materials collected after the reaction indicated the presence of rhodium species present in the small bright spots in Figure 16. Although Rh nanoparticles formed during the thermal decomposition of $[\text{Rh}(\mu\text{-OAc})(\eta^2\text{-C}_2\text{H}_4)_2]_2$ in benzene in the absence of $\text{Cu}(\text{OAc})_2$, the nature of the Rh species in Figure 2.2.35 is ambiguous. Figure 2.2.36 shows compositional mapping in the vicinity of the features associated with Rh, confirming that Rh is present in a separate phase from the Cu component.

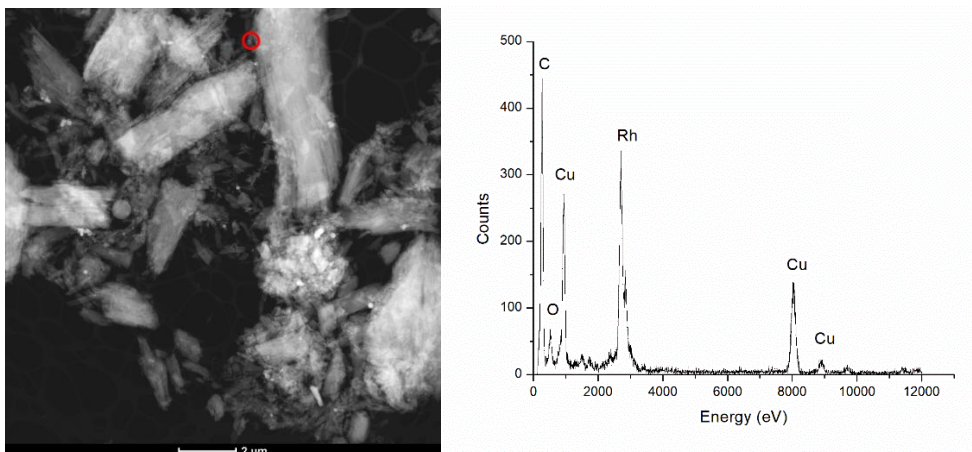


Figure 2.2.35. A STEM image of recovered Rh species formed after 1 h of catalysis with 40 psig ethylene and $[\text{Rh}(\mu\text{-OAc})(\eta^2\text{-C}_2\text{H}_4)_2]_2$ (0.001 mol % Rh relative to benzene) using untreated $\text{Cu}(\text{OAc})_2$ (240 eq. relative to Rh) (left) and EDS analysis of selected single particle circled in red on the left STEM image (right).

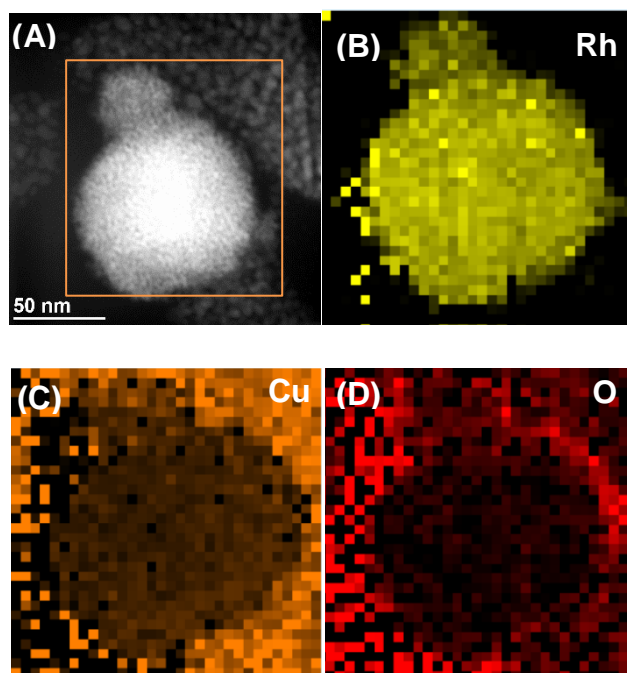


Figure 2.2.36. STEM-EDS maps of recovered Rh species formed after 1 h in the catalysis with 40 psig ethylene and $[\text{Rh}(\mu\text{-OAc})(\eta^2\text{-C}_2\text{H}_4)_2]_2$ (0.001 mol % Rh relative to benzene) using untreated $\text{Cu}(\text{OAc})_2$ (240 eq. relative to Rh). (A) overall dark-field STEM image; (B) EDS map of Rh; (C) EDS maps of Cu; (D) EDS maps of O. Rh, Cu and O are shown in yellow, orange and red, respectively.

We also performed the catalysis with ethylene using the same amount of unactivated $\text{Cu}(\text{OAc})_2$ (48.8 mg, 0.24 mol % relative to benzene) while varying the loading of $[\text{Rh}(\mu\text{-OAc})(\eta^2\text{-C}_2\text{H}_4)_2]_2$ (0.001 mol % Rh, 0.005 mol % Rh, and 0.01 mol % Rh relative to benzene) under 40 psig ethylene at 150 °C (Figure 2.2.37). It was found that the apparent TOF following the induction period decreased from $3.0 \times 10^{-3} \text{ s}^{-1}$ to $1.5 \times 10^{-4} \text{ s}^{-1}$ (using 0.001 mol % Rh, apparent TOF is calculated from 8 h to 12 h; using 0.005 mol % or 0.01 mol % Rh, apparent TOF is calculated from 6 h to 8 h) as the concentration of $[\text{Rh}(\mu\text{-OAc})(\eta^2\text{-C}_2\text{H}_4)_2]_2$ was increased from 0.001 mol % to 0.01 mol % . We hypothesized that the higher concentration of

$[\text{Rh}(\mu\text{-OAc})(\eta^2\text{-C}_2\text{H}_4)_2]_2$ results in more reduced Rh particles, which in turn leads to increased agglomeration following the thermal decomposition, thus decreasing the % of Rh that can leach back into solution. This observation is consistent with previously discussed decomposition and leaching model since the soluble active Rh species are expected to leach more readily from reduced Rh material with smaller particle size.

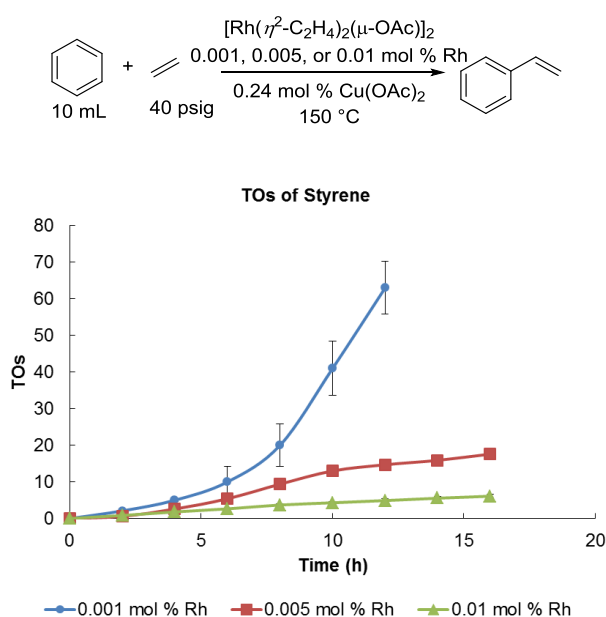


Figure 2.2.37. Plots of TOs versus time for styrene production catalyzed by various loading of $[\text{Rh}(\mu\text{-OAc})(\eta^2\text{-C}_2\text{H}_4)_2]_2$ (0.001 mol % Rh, 0.005 mol % Rh, and 0.01 mol % Rh relative to benzene). Error bars represent the standard deviations based on a minimum of three independent experiments.

In an effort to study the catalytically active Rh species under catalytic conditions where an induction period is not observed (*i.e.*, using activated $\text{Cu}(\text{OAc})_2$ as the oxidant or using 5 equiv. $^{\text{Fl}}\text{DAB}$ ligand), catalytic reactions were stopped after 1 h and filtered. The filtrates were subsequently centrifuged and the supernatants were decanted. The reactivity of the resulting soluble Rh species with ethylene was studied by subjecting the soluble Rh species to catalytic conditions where an induction period

is not observed (*i.e.*, using activated $\text{Cu}(\text{OAc})_2$ as the oxidant or using 5 equiv. $^{\text{Fl}}\text{DAB}$ ligand) (Figure 2.2.38). As expected, no apparent induction period is observed for either of these reactions. For both types of soluble materials, a 20-30% loss of reactivity is observed when compared to the catalysis using $[\text{Rh}(\mu\text{-OAc})(\eta^2\text{-C}_2\text{H}_4)_2]_2$ precursor.

In addition, ICP-OES analysis has been conducted to quantify the amount of Rh content in the solution phase after 1 h of catalysis with $[\text{Rh}(\mu\text{-OAc})(\eta^2\text{-C}_2\text{H}_4)_2]_2$ where induction period is not observed (*i.e.*, using activated $\text{Cu}(\text{OAc})_2$ or an addition of 5 equiv. of $^{\text{Fl}}\text{DAB}$ ligand). The analysis shows that, with activated $\text{Cu}(\text{OAc})_2$, soluble materials contains 68% of Rh relative to the total amount of Rh added before the catalysis, and with 5 equiv. of added $^{\text{Fl}}\text{DAB}$ ligand, 75% of Rh is in the solution (Figure 2.2.38). This result indicates that in either case, at 1 h most of the molecular Rh species have not decomposed to insoluble Rh material but remain in the solution instead. In contrast, as mentioned above, ICP studies of the catalysis using untreated $\text{Cu}(\text{OAc})_2$ found that <1% of starting Rh is in solution after 1 h.

The results of reactivity tests and ICP-OES analysis indicate that the addition of activated $\text{Cu}(\text{OAc})_2$ or diimine ligand helps stabilize soluble molecular Rh species in the reaction solution, and thus the decomposition of $[\text{Rh}(\mu\text{-OAc})(\eta^2\text{-C}_2\text{H}_4)_2]_2$ precursor to form insoluble Rh species is suppressed. However, the ICP analysis shows a rhodium loss of approximately 20-30%, indicating that part of the soluble Rh is converted to a presumably inactive Rh precipitate. This loss in rhodium is consistent with the observed 20-30% loss of reactivity of the soluble Rh species

(Figure 2.2.38).

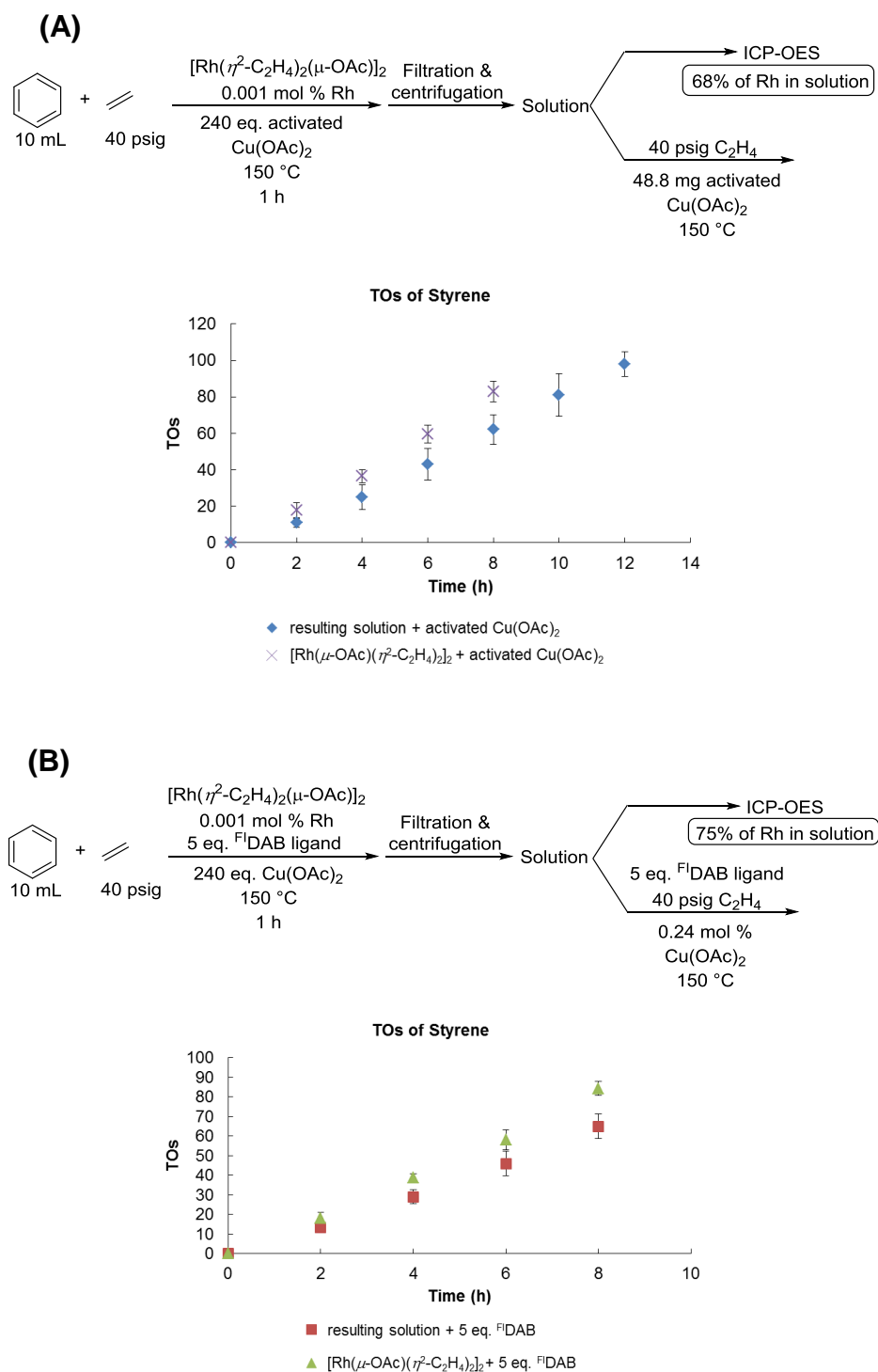
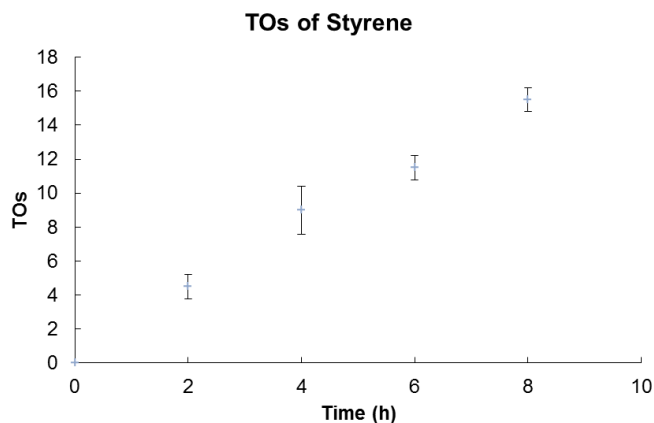


Figure 2.2.38. Plots of TOs versus time for styrene production using the solution phase of the reaction mixture after 1 h of the catalysis with 40 psig ethylene using $[\text{Rh}(\mu\text{-OAc})(\eta^2\text{-C}_2\text{H}_4)_2]_2$ under the conditions where activated $\text{Cu}(\text{OAc})_2$ oxidant is

used (**A**) or 5 eq. of ^{F1}DAB ligand is added (**B**) and its comparison to the catalysis with 40 psig ethylene using $[\text{Rh}(\mu\text{-OAc})(\eta^2\text{-C}_2\text{H}_4)_2]_2$ with the use of activated $\text{Cu}(\text{OAc})_2$ (a) or addition of 5 eq. of ^{F1}DAB ligand (b). TO of styrene was obtained by subtracting TO at 0 h (if any) from the raw TO data. Error bars represent the standard deviations based on a minimum of three independent experiments.

Given that the induction period is not observed in the catalysis using soluble copper oxidants ($\text{Cu}(\text{OHex})_2$), we expected, in contrast to the catalysis using untreated $\text{Cu}(\text{OAc})_2$, no significant change in the amount of soluble Rh during catalysis. We performed reactions with ethylene and 240 equiv. of $\text{Cu}(\text{OHex})_2$ under standard catalytic conditions and performed filtration/centrifugation and decantation after 15 min and 45 min of reaction (the reaction reaches completion at 1 h). We found that 82% and 84% of starting Rh remained (as detected by ICP-OES) at 15 min and 45 min, respectively (Table 2.2.4). In contrast, in the catalysis using untreated $\text{Cu}(\text{OAc})_2$ <1% and 78% of starting Rh is found in the solution phase at the 1 h (during the induction period) and 12 h (after the induction period) time point, respectively (Table 2.2.4). These results are consistent with our hypothesis that Cu(II) oxidants mitigate the conversion of soluble Rh materials to insoluble Rh. Notably, based on the amount of soluble Rh material in Table 1 (soluble Rh is considered to be catalytically active species whereas insoluble Rh material is considered to be inactive), the actual TOF of the catalysis using $\text{Cu}(\text{OAc})_2$ (after the induction period) and $\text{Cu}(\text{OHex})_2$ are $\sim 3.7 \times 10^{-3} \text{ s}^{-1}$ (calculated from 8 h to 16 h) and $\sim 3.7 \times 10^{-2} \text{ s}^{-1}$ (calculated after 1 h) respectively. To eliminate the possibility that the decomposition process may occur before 1 h of catalysis, we ran the standard reaction using activated $\text{Cu}(\text{OAc})_2$ at 125 °C in order to slow down the reaction rate so that we could monitor the reaction



at earlier stages (

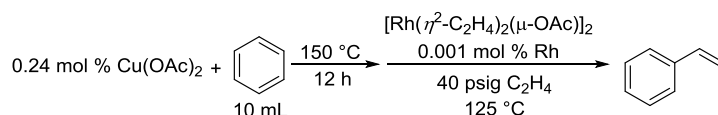
Figure 2.2.39). At 125 °C, an induction period was not observed within 8 h of reaction. In addition, we performed catalysis using $[\text{Rh}(\mu\text{-OAc})(\eta^2\text{-C}_2\text{H}_4)_2]_2$ and untreated $\text{Cu}(\text{OAc})_2$ under standard conditions until 1 h at which time it is anticipated that most of the Rh would be insoluble. The reaction mixture was subsequently treated with activated $\text{Cu}(\text{OAc})_2$ or 5 equiv. of $^{\text{Fl}}\text{DAB}$ ligand and then subjected to the standard catalytic conditions (Figure 2.2.40 and Figure 2.2.41). The new catalysis with either treatment exhibited an induction period. Thus, activated $\text{Cu}(\text{OAc})_2$ or diimine ligand does not likely remove the induction period by facilitating the leaching process of insoluble decomposed Rh species. It is of interest to note that when a benzene solution of $[\text{Rh}(\mu\text{-OAc})(\eta^2\text{-C}_2\text{H}_4)_2]_2$ and 5 equiv. of $^{\text{Fl}}\text{DAB}$ was heated under ethylene in the absence of $\text{Cu}(\text{OAc})_2$ for 1 h and subsequently added to untreated $\text{Cu}(\text{OAc})_2$ and tested under the standard reaction conditions, a significant induction period was observed (Figure 2.2.42). This indicates that excess diimine ligand cannot directly mitigate the degradation of molecular Rh materials. Instead, $^{\text{Fl}}\text{DAB}$ ligand likely suppresses the formation of insoluble Rh species by rapidly transforming commercial $\text{Cu}(\text{OAc})_2$ to activated $\text{Cu}(\text{OAc})_2$, which possesses significantly minimized particle size. In addition, $[\text{Rh}(\mu\text{-OAc})(\eta^2\text{-C}_2\text{H}_4)_2]_2$ was heated in benzene

under ethylene in the absence of $\text{Cu}(\text{OAc})_2$ for 1 h to form insoluble Rh decomposition product. In separate experiments, the resulting reaction mixture was added to activated $\text{Cu}(\text{OAc})_2$ and treated with the standard reaction conditions. Unlike the catalysis using $[\text{Rh}(\mu\text{-OAc})(\eta^2\text{-C}_2\text{H}_4)_2]_2$ precursor (Figure 2.2.10), the catalysis using the insoluble decomposed Rh materials showed no reactivity for the first 2 h under this conditions (Figure 2.2.43), indicating the reduced Rh species formed during thermal decomposition of $[\text{Rh}(\eta^2\text{-C}_2\text{H}_4)_2(\mu\text{-OAc})]_2$ is catalytically inactive, but after a pronounced induction period catalytic activity was observed. This is consistent with our hypothesis that upon continued heating reduced Rh species are re-oxidized by $\text{Cu}(\text{OAc})_2$ and Rh leaches back into solution to form soluble molecular Rh species that catalyze styrene production.

Table 2.2.4. Comparison of amount of soluble Rh material at different time points in the catalysis with 40 psig ethylene (condition: 10 mL benzene, 0.001 mol % Rh complex (relative to benzene) and 240 eq. of Cu(II) (relative to Rh), 150 °C).

Catalytic conditions	untreated $\text{Cu}(\text{OAc})_2$, 1 h	untreated $\text{Cu}(\text{OAc})_2$, 12 h	$\text{Cu}(\text{OHex})_2$, 15 min	$\text{Cu}(\text{OHex})_2$, 45 min
Amount of soluble Rh material*	<1%	78%	82%	84%

* Determined by ICP-OES and calculated relative to the total amount of starting Rh.



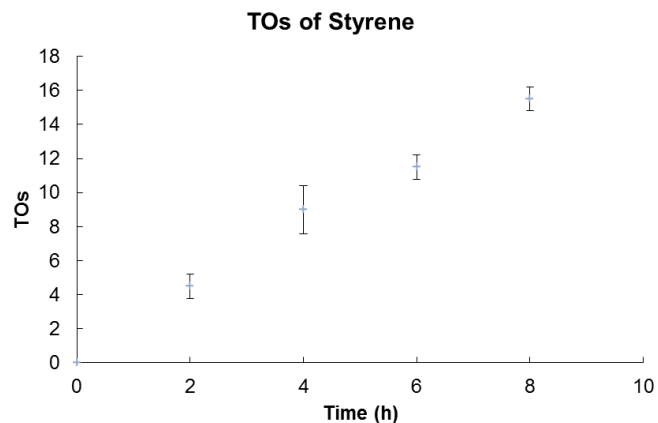


Figure 2.2.39. Plot of TOs versus time for styrene production catalyzed by $[\text{Rh}(\mu\text{-OAc})(\eta^2\text{-C}_2\text{H}_4)_2]_2$ at 125 °C after heating $\text{Cu}(\text{OAc})_2$ (0.24 mol % relative to benzene) in benzene (10 mL) for 12 hours at 150 °C. Each data point is the average of three separate experiments. Error bars represent the standard deviations based on a minimum of three independent experiments.

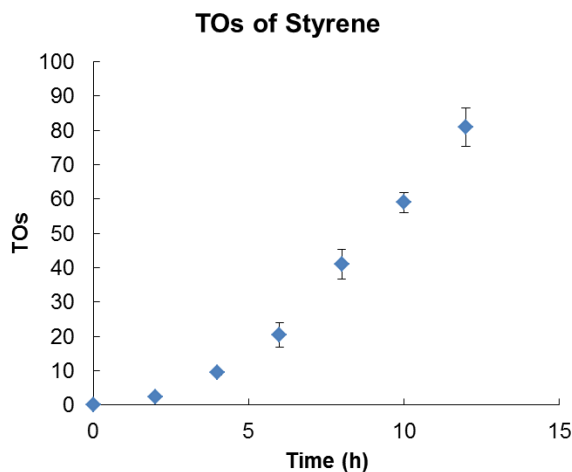
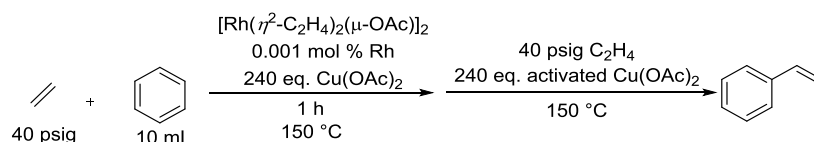


Figure 2.2.40. Plot of TOs versus time for styrene production using the reaction mixture obtained after 1 h of the standard catalytic reaction and activated Cu(OAc)₂ solid. TO of styrene was obtained by subtracting TO at 0 h (if any) from the raw TO data. Each data point is the average of three separate experiments. Error bars represent the standard deviations based on a minimum of three independent experiments.

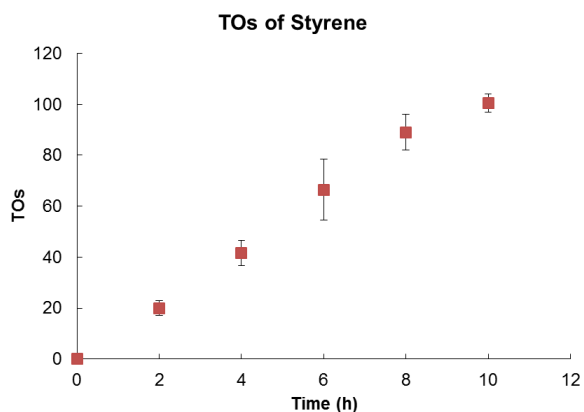
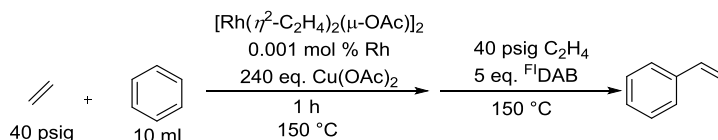


Figure 2.2.41. Plot of TOs versus time for styrene production using the reaction mixture obtained after 1 h of the standard catalytic reaction and commercial Cu(OAc)₂ with the addition of 5 eq. ^F1DAB ligand. TO of styrene was obtained by subtracting TO at 0 h (if any) from the raw TO data. Each data point is the average of three separate experiments. Error bars represent the standard deviations based on a minimum of three independent experiments.

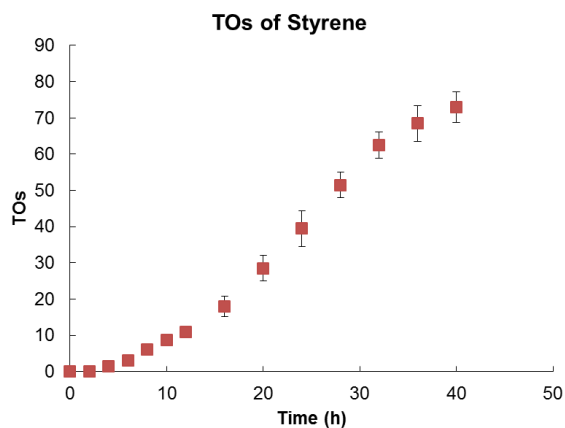
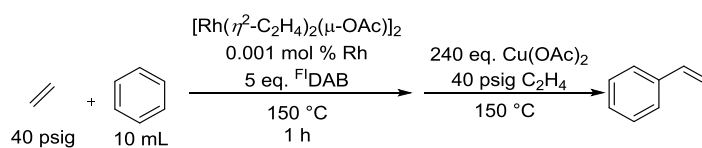


Figure 2.2.42. Plot of TOs versus time for styrene production using commercial Cu(OAc)_2 and the reaction mixture obtained by heating $[\text{Rh}(\mu\text{-OAc})(\eta^2\text{-C}_2\text{H}_4)_2]_2$ (0.001 mol % Rh relative to benzene) and 5 eq. of ^FDAB in benzene (10 mL) for 1 hour at 150 °C under 40 psig ethylene. Each data point is the average of three separate experiments. Error bars represent the standard deviations based on a minimum of three independent experiments.

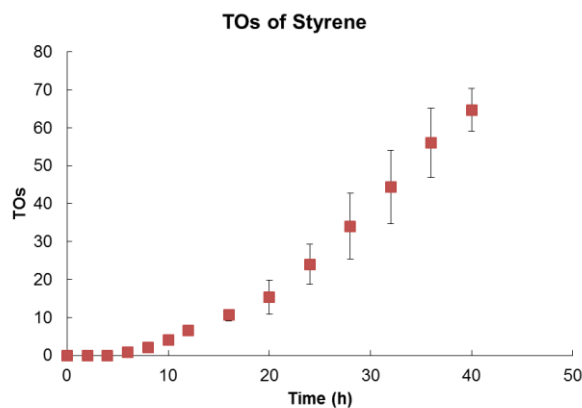
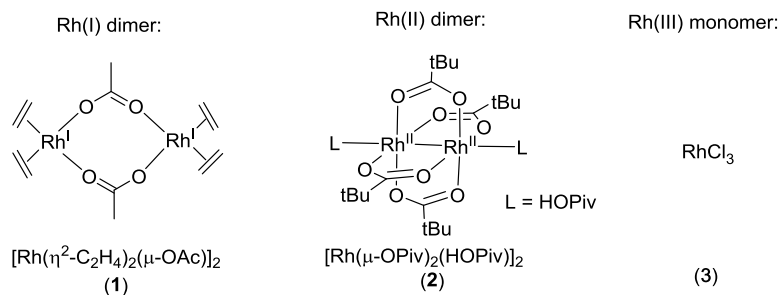


Figure 2.2.43. Plot of TOs versus time for styrene production using activated Cu(OAc)_2 and the reaction mixture obtained by heating $[\text{Rh}(\mu\text{-OAc})(\eta^2\text{-C}_2\text{H}_4)_2]_2$ (0.001 mol % Rh relative to benzene) in benzene (10 mL) for 1 hour at 150 °C under 40 psig ethylene. Each data point is the average of three separate experiments. Error bars represent the standard deviations based on a minimum of three independent experiments.

2.2.7 Experimental Comparison of Rh(I), Rh(II) and Rh(III)

Catalyst Precursors

We probed catalytic styrene production using different molecular Rh complexes as catalyst precursors. These reactions occur at 150 °C and involve a Rh catalyst, benzene, ethylene (C₂H₄), Cu(OPiv)₂ and pivalic acid. Under these conditions, the Rh(I) dimer [Rh(μ-OAc)(η²-C₂H₄)₂]₂ (**1**), the Rh(II) dimer [Rh(μ-OPiv)₂(HOPiv)]₂ (**2**), and RhCl₃ (**3**) all act as catalyst precursors to produce styrene (Scheme 2.2.3 and Figure 2.2.44). Experiments revealed that complex **1** produces styrene rapidly without an observable induction period. In contrast, catalysis with complex **3** shows an induction period of approximately 1.5 hours, after which the rate of catalysis is similar to that using **1**. Calculating TOFs, after any induction period, showed nearly identical results using complexes **1** and **3** as catalyst precursor: the apparent TOF using **1** is $\sim 1.1 \times 10^{-1} \text{ s}^{-1}$ from 0 h to 0.5 h, and the apparent TOF using **3** is $\sim 9.6 \times 10^{-2} \text{ s}^{-1}$ from 1.5 h to 2 h, indicating that the active Rh catalyst from both precursors **1** and **3**, following an induction period for complex **3**, is likely the same species. In contrast, catalysis using the Rh(II) dimer **2** as precursor showed a longer induction period (~6 hours) than complex **3**. Also, catalysis using **2** reveals a lower apparent TOF after the induction period of $\sim 2.8 \times 10^{-2} \text{ s}^{-1}$ (the TOF was calculated from 7 h to 9 h when the TO versus time plots are linear).



Scheme 2.2.3. Structures of three Rh catalyst precursors for Rh(I) dimer $[\text{Rh}(\mu\text{-OAc})(\eta^2\text{-C}_2\text{H}_4)_2]_2$ (**1**), Rh(II) dimer $[\text{Rh}(\mu\text{-OPiv})_2(\text{HOPiv})_2]$ (**2**), and RhCl_3 (**3**).

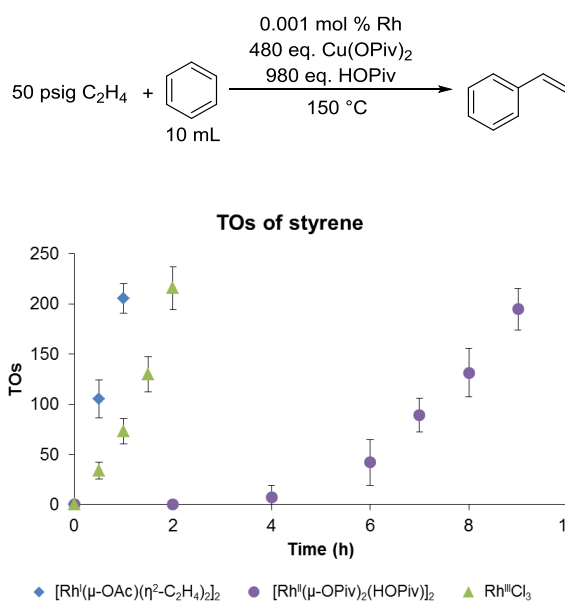


Figure 2.2.44. Comparison of TOs vs time for the conversion of benzene and ethylene to styrene using different molecular Rh catalyst precursors. Each data point is the average of at least three separate experiments. Error bars represent the standard deviations based on a minimum of three independent experiments. Reaction conditions: 0.001 mol % of Rh (relative to benzene), 480 eq. $\text{Cu}(\text{OPiv})_2$ (relative to Rh), 960 eq. HOPiv (relative to Rh), 10 mL benzene, 50 psig ethylene, 150 °C.

2.2.8 Characterization of Rh Resting State and Active Catalyst:

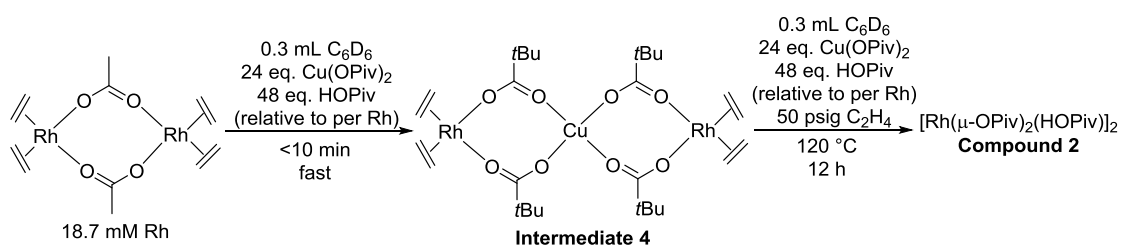
experimental studies

We sought to identify the resting state of the Rh complex starting from complex **1**.

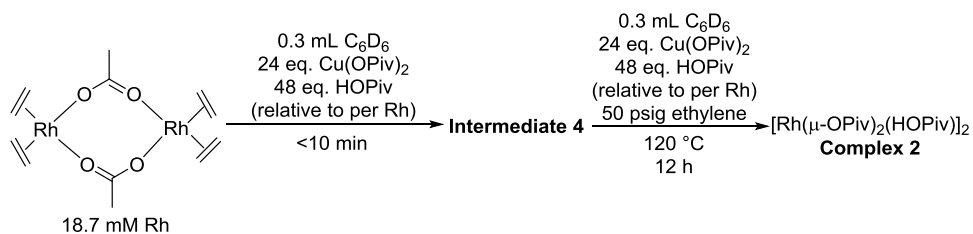
For the conversion of benzene and ethylene to styrene, the catalytic reaction

conditions involve the combination of complex **1**, benzene, ethylene, Cu(OPiv)₂ and pivalic acid (HOPiv).⁵² Our initial studies monitored the transformation of complex **1** in the presence of Cu(OPiv)₂ and HOPiv in benzene-*d*₆ by *in situ* ¹H NMR spectroscopy (Scheme 2.2.4). As observed by ¹H NMR spectroscopy (Figure 2.2.45), approximately 10 minutes after combination of **1** with 24 equivalents of Cu(OPiv)₂ and 48 equivalents of HOPiv (relative to per Rh) at room temperature, [Rh(μ-OAc)(η²-C₂H₄)₂]₂ (18.7 mM Rh) was consumed and a new broad peak was observed at ~4.0 ppm in the ¹H NMR spectrum. This indicates [Rh(μ-OAc)(η²-C₂H₄)₂]₂ was converted to a new Rh complex, which we have characterized (see below) as [Rh^I(μ-OPiv)₂(η²-C₂H₄)₂](μ-Cu) (**4**) (Scheme 2.2.4). After 12 hours at 120 °C in the presence of 50 psig ethylene, Cu(OPiv)₂ and HOPiv in benzene-*d*₆, intermediate **4** is converted to the paddle-wheel dimer [Rh(μ-OPiv)₂(HOPiv)]₂ (**2**), which was readily identified by ¹H NMR spectroscopy with a singlet at ~1.05 ppm (the resulting solution is labeled as solution A for referral later in this chapter). In the absence of ethylene, the formation of [Rh(μ-OPiv)₂(HOPiv)]₂ (**4**) was reproducible with high yields (91(5)% by ¹H NMR spectroscopy, based on 3 independent experiments with the standard deviation provided) and, as expected, accompanied by the release of ethylene (Figure 2.2.46). We confirmed the formation of **2** upon addition of independently prepared [Rh(μ-OPiv)₂(HOPiv)]₂ (prepared according to literature procedures⁷⁸ and confirmed by an X-ray diffraction study, Figure 2.2.47) to a reaction solution. In addition, catalytic styrene production using independently prepared complex **2** (5.60 x 10⁻⁴

mmol, 0.001 mol %Rh) and solution A (initially 5.60×10^{-4} mmol of $[\text{Rh}(\mu\text{-OAc})(\eta^2\text{-C}_2\text{H}_4)_2]_2$) as precursors provided almost identical TOs vs time plots (Scheme 2.2.5). Also, both catalytic reactions showed a similar induction period and reactivity after the induction period (Figure 2.2.48). This result confirms that the majority of $[\text{Rh}(\mu\text{-OAc})(\eta^2\text{-C}_2\text{H}_4)_2]_2$ is converted to $[\text{Rh}(\mu\text{-OPiv})_2(\text{HOPIv})]_2$ under the conditions shown in Scheme 2.2.4.



Scheme 2.2.4. Conversion of $[\text{Rh}(\mu\text{-OAc})(\eta^2\text{-C}_2\text{H}_4)_2]_2$ to $[\text{Rh}(\mu\text{-OPiv})_2(\eta^2\text{-C}_2\text{H}_4)_2]_2(\mu\text{-Cu})$ (**4**) at room temperature and $[\text{Rh}(\mu\text{-OPiv})_2(\text{HOPIv})]_2$ (**2**) at 120°C under 50 psig ethylene.



Formation of complex **2** after heating

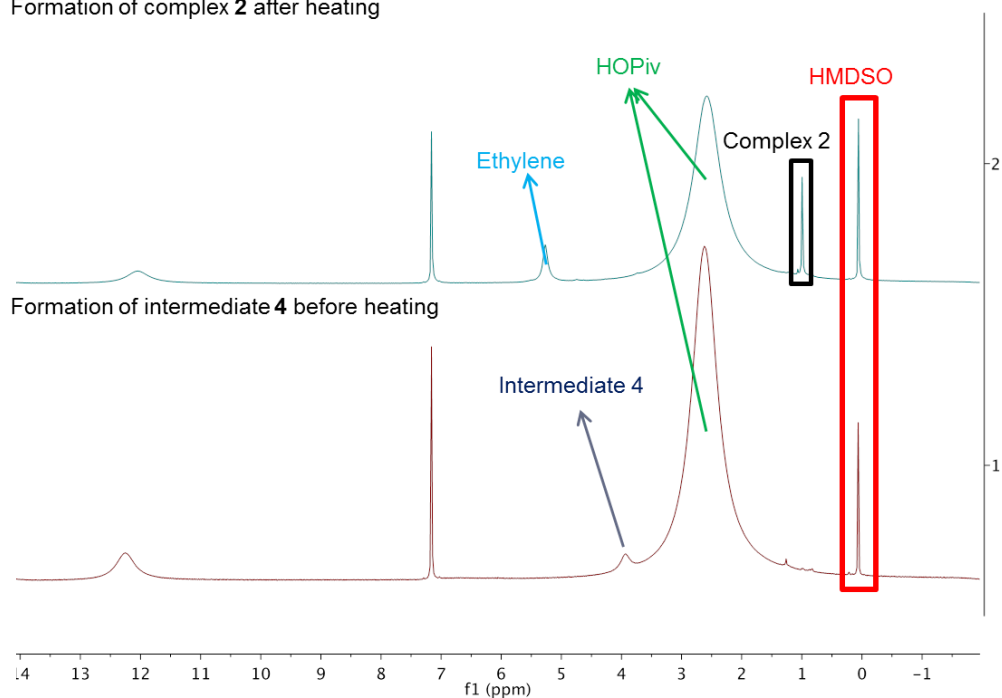
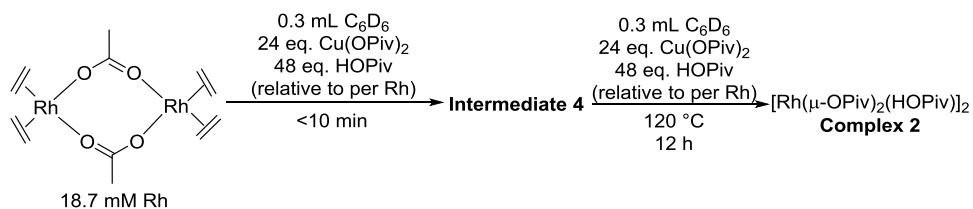


Figure 2.2.45. ^1H NMR spectra for conversion of $[\text{Rh}(\mu\text{-OAc})(\eta^2\text{-C}_2\text{H}_4)_2]_2$ to $[\text{Rh}^{\text{I}}(\mu\text{-OPiv})_2(\eta^2\text{-C}_2\text{H}_4)_2]_2(\mu\text{-Cu})$ (**4**) at room temperature and $[\text{Rh}(\mu\text{-OPiv})_2(\text{HOPIV})]_2$ (**2**) at 120 °C under 50 psig ethylene.



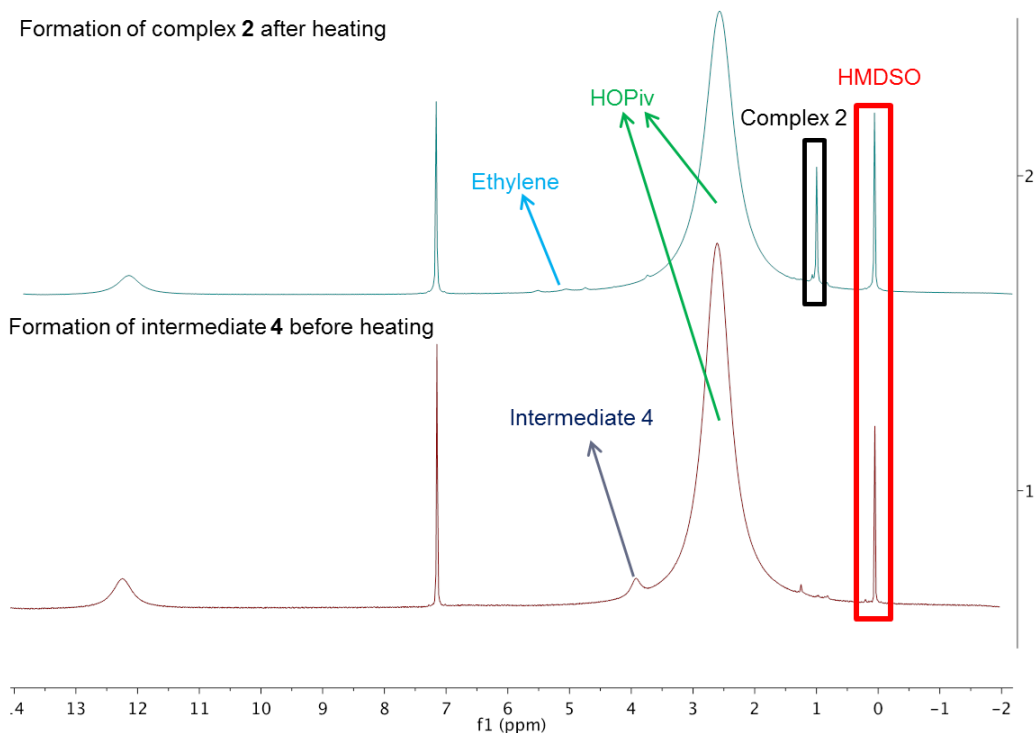


Figure 2.2.46. ^1H NMR spectra for conversion of $[\text{Rh}(\mu\text{-OAc})(\eta^2\text{-C}_2\text{H}_4)_2]_2$ to $[\text{Rh}^{\text{I}}(\mu\text{-OPiv})_2(\eta^2\text{-C}_2\text{H}_4)_2](\mu\text{-Cu})$ at room temperature and $[\text{Rh}(\mu\text{-OPiv})_2(\text{HOPiv})]_2$ at $120\text{ }^\circ\text{C}$ in the absence of ethylene.

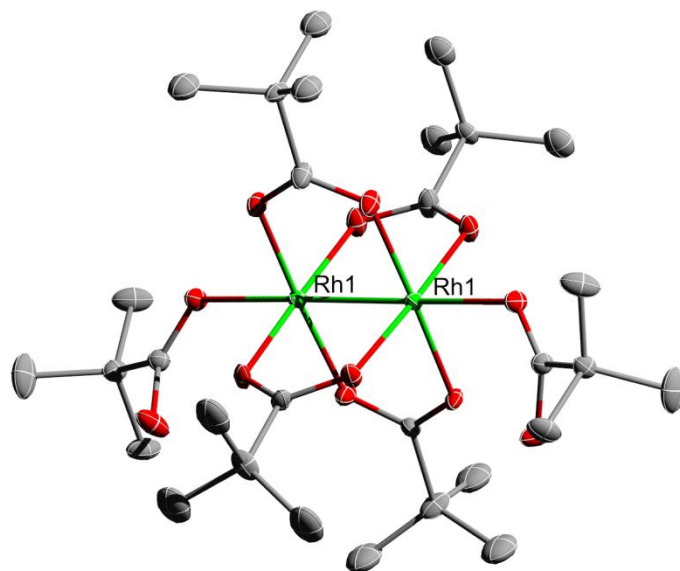
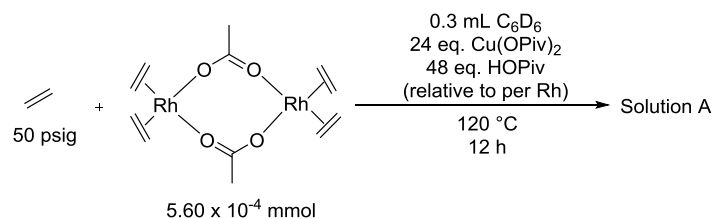


Figure 2.2.47. ORTEP of $[\text{Rh}(\mu\text{-OPiv})_2(\text{HOPiv})]_2$ (**2**) (50% probability). H atoms and solvent molecules are omitted for clarity. Only the major position for the disordered atom is shown.



Scheme 2.2.5. Conversion of $[\text{Rh}(\mu\text{-OAc})(\eta^2\text{-C}_2\text{H}_4)_2]_2$ to solution A (containing $[\text{Rh}(\mu\text{-OPiv})_2(\text{HOPiv})_2]$).

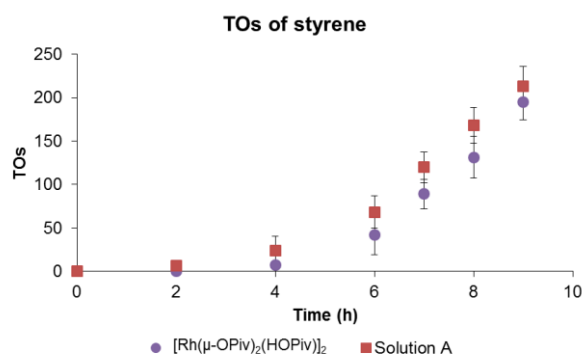
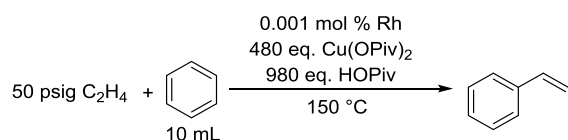


Figure 2.2.48. Comparison of TOs vs time plots for the conversion of benzene and ethylene to styrene using $[\text{Rh}(\mu\text{-OPiv})_2(\text{HOPiv})_2]$ (**2**) and solution A. Each data point is the average of at least three separate experiments and error bars represent the standard deviations based on these independent experiments. Reaction conditions: 0.001 mol % of Rh (relative to benzene), 480 eq. $\text{Cu}(\text{OPiv})_2$ (relative to Rh), 960 eq. HOPiv (relative to Rh), 10 mL benzene, 50 psig ethylene, 150 °C.

We used single-crystal X-ray analysis to validate the structure of intermediate **4**.

X-ray quality crystals of $[\text{Rh}^{\text{I}}(\mu\text{-OPiv})_2(\eta^2\text{-C}_2\text{H}_4)_2]_2(\mu\text{-Cu})$ (**4**) were obtained by treating $[\text{Rh}(\mu\text{-OAc})(\eta^2\text{-C}_2\text{H}_4)_2]_2$ (**1**) with 2 equivalents of $\text{Cu}(\text{OPiv})_2$ and 4 equivalents of HOPiv (relative to Rh) at room temperature. The resulting crystal was characterized as the heterometallic complex $\text{Rh}^{\text{I}}_2\text{Cu}^{\text{II}}(\mu\text{-OPiv})_4(\eta^2\text{-C}_2\text{H}_4)_4$ with bridging pivalate groups between the Rh^{I} s and Cu^{II} (Figure 2.2.49). Reported

examples of structurally characterized trinuclear Rh₂Cu complexes are rare.⁷⁹⁻⁸³ The distance between Rh and Cu atom (3.0095(5) Å) is longer than the sum of the covalent radii of rhodium (1.39 Å) and copper (1.27 Å) in cluster compounds,⁸⁴ and does not fit into the typical range of Rh-Cu bond lengths (2.5-2.6 Å) in this class of Rh₂Cu complexes.⁸¹⁻⁸³ Therefore, we believe only little or no direct Rh-Cu bonding interaction is involved in **4**. The orientation of coordinated ethylene is perpendicular to the Rh coordination square plane, which is characteristic for d⁸ Rh^I(η²-C₂H₄) complexes.^{54, 85} Similar to other reported Rh(I) complexes with ethylene ligand,^{54, 85} The C=C bond distance of coordinated ethylene in **4** is only slightly longer (1.393(6) Å) than that of free ethylene (1.339 Å),⁸⁶ suggesting significant double bond character.

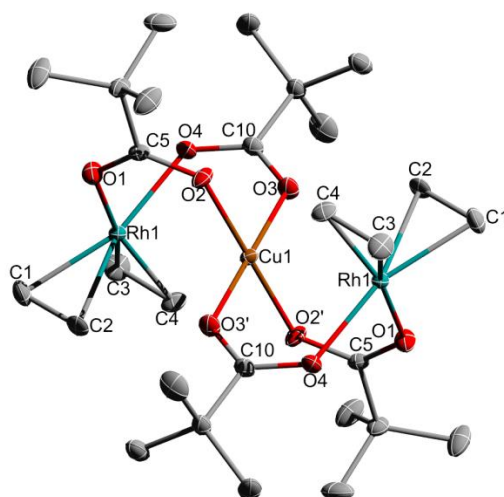
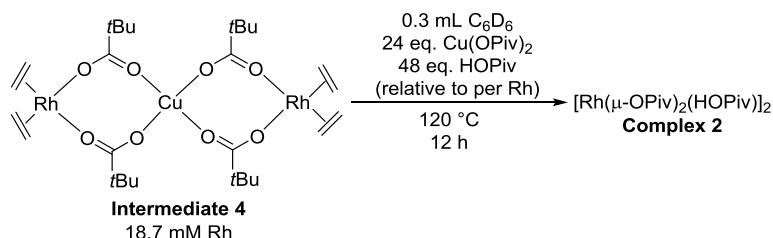


Figure 2.2.49. ORTEP of [Rh^I(μ-OPiv)₂(η²-C₂H₄)₂]₂(μ-Cu) (**4**) (50% probability). H atoms are omitted for clarity. Selected bond lengths (Å): Cu1-O2 1.948(3), Cu1-O3 1.949(3), Rh1-O4 2.078(3), Rh1-C1 2.112(4), Rh1-C2 2.118(3), Rh1-Cu1 3.0095(5), Rh1-O1 2.079(3), Rh1-C3 2.112(4), Rh1-C4 2.122(4), C1-C2 1.393(6), C3-C4 1.402(6). Selected bond angles (°): O4-Rh1-O1 87.78(11), C1-Rh1-C2 38.45(16), C1-Rh1-C3 88.43(18), C1-Rh1-C4 100.63(17), O4-Rh1-C1 160.42(14), O1-Rh1-C1 88.93(15), C3-Rh1-C4 38.66(16), O2'-Cu1-O3' 90.05(12), O2'-Cu1-O3 89.95(12),

O1-C5-O2 125.9(3), O3-C10-O4 125.7(3).

Crystals of **4** were washed with pentane and dried under vacuum. The obtained solid was subjected to the reaction conditions where we observed the conversion of intermediate **4** to complex **2**: 24 equivalents of Cu(OPiv)₂ and 48 equivalents of HOPiv (relative to per Rh, assuming the obtained solid is pure [Rh^I(μ-OPiv)₂(η²-C₂H₄)₂]₂(μ-Cu) at 120 °C for 12 hours. As expected, complete conversion of the obtained solid to **2** was observed by ¹H NMR spectroscopy (Figure 2.2.50). Catalytic styrene production using crystals of **4** showed a statistically identical reactivity compared to the same reaction conditions using complex **1** as catalyst precursor (Figure 2.2.51). Thus, we propose that [Rh^I(μ-OPiv)₂(η²-C₂H₄)₂]₂(μ-Cu) (**4**) is a catalytically relevant intermediate and is likely the catalyst resting state for styrene production (see below for additional evidence). Catalysis using heterometallic complexes and clusters are widely-studied,⁸⁷⁻⁹⁰ examples of Rh-Cu catalyst systems are rare. For example, A Rh-Cu cluster compound Cu₂{Rh₁₂(CO)₃₀} has been reported as the catalyst for CO hydrogenation.⁹¹



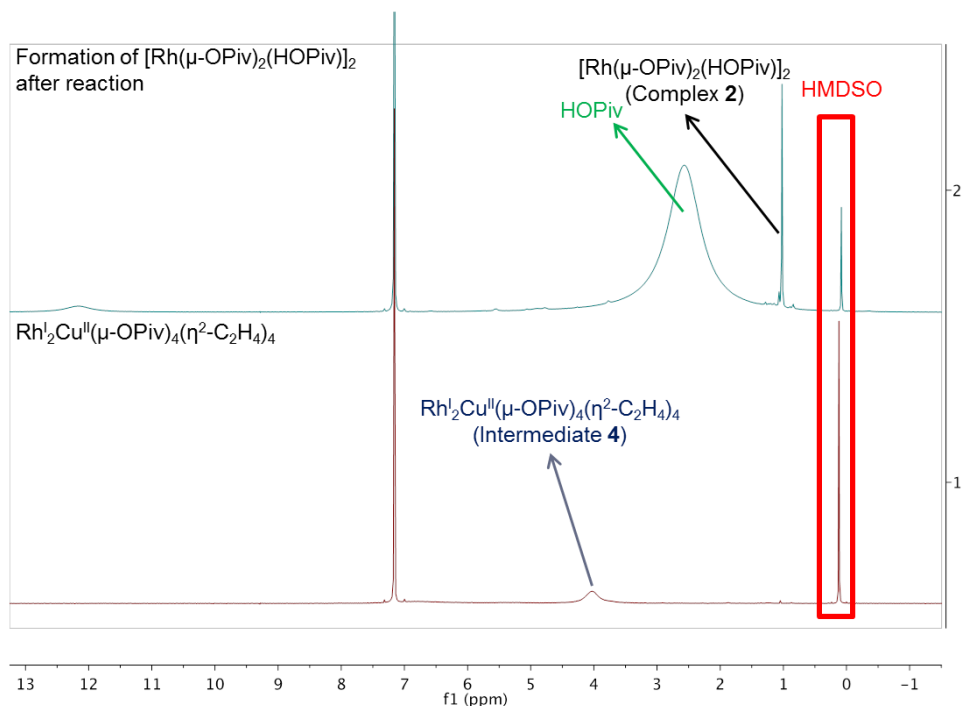


Figure 2.2.50. ^1H NMR spectra for conversion of $[\text{Rh}^{\text{I}}(\mu\text{-OPiv})_2(\eta^2\text{-C}_2\text{H}_4)_2]_2(\mu\text{-Cu})$ (**4**) to $[\text{Rh}(\mu\text{-OPiv})_2(\text{HOPiv})]_2$ (**2**) at 120 °C after 12 hours.

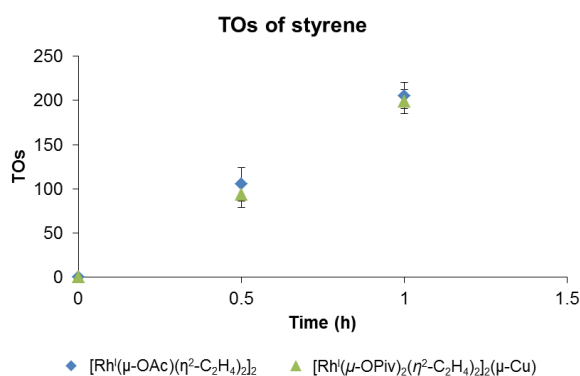
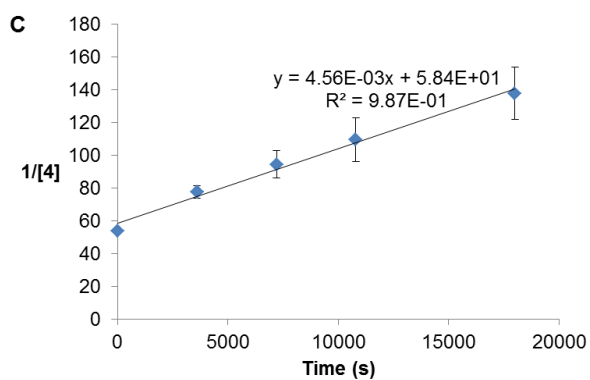
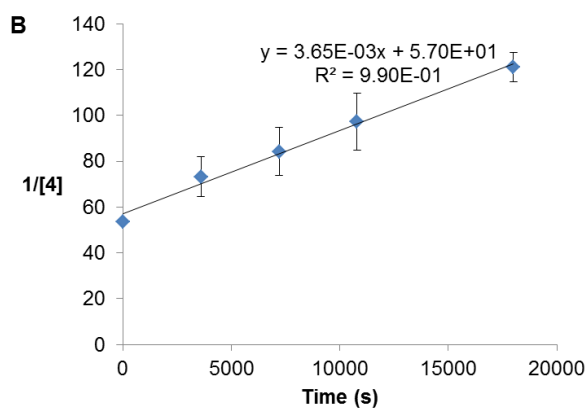
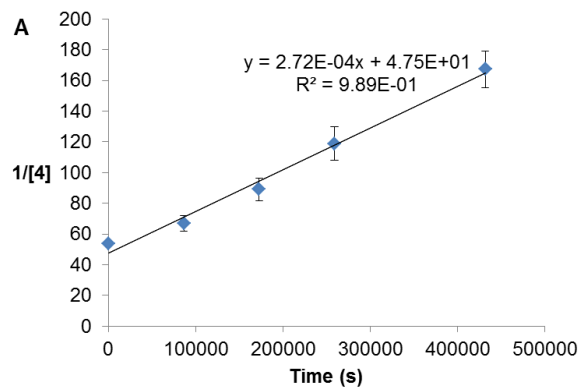


Figure 2.2.51. Comparison of TOs vs time plots for the conversion of benzene and ethylene to styrene using $[\text{Rh}(\mu\text{-OAc})(\eta^2\text{-C}_2\text{H}_4)_2]_2$ (**1**) and $[\text{Rh}^{\text{I}}(\mu\text{-OPiv})_2(\eta^2\text{-C}_2\text{H}_4)_2]_2(\mu\text{-Cu})$ (**4**). Each data point is the average of at least three separate experiments with error bars representing the standard deviations based on these independent experiments. Reaction conditions: 0.001 mol % of Rh (relative to benzene), 480 eq. $\text{Cu}(\text{OPiv})_2$ (relative to Rh), 960 eq. HOPiv (relative to Rh), 10 mL benzene 50 psig ethylene, 150 °C.

Kinetic studies were performed for the conversion of $[\text{Rh}(\mu\text{-OAc})(\eta^2\text{-C}_2\text{H}_4)_2]_2$ (**1**) (18.7 mM Rh) to $[\text{Rh}(\mu\text{-OPiv})_2(\text{HOPiv})]_2$ (**2**) at 21, 45, 50, and 60 °C. Given the

rapid conversion of **1** to **4**, these studies provide kinetic data for the conversion of **4** to **2**. The kinetic plots show a second-order dependence on Rh concentration (Figure 2.2.52). Activation parameters were obtained from an Eyring plot using the observed second-order rate constants (k_{obs}) at four different temperatures (Figure 2.2.52). The ΔH^\ddagger and ΔS^\ddagger were determined to be 16(3) kcal/mol and -19(5) cal/(mol K), respectively. The second-order decay of intermediate **4** and the negative ΔS^\ddagger value are consistent with the rate-limiting conversion of monomeric Rh intermediate to a dimeric Rh product. Thus, we speculated that formation of $[\text{Rh}(\mu\text{-OPiv})_2(\text{HOPiv})]_2$ from intermediate **4** is initialized by breakup of complex **4** into a mononuclear Rh(I) κ^2 -pivalate complex and $\text{Cu}(\text{OPiv})_2$, followed by rate-limiting dimerization and oxidation by $\text{Cu}(\text{OPiv})_2$ to form complex **2** with release ethylene (Scheme 2.2.6. Proposed pathway for conversion of $[\text{RhI}(\mu\text{-OPiv})_2(\eta^2\text{-C}_2\text{H}_4)]_2(\mu\text{-Cu})$ (**4**) to $[\text{Rh}(\mu\text{-OPiv})_2(\text{HOPiv})]_2$ (**2**)). Moreover, in the absence of ethylene, the observed rate constants obtained at 45 and 50 °C were $8(2) \times 10^{-3}$ and $1.2(4) \times 10^{-2} \text{ mol s}^{-1} \text{ L}^{-1}$, respectively, which are higher than the rate constants in the presence of 50 psig ethylene ($3.6(6) \times 10^{-3}$ and $4.6(8) \times 10^{-3} \text{ mol s}^{-1} \text{ L}^{-1}$) (Figure 2.2.53). This indicates that the dissociation of ethylene is involved in kinetically relevant steps, which is consistent with the proposed $[\text{Rh}(\mu\text{-OPiv})_2(\text{HOPiv})]_2$ formation pathway from intermediate **4** (Scheme 2.2.6. Proposed pathway for conversion of $[\text{RhI}(\mu\text{-OPiv})_2(\eta^2\text{-C}_2\text{H}_4)]_2(\mu\text{-Cu})$ (**4**) to $[\text{Rh}(\mu\text{-OPiv})_2(\text{HOPiv})]_2$ (**2**)).



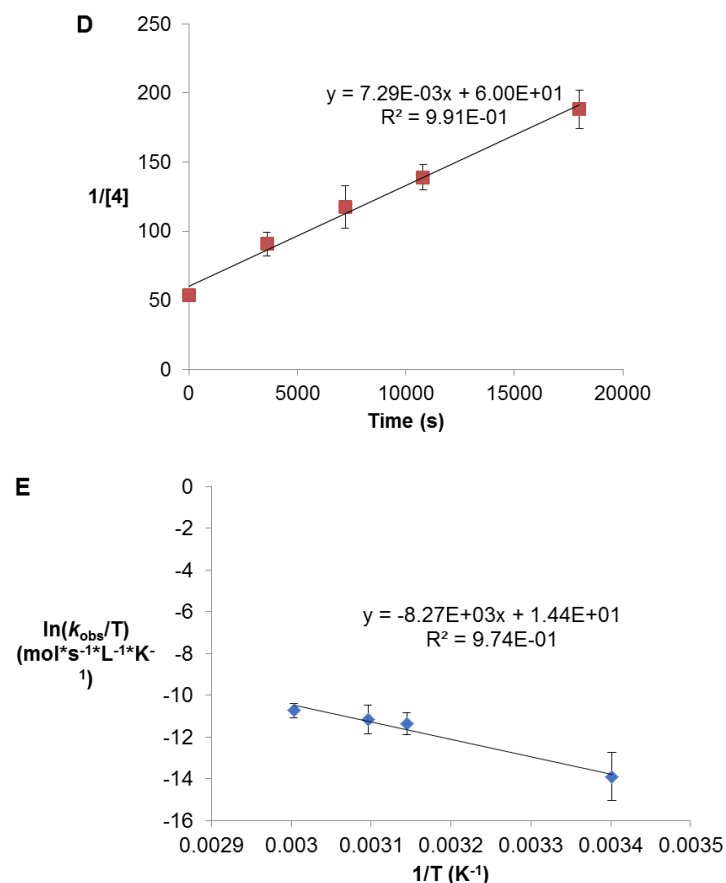
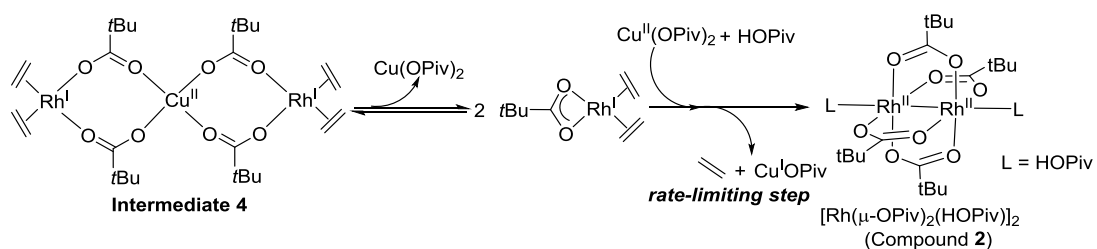


Figure 2.2.52. Kinetic plots and Eyring plot (E) for conversion of $[\text{Rh}^{\text{I}}(\mu\text{-OPiv})_2(\eta^2\text{-C}_2\text{H}_4)_2]_2(\mu\text{-Cu})$ (**4**) to $[\text{Rh}(\mu\text{-OPiv})_2(\text{HOPiv})]_2$ (**2**) at 21 °C (A), 45 °C (B), 50 °C (C), and 60 °C (D) under ethylene. Reaction conditions: 9.35 mM of $[\text{Rh}(\mu\text{-OAc})(\eta^2\text{-C}_2\text{H}_4)_2]_2$ as starting material, 0.3 mL benzene- d_6 , 24 eq. $\text{Cu}(\text{OPiv})_2$ (relative to Rh), 48 eq. HOPiv (relative to Rh), 50 psig ethylene. The rate of decay of **4** was determined based on the amount of complex **2** formed. Each data point is the average of three separate experiments and error bars represent the standard deviations based these independent experiments.



Scheme 2.2.6. Proposed pathway for conversion of $[\text{Rh}^{\text{I}}(\mu\text{-OPiv})_2(\eta^2\text{-C}_2\text{H}_4)_2]_2(\mu\text{-Cu})$ (**4**) to $[\text{Rh}(\mu\text{-OPiv})_2(\text{HOPiv})]_2$ (**2**).

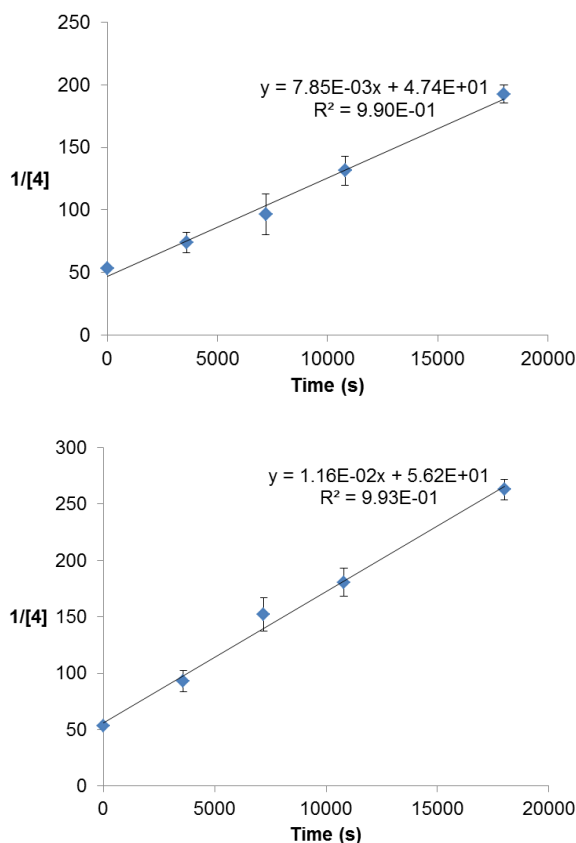


Figure 2.2.53. Kinetic plots for conversion of $[\text{Rh}^{\text{I}}(\mu\text{-OPiv})_2(\eta^2\text{-C}_2\text{H}_4)_2]_2(\mu\text{-Cu})$ (**4**) to $[\text{Rh}(\mu\text{-OPiv})_2(\text{HOPIV})]_2$ (**2**) at 45 °C (top) and 50 °C (bottom) in the absence of ethylene. Reaction conditions: 9.35 mM of $[\text{Rh}(\mu\text{-OAc})(\eta^2\text{-C}_2\text{H}_4)_2]_2$ as starting material, 0.3 mL benzene- d_6 , 24 eq. $\text{Cu}(\text{OPiv})_2$ (relative to Rh), 48 eq. HOPIV (relative to Rh). The rate of decay of **4** is determined based on the amount of complex **2** formed. Each data point is the average of three separate experiments and error bars represent the standard deviations based these independent experiments.

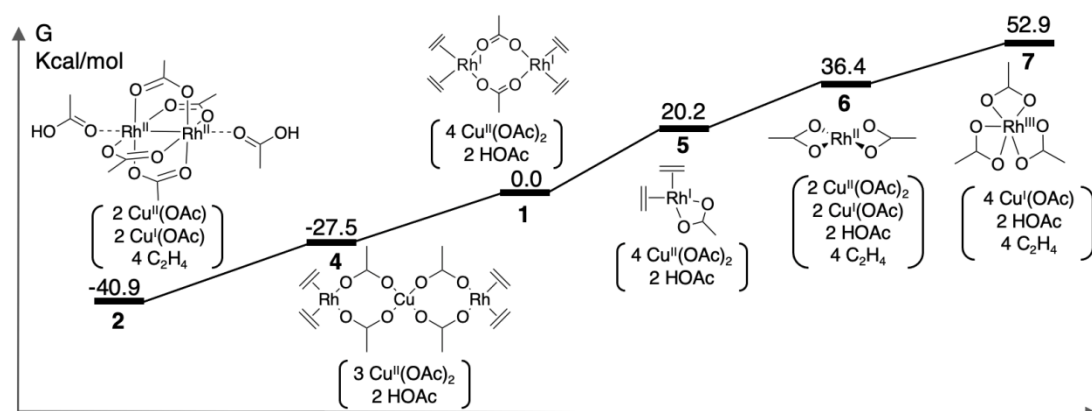
2.2.9 Characterization of Rh Resting State and Active Catalyst:

Computational Studies

All the computational results were performed by Charles B. Musgrave III and Prof. William Goddard III at the California Institute of Technology.

Free energies at 423 K (~150 °C) for several Rh complexes with varying oxidation states are computed (Scheme 2.2.7). $\text{Cu}(\text{OAc})_2$ was used as the oxidant for simplification purposes. To model the catalytic process, we studied one-electron

redox reactions, that is: $\text{Rh}^n + \text{Cu}^{\text{II}} \rightarrow \text{Rh}^{n+1} + \text{Cu}^{\text{I}}$.



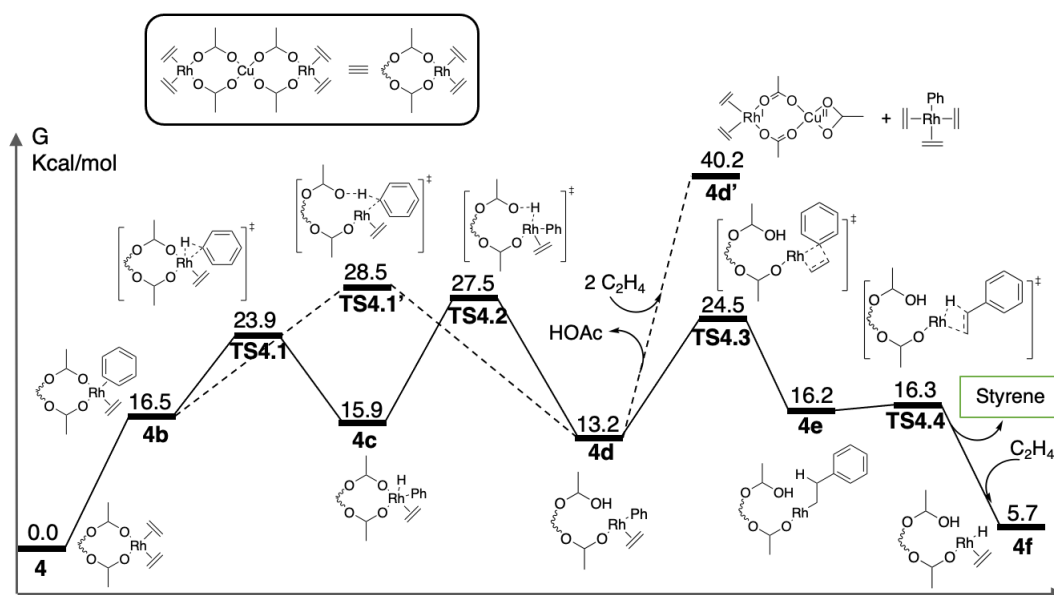
Scheme 2.2.7. B3LYP-D3 free energies at 423 K for (from left to right): $[\text{Rh}^{\text{II}}(\mu\text{-OAc})_2(\text{HOAc})]_2$ (**2**), $\text{Rh}_2^{\text{I}}\text{Cu}^{\text{II}}(\mu\text{-OAc})_4(\eta^2\text{-C}_2\text{H}_4)_4$ (**4**), $[\text{Rh}^{\text{I}}(\mu\text{-OAc})(\eta^2\text{-C}_2\text{H}_4)_2]_2$ (**1**), $\text{Rh}^{\text{I}}(\kappa^2\text{-OAc})(\eta^2\text{-C}_2\text{H}_4)_2$ (**5**), $\text{Rh}^{\text{II}}(\kappa^2\text{-OAc})_2$ (**6**), and $\text{Rh}^{\text{III}}(\kappa^2\text{-OAc})_3$ (**7**). Stoichiometric amounts of $\text{Cu}^{\text{II}}(\text{OAc})_2$, $\text{Cu}^{\text{I}}(\text{OAc})$, C_2H_4 , and HOAc were added to maintain the same number of atoms. Similarly, monomer energies were doubled to be consistent with the dimers. The $\text{Cu}^{\text{I}}(\text{OAc})$ was modeled as a neutral single molecule in (implicit) solution.

$[\text{Rh}(\mu\text{-OAc})(\eta^2\text{-C}_2\text{H}_4)_2]_2$ (**1**) was set as the reference state of 0.0 kcal/mol. The $\text{Rh}(\text{II})$ paddle-wheel dimer $[\text{Rh}^{\text{II}}(\mu\text{-OAc})_2(\text{HOAc})]_2$ (complex **2**) is calculated to be lowest in energy, while the $\text{Rh}(\text{III})$ monomer $\text{Rh}(\kappa^2\text{-OAc})_3$ is calculated to be the highest in energy (Scheme 2.2.7). The dissociation of the $[\text{Rh}(\mu\text{-OAc})(\eta^2\text{-C}_2\text{H}_4)_2]_2$ (**1**) to form two $\text{Rh}(\text{I})$ monomers (**5**) is uphill 20.2 kcal/mol. Oxidation of the monomer **5** by $\text{Cu}(\text{OAc})_2$ is unfavorable with the $\text{Rh}(\text{II})$ and $\text{Rh}(\text{III})$ monomers (**6** and **7**) 36.4 and 52.9 kcal/mol above **1**, respectively. In contrast, computational studies predict oxidation of the $[\text{Rh}(\mu\text{-OAc})(\eta^2\text{-C}_2\text{H}_4)_2]_2$ (**1**) to $[\text{Rh}^{\text{II}}(\mu\text{-OAc})_2(\text{HOAc})]_2$ (**2**) is favorable with downhill 40.9 kcal/mol. This supports the experimentally observed conversion of $[\text{Rh}(\mu\text{-OAc})(\eta^2\text{-C}_2\text{H}_4)_2]_2$ (**1**) to $\text{Rh}_2^{\text{I}}\text{Cu}^{\text{II}}(\mu\text{-OPiv})_4(\eta^2\text{-C}_2\text{H}_4)_4$ (**4**), and eventually to $[\text{Rh}(\mu\text{-OPiv})_2(\text{HOPiv})]_2$ (**2**) at high Rh concentration.

These computational results as well as our experimental observation of the formation of $\text{Rh}^{\text{I}}_2\text{Cu}^{\text{II}}(\mu\text{-OPiv})_4(\eta^2\text{-C}_2\text{H}_4)_4$ (**4**) drove us to study catalytic styrene formation catalyzed by $\text{Rh}^{\text{I}}_2\text{Cu}^{\text{II}}(\mu\text{-OPiv})_4(\eta^2\text{-C}_2\text{H}_4)_4$ (**4**). Coordination of benzene to $\text{Rh}^{\text{I}}_2\text{Cu}^{\text{II}}(\mu\text{-OPiv})_4(\eta^2\text{-C}_2\text{H}_4)_4$ (**4**) is uphill 16.5 kcal/mol (Scheme 2.2.8). From the η^2 -benzene adduct, the formation of a Rh-phenyl intermediate via C–H activation is likely to occur by either two-step oxidative addition/reductive coupling or concerted metalation deprotonation (CMD). DFT calculations indicate a slight preference for stepwise oxidative addition/reductive elimination (barriers of 23.9 and 27.5 kcal/mol for **TS4.1** and **TS4.2**) over CMD (barrier of 28.5 kcal/mol for **TS4.1'**). It is difficult to make a strong case for either mechanism based on the calculation results.

After the benzene C–H activation, the "Rh(Ph)($\eta^2\text{-C}_2\text{H}_4$)" moiety could dissociate from **4d** and bind two equivalents of ethylene to generate $\text{Rh}^{\text{I}}(\text{Ph})(\eta^2\text{-C}_2\text{H}_4)_3$, HOAc and a $\text{Rh}(\eta^2\text{-C}_2\text{H}_4)_2(\mu\text{-OAc})_2\text{Cu}(\kappa^2\text{-OAc})$ (**8**). DFT predicts this transformation is not favorable with **4d'** uphill from the starting state by 40.2 kcal/mol (Scheme 2.2.8). From **4d**, ethylene insertion into the Rh–Ph bond and β -hydride elimination lead to transition state free energies of 24.5 and 16.3 kcal/mol (**TS4.3** and **TS4.4**). Dissociation of styrene upon ligand exchange with ethylene yields free styrene and **4f** at 5.7 kcal/mol above the starting state. Subsequent oxidation of **4f** with $\text{Cu}(\text{OAc})_2$ can produce acetic acid and regenerate the starting catalyst **4**. The calculations predict that the rate-determining step for catalytic styrene formation from starting state **4** for reductive coupling to form coordinated acetic acid with barrier of 27.5 kcal/mol. The calculated activation barrier of 27.5 kcal/mol shows good agreement with the

experimentally determined barrier of 26.9 kcal/mol (calculated from the 0.11 s^{-1} TOF at $150 \text{ }^\circ\text{C}$ via the Eyring equation).



Scheme 2.2.8. B3LYP-D3 free energy profile at 423 K for styrene formation from $[\text{Rh}^{\text{I}}(\mu\text{-OPiv})_2(\eta^2\text{-C}_2\text{H}_4)_2]_2(\mu\text{-Cu})$ (**4**).

Based on these combined experimental and computational results, we hypothesize that $[\text{Rh}^{\text{I}}(\mu\text{-OPiv})_2(\eta^2\text{-C}_2\text{H}_4)_2]_2(\mu\text{-Cu})$ (**4**) is the active catalyst for styrene formation. Further, experimental and computational data are consistent with the $[\text{Rh}(\mu\text{-OPiv})_2(\text{HOPiv})]_2$ being inactive for catalysis but thermodynamically favorable from **4** under catalytic conditions. How does Rh avoid the formation of **2**? We propose that: 1) under catalytic conditions where Rh concentration is low (e.g., 0.112 mM Rh), the formation of $[\text{Rh}(\mu\text{-OPiv})_2(\text{HOPiv})]_2$, which follows 2nd order kinetics in $[\text{Rh}]$, is slow. In contrast, in J-young tube reactions monitored by ^1H NMR spectroscopy, the conversion of $[\text{Rh}(\mu\text{-OAc})(\eta^2\text{-C}_2\text{H}_4)_2]_2$ to $[\text{Rh}(\mu\text{-OPiv})_2(\text{HOPiv})]_2$ is rapid due to higher Rh concentrations (18.7 mM Rh). 2) Under the catalytic conditions with reaction temperature of $150 \text{ }^\circ\text{C}$, the catalytic reaction that involves

$[\text{Rh}^{\text{I}}(\mu\text{-OPiv})_2(\eta^2\text{-C}_2\text{H}_4)_2]_2(\mu\text{-Cu})$ (**4**) is competitive with the conversion of $[\text{Rh}^{\text{I}}(\mu\text{-OPiv})_2(\eta^2\text{-C}_2\text{H}_4)_2]_2(\mu\text{-Cu})$ to $[\text{Rh}(\mu\text{-OPiv})_2(\text{HOPIV})]_2$.

2.3 Summary and Conclusions

Similar catalytic reactivity and product selectivity have been observed in catalysis with ethylene and propylene using a variety of diimine ligated rhodium(I) acetate complexes and $[\text{Rh}(\mu\text{-OAc})(\eta^2\text{-C}_2\text{H}_4)_2]_2$. This observation along with the *in situ* NMR studies of two representative diimine rhodium(I) acetate complexes with diimine ligands indicate that the ligated Rh complexes release diimine ligand and are likely converted into the same catalytically active Rh species under catalytic conditions. In the absence of Cu(II) oxidant, $[\text{Rh}(\mu\text{-OAc})(\eta^2\text{-C}_2\text{H}_4)_2]_2$ initiates ethylene C–H activation and undergoes thermal decomposition to form Rh(0) species as evidenced by ^1H NMR spectroscopy, TEM/EDS and XPS analysis. ICP-OES analysis and reactivity comparison experiments indicate that the generation of catalytically inactive and insoluble Rh from $[\text{Rh}(\mu\text{-OAc})(\eta^2\text{-C}_2\text{H}_4)_2]_2$ occurs in the early stage of catalysis (*i.e.*, during the induction period) when commercial $\text{Cu}(\text{OAc})_2$ is used as the oxidant. However, TEM analysis of the insoluble Rh species showed no evidence of the existence of Rh nanoparticles, and XPS studies indicate that the formed insoluble Rh species are in a higher oxidation state than Rh(0). Yet, when $\text{Cu}(\text{OAc})_2$ is omitted, evidence for the formation of Rh nanoparticles has been obtained either in the absence or presence of silica. We hypothesize that the untreated $\text{Cu}(\text{OAc})_2$ serves to capture

the reduced Rh, as either single atoms or small clusters (which cannot be observed with current data), and this results in insoluble Rh in a higher oxidation state than Rh(0). With continued heating, the Rh trapped by Cu(OAc)₂ can leach back into solution to catalyze arene alkenylation.

The leaching of active soluble Rh species from the insoluble Rh materials results in observed induction periods when using commercial Cu(OAc)₂. Heating Cu(OAc)₂ in benzene prior to catalysis or the addition of extra ^{F1}DAB ligand at the beginning of catalysis is believed to mitigate the decomposition of [Rh(μ-OAc)(η²-C₂H₄)₂]₂ to the insoluble Rh species. In that case, the induction period is not observed or it is shortened. Although *in situ* reduction of soluble Rh to form catalytically active Rh nanoparticles is precedent, to our knowledge, this is the first example of Rh catalyzed reactions attributing the origin of an induction period to a transformation of the initial molecular catalyst precursor into insoluble but catalytically inactive material followed by re-dissolution to form the active and soluble catalyst.

With activated Cu(OAc)₂ or soluble Cu(OHex)₂, the Rh complex [Rh(μ-OAc)(η²-C₂H₄)₂]₂ does not undergo initial decomposition to form insoluble Rh. While we have no direct evidence to determine how activated Cu(OAc)₂ or soluble Cu(OHex)₂ prevent the Rh decomposition, we hypothesize that Rh-H intermediates are likely involved in the reductive decomposition from [Rh(μ-OAc)(η²-C₂H₄)₂]₂ to Rh(0). Perhaps CuX₂ (X = OAc or OHex) with a smaller particle size or enhanced solubility in benzene serves as a more "accessible" oxidant source and thus results in a rapid reaction to convert Rh-H intermediates to Rh-X thus kinetically suppressing Rh

decomposition.

Reactivity comparison experiment using different molecular Rh complexes reveals that Rh(I) species serves as the active catalyst for styrene production. Rh(II) dimer $[\text{Rh}(\mu\text{-OPiv})_2(\text{HOPiv})]_2$ is likely is not involved in the catalytic cycle. $[\text{Rh}^{\text{I}}(\mu\text{-OPiv})_2(\eta^2\text{-C}_2\text{H}_4)_2]_2(\mu\text{-Cu})$, which is formed by reacting $[\text{Rh}(\mu\text{-OAc})(\eta^2\text{-C}_2\text{H}_4)_2]_2$ with $\text{Cu}(\text{OPiv})_2$ oxidant, is a viable the catalyst resting state because it shows nearly identical TOs versus time as the Rh(I) precursor. Under some conditions $[\text{Rh}^{\text{I}}(\mu\text{-OPiv})_2(\eta^2\text{-C}_2\text{H}_4)_2]_2(\mu\text{-Cu})$ is converted to an off-cycle $[\text{Rh}^{\text{II}}(\mu\text{-OPiv})_2(\text{HOPiv})]_2$ species in a process that exhibits second-order kinetics on Rh concentration, but under catalytic conditions the formation of $[\text{Rh}^{\text{II}}(\mu\text{-OPiv})_2(\text{HOPiv})]_2$ is likely minimal and the majority of Rh species are involved in the catalytic cycle. Computational studies reveals that the $[\text{Rh}^{\text{II}}(\mu\text{-OPiv})_2(\text{HOPiv})]_2$ is a low energy global minimum, which is consistent with experimental observations that $[\text{Rh}^{\text{II}}(\mu\text{-OPiv})_2(\text{HOPiv})]$ is in efficient for styrene formation. Combined experimental and DFT calculations are consistent with $[\text{Rh}^{\text{I}}(\mu\text{-OPiv})_2(\eta^2\text{-C}_2\text{H}_4)_2]_2(\mu\text{-Cu})$ remaining intact through the entire catalytic cycle.

These new studies allow us to speculate on the nature of the Rh species responsible for arene alkenylation. Since previous DFT calculations involved $^{\text{Fl}}\text{DAB}$ coordinated Rh,⁵² these modeled intermediates are not likely relevant to the actual catalytic process. However, the details of the previous kinetic studies remain valid, including order in Rh, ethylene, oxidant and benzene under different conditions. The previously published kinetic data are consistent with an active catalyst that is a soluble

mononuclear Rh species, although a binuclear Rh species can form as an intermediate, giving half-order kinetics in Rh, under some conditions.⁵² Our previous kinetic studies, including kinetic isotope effects (C₆H₆ vs. C₆D₆) under different conditions are consistent with benzene C–H activation preceding rate limiting ethylene insertion, and new data reported herein do not contradict these conclusions. Thus, we suggest a similar catalytic cycle to our previous report, without coordination of diimine, is likely,⁵² and a heterometallic complex [Rh^I(μ-OPiv)₂(η²-C₂H₄)₂]₂(μ-Cu) is characterized as the Rh catalyst resting state. More detailed characterization of possible catalytic intermediates will require additional experimental and computational studies.

2.4 Experimental Section

General Considerations. Reactions were performed under anaerobic conditions employing standard Schlenk techniques and/or in a nitrogen-filled glovebox unless specified otherwise. Glovebox purity was maintained by periodic nitrogen purges and was monitored by an oxygen analyzer (O₂ concentration was <15 ppm for all reactions). Tetrahydrofuran (THF) was dried over potassium benzophenone ketyl under N₂. Benzene was dried by passage through columns of activated alumina. Pentane was dried over sodium benzophenone ketyl. Benzene-*d*₆, was used as received and stored under a N₂ atmosphere over 4 Å molecular sieves. Ethylene and propylene were purchased in gas cylinders from GTS-Welco and used as received.

Copper(II) acetate and copper(II) 2-ethylhexanoate were purchased from Alfa Aesar and used as received. Rhodium(II) Acetate Dimer was purchased from Strem Chemicals and used as received. Rhodium(III) chloride hydrate was purchased from Pressure Chemical and used as received. All other reagents were purchased from commercial sources and used as received. $[\text{Rh}(\eta^2\text{-C}_2\text{H}_4)_2(\mu\text{-OAc})]_2$ was prepared according to literature procedures.⁸⁵ All of the diimine ligands (diazbutadienes, or DABs) were synthesized according to literature procedures.⁹²⁻⁹³ $[(^{\text{F1}}\text{DAB})\text{Rh}(\mu\text{-OAc})]_2$ (**3**) was synthesized according to literature procedures.⁵²

Measurement of the ^1H , ^{13}C , and ^{19}F NMR spectra were performed on a Varian Mercury 600 MHz spectrometer. All ^1H and ^{13}C spectra are referenced against residual proton signals (^1H NMR) or ^{13}C resonances (^{13}C NMR) of deuterated solvents. GC/FID was performed using a Shimadzu GC-2014 system with a 30 m x 90.25 mm HP5 column with 0.25 μm film thickness. Infrared spectra were collected on a Shimadzu IRAffinity-1 FT-IR instrument using KBr pellets. UV-vis spectra were collected on a Perkin Elmer Lambda 25 UV/VIS Spectrometer. SEM images were captured using a FEI Quanta 650 Scanning Electron Microscope (SEM). Phase identification was performed using x-ray diffraction on a PANalytical X'Pert Pro MPD with a Cu source operating at 45 kV and 40 mA. The single-crystal X-ray diffraction details are given in the supporting information. Specific surface area was obtained by N_2 physisorption at 77 K based on the Brunauer-Emmett-Teller (BET) method on a Micromeritics ASAP 2020 analyzer. ICP-OES analysis were performed by Galbraith Laboratories, Knoxville, TN

To sample reaction mixtures in Fisher-Porter reactors, the reactors were cooled to room temperature, sampled under N₂, recharged with olefin, and reheated. Aliquots of the reaction mixture (<100 μL) were analyzed by GC/FID using relative peak areas versus the internal standard (hexamethylbenzene). Styrene, allylbenzene, α-methylstyrene, trans-β-methylstyrene, and cis-β-methylstyrene production was quantified using linear regression analysis of gas chromatograms of standard samples of authentic product. A plot of peak area ratios versus molar ratios gave a regression line using hexamethylbenzene (HMB) as the internal standard. The slope and correlation coefficient of the regression lines were 1.67 and 0.99 (styrene), 0.87 and 0.99 (trans-stilbene), 1.40 and 0.99 (allylbenzene), 1.23 and 0.99 (α-methylstyrene), 1.47 and 0.99 (cis-β-methylstyrene), 1.38 and 0.99 (trans-β-methylstyrene) respectively.

All Density Functional Theory (DFT) calculations were performed by the Goddard group (Caltech) using the Jaguar software version 10.9 by Schrodinger Inc.⁹⁴ Structure optimizations were performed using the B3LYP⁹⁵ flavor of DFT including the Grimme-Becke-Johnson D3 correction for London dispersion.⁹⁶ Non-metal atoms were described by the triple-zeta 6-311G**++ basis set⁹⁷ while Rh and Cu were treated with the Los Alamos small-core (18 explicit electrons) effective core potential (LACV3P**++).⁹⁸⁻⁹⁹ Ultra-fine DFT grids were used for all calculations.

Vibrational frequency calculations at 423 K were performed at the B3LYP-D3 level and used to predict thermochemical properties including zero point energies, enthalpies as a function of temperature, and entropies as a function of temperature.

These frequency calculations were also used to confirm local minima (no negative eigenvalues in Hessian) and transition states (1 negative eigenvalue in Hessian).

In such calculations there are 3 translational degrees of freedom (dof) and 3 rotational dof leading to large entropies, but in solvent these dof become hindered librational dof, reducing the entropy by 40 to 60 %. We assume in this paper a factor of 50%. This becomes an issue for reactions that change the number of molecules.

All calculations included implicit solvent treatment. Solvent effects were implemented via the Poisson-Boltzmann finite element method (PBF).¹⁰⁰⁻¹⁰¹ A dielectric constant of 2.284 and a probe radius of 2.6 Å were used to represent benzene.

Procedure for TEM/EDS Experiments for TEM/EDS Experiments. Samples analyzed by transmission electron microscopy (TEM) were prepared by dispersing the powders in cyclohexane (99.5%, anhydrous, Sigma-Aldrich) and sonicating for 1 minute before mounting on Au-supported holey carbon grids. The catalyst samples were imaged using a FEI Titan 80–300 operating at 300 kV. The sample was also characterized by an energy dispersive spectrometer (EDS) system in the scanning mode of TEM for single-nanoparticle composition analyses and elemental mapping. Lattice spacings were determined from selected-area electron diffraction and Fourier transforms of high resolution TEM images.

Procedure for XPS Experiments. X-ray photoelectron spectroscopy (XPS) was performed using a Phi VersaProbe III with a monochromatic Al K α X-ray source (1486.7 eV) and a hemispherical analyzer; instrument base pressure was $\sim 10^{-7}$ Pa. Due

to the air-sensitivity of Rh catalysts, a PHI vacuum transfer vessel (Model 04-111) was used to protect the sample from exposure to ambient atmosphere during transfer from the glovebox to the XPS analysis chamber. An X-ray beam of 100 μm was utilized and was rastered over 1.4 mm to reduce the X-ray flux on the target. The electron-energy analyzer was operated with a pass energy of 55 eV for high-resolution scans with a 50 ms per step dwell time. Dual-charge compensation, using a low-energy flood gun with a bias of 1 eV and a low-energy Ar^+ beam, was utilized during data acquisition. The Si $2p_{3/2}$ peak for SiO_2 (103.5 eV) and the C1s (284.6 eV) peak were used as a binding energy references for the spectra.

Generation of diimine rhodium complexes. To a stirring solution of $[\text{Rh}(\eta^2\text{-C}_2\text{H}_4)_2(\mu\text{-OAc})]_2$ (200 mg, 0.368 mmol) in THF (25 mL), the diimine ligand (0.735 mmol) was added, and the mixture was stirred for 1 h. The solvent was removed under vacuum, and the solid was washed with pentane (c.a. 100 mL) and dried to yield the corresponding *in situ* rhodium catalyst. X-ray quality crystals of representative complex **6** were grown by the vapor diffusion method using benzene and *n*-pentane. X-ray quality crystals of representative $[(^{\text{F1}}\text{DAB})\text{Rh}(\text{-OAc})]_2$ (**3**) were grown by vapor diffusion using THF and *n*-pentane. The characterization data for the representative complex **6** are as follows. ^1H NMR (600 MHz, Benzene- d_6): δ 7.27 (t, $J = 7.5$ Hz, 2H, *p*-Ar-*H*), 7.17 (d, $J = 7.6$ Hz, 4H, *m*-Ar-*H*), 2.41 (s, 12H, *o*- CH_3), 1.47 (s, 3H, N=C- CH_3), -0.80 (s, 6H, N=C- CH_3). ^{13}C NMR (151 MHz, Benzene- d_6): δ 186.60 (N=C- CH_3), 156.09 (COOCH_3), 154.66 (ipso-Ar-C), 130.77 (*o*-Ar-C), 127.82 (*m*-Ar-C), 125.47 (*p*-Ar-C), 23.15 (COOCH_3), 19.45 (*o*- CH_3), 18.73

(N=C-CH₃). Anal. Calcd for C₂₂H₂₇N₂O₂Rh: C: 58.15; H: 5.99; N: 6.17. Found: C: 58.18; H: 5.99; N: 6.17. The ¹H, ¹³C, and ¹⁹F NMR data for the representative [(^{F1}DAB)Rh(μ-OAc)]₂ (**3**) have been reported.⁵² The elemental analysis data for [(^{F1}DAB)Rh(μ-OAc)]₂ are as follows. Anal. Calcd for C₁₈H₉F₁₀N₂O₂Rh: C: 37.39; H: 1.57; N: 4.85. Found: C: 37.69; H: 2.33; N: 5.20.

Synthesis of silica-supported Rh nanoparticles. Silica-supported Rh nanoparticle catalysts were prepared via an ion exchange of the Rh precursor using Davisil 636 silica (Sigma-Aldrich) as a support.¹⁰²⁻¹⁰³ For example, the rhodium(III) chloride hydrate precursor (0.250 g, 99%, Sigma-Aldrich) was dissolved in a solution of aqueous ammonia (5.428 cm³ ammonium hydroxide, ACS plus, Fisher Scientific, in 282 cm³ distilled deionized water). The metal solution was added dropwise over 10 min to 4.75 g of acid-washed Davisil 636 silica in 114 cm³ of distilled deionized water at 343 K. The metal salt and silica slurry was stirred for 60 min at 343 K, and then cooled to room temperature. The mixture was washed with water and vacuum dried overnight. After calcination in flowing air (medical grade, GTS-Welco) at 673 K for 2 h, the sample was pre-reduced in flowing H₂ (99.999%, GTS-Welco) at 523 K for 2 h.

Catalytic alkenylation of benzene with ethylene and propylene using Cu(OAc)₂ (untreated Cu(OAc)₂, dried Cu(OAc)₂, ball-milled Cu(OAc)₂) or Cu(OHex)₂ with or without the addition of additives (i.e., excess ^{F1}DAB ligand, Cu₂O, CuO, CuOAc, or/and HOAc). Representative catalytic reactions are described here. A stock solution containing an diimine rhodium complex or

$[\text{Rh}(\eta^2\text{-C}_2\text{H}_4)_2(\mu\text{-OAc})]_2$ (0.011 mmol, 0.001 mol % of Rh relative to benzene), hexamethylbenzene (0.073 g, 0.46 mmol), and benzene (200 mL) was prepared in a volumetric flask. Fisher-Porter reactors were charged with stock solution (10 mL) copper(II) acetate (240 equiv. relative to per Rh, 0.049 g, 0.27 mmol) and additives (if any). The vessels were sealed, pressurized with ethylene (40 psig) or propylene (25 psig), and subsequently stirred and heated to 150 °C. For the catalysis with ethylene, the reactions were sampled every 4 h until 24 h. For the catalysis with propylene, the reactions were sampled until 48 h when the solution turned yellowish brown and Cu oxidant is consumed.

Kinetics of thermal decomposition of $[\text{Rh}(\eta^2\text{-C}_2\text{H}_4)_2(\mu\text{-OAc})]_2$ in the absence of $\text{Cu}(\text{OAc})_2$. The experiment at 100 °C in benzene- d_6 is used here as an example: 0.0075g (0.017 mmol) of $[\text{Rh}(\eta^2\text{-C}_2\text{H}_4)_2(\mu\text{-OAc})]_2$ was dissolved with 1.5 mL benzene- d_6 in a volumetric flask. The solution was then equally distributed into three J-Young pressure NMR tubes. Each NMR tubes was pressurized with 35 psig N_2 to prevent the solvent from boiling. The J-Young tubes were heated in a 100 °C oil bath. Every 20 mins, the J. Young tubes were taken out of the oil bath and cooled to room temperature with water. After ^1H NMR spectra were acquired, the J-Young tubes were put back into the oil bath. The experiment was stopped when the resonances from the Rh complex were no longer observed in the ^1H NMR spectra.

Isolation of black precipitates formed during thermal decomposition of $[\text{Rh}(\eta^2\text{-C}_2\text{H}_4)_2(\mu\text{-OAc})]_2$ in the absence of $\text{Cu}(\text{OAc})_2$. A stock solution containing $[\text{Rh}(\eta^2\text{-C}_2\text{H}_4)_2(\mu\text{-OAc})]_2$ (0.011 mmol, 0.001 mol % of Rh relative to benzene) and

benzene (200 mL) was prepared in a volumetric flask. Fisher-Porter reactors were charged with stock solution (10 mL). The vessels were sealed, pressurized with ethylene (40 psig), and subsequently stirred and heated to 150 °C for 1 h. The resulting reaction mixtures were decanted after centrifuging to leave only black precipitates and remove any soluble materials. The solid was subsequently sonicated in cyclohexane, decanted, and the remaining solid was deposited on the grid for TEM/EDS analysis or collected for XPS analysis.

Catalytic alkenylation of benzene with ethylene and propylene after Cu(OAc)₂ preheating treatment in benzene. A stock solution containing hexamethylbenzene (0.073 g, 0.46 mmol), and benzene (200 mL) was prepared in a volumetric flask. Fisher-Porter reactors were charged with stock solution (10 mL) and copper(II) acetate (0.050 g, 0.28 mmol). The vessels were sealed, pressurized with N₂ (70 psig), and subsequently stirred and heated to 150 °C for 2, 4, 6, 8, 10, 12, or 24 h. A stock solution containing [Rh(η^2 -C₂H₄)₂(μ -OAc)]₂ (0.0049 g, 0.022 mmol), and benzene (2 mL) was prepared in a volumetric flask. After preheating, the reactors were cooled to room temperature, brought into the glovebox, and charged with 0.1 mL of stock solution containing [Rh(η^2 -C₂H₄)₂(μ -OAc)]₂. The vessels were sealed, pressurized with ethylene (40 psig) or propylene (25 psig), and subsequently stirred and heated to 150 or 125 °C. For the catalysis with ethylene, the reactions were sampled every 2 h until 12 h. For the catalysis with propylene, the reactions were sampled until 48 h when the solution turned yellowish brown and Cu oxidant is consumed.

Procedure for ball miller. 5g Cu(OAc)₂ powder and tungsten carbide grinding

balls with a weight ratio of 1:5 were added to a high density polyethylene bottle sealed in a glovebox under Argon atmosphere. The well-sealed jar was then loaded in SPEX 8000 apparatus and vibrationally ball milled for 10 minutes. The resulting powder was used for catalysis.

Catalytic alkenylation of benzene with ethylene using insoluble solid materials or supernatant isolated from the reaction mixture after the catalytic styrene production. A representative catalytic reaction is described here. A stock solution containing $[\text{Rh}(\eta^2\text{-C}_2\text{H}_4)_2(\mu\text{-OAc})]_2$ (0.011 mmol, 0.001 mol % of Rh relative to benzene), hexamethylbenzene (0.073 g, 0.46 mmol), and benzene (200 mL) was prepared in a volumetric flask. Fisher-Porter reactors were charged with stock solution (10 mL) and copper(II) acetate (240 equiv. relative to per Rh, 0.049 g, 0.27 mmol). The vessels were sealed, pressurized with ethylene (40 psig) or propylene (25 psig), and subsequently stirred and heated to 150 °C for 1 h. The reactors were cooled to room temperature and brought into the glovebox. Each reaction mixture was filtered through a frit. The filtrate was centrifuged in order to separate any remaining insoluble solid that passed through the frits. The insoluble solid materials collected from the filtration and centrifugation were combined. For the use of ICP-OES measurement, volatile species from the supernatant were removed under vacuum and the remaining solid was sent for analysis. For the catalysis using the supernatant, new Fisher-Porter reactors were charged with copper(II) acetate (0.049 g, 0.27 mmol) and the supernatant. For the catalysis using the insoluble solid material, new Fisher-Porter reactors were charged with hexamethylbenzene (0.018 g, 0.11 mmol) and the solid

material. The vessels were sealed, pressurized with ethylene (40 psig), and subsequently stirred and heated to 150 °C. The reactions were sampled every 2 h until 12 h.

Isolation of recovered Rh species from catalytic reactions for the use of TEM/EDS and XPS analysis. After catalytic reactions, the reactors were cooled to room temperature and brought into the glovebox. Volatile species from the reaction mixture were removed under vacuum and the remaining solid was collected for analysis. For the use of XPS analysis, the samples were sealed in a vacuum transfer vessel in the glovebox prior to analysis.

Reaction of diimine rhodium complexes with ethylene. A representative catalytic reaction is described here. A J-Young pressure NMR tube was charged with 0.5 mL benzene- d_6 and 0.0058 g (0.005 mmol) of $[(^{\text{Fl}}\text{DAB})\text{Rh}(\mu\text{-OAc})]_2$. A ^1H NMR spectrum was obtained before the tube was purged and pressurized with ethylene (~10 psig). Immediately after being treated with ethylene, the solution changed from purple to yellow. ^1H NMR spectra were subsequently acquired at 0, 24 and 48 h.

Isolation of the insoluble solid materials (activated $\text{Cu}(\text{OAc})_2$) and supernatant obtained after $\text{Cu}(\text{OAc})_2$ preheating treatment and catalytic alkenylation of benzene by $[\text{Rh}(\mu\text{-OAc})(\eta^2\text{-C}_2\text{H}_4)_2]_2$ using these solid materials activated $\text{Cu}(\text{OAc})_2$ and supernatant. A stock solution (#1) containing hexamethylbenzene (0.073 g, 0.46 mmol) and benzene (200 mL) was prepared in a volumetric flask. Fisher-Porter reactors were charged with the stock solution (10 mL) and copper(II) acetate (0.050 g, 0.28 mmol). The vessels were sealed, pressurized

with N₂ (70 psig), and subsequently stirred and heated to 150 °C for 12 h. After the 12 h heating period, the reactors were allowed to cool to room temperature and brought into the glovebox. The reaction mixture was vacuum filtered through a fine porosity frits. The filtrate was centrifuged in order to separate any remaining insoluble materials that passed through the frit. The insoluble solid materials collected from the filtration and the centrifugation were combined and served as **activated Cu(OAc)₂** for the use of TGA, Powder-XRD, IR spectroscopy, SEM analysis and catalysis. A second stock solution (#2) containing [Rh(η^2 -C₂H₄)₂(μ -OAc)]₂ (0.0049 g, 0.022 mmol) and benzene (2 mL) was prepared in a volumetric flask. New Fisher-Porter reactors were charged with stock solution #2 (0.1 mL), copper(II) acetate (0.049 g, 0.27 mmol) and the supernatant. A third stock solution (#3) containing hexamethylbenzene (0.073 g, 0.46 mmol) and benzene (200 mL) was prepared in a volumetric flask. New Fisher-Porter reactors were charged with stock solution #3 (0.1 mL) and the filtrate after the centrifugation. The vessels were sealed, pressurized with ethylene (40 psig), and subsequently stirred and heated to 150 °C. The reactions were sampled every 2 or 4 h until the solution turned yellowish brown and Cu(II) oxidant was consumed.

Catalytic alkenylation of benzene with ethylene after Cu(OAc)₂ preheating treatment in hexane. Fisher-Porter reactors were charged with hexane (10 mL) and copper(II) acetate (0.050 g, 0.28 mmol). The vessels were sealed, pressurized with N₂ (70 psig), and subsequently stirred and heated to 150 °C for 12 h. After preheating, the reactors were allowed to cool to room temperature and then brought into the glovebox. Each reaction mixture was filtered through a fine porosity frit. The filtrate

was centrifuged in order to separate any remaining insoluble solid that passed through the frit. The insoluble solid material collected from the filtration and centrifugation were combined. A stock solution containing $[\text{Rh}(\eta^2\text{-C}_2\text{H}_4)_2(\mu\text{-OAc})_2]$ (0.0049 g, 0.022 mmol) and benzene (2 mL) was prepared in a volumetric flask. New Fisher-Porter reactors were charged with stock solution (0.1 mL), the solid material and hexamethylbenzene (0.018 g, 0.11 mmol). The vessels were sealed, pressurized with ethylene (40 psig), and subsequently stirred and heated to 150 °C. The reactions were sampled every 2 h until 12 h.

Procedure for thermogravimetric analysis (TGA): TGA experiments were performed using a SDT Q600 instrument. Before each measurement, the TGA instrument was evacuated and then purged with dinitrogen to remove residual dioxygen. Approximately 10 mg of sample were heated in a 40 sccm synthetic air (20 vol% O₂ in He) flow to 400 °C in a constant ramp rate of 10 °C min⁻¹.

Catalytic alkenylation of benzene with ethylene using Cu(OAc)₂ with the addition of solid Cu species obtained after the standard catalytic reaction. A stock solution containing $[\text{Rh}(\eta^2\text{-C}_2\text{H}_4)_2(\mu\text{-OAc})_2]$ (0.011 mmol, 0.001 mol % of Rh relative to benzene), hexamethylbenzene (0.073 g, 0.46 mmol) and benzene (200 mL) was prepared in a volumetric flask. Fisher-Porter reactors were charged with stock solution (10 mL) and copper(II) acetate (240 equiv. relative to Rh, 0.049 g, 0.27 mmol). The vessels were sealed, pressurized with ethylene (40 psig), and subsequently stirred and heated to 150 °C for 24 h. The reactors were allowed to cool to room temperature and brought into the glovebox. The resulting reaction mixture

was filtered through a fine porosity frit to separate insoluble solid material. A stock solution containing $[\text{Rh}(\eta^2\text{-C}_2\text{H}_4)_2(\mu\text{-OAc})_2]$ (0.0049 g, 0.022 mmol) and benzene (2 mL) was prepared in a volumetric flask. New Fisher-Porter reactors were charged with stock solution (10 mL), copper(II) acetate (240 equiv. relative to per Rh, 0.049 g, 0.27 mmol), and insoluble solid materials. The vessels were sealed, pressurized with ethylene (40 psig), and subsequently stirred and heated to 150 °C. The reactions were sampled every 2 h until 12 h.

Catalytic alkenylation of benzene with ethylene with the addition of poisoning reagents (*i.e.*, PPh_3 , $\text{P}(\text{OCH}_2)_3\text{CEt}$ or 1,10-Phenanthroline). Stock solution #1 containing $[\text{Rh}(\eta^2\text{-C}_2\text{H}_4)_2(\mu\text{-OAc})_2]$ (0.011 mmol, 0.001 mol % of Rh relative to benzene), hexamethylbenzene (0.073 g, 0.46 mmol), and benzene (200 mL) was prepared in a volumetric flask. Stock solution #2 containing the poisoning reagent (0.11 mmol, 0.001 mol % of Rh relative to benzene) and benzene (10 mL) was prepared in a volumetric flask. Fisher-Porter reactors were charged with stock solution #1 (10 mL), activated copper(II) acetate (240 equiv. relative to per Rh, 0.049 g, 0.27 mmol) and stock solution #2 (0.1 mL for 1 equiv. of poisoning reagents, 0.05 mL for 0.5 equiv. of poisoning reagents, 0.025 mL for 0.25 equiv. of poisoning reagents). The vessels were sealed, pressurized with ethylene (40 psig), and subsequently stirred and heated to 150 °C. The reactions were sampled every 2 h until 12 h.

Isolation of the insoluble solid materials obtained after preheating copper(II) acetate with $^{\text{Fl}}\text{DAB}$. A stock solution containing $^{\text{Fl}}\text{DAB}$ (0.047g, 0.112 mmol) and

benzene (200 mL) was prepared in a volumetric flask. Fisher-Porter reactors were charged with stock solution (10 mL) and copper(II) acetate (0.050 g, 0.28 mmol). The vessels were sealed, pressurized with N₂ (70 psig), and subsequently stirred and heated to 150 °C for 2 h. After preheating, the reactors were allowed to cool to room temperature and brought into the glovebox. Each reaction mixture was filtered through a fine porosity frit. The filtrate was centrifuged in order to separate any remaining insoluble solid that passed through the frits. The insoluble solid materials collected from the filtration and centrifugation were combined for the use of Powder-XRD, IR spectroscopy and catalysis.

Isolation of SiO₂ captured reduced Rh species. A stock solution containing [Rh(η^2 -C₂H₄)₂(μ -OAc)]₂ (0.011 mmol, 0.001 mol % of Rh relative to benzene) and benzene (200 mL) was prepared in a volumetric flask. Fisher-Porter reactors were charged with stock solution (10 mL) and 50 mg of mesoporous SiO₂. The vessels were sealed, pressurized with ethylene (40 psig), and subsequently stirred and heated to 150 °C for 1 h. The reactors were allowed to cool to room temperature and brought into the glovebox. Volatile species from the reaction mixture were removed under vacuum and the remaining solid was collected for analysis. For the use of XPS analysis, the samples were sealed in a vacuum transfer vessel in the glovebox prior to analysis.

Catalytic alkenylation of benzene with ethylene using the reaction mixture obtained after 1 h of the standard catalytic reaction. A representative catalytic reaction is described. A stock solution containing [Rh(η^2 -C₂H₄)₂(μ -OAc)]₂ (0.011

mmol, 0.001 mol % of Rh relative to benzene), hexamethylbenzene (0.073 g, 0.46 mmol), and benzene (200 mL) was prepared in a volumetric flask. Fisher-Porter reactors were charged with stock solution (10 mL) and copper(II) acetate (240 equiv. relative to per Rh, 0.049 g, 0.27 mmol). The vessels were sealed, pressurized with ethylene (40 psig), and subsequently stirred and heated to 150 °C for 1 h. The reactors were allowed to cool to room temperature and brought into the glovebox. Activated copper(II) acetate (0.049 g, 0.27 mmol) was added to the reactors. The vessels were resealed, pressurized with ethylene (40 psig), and subsequently stirred and heated to 150 °C. The reactions were sampled every 2h until 12 h.

Catalytic alkenylation of benzene with ethylene using the reaction mixture obtained by heating $[\text{Rh}(\mu\text{-OAc})(\eta^2\text{-C}_2\text{H}_4)_2]_2$ with or without $^{\text{Fl}}\text{DAB}$ in benzene for 1 h. A stock solution containing $[\text{Rh}(\eta^2\text{-C}_2\text{H}_4)_2(\mu\text{-OAc})]_2$ (0.011 mmol, 0.001 mol % of Rh relative to benzene), $^{\text{Fl}}\text{DAB}$ (0.047g, 0.112 mmol) (if any), hexamethylbenzene (0.073 g, 0.46 mmol) and benzene (200 mL) was prepared in a volumetric flask. Fisher-Porter reactors were charged with stock solution (10 mL). The vessels were sealed, pressurized with ethylene (40 psig), and subsequently stirred and heated to 150 °C for 1 h. The reactors were allowed to cool to room temperature and brought into the glovebox. Copper(II) acetate (0.049 g, 0.27 mmol) was added to reactors. The vessels were resealed, pressurized with ethylene (40 psig), and subsequently stirred and heated to 150 °C. The reactions were sampled every 2 h within the first 12 hours and then every 4 h until 40 h when the solution turned yellowish brown and Cu oxidant is consumed.

Styrene production using $[\text{Rh}(\eta^2\text{-C}_2\text{H}_4)_2(\mu\text{-OAc})]_2$, $[\text{Rh}(\mu\text{-OPiv})_2(\text{HOPiv})]_2$ or $[\text{Rh}^{\text{I}}(\mu\text{-OPiv})_2(\eta^2\text{-C}_2\text{H}_4)_2]_2(\mu\text{-Cu})$ as catalyst precursor and copper(II) pivalate as oxidant. A stock solution containing or $[\text{Rh}(\eta^2\text{-C}_2\text{H}_4)_2(\mu\text{-OAc})]_2$, $[\text{Rh}(\mu\text{-OPiv})_2(\text{HOPiv})]_2$ or $[\text{Rh}^{\text{I}}(\mu\text{-OPiv})_2(\eta^2\text{-C}_2\text{H}_4)_2]_2(\mu\text{-Cu})$ (0.0056 mmol, 0.001 mol % of Rh relative to benzene), hexamethylbenzene (0.073 g, 0.46 mmol), and benzene (200 mL) was prepared in a volumetric flask. Fisher-Porter reactors were charged with stock solution (10 mL), copper(II) pivalate (240 equiv. relative to per Rh, 0.072 g, 0.27 mmol) and pivalic acid (480 equiv. relative to per Rh, 0.0550 g, 0.539 mmol). The vessels were sealed, pressurized with ethylene (50 psig), and subsequently stirred and heated to 150 °C. To analyze reaction mixture samples by GC-FID, the reactors were cooled to room temperature, sampled under N₂, recharged with gases, and reheated. Aliquots of the resulting solution (< 100 µL) were washed with saturated sodium carbonate solution (0.25 mL). The aqueous and organic layers were separated. The resulting organic layers were analyzed by GC/FID.

Styrene production using RhCl_3 as catalyst precursor and copper(II) pivalate as oxidant. Under air, a stock solution containing rhodium chloride trihydrate (0.0118 g, 0.0449 mmol) and distilled water (2 mL) was prepared in a volumetric flask. Fisher-Porter reactors were charged with 0.05 mL stock solution (contains 0.0011 mmol Rh) and placed under dynamic vacuum at 40 °C for 2 hours to remove water. The Fisher-Porter reactors were then brought into the nitrogen-filled glovebox and charged with hexamethylbenzene (0.0182 g, 0.1121 mmol), additives (2000 eq. of relative to per Rh), copper(II) pivalate (240 equiv. relative to per Rh,

0.072 g, 0.27 mmol), pivalic acid (480 equiv. relative to per Rh, 0.0550 g, 0.539 mmol) and benzene (10 mL). The vessels were sealed, pressurized with ethylene (50 psig), stirred and heated to 150 °C. To analyze reaction mixture samples by GC-FID, the reactors were cooled to room temperature, sampled under N₂, recharged with gases, and reheated. Aliquots of the resulting solution (< 100 µL) were washed with saturated sodium carbonate solution (0.25 mL). The aqueous and organic layers were separated. The resulting organic layers were analyzed by GC/FID.

Styrene production using solution A and copper(II) pivalate as oxidant. A stock solution containing $[\text{Rh}(\eta^2\text{-C}_2\text{H}_4)_2(\mu\text{-OAc})_2]$ (8.2 mg, 0.0373 mmol Rh) and benzene-*d*₆ (10 mL) was prepared in a volumetric flask. A J-Young pressure NMR tube was charged with stock solution (0.3 mL), copper(II) pivalate (24 equiv. relative to per Rh, 7.2 mg, 0.027 mmol), pivalic acid (48 equiv. relative to per Rh, 5.5 mg, 0.054 mmol). Each NMR tube was purged and pressurized with ethylene. Then the tube was heated in a 120 °C oil bath for 12 h. The J. Young tubes were taken out of the oil bath, cooled to room temperature and subsequently brought to the nitrogen-filled glovebox. In the glovebox, Fisher-Porter reactors were charged with solution from the J. Young tube reaction, hexamethylbenzene (0.0182 g, 0.112 mmol), copper(II) pivalate (240 equiv. relative to per Rh, 0.072 g, 0.27 mmol) and pivalic acid (480 equiv. relative to per Rh, 0.0550 g, 0.539 mmol). The vessels were sealed, pressurized with ethylene (50 psig), and subsequently stirred and heated to 150 °C. To analyze reaction mixture samples by GC-FID, the reactors were cooled to room temperature, sampled under N₂, recharged with gases, and reheated. Aliquots of the

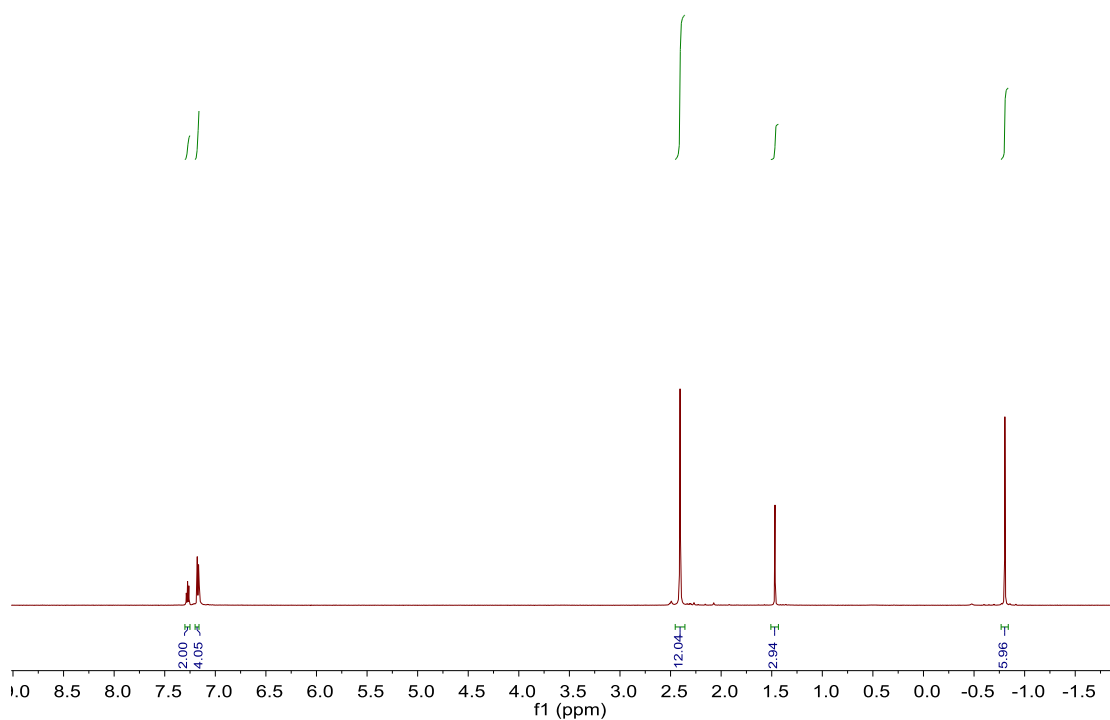
resulting solution (< 100 μL) were washed with saturated sodium carbonate solution (0.25 mL). The aqueous and organic layers were separated. The resulting organic layers were analyzed by GC/FID.

In Situ ^1H NMR Studies of conversion of $[\text{Rh}(\eta^2\text{-C}_2\text{H}_4)_2(\mu\text{-OAc})_2$ to $[\text{Rh}(\mu\text{-OPiv})_2(\text{HOPiv})_2]$. A stock solution containing $[\text{Rh}(\eta^2\text{-C}_2\text{H}_4)_2(\mu\text{-OAc})_2$ (8.2 mg, 0.0373 mmol Rh, 18.7 mM Rh) and benzene- d_6 (2 mL) was prepared in a volumetric flask. A J-Young pressure NMR tube was charged with stock solution (0.3 mL), copper(II) pivalate (24 equiv. relative to per Rh, 0.036 g, 0.135 mmol), pivalic acid (48 equiv. relative to per Rh, 0.0275 g, 0.27 mmol) and hexamethyldisiloxane (HMDSO, internal standard). A ^1H NMR spectrum was obtained immediately after pressurizing each tube with N_2 (~20 psig). If needed, the tube was purged with ethylene to remove N_2 and pressurized with ethylene. Then the tube was heated in an oil bath. At each time point, the J. Young tubes were taken out of the oil bath and cooled to room temperature with water for NMR measurement. After ^1H NMR spectra were obtained, the J-Young tubes were put back into the oil bath. The relaxation delay time (d1) for ^1H NMR was set to 10 s. The rate of decay of **4** was determined based on the amount of $[\text{Rh}(\mu\text{-OPiv})_2(\text{HOPiv})_2]$ (**2**) formed. Concentration of **2** were determined based on the integration ratio between $[\text{Rh}(\mu\text{-OPiv})_2(\text{HOPiv})_2]$ peak and the HMDSO peak in the ^1H NMR spectra.

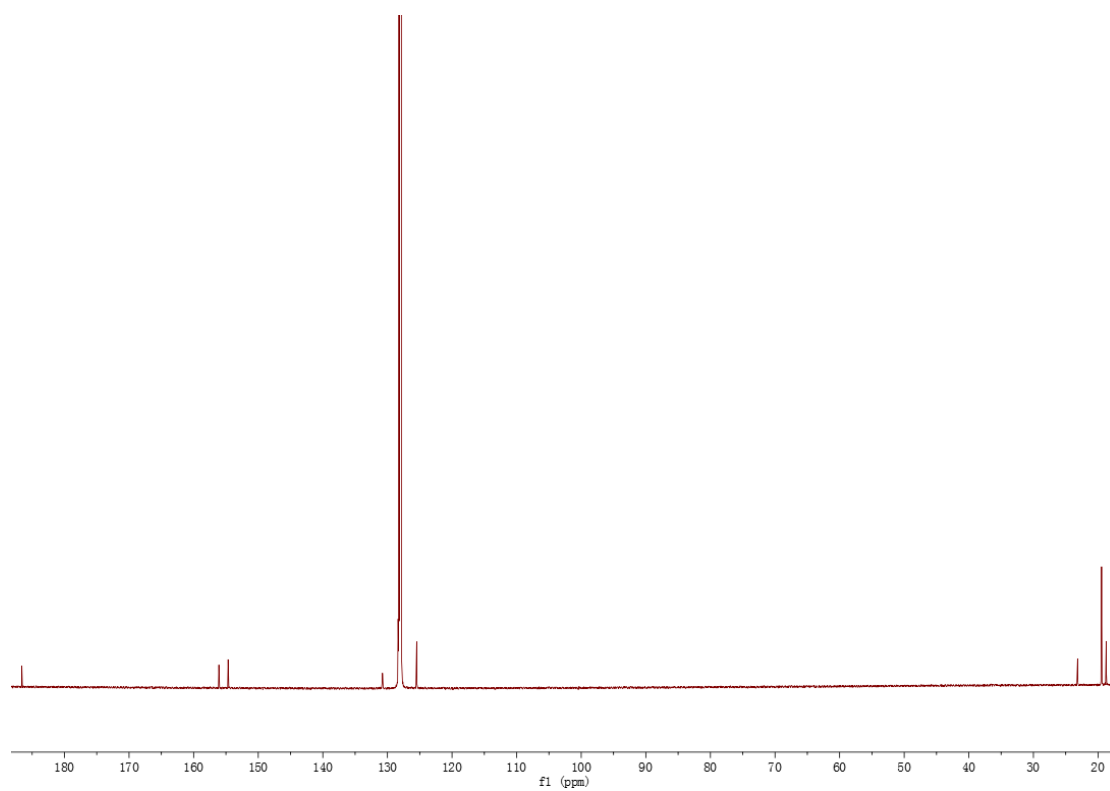
Generation of $[\text{Rh}^{\text{I}}(\mu\text{-OPiv})_2(\eta^2\text{-C}_2\text{H}_4)_2(\mu\text{-Cu})]$ (4**).** To a solution of $[\text{Rh}(\eta^2\text{-C}_2\text{H}_4)_2(\mu\text{-OAc})_2$ (4.9 mg, 0.0224 mmol Rh) in benzene (1 mL), copper(II) pivalate (1 equiv. relative to per Rh, 6.5 mg, 0.0224 mmol), pivalic acid (2 equiv.

relative to per Rh, 4.6 mg, 0.0448 mmol) was added. Crystals suitable for X-ray analysis were obtained by slowly evaporating benzene solvent. Crystals of **4** were washed with pentane and dried under vacuum. The obtained solid was collected for NMR and catalysis studies.

In Situ ¹H NMR Studies of conversion of [Rh^I(μ-OPiv)₂(η²-C₂H₄)₂]₂(μ-Cu) to [Rh(μ-OPiv)₂(HOPIv)]₂. A J-Young pressure NMR tube was charged with benzene-*d*₆ (0.3 mL), [Rh^I(μ-OPiv)₂(η²-C₂H₄)₂]₂(μ-Cu) (2.2 mg, 18.7 mM Rh), hexamethyldisiloxane (HMDSO, internal standard). A ¹H NMR spectrum was obtained before the tube was changed with copper(II) pivalate (24 equiv. relative to per Rh, 0.036 g, 0.135 mmol) and pivalic acid (48 equiv. relative to per Rh, 0.0275 g, 0.27 mmol). Each NMR tube was pressurized with 20 psig N₂. Then the tube was heated in a 120 °C oil bath. ¹H NMR spectra were subsequently acquired after 12 hours.



Scheme 2.4.1. ^1H NMR spectrum of complex **6** (600 MHz, C_6D_6).



Scheme 2.4.2. ^{13}C $\{^1\text{H}\}$ NMR spectrum of complex **6** (151 MHz, C_6D_6).

2.5 References

- (1) Olah, G. A.; Molnár, Á.: *Hydrocarbon Chemistry*; 2nd ed.; Wiley-Interscience: Hoboken, NJ, 2003.
- (2) Perego, C.; Pollesel, P.: Chapter 2 - Advances in Aromatics Processing Using Zeolite Catalysts. *Advances in Nanoporous Materials*; Stefan, E., Ed.; Elsevier, 2010; Vol. Volume 1; pp 97-149.
- (3) Chen, S.-S. Styrene. *Kirk-Othmer Encyclopedia of Chemical Technology*; John Wiley & Sons, Inc: Hoboken, New Jersey, 2000; pp 325-357.
- (4) Wittcoff, H. A., Reuben, B. G. and Plotkin, J. S. Chemicals and Polymers from Ethylene. *Industrial Organic Chemicals*; John Wiley & Sons, Inc: Hoboken, New Jersey, 2004; pp 100-166.
- (5) Process Evaluation/Research Planning (PERP) Program Report. *Styrene/Ethylbenzene*; PERP Report 91-9, Chem Systems, Inc.: New York, 1992.
- (6) Perego, C.; Ingallina, P. Recent advances in the industrial alkylation of aromatics: new catalysts and new processes. *Catal. Today* **2002**, *73*, 3-22.
- (7) Perego, C.; Ingallina, P. Combining alkylation and transalkylation for alkylaromatic production. *Green Chem.* **2004**, *6*, 274-279.
- (8) Čejka, J.; Wichterlová, B. Acid-Catalyzed Synthesis of Mono- and Dialkyl Benzenes over Zeolites: Active Sites, Zeolite Topology, and Reaction Mechanisms. *Catal. Rev.: Sci. Eng.* **2002**, *44*, 375-421.
- (9) Olah, G. A.; Molnár, Á.: *Hydrocarbon Chemistry*; 2nd ed.; Wiley-Interscience: Hoboken, NJ, 2003. pp. 283.
- (10) Lucchini, M.; Galeotti, A. International Patent WO2007073918A1, 2007.
- (11) Gerzeliev, I. M.; Khadzhiev, S. N.; Sakharova, I. E. Ethylbenzene synthesis and benzene transalkylation with diethylbenzenes on zeolite catalysts. *Pet. Chem.* **2011**, *51*, 39-48.
- (12) Heck, R. F. In *Organic Reactions*; Duaben, W. G., Ed.; John Wiley and Sons: New York, 1982; Vol. 27, p 345-390.
- (13) Heck, R. F. In *Comp. Org. Syn.*; Trost, B. M., Fleming, I., Semmelhack, M. F., Eds.; Pergamon Press: Oxford, 1999; Vol. 4, p 833-863.
- (14) Beletskaya, I. P.; Cheprakov, A. V. The Heck Reaction as a Sharpening Stone of Palladium Catalysis. *Chem. Rev.* **2000**, *100*, 3009-3066.
- (15) McCartney, D.; Guiry, P. J. The asymmetric Heck and related reactions. *Chem. Soc. Rev.* **2011**, *40*, 5122-5150.
- (16) Lail, M.; Arrowood, B. N.; Gunnoe, T. B. Addition of Arenes to Ethylene and Propene Catalyzed by Ruthenium. *J. Am. Chem. Soc.* **2003**, *125*, 7506-7507.
- (17) Lail, M.; Bell, C. M.; Conner, D.; Cundari, T. R.; Gunnoe, T. B.; Petersen, J. L. Experimental and Computational Studies of Ruthenium(II)-Catalyzed Addition of Arene C-H Bonds to Olefins. *Organometallics* **2004**, *23*, 5007-5020.
- (18) McKeown, B. A.; Foley, N. A.; Lee, J. P.; Gunnoe, T. B. Hydroarylation of Unactivated Olefins Catalyzed by Platinum(II) Complexes. *Organometallics* **2008**, *27*, 4031-4033.

-
- (19) Foley, N. A.; Lee, J. P.; Ke, Z.; Gunnoe, T. B.; Cundari, T. R. Ru(II) Catalysts Supported by Hydridotris(pyrazolyl)borate for the Hydroarylation of Olefins: Reaction Scope, Mechanistic Studies, and Guides for the Development of Improved Catalysts. *Acc. Chem. Res.* **2009**, *42*, 585-597.
- (20) Andreatta, J. R.; McKeown, B. A.; Gunnoe, T. B. Transition Metal Catalyzed Hydroarylation of Olefins using Unactivated Substrates: Recent Developments and Challenges. *J. Organomet. Chem.* **2011**, *696*, 305-315.
- (21) McKeown, B. A.; Gonzalez, H. E.; Friedfeld, M. R.; Gunnoe, T. B.; Cundari, T. R.; Sabat, M. Mechanistic Studies of Ethylene Hydrophenylation Catalyzed by Bipyridyl Pt(II) Complexes. *J. Am. Chem. Soc.* **2011**, *133*, 19131-19152.
- (22) Joslin, E. E.; McMullin, C. L.; Gunnoe, T. B.; Cundari, T. R.; Sabat, M.; Myers, W. H. Catalytic Hydroarylation of Ethylene using TpRu(L)(NCMe)Ph (L = 2,6,7-Trioxa-1-phosphabicyclo[2,2,1]heptane): Comparison to TpRu(L')(NCMe)Ph Systems (L' = CO, PMe₃ or P(OCH₂)₃CEt). *Organometallics* **2012**, *31*, 6851-6860.
- (23) McKeown, B. A.; Gonzalez, H. E.; Michaelos, T.; Gunnoe, T. B.; Cundari, T. R.; Crabtree, R. H.; Sabat, M. Control of Olefin Hydroarylation Catalysis via a Sterically and Electronically Flexible Pt^{II} Catalyst Scaffold. *Organometallics* **2013**, *32*, 3903-3913.
- (24) McKeown, B. A.; Gonzalez, H. E.; Friedfeld, M. R.; Brosnahan, A. M.; Gunnoe, T. B.; Cundari, T. R.; Sabat, M. Pt^{II} Catalyzed Ethylene Hydrophenylation: Switching Selectivity between Alkyl and Vinyl Benzene Production. *Organometallics* **2013**, *32*, 2857-2865.
- (25) McKeown, B. A.; Gonzalez, H. E.; Gunnoe, T. B.; Cundari, T. R.; Sabat, M. Pt^{II} Catalyzed Ethylene Hydrophenylation: Influence of Dipyridyl Chelate Ring Size on Catalyst Activity and Longevity. *ACS Catal.* **2013**, *3*, 1165-1171.
- (26) McKeown, B. A.; Prince, B. M.; Ramiro, Z.; Gunnoe, T. B.; Cundari, T. R. Pt(II) Catalyzed Hydrophenylation of α -Olefins: Variation of Linear/Branched Products as a Function of Ligand Donor Ability. *ACS Catal.* **2014**, *4*, 1607-1615.
- (27) Burgess, S. A.; Joslin, E. E.; Gunnoe, T. B.; Cundari, T. R.; Sabat, M.; Myers, W. H. Hydrophenylation of Ethylene using a Cationic Ru(II) Catalyst: Comparison to a Neutral Ru(II) Catalyst. *Chem. Sci.* **2014**, *5*, 4355-4366.
- (28) Bhalla, G.; Bischof, S. M.; Ganesh, S. K.; Liu, X. Y.; Jones, C. J.; Borzenko, A.; Tenn, W. J., III; Ess, D. H.; Hashiguchi, B. G.; Lokare, K. S.; Leung, C. H.; Oxgaard, J.; Goddard, W. A., III; Periana, R. A. Mechanism of efficient anti-Markovnikov olefin hydroarylation catalyzed by homogeneous Ir(III) complexes. *Green Chem.* **2011**, *13*, 69-81.
- (29) Luedtke, A. T.; Goldberg, K. I. Intermolecular hydroarylation of unactivated olefins catalyzed by homogeneous platinum complexes *Angew. Chem. Int. Ed.* **2008**, *47*, 7694-7696.
- (30) Karshtedt, D.; Bell, A. T.; Tilley, T. D. Pt-Ag Catalyst System for Hydroarylations with Unactivated Arenes and Olefins. *Organometallics* **2004**, *23*, 4169-4171.

-
- (31) Karshtedt, D.; McBee, J. L.; Bell, A. T.; Tilley, T. D. Stoichiometric and Catalytic Arene Activations by Platinum Complexes Containing Bidentate Monoanionic Nitrogen-Based Ligands. *Organometallics* **2006**, *25*, 1801-1811.
- (32) Bhalla, G.; Oxgaard, J.; Goddard III, W. A.; Periana, R. A. Hydrovinylation of Olefins Catalyzed by an Iridium Complex via CH Activation. *Organometallics* **2005**, *24*, 5499-5502.
- (33) Bhalla, G.; Oxgaard, J.; Goddard III, W. A.; Periana, R. A. Anti-Markovnikov Hydroarylation of Unactivated Olefins Catalyzed by a Bis-tropolonato Iridium(III) Organometallic Complex. *Organometallics* **2005**, *24*, 3229-3232.
- (34) Periana, R. A.; Liu, X. Y.; Bhalla, G. Novel bis-acac-O,O-Ir(III) catalyst for anti-Markovnikov, hydroarylation of olefins operates by arene CH activation. *Chem. Commun.* **2002**, *24*, 3000-3001.
- (35) Bowring, M. A.; Bergman, R. G.; Tilley, T. D. Disambiguation of Metal and Brønsted Acid Catalyzed Pathways for Hydroarylation with Platinum(II) Catalysts. *Organometallics* **2011**, *30*, 1295-1298.
- (36) Jones, W. D.; Maguire, J. A.; Rosini, G. P. Thermal and photochemical substitution reactions of CpRe(PPh₃)₂H₂ and CpRe(PPh₃)H₄. Catalytic insertion of ethylene into the C-H bond of benzene. *Inorg. Chim. Acta* **1998**, *270*, 77-86.
- (37) Sen, A.; Lai, T.-W. Catalysis by solvated transition-metal cations. Novel catalytic transformations of alkenes by tetrakis(acetonitrile)palladium ditetrafluoroborate. Evidence for the formation of incipient carbonium ions as intermediates. *J. Am. Chem. Soc.* **1981**, *103*, 4627-4629.
- (38) Suslick, B. A.; Liberman-Martin, A. L.; Wambach, T. C.; Tilley, T. D. Olefin Hydroarylation Catalyzed by (pyridyl-indolate)Pt(II) Complexes: Catalytic Efficiencies and Mechanistic Aspects. *ACS Catal.* **2017**, *7*, 4313-4322.
- (39) Hong, P.; Yamazaki, H. Rhodium carbonyl-catalyzed activation of carbon-hydrogen bonds for application in organic synthesis.: V. phenylation of olefins with benzenes. *J. Mol. Catal.* **1984**, *26*, 297-311.
- (40) Taube, D.; Periana, R.; Matsumoto, T. U.S. Patent 6127590A, 2000.
- (41) Fujiwara, Y.; Moritani, I.; Danno, S.; Asano, R.; Teranishi, S. Aromatic substitution of olefins. VI. Arylation of olefins with palladium(II) acetate. *J. Am. Chem. Soc.* **1969**, *91*, 7166-7169.
- (42) Yamada, T.; Sakakura, A.; Sakaguchi, S.; Obora, Y.; Ishii, Y. Oxidative arylation of ethylene with benzene catalyzed by Pd(OAc)₂/heteropoly acid/O₂ system. *New J. Chem.* **2008**, *32*, 738-742.
- (43) Kubota, A.; Emmert, M. H.; Sanford, M. S. Pyridine Ligands as Promoters in Pd^{II/0}-Catalyzed C-H Olefination Reactions *Org. Lett.* **2012**, *14*, 1760-1763.
- (44) Sasaki, K.; Sakakura, T.; Tokunaga, Y.; Wada, K.; Tanaka, M. C=C Double Bond Insertion in Catalytic C-H Activation. Dehydrogenative Cross Coupling of Arenes with Olefins. *Chem. Lett.* **1988**, *17*, 685-688.
- (45) Weissman, H.; Song, X.; Milstein, D. Ru-Catalyzed Oxidative Coupling of Arenes with Olefins Using O₂. *J. Am. Chem. Soc.* **2001**, *123*, 337-338.
- (46) Takaya, M.; Hajime, Y. Oxidative Arylation of Ethylene with Benzene to Produce Styrene. *Chem. Lett.* **2000**, *29*, 1064-1065.

-
- (47) Ritleng, V.; Sirlin, C.; Pfeffer, M. Ru-, Rh-, and Pd-Catalyzed C–C Bond Formation Involving C–H Activation and Addition on Unsaturated Substrates: Reactions and Mechanistic Aspects. *Chem. Rev.* **2002**, *102*, 1731-1770.
- (48) Jia, X.; Gary, J. B.; Gu, S.; Cundari, T. R.; Gunnoe, T. B. Oxidative Hydrophenylation of Ethylene Using a Cationic Ru(II) Catalyst: Styrene Production with Ethylene as the Oxidant. *Isr. J. Chem.* **2017**, *57*, 1037-1046.
- (49) McKeown, B. A., Habgood, L. G., Cundari, T. R., Gunnoe, T. B.: Alkylation of Arenes Without Chelation Assistance: Transition Metal Catalysts with d^6 Electron Configurations. *Catalytic Hydroarylation of Carbon-Carbon Multiple Bonds*; Ackermann, L.; Gunnoe, T. B.; Habgood, L. G., Eds.; Wiley-VCH, Weinheim: 2018, pp 83-106.
- (50) Evano, G.; Theunissen, C. Beyond Friedel and Crafts: Innate Alkylation of C–H Bonds in Arenes. *Angew. Chem. Int. Ed.* **2019**, *58*, 7558-7598.
- (51) Vaughan, B. A.; Webster-Gardiner, M. S.; Cundari, T. R.; Gunnoe, T. B. A rhodium catalyst for single-step styrene production from benzene and ethylene. *Science* **2015**, *348*, 421-424.
- (52) Vaughan, B. A.; Khani, S. K.; Gary, J. B.; Kammert, J. D.; Webster-Gardiner, M. S.; McKeown, B. A.; Davis, R. J.; Cundari, T. R.; Gunnoe, T. B. Mechanistic Studies of Single-Step Styrene Production Using a Rhodium(I) Catalyst. *J. Am. Chem. Soc.* **2017**, *139*, 1485-1498.
- (53) Webster-Gardiner, M. S.; Chen, J.; Vaughan, B. A.; McKeown, B. A.; Schinski, W.; Gunnoe, T. B. Catalytic Synthesis of “Super” Linear Alkenyl Arenes Using an Easily Prepared Rh(I) Catalyst. *J. Am. Chem. Soc.* **2017**, *139*, 5474-5480.
- (54) Chen, J.; Nielsen, R. J.; Goddard III, W. A.; McKeown, B. A.; Dickie, Diane A.; Gunnoe, T. B. Catalytic Synthesis of Superlinear Alkenyl Arenes Using a Rh(I) Catalyst Supported by a “Capping Arene” Ligand: Access to Aerobic Catalysis. *J. Am. Chem. Soc.* **2018**, *140*, 17007-17018
- (55) Tran, B. L.; Fulton, J. L.; Linehan, J. C.; Lercher, J. A.; M.Bullock, R. Rh(CAAC)-Catalyzed Arene Hydrogenation: Evidence for Nanocatalysis and Sterically Controlled Site-Selective Hydrogenation. *ACS Catal.* **2018**, *8*, 8441-8449.
- (56) Bayram, E.; Linehan, J. C.; Fulton, J. L.; Roberts, J. A. S.; Szymczak, N. K.; Smurthwaite, T. D.; Ö zkar, S.; Balasubramanian, M.; Finke, R. G. Is It Homogeneous or Heterogeneous Catalysis Derived from $[\text{RhCp}^*\text{Cl}_2]_2$? In Operando XAFS, Kinetic, and Crucial Kinetic Poisoning Evidence for Subnanometer Rh_4 Cluster-Based Benzene Hydrogenation Catalysis. *J. Am. Chem. Soc.* **2011**, *133*, 18889-18902.
- (57) Bayram, E.; Linehan, J. C.; Fulton, J. L.; Szymczak, N. K.; Finke, R. G. Determination of the Dominant Catalyst Derived from the Classic $[\text{RhCp}^*\text{Cl}_2]_2$ Precatalyst System: Is It SingleMetal Rh_1Cp^* -Based, Subnanometer Rh_4 Cluster-Based, or Rh(0) Nanoparticle-Based Cyclohexene Hydrogenation Catalysis at Room Temperature and Mild Pressures? *ACS Catal.* **2015**, *5*, 3876-3886.
- (58) Pun, D.; Diao, T. N.; Stahl, S. S. Aerobic Dehydrogenation of Cyclohexanone to Phenol Catalyzed by $\text{Pd}(\text{TFA})_2/2$ -Dimethylaminopyridine: Evidence for the Role of Pd Nanoparticles. *J. Am. Chem. Soc.* **2013**, *135*, 8213-8221.

-
- (59) Yu, K.; Sommer, W.; Richardson, J. M.; Weck, M.; Jones, C. W. Evidence that SCS Pincer Pd(II) Complexes are only Precatalysts in Heck Catalysis and the Implications for Catalyst Recovery and Reuse. *Adv. Synth. Catal.* **2005**, *347*, 161-171.
- (60) Phan, N. T. S.; Van Der Sluys, M.; Jones, C. W. On the Nature of the Active Species in Palladium Catalyzed Mizoroki–Heck and Suzuki–Miyaura Couplings–Homogeneous or Heterogeneous Catalysis, A Critical Review. *Adv. Synth. Catal.* **2006**, *348*, 609-679.
- (61) Watzky, M. A.; Finke, R. G. Transition Metal Nanocluster Formation Kinetic and Mechanistic Studies. A New Mechanism When Hydrogen Is the Reductant: Slow, Continuous Nucleation and Fast Autocatalytic Surface Growth. *J. Am. Chem. Soc.* **1997**, *119*, 10382-10400.
- (62) Laxson, W. W.; Finke, R. G. Nucleation is Second Order: An Apparent Kinetically Effective Nucleus of Two for Ir(0)_n Nanoparticle Formation from [(1,5-COD)Ir^I P₂W₁₅Nb₃O₆₂]⁸⁻ Plus Hydrogen. *J. Am. Chem. Soc.* **2014**, *136*, 17601-17615.
- (63) Ozkar, S.; Finke, R. G. Nanoparticle Nucleation is Tetramolecular in Metal and Involves Hydrogen: Evidence for a Kinetically Effective Nucleus of Three {Ir₃H_{2x}P₂W₁₅Nb₃O₆₂}⁶⁻ in Ir(0)_n Nanoparticle Formation From [(1,5-COD)Ir^I P₂W₁₅Nb₃O₆₂]⁸⁻ Plus Dihydrogen. *J. Am. Chem. Soc.* **2017**, *139*, 5444-5457.
- (64) Bukan, B.; Duman, S. Green dehydrogenation of dimethylamine-borane catalyzed by in situ generated ruthenium nanoclusters in presence of various supporters and its comparison with classical methods, *Int. J. Hydrog. Energy* **2018**, *43*, 8278-8289.
- (65) Yan, N.; Yuan, Y.; Dyson, P. J. Nanometallic Chemistry: Deciphering Nanoparticle Catalysis from the Perspective of Organometallic Chemistry and Homogeneous Catalysis. *Dalton Trans.* **2013**, *42*, 13294-13304.
- (66) Vance, J. R.; Schafer, A.; Robertson, A. P. M.; Lee, K.; Turner, J.; Whittell, G. R.; Manners, I. Iron-Catalyzed Dehydrocoupling/Dehydrogenation of Amine–Boranes. *J. Am. Chem. Soc.* **2014**, *136*, 3048-3064.
- (67) Sonnenberg, J. F.; Coombs, N.; Dube, P. A.; Morris, R. H. Iron Nanoparticles Catalyzing the Asymmetric Transfer Hydrogenation of Ketones. *J. Am. Chem. Soc.* **2012**, *134*, 5893-5899.
- (68) Sonnenberg, J. F.; Morris, R. H. Evidence for Iron Nanoparticles Catalyzing the Rapid Dehydrogenation of Ammonia-Borane. *ACS Catal.* **2013**, *3*, 1092-1102.
- (69) Tetrick, S. M.; Tham, F. S.; Cutler, A. R. Re₂Rh₂ μ₃-[η¹-C(Re):η¹-O(Rh):η¹-O'(Rh')] Bis(carbon dioxide) Complexes [(η⁵-C₅R₅)(L)(NO)Re(CO₂)Rh(η⁴-diene)]₂ That Are Structurally Related to Rhodium(I) Carboxylate Dimers [Rh(O₂CR)(η⁴-diene)]₂. *J. Am. Chem. Soc.* **1997**, *119*, 6193-6194.
- (70) Esteruelas, M. A.; Lahuerta, O.; Modrego, J.; Nurnberg, O.; Oro, L. A.; Rodriguez, L.; Sola, E.; Werner, H. Synthesis, characterization, and reactivity of rhodium carboxylate dimers [Rh(μ-OOCCR₃)(CO)(PCy₃)]₂ (R = H, F). X-ray crystal structure of [Rh₂(μ-OOCCH₃)(μ-η¹:η²-C₂Ph)(CO)₂(PCy₃)₂]. *Organometallics* **1993**, *12*, 266-275.

- (71) Balch, A. L. Dimeric rhodium(I) and rhodium(II) complexes with bridging phosphine or arsine ligands. *J. Am. Chem. Soc.* **1976**, *98*, 8049-8054.
- (72) Balch, A. L.; Tulyathan, B. *Inorg. Chem.* Interactions between rhodium(I) centers in dimeric complexes. **1977**, *16*, 2840-2845.
- (73) Gonsalvi, L.; Gaunt, J. A.; Adams, H.; Castro, A.; Sunley, G. J.; Haynes, A. Quantifying Steric Effects of α -Diimine Ligands. Oxidation Addition of MeI to Rhodium(I) and Migratory Insertion of Rhodium(III) Complexes. *Organometallics* **2003**, *22*, 1047-1054.
- (74) Bikrani, M.; Mail, R. E.; Garralda, M. A.; Ibarlucea, L.; Pinilla, E.; Torres, M. R. *J. Organomet. Chem.* **2000**, *601*, 311-319.
- (75) Meyers, C.; Maes, B. U. W.; Loones, K. T. J.; Bal, G.; Lemiere, G. L. F.; Dommissie, R. A. Study of a New Rate Increasing "Base Effect" in the Palladium-Catalyzed Amination of Aryl Iodides. *J. Org. Chem.* **2004**, *69*, 6010-6017.
- (76) Gibson, V. C.; Tomov, A.; Wass, D. F.; White, A. J. P.; Williams, D. J. Ethylene polymerisation by a copper catalyst bearing α -diimine ligands. *J. Chem. Soc., Dalton Trans.* **2002**, 2261-2262.
- (77) Tian, J.; He, X.; Liu, J.; Deng, X.; Chen, D. Palladium (II) and copper (II) chloride complexes bearing bulky α -diimine ligands as catalysts for norbornene vinyl-addition (co)polymerization. *RSC Adv.* **2016**, *6*, 22908-22916.
- (78) Mikuriya, M.; Yamamoto, J.; Ishida, H.; Yoshioka, D.; Handa, M. Preparation and Crystal Structure of Tetrakis(μ -pivalato-O,O')bis[(pivalic acid-O)rhodium(II)]. *X-Ray Struct. Anal. Online* **2011**, *27*, 7-8.
- (79) Barnett, H. J.; Hill, A. F. A Dirhoda-Heterocyclic Carbene. *Angew. Chem. Int. Ed.* **2020**, *59*, 4274-4277.
- (80) Carriedo, G. A.; Howard, J. A. K.; Stone, F. G. A. Chemistry of Di- and Tri-Metal Complexes with Bridging Carbene or Carbyne Ligands. Part 24. Complexes of the Pentamethylcyclopentadienylcopper Group and the Crystal Structures of the Compounds [CupTW(μ -₃CC₆H₄Me-4)(Co)₂(PMe₃)₂(H-C₅H₅)(H-C₅Me₅)] and [CuRh₂(μ -Co)₂(H-C₅Me₅)₃]. *J. Chem. Soc., Dalton Trans.* **1984**, 1555-1561.
- (81) Bachechi, F.; Bianchini, C.; Meli, A. X-Ray Structural Analyses of Copper(I) and Silver(I) Adducts of the Rh(III) Trihydride [(Triphos)RhH₃], with Triphos=CH₃C(CH₂PPh₂)₃. *Inorg. Chim. Acta* **1993**, *213*, 269-277.
- (82) Grazia Arena, C.; Faraone, F.; Lanfranchi, M.; Rotondo, E.; Tiripicchio, A. Steric Effects of the 2-(Diphenylphosphino)-6-Methoxypyridine Short-Bite Bridging Ligand in the Synthesis of Binuclear Complexes. Crystal and Molecular Structure of [Rh₂Cu(CO)₂(Ph₂PPyOMe)₂(μ -Cl)₂]BF₄·CH₂Cl₂. *Inorganic Chemistry* **1992**, *31*, 4797-4802.
- (83) Bruno, G.; Lo Schiavo, S.; Rotondo, E.; Piraino, P.; Faraone, F. Synthesis of Triangular Mixed-Metal Clusters by the Addition of Copper Electrophiles to an Electron-Rich Rhodium-Rhodium Bond. X-Ray Crystal Structures of [Rh₂(η -C₅H₅)₂(μ -Co)(μ -Ph₂PCH₂PPh₂)(μ -CuI)] and [Rh₂(η -C₅H₅)₂(μ -Co)(μ -Ph₂PCH₂PPh₂)(μ -AgO₂CCH₃)]. *Organometallics* **1987**, *6*, 2502-2507.

-
- (84) Churchill, M. R.; Bezman, S. A.; Osborn, J. A.; Wormald, J. Synthesis and Molecular Geometry of Hexameric Triphenylphosphinocopper(I) Hydride and the Crystal Structure of $H_6Cu_6(PPh_3)_6 \cdot HCONMe_2$ [Hexameric Triphenylphosphino Copper(I) Hydride Dimethylformamide]. *Inorganic Chemistry* **1972**, *11*, 1818-1825.
- (85) Werner, H.; Poelsma, S.; Schneider, M. E.; Windmüller, B.; Barth, D. Synthesis and Reactivity of Bis(ethene) Rhodium(I) and Iridium(I) Carboxylato Complexes. *Chem. Ber.* **1996**, *129*, 647-652.
- (86) Herzberg, G. Electronic Spectra and Electronic Structure of Polyatomic Molecules; Van Nostrand: New York, 1966.
- (87) Das, D.; Mohapatra, S. S.; Roy, S. Recent Advances in Heterobimetallic Catalysis across a “Transition Metal–Tin” Motif. *Chem. Soc. Rev.* **2015**, *44*, 3666-3690.
- (88) Campos, J. Bimetallic Cooperation across the Periodic Table. *Nature Reviews Chemistry* **2020**.
- (89) Buchwalter, P.; Rosé J.; Braunstein, P. Multimetallic Catalysis Based on Heterometallic Complexes and Clusters. *Chem. Rev.* **2015**, *115*, 28-126.
- (90) Mata, J. A.; Hahn, F. E.; Peris, E. Heterometallic Complexes, Tandem Catalysis and Catalytic Cooperativity. *Chemical Science* **2014**, *5*, 1723-1732.
- (91) Walker, W. E.; Brown, E. S.; Pruett, R. L. U.S. Patent 4,320,064, 1975, Union Carbide Co.
- (92) Webster-Gardiner, M. S.; Pizsel, P. E.; Fu, R.; McKeown, B. A.; Nielsen, R. J.; Goddard, W. A., III; Gunnoe, T. B. Electrophilic Rh^I catalysts for arene H/D exchange in acidic media: Evidence for an electrophilic aromatic substitution mechanism. *J. Mol. Catal. A: Chem.* **2017**, *426*, 381-388.
- (93) Zhong, A. H.; Labinger, J. A.; Bercaw, J. E. C–H Bond Activation by Cationic Platinum(II) Complexes: Ligand Electronic and Steric Effects. *J. Am. Chem. Soc.* **2002**, *124*, 1378-1399.
- (94) Bochevarov, A. D.; Harder, E.; Hughes, T. F.; Greenwood, J. R.; Braden, D. A.; Philipp, D. M.; Rinaldo, D.; Halls, M. D.; Zhang, J.; Friesner, R. A. Jaguar: A High-Performance Quantum Chemistry Software Program with Strengths in Life and Materials Sciences. *Int. J. Quantum Chem* **2013**, *113*, 2110-2142.
- (95) Becke, A. D. Density - Functional Thermochemistry. Iii. The Role of Exact Exchange. *The Journal of Chemical Physics* **1993**, *98*, 5648-5652.
- (96) Grimme, S.; Antony, J.; Ehrlich, S.; Krieg, H. A Consistent and Accurate Ab Initio Parametrization of Density Functional Dispersion Correction (Dft-D) for the 94 Elements H-Pu. *The Journal of Chemical Physics* **2010**, *132*, 154104.
- (97) Hehre, W. J.; Ditchfield, R.; Pople, J. A. Self—Consistent Molecular Orbital Methods. Xii. Further Extensions of Gaussian—Type Basis Sets for Use in Molecular Orbital Studies of Organic Molecules. *The Journal of Chemical Physics* **1972**, *56*, 2257-2261.
- (98) Kahn, L. R.; Goddard, W. A. Ab Initio Effective Potentials for Use in Molecular Calculations. *The Journal of Chemical Physics* **1972**, *56*, 2685-2701.
- (99) Roy, L. E.; Hay, P. J.; Martin, R. L. Revised Basis Sets for the Lanl Effective Core Potentials. *J Chem Theory Comput* **2008**, *4*, 1029-1031.

-
- (100) Friedrichs, M.; Zhou, R.; Edinger, S. R.; Friesner, R. A. Poisson–Boltzmann Analytical Gradients for Molecular Modeling Calculations. *The Journal of Physical Chemistry B* **1999**, *103*, 3057-3061.
- (101) Tannor, D. J.; Marten, B.; Murphy, R.; Friesner, R. A.; Sitkoff, D.; Nicholls, A.; Honig, B.; Ringnalda, M.; Goddard, W. A. Accurate First Principles Calculation of Molecular Charge Distributions and Solvation Energies from Ab Initio Quantum Mechanics and Continuum Dielectric Theory. *J. Am. Chem. Soc.* **1994**, *116*, 11875-11882.
- (102) Lam, Y. M.; Boudart, M. Preparation of Small Au–Pd Particles on Silica. *J. Catal.* **1977**, *50*, 530–540.
- (103) Kaylor, N.; Xie, J.; Kim, Y.-S.; Pham, H. N.; Datye, A. K.; Lee, Y.-K.; Davis, R. J. Vapor Phase Deoxygenation of Heptanoic Acid over Silica-Supported Palladium and Palladium-Tin Catalysts. *J. Catal.* **2016**, *344*, 202-212.

3 Rhodium-Catalyzed Arene Alkenylation Using Only Dioxygen as Oxidant

This chapter is adapted from “Rhodium-Catalyzed Arene Alkenylation Using Only Dioxygen as Oxidant.” Zhu, W.; Gunnoe, T. B. *ACS Catal.* **2020**, *10*, 11519–11531”.

Copyright 2020 American Chemical Society

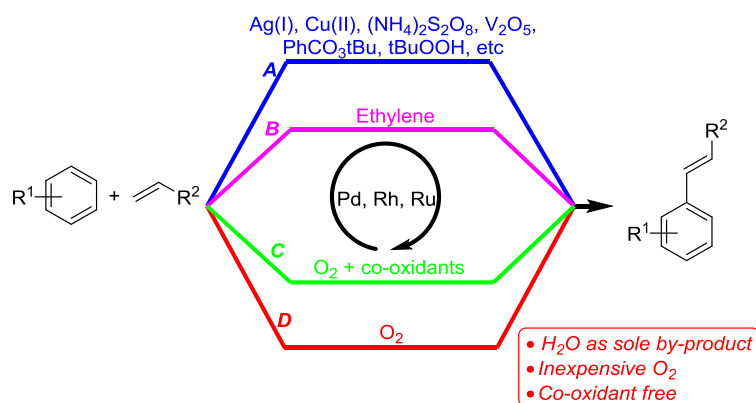
3.1 Introduction

Alkyl and alkenyl arenes are produced on a large scale for use in the manufacture of commodity and fine chemicals.¹⁻⁴ For example, in 2018 the global consumption of ethylbenzene was ~40 million tons with styrene production from ethylbenzene on a scale of ~38 million tons.⁵⁻⁸ Commercial synthesis of alkyl arenes, which are often precursors to alkenyl arenes, usually involves either acid-catalyzed Friedel-Crafts or zeolite-mediated arene alkylation.¹⁻⁷ Both of these processes involve acidic catalysis, which can result in the generation of polyalkylated arene products.⁹ As a result energy-intensive distillation and a transalkylation process are often required to increase the yield of monoalkylated products.⁵⁻⁷ Additionally, when using α -olefins acid catalysts do not produce 1-aryl alkanes (i.e., anti-Markovnikov products) since the formation of carbocationic intermediates from the olefin leads to the exclusive formation of *n*-aryl alkanes ($n > 1$; i.e., Markovnikov products). Palladium-catalyzed aryl-carbon coupling reactions can produce alkyl or alkenyl arenes using aryl halides or pseudo halides, but they require arene halogenation and often a stoichiometric amount of metal-containing reagent.¹⁰⁻¹⁵

Olefin hydroarylation with unfunctionalized hydrocarbons catalyzed by molecular Ni,^{16, 17} Ir,¹⁸⁻²³ Ru²⁴⁻³¹ or Pt³²⁻⁴⁰ complexes has been demonstrated for arene alkylation using olefins. In contrast to acid-catalyzed arene alkylation, these transition metal-catalyzed olefin hydroarylation reactions generate both 1-aryl and *n*-aryl alkanes ($n > 1$) when using α -olefins such as propene and 1-hexene. However, these catalysts have drawbacks including low selectivity for anti-Markovnikov products (and, in some cases, selectivity for Markovnikov products), limited catalyst longevity, and an inability to selectively produce alkenyl arenes. The recent Ni catalyst reported by Hartwig and coworkers gives exceptionally high selectivity for anti-Markovnikov alkyl arenes (>50:1 in most cases) when using α -olefins.¹⁶

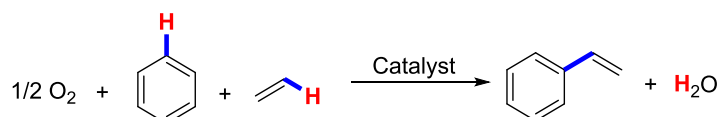
Late transition metal catalysts have been developed to convert unactivated arenes and olefins to alkenyl arenes using hydrocarbons in the presence of oxidant (Scheme 3.1.1A). Examples of Pd- and Rh-catalyzed arene alkenylation under anaerobic conditions that require stoichiometric consumption of oxidants such as $(\text{NH}_4)_2\text{S}_2\text{O}_8$,⁴¹ AgOAc,⁴² V_2O_5 ,⁴³ PhCO_3tBu ,⁴⁴ tBuOOH ⁴⁵ or copper(II) carboxylates⁴⁶⁻⁵⁰ have been reported. In addition, we previously reported a cationic Ru(II) complex $[(\text{MeOTTM})\text{Ru}(\text{P}(\text{OCH}_2)_3\text{CEt})(\text{NCMe})\text{Ph}][\text{BAR}'_4]$ (MeOTTM = 4,4',4''-(methoxymethanetriyl)-tris(1-benzyl-1H-1,2,3-triazole); BAR'_4 = tetrakis[3,5-bis(trifluoromethyl)phenyl]borate) catalyzes the conversion of ethylene and benzene with 53 turnovers (TOs) of styrene with ethylene serving as oxidant to form ethane (Scheme 3.1.1B).⁵¹ Hong and coworkers reported that $\text{Rh}_4(\text{CO})_{12}$ catalyzes the conversion of benzene and ethylene in the presence of carbon monoxide

to give 472 TOs of styrene and 809 TOs of 3-pentanone.⁵² Recently, we demonstrated the Rh-catalyzed production of alkenyl arenes from benzene and olefins using $[\text{Rh}(\mu\text{-OAc})(\eta^2\text{-C}_2\text{H}_4)_2]_2$ as catalyst precursor with high TOs (> 800 TOs of styrene and > 1470 TOs of propenylbenzene) and near-quantitative yield (> 95%) relative to the Cu(II) oxidant.⁵³⁻⁵⁵



Scheme 3.1.1. Arene alkenylation consuming stoichiometric oxidants (A), ethylene (B), dioxygen in the presence (C) or absence (D) of co-oxidants.

While the above listed reactions are important advancements, the use of dioxygen as the *in situ* and sole oxidant offers potential advantages since dioxygen is inexpensive (especially when the source is unpurified air) and the only waste is water (Scheme 3.1.2). However, direct use of dioxygen presents challenges, including: 1) the radical nature of dioxygen can lead to undesirable odd-electron reactions; 2) dioxygen can react with low-valent metals to generate metal oxo or peroxy products that are incapable of catalysis; and 3) mechanisms for the reaction of dioxygen to sequester reducing equivalents, such as hydrogen in this case, are not well understood.



Scheme 3.1.2. Arene alkenylation using O₂ as the oxidant to produce alkenyl arene and water (depicted with benzene and ethylene).

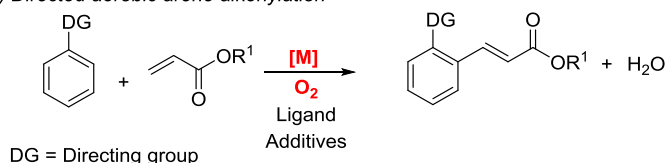
The Matsumoto, Periana and Fujiwara groups studied Pd- and Rh-catalyzed aerobic benzene ethenylation to form styrene in which the Cu(II) or Ag(I) is present as a co-oxidant and is regenerated *in situ* using air or dioxygen (Scheme 3.1.1C).⁵⁶⁻⁵⁸ The overall process is akin to the commercialized Wacker-Hoechst process for ethylene oxidation in which the CuCl₂ oxidant is regenerated either *in situ* by dioxygen or *ex situ* in a separate reactor by air.^{4, 59} Subsequently, examples of aerobic benzene alkenylation using benzoquinone⁶⁰ or polyoxometalates⁶¹⁻⁶³ as the co-oxidant were reported. We reported conditions for the formation of styrene from benzene and ethylene catalyzed by Pd(OAc)₂ using copper(II) pivalate (Cu(OPiv)₂) in the presence of purified dioxygen to yield ~2400 TOs of styrene with > 85% selectivity.⁶⁴ The keys to increase selectivity for styrene are applying low ethylene pressure (20 psig) to reduce the production of undesired vinyl pivalate and high reaction temperature (180 °C) to facilitate the conversion of vinyl pivalate and benzene to styrene.⁶⁴ We recently developed a Rh-catalyzed aerobic alkenylation reaction for synthesis of stilbene derivatives from simple arenes and styrenes in good to high yield with good functional group tolerance.⁶⁵ The reaction proceeds with air as a terminal oxidant in the presence of air-recyclable copper(II) pivalate co-oxidant. Unfortunately, the limited stability of the Cu(II) carboxylate co-oxidant gives rise to the formation of side products (*e.g.*, phenyl carboxylate) that result from its thermal degradation.

Pd- and Ru-catalyzed arene alkenylation using electron-deficient acrylates as the alkene source with dioxygen as the direct oxidant were reported (Scheme 3.1.1D,

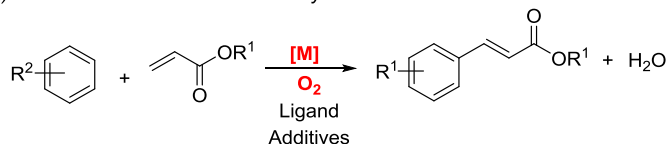
Scheme 3.1.3A and B).⁶⁶⁻⁶⁹ Only a few examples exist for aerobic styrene production from benzene and ethylene in the absence of a co-oxidant (Scheme 3.1.3C and Scheme 3.1.4). Shue demonstrated that Pd(OAc)₂ can catalyze benzene ethylation under oxygen to yield 6 TOs of styrene at 80 °C.⁷⁰ Matsumoto, Periana and coworkers reported Pd and Rh catalysts with the addition of acetylacetonone afford 47 and 23 TOs of styrene, respectively.^{56, 57} Milstein and coworkers reported a Ru(II) catalyst that yields 19 TOs of styrene under dioxygen and carbon monoxide.⁷¹ Despite the significant advancement of these catalytic processes, they give low TOs and require high pressure of pure dioxygen and/or the use of carbon monoxide.

Previous work:

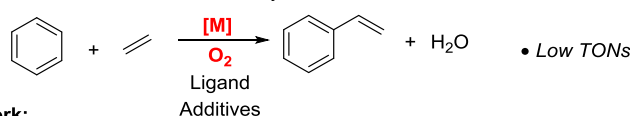
A) Directed aerobic arene alkenylation



B) Non-directed aerobic arene alkenylation with electron-deficient olefins

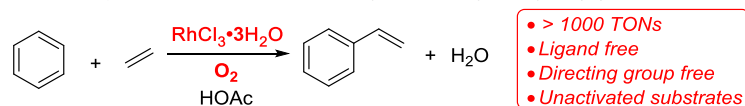


C) Non-directed aerobic arene alkenylation with unactivated olefins

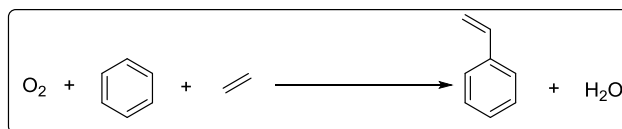


This work:

D) Non-directed ligand-free aerobic arene alkenylation catalyzed by Rh(III)



Scheme 3.1.3. Metal-catalyzed arene alkenylation using only air or dioxygen as oxidant in the absence of co-oxidants.



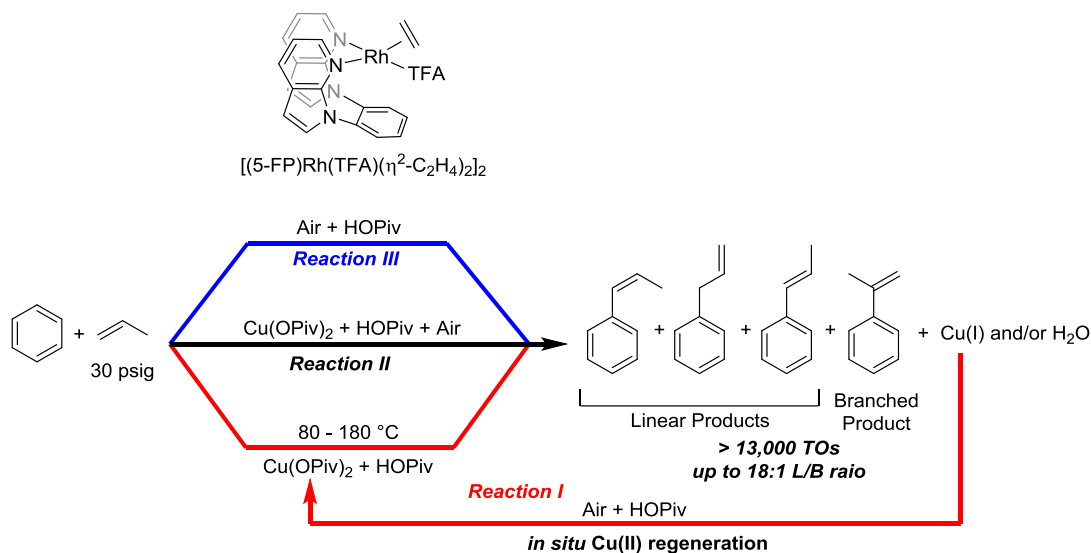
Catalyst Precursor	Rh(acac)(CO) ₂	Pd(OAc) ₂	RuCl ₃ ·3H ₂ O	Pd(OAc) ₂
Additives	acacH and HOAc	acacH and HOAc	CO gas	
Temperature	180 °C	180 °C	180 °C	80 °C
TOs	23	47	19	6

acac = acetylacetonato
 Hacac = acetylacetone

Scheme 3.1.4. Examples of catalyst for aerobic benzene ethylation using dioxygen as the direct oxidant.

Our group initially found that the conversion of benzene and ethylene to styrene catalyzed by $[\text{Rh}(\mu\text{-OAc})(\eta^2\text{-C}_2\text{H}_4)]_2$ was sluggish in the presence of dioxygen or air. We speculated that aerobic deactivation of the Rh catalyst might result from the conversion of square planar Rh(I) complexes to six-coordinate octahedral Rh(III) peroxide complexes. We hypothesized that blocking one of the coordination sites of the Rh center would destabilize octahedral Rh(III) peroxide intermediates and thus permit catalysis under aerobic conditions. we recently demonstrated that $(5\text{-FP})\text{Rh}(\text{TFA})(\eta^2\text{-C}_2\text{H}_4)$ (TFA = trifluoroacetate, 5-FP = 1,2-bis(*N*-7-azaindolyl)benzene) enhances catalyst longevity compared to simple $[\text{Rh}(\mu\text{-OAc})(\eta^2\text{-C}_2\text{H}_4)]_2$ salt catalyst precursors, and allows *in situ* recycling of the Cu(II) oxidant using air to achieve ~800 TOs (Reaction I, Scheme 3.1.5).⁷² We also demonstrated that $(5\text{-FP})\text{Rh}(\text{TFA})(\eta^2\text{-C}_2\text{H}_4)$ can catalyze aerobic benzene alkenylation in the presence of $\text{Cu}(\text{OPiv})_2$ with air as the *in situ* terminal oxidant to produce > 13,000 TOs of propenylbenzene products with no evidence of catalyst deactivation (Reaction II, Scheme 3.1.5).⁷² In addition, catalysis using dioxygen as the sole oxidant

in the absence of Cu(II) (Reaction III, Scheme 3.1.5) afforded > 500 TOs after 240 h.⁷² At 80 °C, an 18:1 L:B ratio (L = anti-Markovnikov products, B = Markovnikov product, see Scheme 3.1.5) of alkenyl arenes has been observed.⁷²



Scheme 3.1.5. (5-FP)Rh(TFA)(η^2 -C₂H₄) catalyzed benzene propenylation using Cu(OPiv)₂/air as oxidants under aerobic/anaerobic conditions.

We expanded our studies of aerobic Rh-catalyzed arene alkenylation by including the use of RhCl₃ as catalyst precursor and unpurified air (and purified dioxygen) as the only oxidant (Scheme 3.1.3D). The newly-discovered aerobic method does not require additional additives or ligands, and > 1000 TOs of alkenyl benzene products are achieved under optimized conditions. Limitations of the aerobic process compared to the use of Cu(II) as a co-oxidant are also discussed.

3.2 Results and Discussion

We initially investigated RhCl₃ as a catalyst precursor for the aerobic oxidation

of benzene ethenylation (Table 3.2.1). For all catalytic reactions shown in Table 3.2.1, the TOs are the average of a minimum of three experiments. Heating a 10 mL benzene solution of RhCl_3 (0.112 mM) under 70 psig of ethylene with 1 atm of air at 150 °C reveals no styrene production after 60 hours (Table 3.2.1, entry 1). Under these conditions, the formation of black precipitate, presumed to be elemental Rh,⁷³ is observed. However, the addition of 2000 eq. of HOAc (relative to the Rh) under otherwise identical conditions produces 70(8) TOs of styrene at a constant rate for 60 hours (Figure 3.2.1 and Table 3.2.1, entry 2) coupled with formation of trace amounts of phenyl acetate, vinyl acetate, benzaldehyde and stilbene (< 1 TO for each product) as well as 5(1) TOs of biphenyl (see Table 3.2.2). We previously reported that in the absence of Cu(II) oxidant, $[\text{Rh}(\mu\text{-OAc})(\eta^2\text{-C}_2\text{H}_4)_2]_2$ catalyst precursor decomposes to Rh(0) in benzene at 90 °C under ethylene pressure.⁷³ Although the details are unknown, we speculate that HOAc suppresses reductive decomposition of the Rh catalyst to form Rh(s) by serving as a reactive oxidant. Replacing HOAc with the same amount of other carboxylic acids afforded less satisfactory results (Figure 3.2.1 and Table 3.2.1, entries 3-5). Substituting the carboxylic acid with 2000 eq. of carboxylate salts is partially effective, providing less than 12 TOs of styrene product after 96 hours (Table 3.2.1, entries 6-9), whereas the use of NaCl or KCl under the identical conditions revealed no styrene production after 96 hours (Table 3.2.1, entries 10 and 11). These results suggest that a carboxylate group is required for successful reaction, which we attribute to Rh-mediated benzene C–H activation via a concerted metalation–deprotonation (CMD) mechanism that is facilitated by the presence of Rh-

–OCOR groups.⁷⁴⁻⁷⁸ Increasing the loading of acid by using benzene/acetic acid in a 1:1 (v/v) mixture increases catalytic rate (Figure 3.2.2) with 165(17) TOs of styrene production after 60 hours (Table 3.2.1, entry 12). For example, the apparent turnover frequency (TOF) after 12 hours for the catalysis with 2000 eq. of HOAc is $2.5 \times 10^{-3} \text{ s}^{-1}$ while the apparent TOF at the same time point for the catalysis using a 1:1 (v/v) mixture of benzene/acetic acid is $9.7 \times 10^{-3} \text{ s}^{-1}$. Small quantities of the by-products phenyl acetate (11(2) TOs), benzaldehyde (22(2) TOs), stilbene (4(2) TOs) and biphenyl (7(1) TOs) were also detected (Table 3.2.2). Changing the benzene/HOAc ratio (v/v) from 1:1 to 1:3 and 3:1 did not influence the catalytic performance (Figure 3.2.2 and Table 3.2.1, entries 13 and 14). Using the Rh(I) complex $[\text{Rh}(\mu\text{-OAc})(\eta^2\text{-C}_2\text{H}_4)_2]_2$ (0.112 mM Rh) as the catalyst precursor revealed statistically identical TOs versus time plots compared to RhCl_3 catalysis under the same conditions (Table 3.2.1, entry 15, see Supporting Information Figure 3.2.3). This suggests that the two Rh catalyst precursors, $[\text{Rh}(\mu\text{-OAc})(\eta^2\text{-C}_2\text{H}_4)_2]_2$ and RhCl_3 , are possibly converted into the same catalytically active Rh species under catalytic conditions. Control reactions in the absence of rhodium reveal no reaction (Table 3.2.1, entry 16).

Table 3.2.1. Optimization of the rhodium catalyzed aerobic benzene alkenylation using air as oxidant.^a

c1ccccc1 + C=C $\xrightarrow[70 \text{ psig}]{0.112 \text{ mM RhCl}_3 \cdot 3\text{H}_2\text{O}}$ C=Cc1ccccc1
 1 atm air, acid or salt, 150 °C, 60 h

Entry	Volume of benzene (mL)	Additives	TOs ^b

1	10	-	0
2	10	2000 eq. HOAc	70(8)
3	10	2000 eq. HOPiv	40(6)
4	10	2000 eq. acetic anhydride	46(5)
5	10	2000 eq. HTFA	0
6	10	2000 eq. NaOAc	10(4) ^c
7	10	2000 eq. KOAc	8(3) ^c
8	10	2000 eq. Na ₂ CO ₃	11(3) ^c
9	10	2000 eq. Na ₂ SO ₄	3(1) ^c
10	10	2000 eq. NaCl	0 ^c
11	10	2000 eq. KCl	0 ^c
12	5	5 mL HOAc	165(17)
13	2	8 mL HOAc	186(21)
14	8	2 mL HOAc	159(29)
15	5	5 mL HOAc	153(22) ^d
16	5	5 mL HOAc	0 ^e
17	5	5 mL HOAc + 2000 eq. NaOAc	84(19)
18	5	5 mL HOAc + 2000 eq. KOAc	96(25)
19	5	5 mL HOAc + 50 eq. acetylacetone	134(8)
20	5	5 mL HOAc + 0.05 mL H ₂ O	170(18)
21	5	5 mL HOAc + 1 mL H ₂ O	151(35)

^a Unless otherwise noted, reaction conditions are 0.112 mM RhCl₃, 1 atm air, 70 psig C₂H₄, 60 h, 150 °C. The reactions were sampled every 12 h until 60 h. Each data point represents the average of three separate experiments. Values in parentheses represent the standard deviations based on a minimum of three independent experiments. ^b TOs are obtained by GC-FID. ^c TO is obtained at 96 h. ^d [Rh(μ-OAc)(η²-C₂H₄)₂]₂ (0.112 mM Rh) used. ^e Without Rh source.

Table 3.2.2. Product distributions for aerobic benzene alkenylation with ethylene under typical reaction conditions (1).

Product	TOs
Styrene	70(8)
Phenyl acetate	<1
Benzaldehyde	<1
Stilbene	<1
Biphenyl	5(1)

Product	TOs
Styrene	165(17)
Phenyl acetate	11(2)
Benzaldehyde	22(2)
Stilbene	4(2)
Biphenyl	7(1)

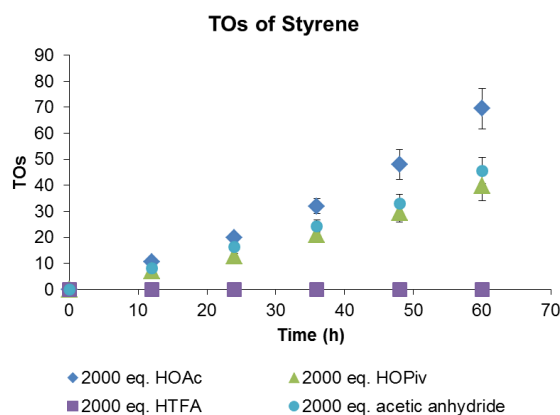


Figure 3.2.1. Comparison of TOs vs time for aerobic benzene alkenylation with ethylene in presence of acids. Reaction conditions: 10 mL of benzene, 0.112 mM RhCl₃, 70 psig ethylene, 1 atm air, 150 °C. Equivalents of acid or acetic anhydride are relative to RhCl₃. Each data point represents the average of three separate experiments. Error bars represent the standard deviations based on a minimum of three independent experiments.

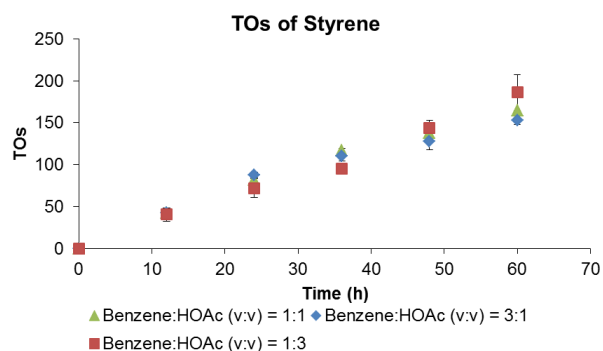


Figure 3.2.2. Comparison of TOs vs time for aerobic benzene alkenylation using different volume ratios of benzene and acetic acid. Reaction conditions: 10 mL of a benzene/acetic acid solution, 0.112 mM RhCl_3 , 70 psig ethylene, 1 atm air, 150 °C. Each data point represents the average of three separate experiments. Error bars represent the standard deviations based on a minimum of three independent experiments.

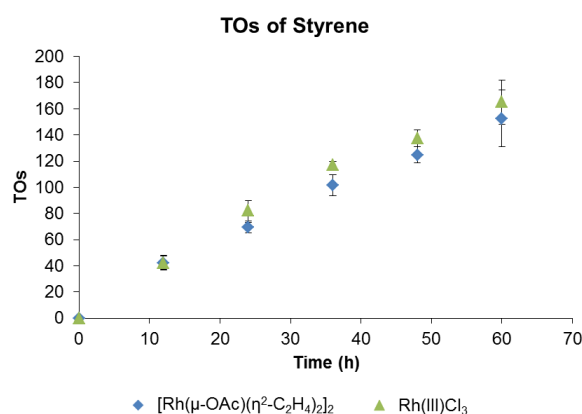


Figure 3.2.3. Comparison of TOs vs time for aerobic benzene alkenylation with ethylene catalyzed by $[\text{Rh}(\mu\text{-OAc})(\eta^2\text{-C}_2\text{H}_4)_2]_2$ and RhCl_3 . Reaction conditions: 5 mL benzene, 5 mL HOAc, 0.112 mM Rh, 70 psig ethylene, 1 atm air, 150 °C. Each data point represents the average of three separate experiments. Error bars represent the standard deviations based on a minimum of three independent experiments.

Using 0.112 mM RhCl_3 , 1:1 benzene/HOAc (v/v) solution, 70 psig C_2H_4 and 1 atm of air at 150 °C as a standard set of conditions, the inclusion of additives such as acetylacetone or carboxylate salts does not result in an increased catalytic rate or yield (Figure 3.2.4 and Table 3.2.1, entries 17-19). Notably, adding 0.05 or 1.00 mL of distilled water has negligible impact on the rate of styrene production (Figure 3.2.5 and Table 3.2.1, entries 20 and 21). These results suggest that the catalytic reaction is

not significantly influenced by the formation of water as a by-product.

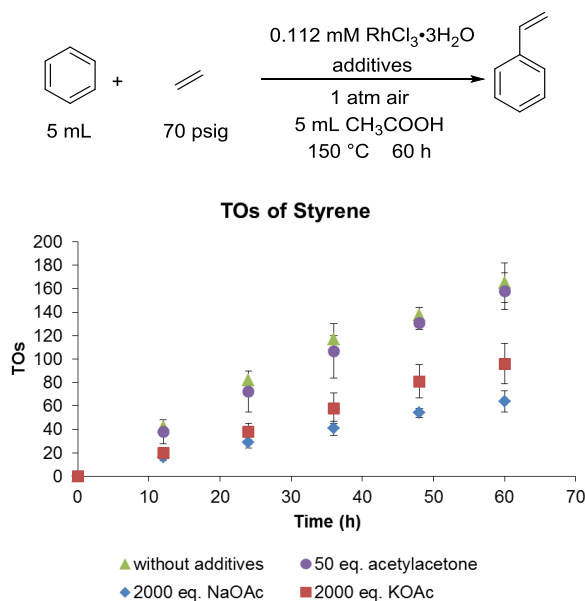


Figure 3.2.4. Comparison of TOs vs time for aerobic benzene alkenylation with ethylene in the absence or presence of additives. Reaction conditions: 5 mL C₆H₆, 5 mL HOAc, 0.112 mM RhCl₃, 70 psig ethylene, 1 atm air, 150 °C. Each data point represents the average of three separate experiments. Equivalents of additives are relative to RhCl₃. Error bars represent the standard deviations based on a minimum of three independent experiments.

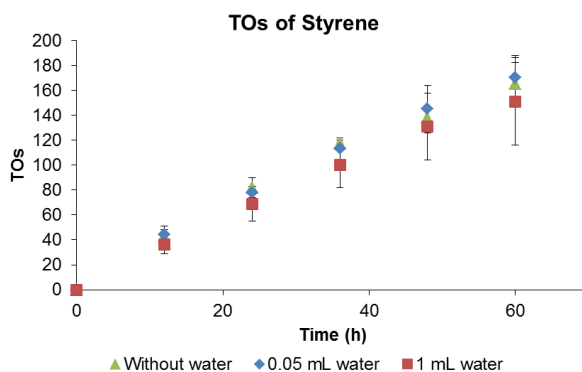


Figure 3.2.5. Comparison of TOs vs time for aerobic benzene alkenylation with ethylene in the absence or presence of water. Reaction conditions: 5 mL benzene, 5 mL HOAc, 0.112 mM RhCl₃, 70 psig ethylene, 1 atm air, 150 °C. Each data point represents the average of three separate experiments. Error bars represent the standard deviations based on a minimum of three independent experiments.

The effect of temperature on catalysis was investigated under the standard set of conditions (Figure 3.2.6). Generally, catalyst activity is increased by raising the

temperature from 120 to 170 °C. However, further increasing the temperature to 180 °C (ethylene pressure was decreased to 50 psig due to the pressure limit of the Fisher-Porter reactor) led to reduced catalyst efficacy (39(9) TOs at 180 °C versus 226(31) TOs at 150 °C after 36 h). This likely results from low solubility of ethylene in benzene at high temperature. Thus, the optimal temperature appears to be 170 °C.

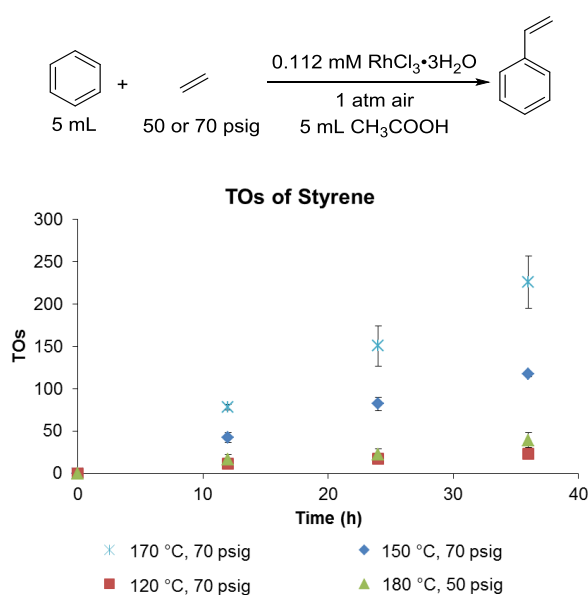


Figure 3.2.6. Effect of reaction temperature on aerobic benzene alkenylation reaction. Reaction conditions: 5 mL C₆H₆, 5 mL HOAc, 0.112 mM RhCl₃, 1 atm air. Each data point represents the average of three separate experiments. Error bars represent the standard deviations based on a minimum of three independent experiments.

Under the standard set of conditions, we probed aerobic benzene alkenylation with propylene at 150 and 170 °C (Figure 3.2.7). The catalyst is more active at 170 °C than at 150 °C, showing a similar trend to that observed in aerobic catalysis with ethylene. The catalyst is selective for anti-Markovnikov (herein, called linear) 1-phenylpropylene products over Markovnikov (branched) 2-phenylpropylene products, indicating a non-acid catalyzed process. The linear/branched product (L/B) ratio increases with reaction time, and the rate of increase is more rapid at 170 °C than

at 150 °C. We speculated that the increase of L/B ratio results from different rates of reaction of the four phenylpropylene products instead of the change of intrinsic catalyst L/B selectivity. To test this hypothesis, we added the four phenylpropylene products (the concentrations are approximately those of phenylpropylene products after 24 h of catalysis at 170 °C) at the beginning of a catalytic reaction using benzene and ethylene to produce styrene. As catalytic styrene production proceeds, the L/B ratio increased from an initial 5.5:1 to 8.3(3):1 after 12 hours and was determined to be 35(3):1 after 36 hours (Figure 3.2.8). This trend is similar to the observations in aerobic benzene alkenylation with propylene. Next, we speculated that the aerobic benzene alkenylation possibly produces H₂O₂ as a by-product.⁷⁹⁻⁸¹ Thus, we studied the influence of H₂O₂ on the rate of phenylpropylene consumption. The L/B ratio increases more rapidly in the presence of added H₂O₂ with the L/B ratio increasing from an initial 5.5:1 to 45(4):1 and then 144(27):1 after 36 hours when 100 and 500 equivalents of H₂O₂ (relative to Rh) was added at the start of the reaction (Figure 3.2.8). The isomerization of branched α -methylstyrene to linear products catalyzed by Rh could increase the observed L/B ratio. To study this possible isomerization, we added 50 equivalents of α -methylstyrene (relative to Rh) at the beginning of a catalytic reaction using benzene and ethylene to produce styrene. After 36 h of reaction, linear phenylpropylene products were not observed (Scheme 3.2.1), indicating the isomerization of branched α -methylstyrene to linear phenylpropylene products does not occur under the catalytic conditions.

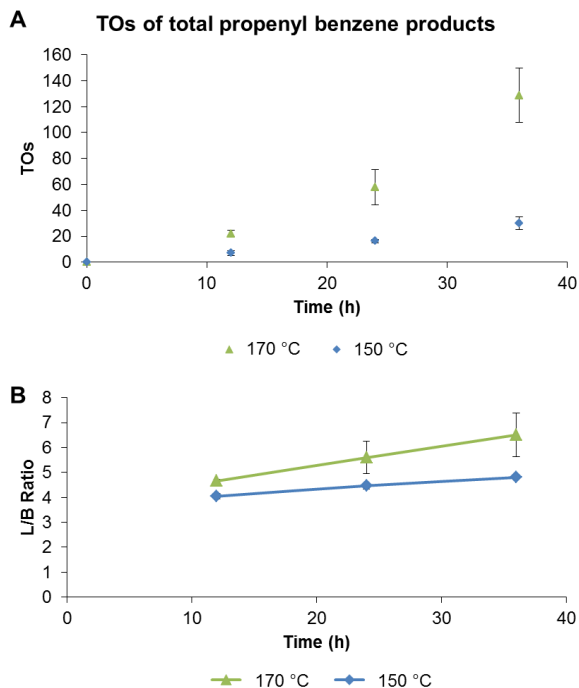
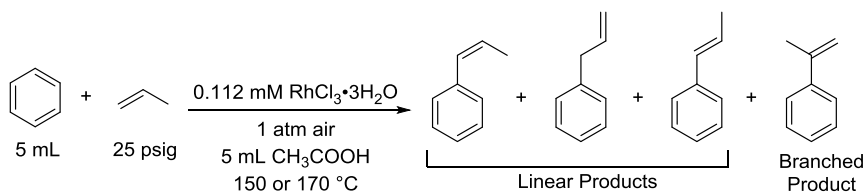


Figure 3.2.7. Plots of TOs of total products versus time (**A**) and L/B ratio versus time (**B**) for aerobic benzene alkenylation with propylene at 150 and 170 °C. Reaction conditions: 5 mL C₆H₆, 5 mL HOAc, 0.112 mM RhCl₃, 25 psig propylene, 1 atm air, 170 °C. Each data point represents the average of three separate experiments. Error bars represent the standard deviations based on a minimum of three independent experiments.

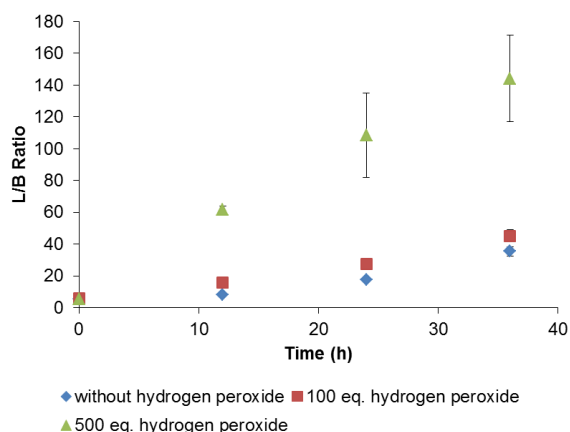
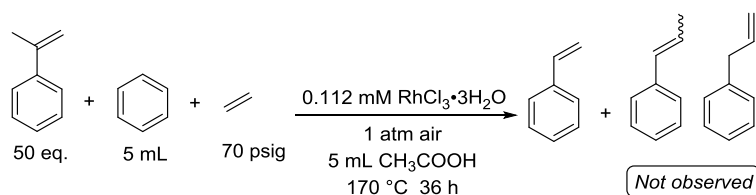


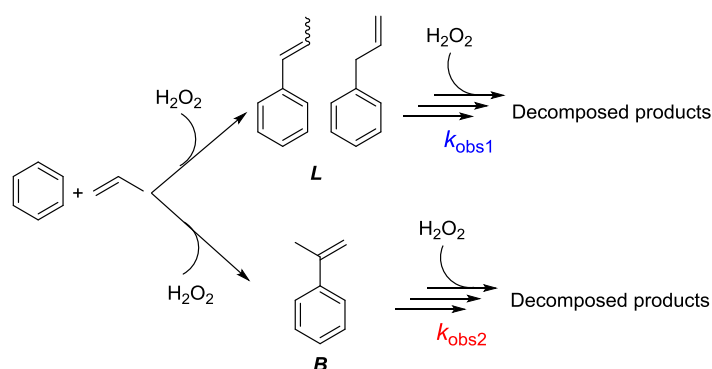
Figure 3.2.8. Plots of L/B ratio of 4 phenylpropylene products versus time under catalytic conditions. Reaction conditions: 5 mL C₆H₆, 5 mL HOAc, 0.112 mM RhCl₃, 70 psig ethylene, 1 atm air, 23 eq. of allylbenzene, 9 eq. of α -methylstyrene, 3 eq. of cis- β -methylstyrene, 23 eq. of trans- β -methylstyrene, 170 °C. Each data point

represents the average of three separate experiments. Error bars represent the standard deviations based on a minimum of three independent experiments.



Scheme 3.2.1. Aerobic benzene alkenylation with ethylene in presence of α -methylstyrene

We speculate that the observed increase in L/B ratio is controlled by the different rates of reaction of the four phenylpropylene products with H_2O_2 (k_{obs1} and k_{obs2} in Scheme 3.2.2). If k_{obs1} is smaller than k_{obs2} , α -methylstyrene will be consumed more rapidly than the linear products once H_2O_2 is formed. In that case, the unreacted phenylpropylene products give rise to higher observed L/B ratio than the intrinsic catalyst L/B selectivity, and the observed L/B ratio will increase over time.



$$\text{Decay rate of } L = \frac{d[L]}{dt} \quad \text{Decay rate of } B = \frac{d[B]}{dt}$$

$$\frac{d[L]}{dt} = k_{\text{obs1}}[L][\text{H}_2\text{O}_2] \quad \frac{d[B]}{dt} = k_{\text{obs2}}[B][\text{H}_2\text{O}_2] \quad \frac{d[L]}{dt} / \frac{d[B]}{dt} = \frac{k_{\text{obs1}}[L][\text{H}_2\text{O}_2]}{k_{\text{obs2}}[B][\text{H}_2\text{O}_2]} = \frac{k_{\text{obs1}}[L]}{k_{\text{obs2}}[B]}$$

Scheme 3.2.2. Explanation for the increase of observed L/B ratio during the aerobic benzene alkenylation with propylene based on product reaction with hydrogen peroxide.

When the catalyst loading is reduced to 0.022 mM of RhCl_3 , 277(25) TOs of styrene can be reached accompanied by 93(12) TOs of benzaldehyde after 72 h under the standard set of conditions (Figure 3.2.9 and Figure 3.2.10). Continued reaction for

an additional 24 h does not increase the TOs of styrene (268(37) TOs), but higher TOs of benzaldehyde (169(20) TOs) are observed. Increasing the benzene/HOAc ratio (v/v) from 1:1 to 4:1 and 9:1 increases the production of styrene. Performing catalysis with a 9:1 benzene/HOAc ratio (v/v) yields 1031(74) TOs of styrene and 353(37) TOs of benzaldehyde after 192 h (Figure 3.2.9 and Figure 3.2.10). The formation of 341(45) TOs of biphenyl, 72(12) TOs of PhOAc, and 119(28) TOs of stilbene were also observed (Table 3.2.3). Benzaldehyde likely forms from non-metal-catalyzed oxidative cleavage of styrene by dioxygen.⁸² We believe that as the reaction progresses, under some conditions the benzene alkenylation becomes slow likely due to catalyst deactivation whereas benzaldehyde production from styrene becomes competitive as the amount of styrene increases.

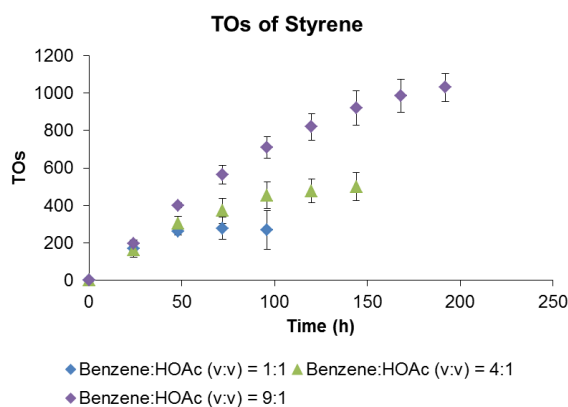


Figure 3.2.9. Comparison of TOs of styrene vs time for aerobic benzene alkenylation with ethylene using different volume ratios of benzene and acetic acid. Reaction conditions: 10 mL of a benzene/acetic acid solution, 0.022 mM RhCl₃, 70 psig ethylene, 1 atm air, 170 °C. Each data point represents the average of three separate experiments. Error bars represent the standard deviations based on a minimum of three independent experiments.

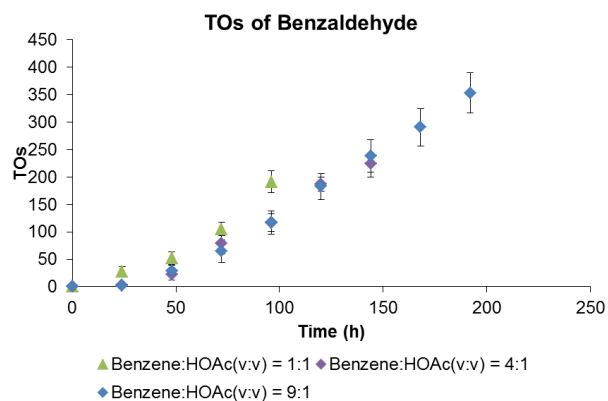
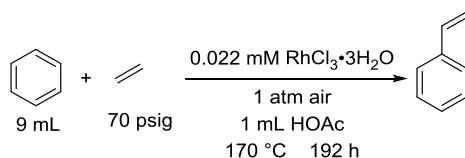


Figure 3.2.10. Comparison of TOs of benzaldehyde vs time for aerobic benzene alkenylation with ethylene using different volume ratios of benzene and acetic acid. Reaction conditions: 10 mL of a benzene/acetic acid solution, 5 mL HOAc, 0.112 mM RhCl₃, 70 psig ethylene, 1 atm air, 170 °C. Each data point represents the average of three separate experiments. Error bars represent the standard deviations based on a minimum of three independent experiments. To avoid the decay of internal standard hexamethylbenzene under aerobic conditions as the catalysis proceeds for long, hexamethylbenzene was not added at the beginning of the catalysis. Instead, external hexamethylbenzene was added while sampling

Table 3.2.3. Product distributions for aerobic benzene alkenylation with ethylene under typical reaction conditions (2).



Product	TOs
Styrene	1031(74)
Phenyl acetate	72(12)
Benzaldehyde	353(37)
Stilbene	119(28)
Biphenyl	341(45)

We performed a series of kinetic studies on three reaction components (ethylene, Rh catalyst and dioxygen; Figure 3.2.11). Under the standard set of conditions at 170 °C, a first-order dependence on ethylene concentration was revealed under ethylene pressure ranging from 25 psig to 50 psig (Figure 3.2.11A), and saturation kinetics were observed when the catalysis was run at ethylene pressure > 50 psig (Figure 3.2.12). This is in contrast to the previously reported *inverse* first-order

dependence on ethylene concentration for Ir(III),¹⁹ Pt(II)³⁶ or Ru(II)²⁵ catalyzed ethylene hydroarylation. For the Ir(III), Pt(II) and Ru(II) catalysts, the inverse dependence on ethylene concentration resulted from the formation of off-cycle $M(\text{CH}_2\text{CH}_2\text{Ph})(\eta^2\text{-C}_2\text{H}_4)$ ($M = \text{cis}(\text{acac-O,O})_2\text{Ir}$, $\text{TpRu}(\text{CO})$ or $[(^t\text{bpy})\text{Pt}]^+$, $\text{acac} =$ acetylacetonate, $\text{Tp} =$ hydridotris(pyrazolyl)borate, $^t\text{bpy} =$ 4,4'-di-*tert*-butyl-2,2'-bipyridine) resting states, which block benzene coordination that is required for C–H bond activation.^{21, 29, 40} The rate dependence on Rh concentration is near first-order using 0.022 mM to 1.121 mM of RhCl_3 (Figure 3.2.11B), which is inconsistent with a catalytic pathway that proceeds through a binuclear Rh intermediate or transition state. To study the dependence on dioxygen pressure, we decreased the reaction temperature to 150 °C, which provides a direct comparison to previously reported Rh-catalyzed anaerobic benzene alkenylation using Cu(II) as the oxidant at 150 °C.⁸³ A first-order dependence on dioxygen pressure using 1.0 to 2.5 atm of dioxygen was observed (Figure 3.2.11C). This suggests that the reaction of a Rh intermediate with the dioxygen oxidant is a kinetically relevant step. Performing aerobic catalysis in C_6H_6 and C_6D_6 independently in separate reactors shows a primary kinetic isotope effect (KIE) of 2.7(6) (Scheme 3.2.3), which is consistent with reported values for Rh-mediated C–H activation reactions.⁸³⁻⁸⁵ The KIE result indicates that benzene C–H bond activation likely occurs before or during the rate limiting step. Catalysis using $\text{CD}_3\text{CO}_2\text{D}$ reveals a statistically identical rate to the catalysis using $\text{CH}_3\text{CO}_2\text{H}$ within 12 hours (Figure 3.2.13), suggesting that the proton from acetic acid is not involved in kinetically relevant steps.

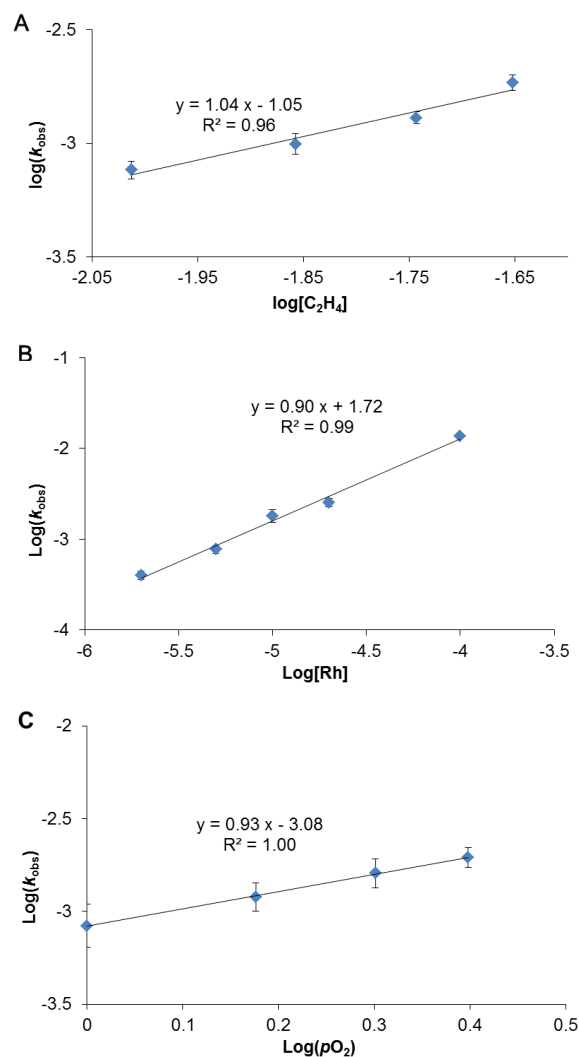


Figure 3.2.11. Log–log plots of observed rate constants (k_{obs}) versus (A) concentration of C_2H_4 . Reaction conditions: 5 mL C_6H_6 , 5 mL HOAc, 0.112 mM RhCl_3 , 1 atm air, 170 °C. (B) k_{obs} versus concentration of RhCl_3 . Reaction conditions: 5 mL C_6H_6 , 5 mL HOAc, 70 psig C_2H_4 , 1 atm air, 170 °C. (C) k_{obs} versus pressure of O_2 . Reaction conditions: 5 mL C_6H_6 , 5 mL HOAc, 70 psig C_2H_4 , 0.112 mM RhCl_3 , 150 °C. Each reaction was run in triplicate. The reactions were sampled every 4 h until 12 h. Each trial produces styrene at a constant rate within 12 hours (Figure S7-S9). Observed rate constants (k_{obs}) were extracted from the initial rate regime (from 0 to 4 h) of styrene TOs versus time plots (Figure S7-S9). The concentration of ethylene dissolved in benzene under various ethylene pressures at 170 °C was determined according to a reported method.⁸⁶ Each data point represents the average of three separate experiments. Error bars represent the standard deviations based on a minimum of three independent experiments.

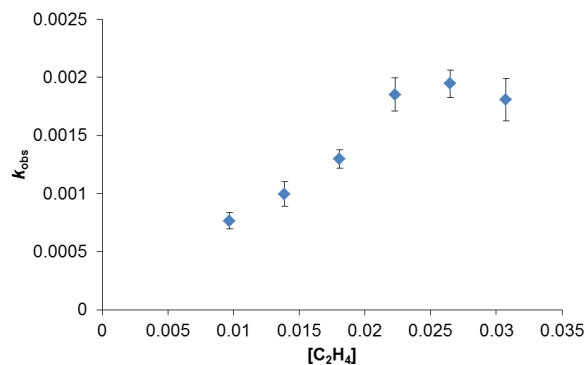
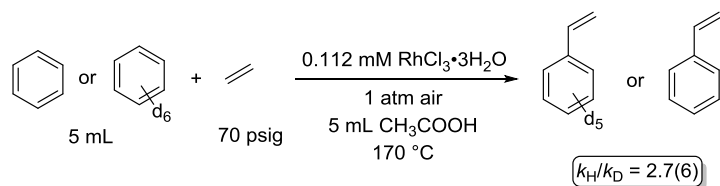


Figure 3.2.12. Plot of k_{obs} versus $[\text{C}_2\text{H}_4]$. Reaction conditions: 5 mL C_6H_6 , 5 mL HOAc, 0.112 mM $\text{RhCl}_3 \cdot 3\text{H}_2\text{O}$, 1 atm air, 170 °C. Each data point represents the average of three separate experiments. Error bars represent the standard deviations based on a minimum of three independent experiments.



Scheme 3.2.3. Kinetic isotope experiment using two parallel reactions with C_6H_6 versus C_6D_6 . Each reaction was run in triplicate. The reactions were sampled every 4 h until 12 h. Each trial produces styrene at a constant rate within 12 hours (Figure S10). k_{H} and k_{D} values were determined using average initial rates (from 0 to 4 h) of three separate experiments. The reported error represents the propagated standard deviation of all values.

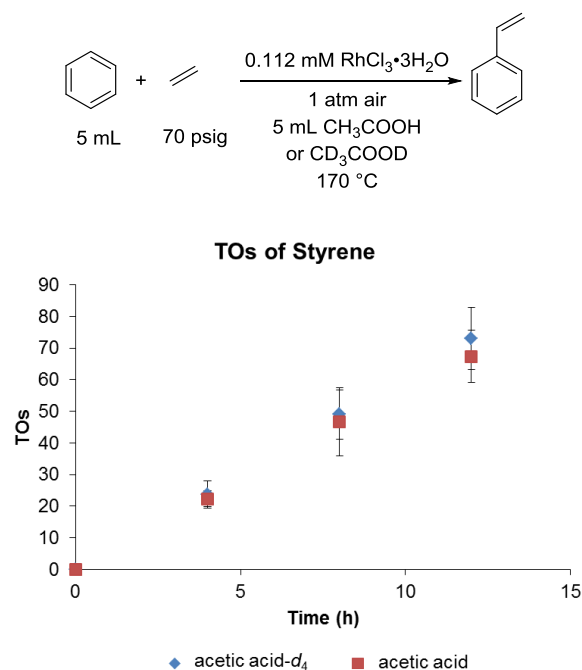
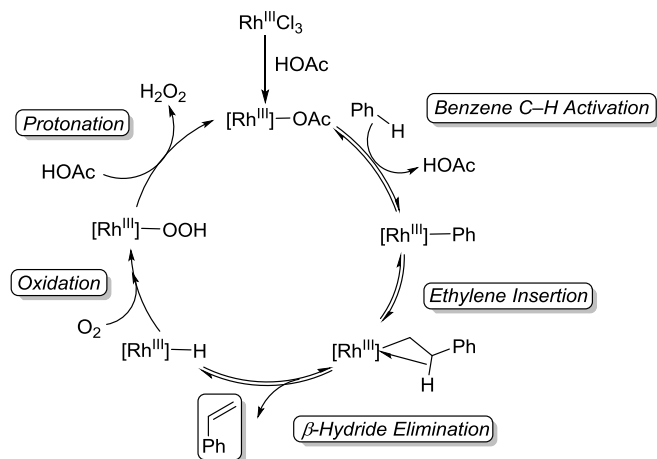


Figure 3.2.13. Comparison of TOs vs time for aerobic benzene alkenylation with

ethylene in acetic acid- d_4 and perprotio acetic acid. Reaction conditions: 5 mL benzene, 5 mL acetic acid- d_4 or perprotio acetic acid, 0.112 mM Rh, 70 psig ethylene, 1 atm air, 170 °C. Each data point represents the average of three separate experiments. Error bars represent the standard deviations based on a minimum of three independent experiments.

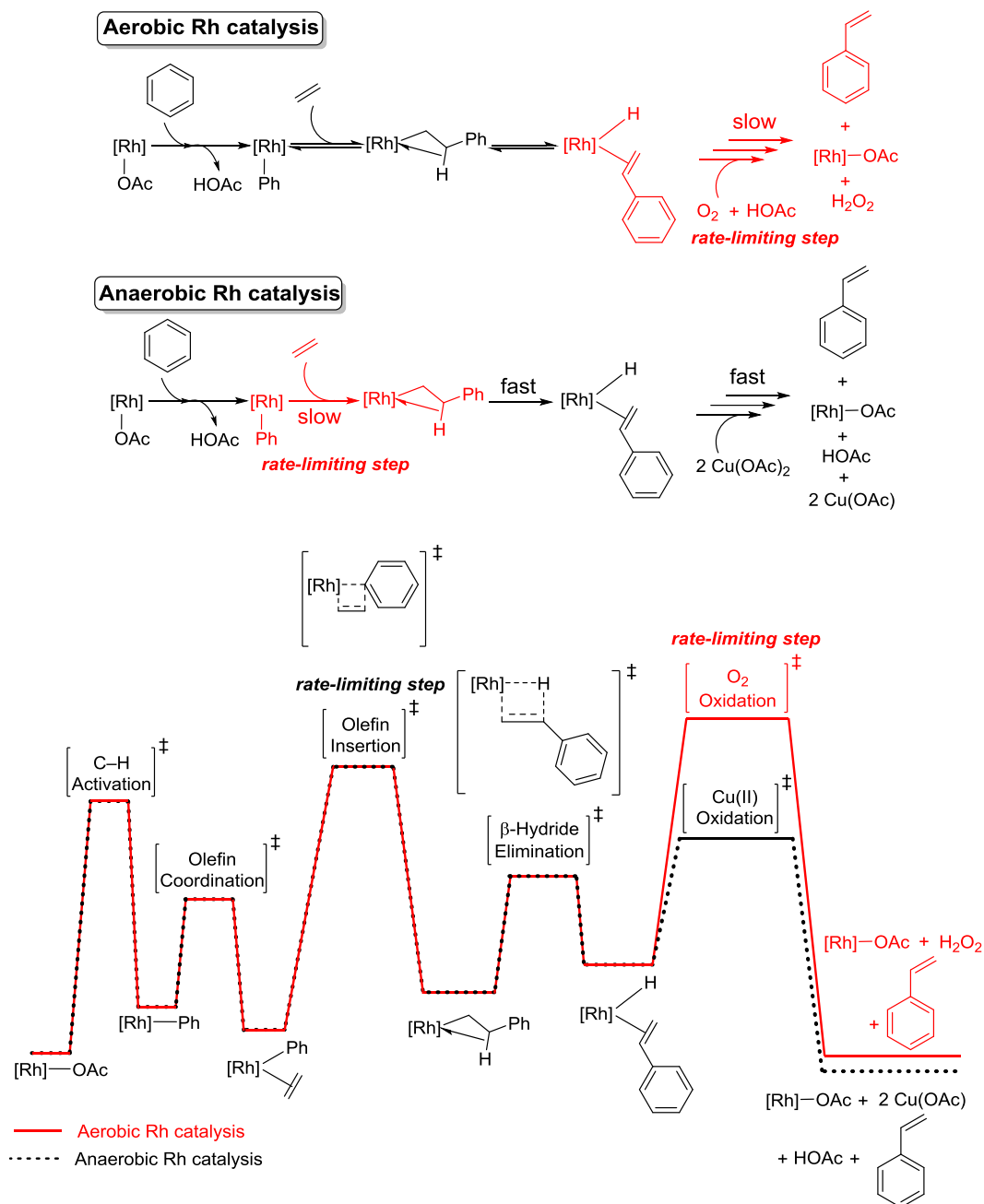
Based on the experimental results, a plausible catalytic cycle for Rh-catalyzed aerobic styrene production is illustrated in Scheme 3.2.4. First, a Rh acetate species is generated through the reaction of RhCl_3 precursor with HOAc, followed by benzene C–H activation via a concerted metalation–deprotonation mechanism (CMD) pathway using an acetate ligand. Ethylene coordination and migratory insertion into the Rh–Ph bond forms a Rh– $\text{CH}_2\text{CH}_2\text{Ph}$ intermediate, which undergoes β -hydride elimination to provide styrene and a Rh–H intermediate. Next, dioxygen reacts with the Rh–H intermediate, most likely to form a Rh–OOH complex. Mechanisms for the insertion of dioxygen into late metal-hydrides, such as Pd,⁸⁷⁻⁹⁴ Ir,⁹⁵⁻⁹⁹ Rh,^{79-81, 100, 101} and Pt^{102, 103} to generate a metal-hydroperoxo species have been demonstrated. Protonation of Rh–OOH regenerates the catalytically active Rh–OAc intermediate and releases hydrogen peroxide. More detailed studies are needed to probe the oxidation state of the Rh catalyst and characterize possible catalytic intermediates, although under the oxidizing conditions it seems likely that the Rh(III) oxidation state is maintained.



Scheme 3.2.4. Proposed mechanism for aerobic styrene production using RhCl_3 as a catalyst precursor in the presence of HOAc.

Under anaerobic conditions for Rh-catalyzed styrene production, catalysis using Cu(II) as oxidant shows a first-order dependence on ethylene concentration over a concentration ranging from 79 mM to 237 mM and a near zero-order kinetic dependence on the concentration of Cu(II).⁸³ In addition, for comparative conversion of C_6H_6 and C_6D_6 , a primary KIE value > 2.5 was observed. Based on these kinetic data, for the Cu(II) process we proposed that benzene C–H activation occurs before the rate-determining olefin insertion step whereas the reaction of Rh with Cu(II) likely occurs after the olefin insertion step. Hence, the C–H bond activation and the reaction with ethylene are kinetically relevant to the overall catalytic process whereas the reaction of a Rh intermediate, likely a Rh–H, with Cu(II) is kinetically irrelevant. This also explains why the rate of catalysis is independent of the concentration of Cu(II). Similar to catalysis using Cu(II) oxidant under anaerobic conditions, Rh catalysis under aerobic conditions without Cu(II) shows a first-order dependence on ethylene concentration under ethylene pressure below 50 psig and primary KIE when

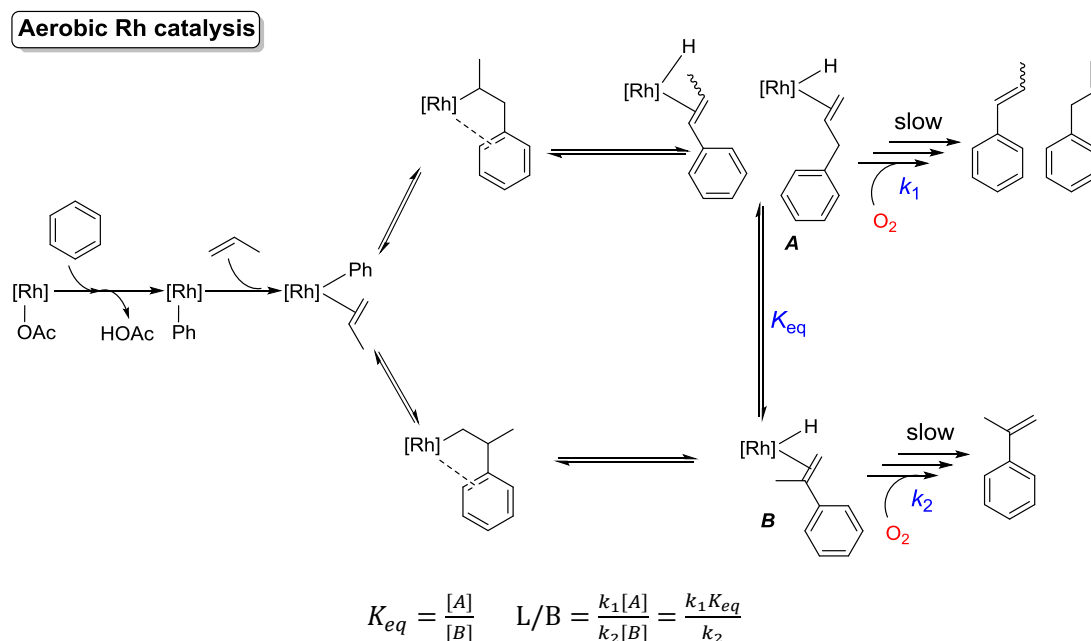
comparing reaction rate using of C₆H₆ and C₆D₆. However, a first-order dependence on the concentration of dioxygen is observed, which is in contrast with a near zero-order dependence on the concentration of Cu(II) oxidant under anaerobic conditions. These observations indicate that benzene C–H activation, the reaction of a Rh intermediate with dioxygen and with ethylene are all kinetically relevant steps. The kinetic studies are in agreement with our proposed mechanism (Scheme 3.2.5) in which C–H activation and olefin insertion occur before the rate-determining step, which is proposed to be the reaction of Rh–H with O₂. The different kinetic dependence on oxidant under aerobic conditions using O₂ and anaerobic conditions using Cu(II) are consistent with the possibility of a slower reaction of a Rh–H intermediate with dioxygen than the analogous reaction using Cu(II) under the anaerobic conditions. This could lead to a shift of rate-limiting steps from olefin insertion (under anaerobic conditions)⁸³ to net dioxygen insertion (regardless of specific mechanism) into a Rh–H bond after olefin insertion (under aerobic conditions) (Scheme 3.2.5). Assuming changing the oxidant from Cu(II) to O₂ does not affect the rate of C–H activation, olefin insertion and β-hydride elimination (which is likely a simplification), a reduced TOF when using O₂ as the sole oxidant is expected. Consistent with this expectation, at 150 °C in the presence of 0.112 mM Rh catalyst, the maximum apparent TOF ($2.1 \times 10^{-3} \text{ s}^{-1}$, calculated based on TO after 12 hours) achieved under aerobic conditions using 2.5 atm O₂ is lower than the optimized TOF ($2.8 \times 10^{-3} \text{ s}^{-1}$, calculated when maximum apparent TOF is achieved after the induction period) under anaerobic conditions using Cu(OAc)₂ oxidant.⁷³



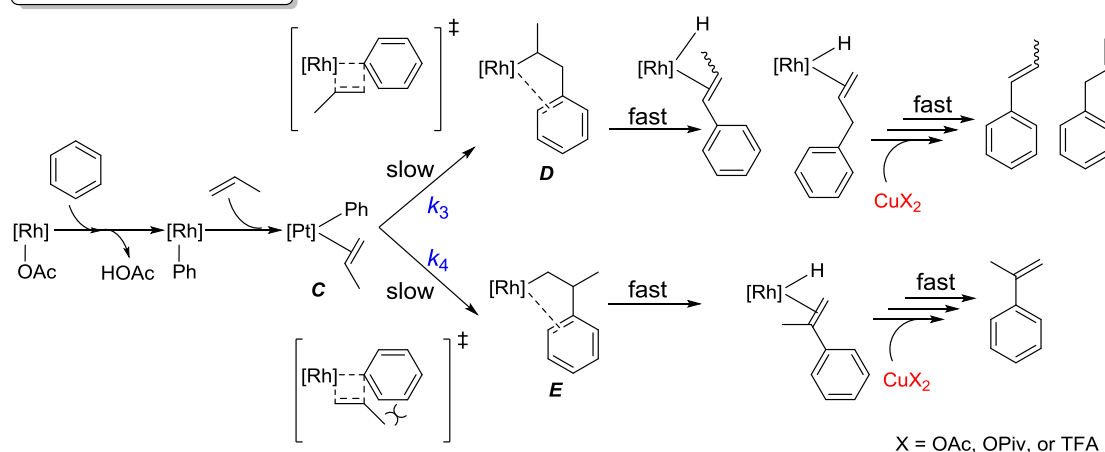
Scheme 3.2.5. Comparison of mechanistic pathway (top) and reaction coordinate (bottom) of Rh-catalyzed benzene ethylation under aerobic and anaerobic conditions.

We recently demonstrated that anaerobic benzene propenylation catalyzed by $[\text{Rh}(\mu\text{-OAc})(\eta^2\text{-C}_2\text{H}_4)_2]_2$ produces phenylpropylene products with ~8:1 ratio of linear 1-phenylpropylene products to branched α -methylstyrene when $\text{Cu}(\text{OAc})_2$ or

Cu(OPiv)₂ is used as the *in situ* oxidant,⁵⁴ which is a higher L/B selectivity than Rh-catalyzed aerobic benzene propenylation presented herein. Under Curtin–Hammett conditions, the equilibrium constant between two interconverting insertion products and the relative rates of product formation after the olefin insertion step determine the selectivity between linear and branched products.⁵⁵ Based on our hypothesis that the reaction involves the dioxygen oxidant after the olefin insertion step is the rate-limiting step under aerobic conditions, we speculate that L/B selectivity is controlled by K_{eq} in Scheme 3.2.6 and the relative ΔG^\ddagger for the rates of subsequent steps (Scheme 3.2.6; L/B ratio = $\frac{k_1 K_{eq}}{k_2}$). In contrast, under anaerobic conditions, L/B ratio is likely governed by the kinetic selectivity of rate-limiting olefin insertion (Scheme 3.2.6; L/B ratio = $\frac{k_3}{k_4}$). Therefore, the change in rate-limiting steps is likely responsible for the decreased L/B selectivity under aerobic conditions.



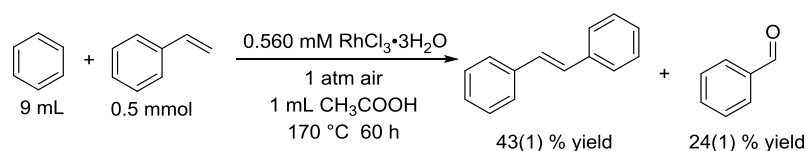
Anaerobic Rh catalysis



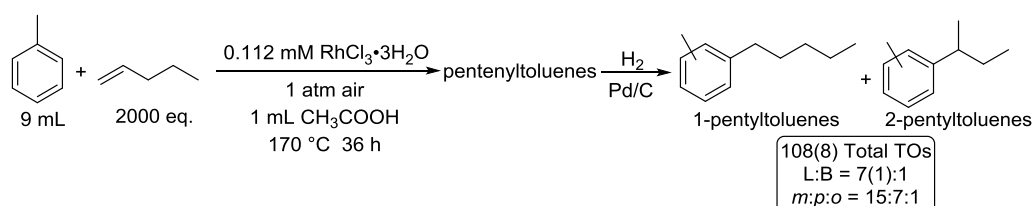
$$\frac{d[D]}{dt} = k_3[C] \quad \frac{d[E]}{dt} = k_4[C] \quad L/B = \frac{d[D]}{dt} / \frac{d[E]}{dt} = \frac{k_3[C]}{k_4[D]} = \frac{k_3}{k_4}$$

Scheme 3.2.6. Possible explanation for different linear/branched product selectivity of aerobic and anaerobic Rh catalysis.

We explored the versatility of the Rh-catalyzed aerobic alkenylation by probing substituted olefins and arenes. We have reported a Rh-catalyzed alkenylation reaction for synthesis of stilbene derivatives from arenes and styrenes using a sub-stoichiometric amount of Cu(II) carboxylate as a co-oxidant, which is regenerated by air.⁶⁵ Using this aerobic alkenylation protocol, trans-stilbene can be prepared from benzene and styrene in 43(1)% yield after 60 hours (Scheme 3.2.7). For this aerobic reaction, 24(1)% of styrene was converted to benzaldehyde, which limits the yield of the stilbene product. Also, we have demonstrated Rh-catalyzed alkenylation of toluene with 1-pentene using Cu(II) oxidant to form meta- and para substituted 1-pentenyltoluenes and 2-pentenyltoluenes.⁴⁸ Under the aerobic alkenylation conditions, 1-pentene and toluene were transformed into the desired 1-pentenyltoluenes and 2-pentenyltoluenes. Upon hydrogenation, 108(8) TOs of pentyltoluenes with L:B ratio (i.e., 1-pentyltoluenes/2-pentyltoluenes) of 7(1):1 and a meta:para:ortho ratio of ~15:7:1 (Scheme 3.2.8).



Scheme 3.2.7. Rh-catalyzed aerobic benzene alkenylation with styrene to produce trans-stilbene. Reaction conditions: 9 mL benzene, 1 mL acetic acid, 0.5 mmol styrene, 0.560 mM $\text{RhCl}_3 \cdot 3\text{H}_2\text{O}$, 1 atm air, 170 °C. Yields, which were determined by GC, represent the average of three separate experiments based on the amount of styrene. The standard deviations given in parentheses are based on three independent experiments.



Scheme 3.2.8. Rh-catalyzed aerobic alkenylation of toluene with 1-pentene. Reaction conditions: 9 mL toluene, 1 mL acetic acid, 2000 equivalent of 1-pentene relative to Rh, 0.112 mM $\text{RhCl}_3 \cdot 3\text{H}_2\text{O}$, 1 atm air, 170 °C. Hydrogenation was achieved using 10% Pd/C under hydrogen atmosphere. The reaction was run in triplicate. The standard deviations given in parentheses are based on three independent experiments. The L:B ratio in the graphic is the ratio of anti-Markovnikov to Markovnikov products.

3.3 Summary and Conclusions

In conclusion, we have developed a Rh-catalyzed step-economical aerobic benzene alkenylation reaction that produces H_2O as the sole by-product from oxidation step. Notable hallmarks include: (1) the catalysis uses commercially-available RhCl_3 salt as catalyst precursor in the absence of additional additives and ligand, (2) the catalysis can use unpurified air or oxygen as the sole oxidant and does not require other co-oxidants, (3) the Rh catalysts can achieve a $\text{TON} > 1000$ under optimized conditions. A first-order dependence on O_2 oxidant was observed, which is indicative of a kinetically relevant O_2 oxidation step. Based on this

hypothesis, the reduced L/B selectivity relative to the anaerobic Rh catalysis using Cu(II) oxidants is likely a result of Curtin–Hammett conditions. The aerobic alkenylation protocol is successfully applied to synthesis of trans-stilbene from benzene and styrene and conversion of toluene and 1-pentene to pentenyltoluenes. Targets for future catalyst improvement include enhancing catalyst reactivity, which would allow a lower reaction temperature to potentially inhibit benzaldehyde formation.

3.4 Experimental Section

General Considerations. Glovebox purity was maintained by periodic nitrogen purges and was monitored by an oxygen analyzer (O_2 concentration was < 15 ppm for all reactions). Benzene was dried by passage through columns of activated alumina. Benzene- d_6 was used as received and stored under a N_2 atmosphere over 4 Å molecular sieves. Ethylene, propylene, hydrogen and dioxygen were purchased in gas cylinders from GTS-Welco and used as received. Rhodium trichloride trihydrate was purchased from Pressure Chemical and used as received. All other reagents were purchased from commercial sources and used as received. $[\text{Rh}(\eta^2\text{-C}_2\text{H}_4)_2(\mu\text{-OAc})_2]$ was prepared according to a literature procedure.⁵⁴ GC/FID was performed using a Shimadzu GC-2014 system with a 30 m x 90.25 mm HP5 column with 0.25 μm film thickness. GC–MS was performed using a Shimadzu GCMS-QP2010 Plus instrument with a 30 m x 0.25 mm SHRXI-5MS column with a 0.25 μm thickness using electron

impact (EI) ionization was used. *The mixture of hydrocarbons and air is flammable and potentially explosive. We advise taking proper safety precaution (e.g., blast shield, burst valves for pressure relief) and avoiding any possible ignition source.*

To analyze reaction mixture samples by GC-FID, the reactors were cooled to room temperature, sampled under N₂, recharged with gases, and reheated. For reaction mixtures containing the internal standard hexamethylbenzene, aliquots of the reaction mixture (< 100 μL) were sampled, diluted with benzene (0.25 mL), and washed with saturated sodium carbonate solution (0.25 mL). The aqueous and organic layers were separated. The resulting organic layers were analyzed by GC/FID. The reaction mixtures without the internal standard hexamethylbenzene required addition of external hexamethylbenzene while sampling. A stock solution containing hexamethylbenzene (0.0364 g, 0.2243 mmol) and benzene (100 mL) was prepared in a volumetric flask. 100 μL of reaction mixture and 0.5 mL stock solution were measured by microsyringes and combined together. Aliquots of the resulting solution (< 100 μL) were washed with saturated sodium carbonate solution (0.25 mL). The aqueous and organic layers were separated. The resulting organic layers were analyzed by GC/FID.

Vinyl acetate, styrene, benzaldehyde, phenyl acetate, biphenyl, *trans*-stilbene, allylbenzene, α -methylstyrene, *cis*- β -methylstyrene and *trans*- β -methylstyrene production were quantified using linear regression analysis of gas chromatograms of standard samples of authentic products. A plot of peak area ratios versus molar ratios gave a regression line using hexamethylbenzene as the internal standard. The slopes

and correlation coefficients of the regression lines were 5.83 and 0.99 (vinyl acetate), 1.78 and 0.99 (styrene), 2.24 and 0.99 (benzaldehyde), 1.67 and 0.99 (phenyl acetate), 1.07 and 0.99 (biphenyl), 0.87 and 0.99 (*trans*-stilbene), 1.40 and 0.99 (allylbenzene), 1.23 and 0.99 (α -methylstyrene), 1.47 and 0.99 (*cis*- β -methylstyrene), 1.38 and 0.99 (*trans*- β -methylstyrene) respectively.

To analyze reaction mixture samples by GC-MS, plots of peak areas versus molar ratios gave regression lines using cyclooctane as the internal standard. 1-tolyl-1-pentane production was quantified using linear regression analysis of gas chromatograms of standard samples of authentic products. The slope and correlation coefficient of the regression lines were 1.34 and 0.998 (1-m-tolyl-1-pentane), 1.85 and 0.997 (1-p-tolyl-1-pentane) and 1.84 and 0.998 (1-o-tolyl-1-pentane), respectively. The production of 2-tolyl-2-pentenes was quantified using the slope and correlation coefficient for a fit of cumene versus n-propylbenzene, which enabled an approximation of the ratio of 1-tolyl-1-pentenes to 2-tolyl-2-pentenes. The slope and correlation coefficient of the regression line were 1.24 and 0.98 for cumene versus n-propylbenzene, respectively.

Catalytic alkenylation of benzene with ethylene and propylene using RhCl_3 as catalyst precursor and air or dioxygen as oxidant. A representative catalytic reaction is described here. Under air, a stock solution containing rhodium chloride trihydrate (0.0118 g, 0.0449 mmol) and distilled water (2 mL) was prepared in a volumetric flask. Fisher-Porter reactors were charged with 0.05 mL stock solution (contains 0.0011 mmol Rh) and placed under dynamic vacuum at 40 °C for 2 hours to

remove water. The Fisher-Porter reactors were then brought into the glovebox and charged with hexamethylbenzene (0.0182 g, 0.1121 mmol), additives (2000 eq. of relative to per Rh), and benzene (10 mL) or a benzene (5 mL)/acetic acid (5 mL) mixture. The vessels were sealed, purged with air or dioxygen, and pressurized with ethylene (70 psig) or propylene (25 psig). For the reaction under 60, 50, 40, 30 or 20 psig ethylene, after charged with air and ethylene, the vessels were subsequently pressurized with N₂ up to 80 psig as top pressure. Then the reactors were stirred and heated to 150 or 170 °C. The reaction mixtures without the internal standard hexamethylbenzene required addition of external hexamethylbenzene while sampling. Since the mixture of hydrocarbon gas and air/O₂ is flammable and explosive, it is important to be aware of explosive limits. The lower and upper explosive limit of ethylene and propylene (LEL and UEL) in air is 2.7 and 36.0 for ethylene and 2.0 and 11.1 for propylene (concentrations in percent by volume).¹⁰⁴ In our reactions with air, ethylene in the reactors is at a concentration in air higher than the UEL. Thus, the mixture of hydrocarbon gas and air under our conditions will be outside the explosive region. We advise taking proper safety precaution (*e.g.*, blast shield, burst valves for pressure relief) and avoiding any possible ignition source in reactions with air or O₂. The reactions were sampled every 12 h until 60 h or every 4 h until 12 h. The resulting product mixture was analyzed by GC-FID.

Catalytic alkenylation of benzene with ethylene and propylene using [Rh(η^2 -C₂H₄)₂(μ -OAc)]₂ as catalyst precursor and air or dioxygen as oxidant. In the glovebox, a stock solution containing [Rh(η^2 -C₂H₄)₂(μ -OAc)]₂ (0.0111 g, 0.0224

mmol), hexamethylbenzene (0.3640 g, 2.2430 mmol), and benzene (100 mL) was prepared in a volumetric flask. Fisher-Porter reactors were charged with stock solution (5 mL) and acetic acid (5 mL). The vessels were sealed, purged with air (1 atm) and pressurized with ethylene (70 psig), and subsequently stirred and heated to 150 °C. The mixture of hydrocarbon gas and air is flammable and explosive, we advise taking proper safety precaution (*e.g.*, blast shield, burst valves for pressure relief) and avoiding any possible ignition source. The reactions were sampled every 12 h until 60 h. The resulting product mixture was analyzed by GC–FID.

Catalytic alkenylation of benzene with styrene using RhCl₃ as catalyst precursor and air as oxidant. Under air, a stock solution containing rhodium(III) chloride trihydrate (0.059 g, 0.224 mmol) and distilled water (2 mL) was prepared in a volumetric flask. Fisher-Porter reactors were charged with 0.05 mL stock solution (0.0056 mmol Rh) and placed under dynamic vacuum at 40 °C for 2 hours to remove water. The Fisher-Porter reactors were then brought into the glovebox and charged with benzene (9 mL), styrene (0.5 mmol) and acetic acid (1 mL). The vessels were sealed, purged with air, and pressurized with dinitrogen. The mixtures were stirred and heated to 170 °C. The reactions were sampled at 60 h. The resulting product mixture was analyzed by GC–FID.

Catalytic alkenylation of toluene with 1-pentene using RhCl₃ as catalyst precursor and air as oxidant. Under air, a stock solution containing rhodium(III) chloride trihydrate (0.0118 g, 0.0449 mmol) and distilled water (2 mL) was prepared in a volumetric flask. Fisher-Porter reactors were charged with 0.05 mL stock solution

(0.0011 mmol Rh) and placed under dynamic vacuum at 40 °C for 2 hours to remove water. The Fisher-Porter reactors were then brought into the glovebox and charged with toluene (9 mL), 1-pentene (2000 equivalent relative to Rh), and acetic acid (1 mL). The vessels were sealed, purged with air, and pressurized with dinitrogen. The mixtures were stirred and heated to 170 °C. The reactions were sampled at 36 h. A stock solution containing cyclooctane (63 µL, 50 equiv relative to Rh) and benzene (10 mL) was prepared in a volumetric flask. Next, 200 µL of the reaction mixture and 200 µL of the stock solution were measured and combined. Aliquots of the resulting solution (< 200 µL) were washed with saturated sodium carbonate solution (0.25 mL). The aqueous and organic layers were separated. The resulting organic layers were subject to hydrogenation..

Hydrogenation Procedure. A Fischer–Porter reactor was charged with aliquots of the reaction mixture, 8 mg of 10% Pd/C and 4 mL of ethanol. The vessels were sealed and pressurized with 100 psi of H₂ after the headspace was evacuated. The reactor was stirred at room temperature overnight. The resulting product mixture was analyzed by GC–MS.

3.5 References

1. Olah, G. A.; Molnár, Á. *Hydrocarbon Chemistry*; Wiley-Interscience: Hoboken: NJ, 2003; pp 283.
2. Perego, C.; Pollesel, P. *Advances in Aromatics Processing Using Zeolite Catalysts. Advances in Nanoporous Materials*; Elsevier: 2010; Vol. 1, pp 97-149.
3. Chen, S. S. *Kirk-Othmer Encyclopedia of Chemical Technology*; John Wiley & Sons, Inc.: Hoboken: NJ, 2000; pp 325-357.
4. Wittcoff, H. A.; Reuben, B. G.; Plotkin, J. S. *Chemicals and Polymers from*

Ethylene. In *Industrial Organic Chemicals*; John Wiley & Sons, Inc.: Hoboken: NJ, 2004; pp 100-166.

5. Čejka, J.; Wichterlová, B. Acid-Catalyzed Synthesis of Mono- and Dialkyl Benzenes over Zeolites: Active Sites, Zeolite Topology, and Reaction Mechanisms. *Cat. Rev.* **2002**, *44*, 375-421.

6. Perego, C.; Ingallina, P. Recent Advances in the Industrial Alkylation of Aromatics: New Catalysts and New Processes. *Catal. Today* **2002**, *73*, 3-22.

7. Perego, C.; Ingallina, P. Combining Alkylation and Transalkylation for Alkylaromatic Production. *Green Chem.* **2004**, *6*, 274-279.

8. Garside, M. Guide to the Business of Chemistry - 2019; American Chemistry Council: 2019.

9. Caro, J.; Noack, M.; Ernst, S. Chapter 1 - Zeolite Membranes – Status and Prospective. In *Advances in Nanoporous Materials*; Elsevier: 2010; Vol. 1, pp 1-96.

10. Negishi, E.-i.; Anastasia, L. Palladium-Catalyzed Alkynylation. *Chem. Rev.* **2003**, *103*, 1979-2018.

11. Stille, J. K. The Palladium-Catalyzed Cross-Coupling Reactions of Organotin Reagents with Organic Electrophiles. *Angew. Chem. Int. Ed.* **1986**, *25*, 508-524.

12. Beletskaya, I. P.; Cheprakov, A. V. The Heck Reaction as a Sharpening Stone of Palladium Catalysis. *Chem. Rev.* **2000**, *100*, 3009-3066.

13. Suzuki, A. Organoborates in New Synthetic Reactions. *Acc. Chem. Res.* **1982**, *15*, 178-184.

14. Varun, B. V.; Dhineshkumar, J.; Bettadapur, K. R.; Siddaraju, Y.; Alagiri, K.; Prabhu, K. R. Recent Advancements in Dehydrogenative Cross Coupling Reactions for C–C Bond Formation. *Tetrahedron Lett.* **2017**, *58*, 803-824.

15. Biffis, A.; Centomo, P.; Del Zotto, A.; Zecca, M. Pd Metal Catalysts for Cross-Couplings and Related Reactions in the 21st Century: A Critical Review. *Chem. Rev.* **2018**, *118*, 2249-2295.

16. Saper, N. I.; Ohgi, A.; Small, D. W.; Semba, K.; Nakao, Y.; Hartwig, J. F. Nickel-Catalysed Anti-Markovnikov Hydroarylation of Unactivated Alkenes with Unactivated Arenes Facilitated by Non-Covalent Interactions. *Nature Chemistry* **2020**, *12*, 276-283.

17. Bair, J. S.; Schramm, Y.; Sergeev, A. G.; Clot, E.; Eisenstein, O.; Hartwig, J. F. Linear-Selective Hydroarylation of Unactivated Terminal and Internal Olefins with Trifluoromethyl-Substituted Arenes. *J. Am. Chem. Soc.* **2014**, *136*, 13098-13101.

18. Matsumoto, T.; Taube, D. J.; Periana, R. A.; Taube, H.; Yoshida, H. Anti-Markovnikov Olefin Arylation Catalyzed by an Iridium Complex. *J. Am. Chem. Soc.* **2000**, *122*, 7414-7415.

19. Periana, R. A.; Liu, X. Y.; Bhalla, G. Novel Bis-Acac-O, O–Ir (III) Catalyst for Anti-Markovnikov, Hydroarylation of Olefins Operates by Arene C–H Activation. *Chem. Commun.* **2002**, 3000-3001.

20. Bhalla, G.; Liu, X. Y.; Oxgaard, J.; Goddard, W. A.; Periana, R. A. Synthesis, Structure, and Reactivity of O-Donor Ir(III) Complexes: C–H Activation Studies with Benzene. *J. Am. Chem. Soc.* **2005**, *127*, 11372-11389.

21. Bhalla, G.; Bischof, S. M.; Ganesh, S. K.; Liu, X. Y.; Jones, C. J.;

Borzenko, A.; Tenn, W. J.; Ess, D. H.; Hashiguchi, B. G.; Lokare, K. S.; Leung, C. H.; Oxgaard, J.; Goddard, W. A.; Periana, R. A. Mechanism of Efficient Anti-Markovnikov Olefin Hydroarylation Catalyzed by Homogeneous Ir(III) Complexes. *Green Chem.* **2011**, *13*, 69-81.

22. Bhalla, G.; Oxgaard, J.; Goddard, W. A.; Periana, R. A. Anti-Markovnikov Hydroarylation of Unactivated Olefins Catalyzed by a Bis-Tropolonato Iridium(III) Organometallic Complex. *Organometallics* **2005**, *24*, 3229-3232.

23. Crisenza, G. E. M.; McCreanor, N. G.; Bower, J. F. Branch-Selective, Iridium-Catalyzed Hydroarylation of Monosubstituted Alkenes Via a Cooperative Destabilization Strategy. *J. Am. Chem. Soc.* **2014**, *136*, 10258-10261.

24. Lail, M.; Arrowood, B. N.; Gunnoe, T. B. Addition of Arenes to Ethylene and Propene Catalyzed by Ruthenium. *J. Am. Chem. Soc.* **2003**, *125*, 7506-7507.

25. Lail, M.; Bell, C. M.; Conner, D.; Cundari, T. R.; Gunnoe, T. B.; Petersen, J. L. Experimental and Computational Studies of Ruthenium(II)-Catalyzed Addition of Arene C-H Bonds to Olefins. *Organometallics* **2004**, *23*, 5007-5020.

26. Foley, N. A.; Lail, M.; Gunnoe, T. B.; Cundari, T. R.; Boyle, P. D.; Petersen, J. L. Combined Experimental and Computational Study of TpRu{P(Pyr)₃}(NCMe)Me (Pyr = N-Pyrrolyl): Inter- and Intramolecular Activation of C-H Bonds and the Impact of Sterics on Catalytic Hydroarylation of Olefins. *Organometallics* **2007**, *26*, 5507-5516.

27. Foley, N. A.; Lail, M.; Lee, J. P.; Gunnoe, T. B.; Cundari, T. R.; Petersen, J. L. Comparative Reactivity of TpRu(L)(NCMe)Ph (L = Co or PMe₃): Impact of Ancillary Ligand L on Activation of Carbon-Hydrogen Bonds Including Catalytic Hydroarylation and Hydrovinylation/Oligomerization of Ethylene. *J. Am. Chem. Soc.* **2007**, *129*, 6765-6781.

28. Foley, N. A.; Ke, Z.; Gunnoe, T. B.; Cundari, T. R.; Petersen, J. L. Aromatic C-H Activation and Catalytic Hydrophenylation of Ethylene by TpRu{P(OCH₂)₃CEt}(NCMe)Ph. *Organometallics* **2008**, *27*, 3007-3017.

29. Foley, N. A.; Lee, J. P.; Ke, Z.; Gunnoe, T. B.; Cundari, T. R. Ru (II) Catalysts Supported by Hydridotris(Pyrazolyl)Borate for the Hydroarylation of Olefins: Reaction Scope, Mechanistic Studies, and Guides for the Development of Improved Catalysts. *Acc. Chem. Res.* **2009**, *42*, 585.

30. Joslin, E. E.; McMullin, C. L.; Gunnoe, T. B.; Cundari, T. R.; Sabat, M.; Myers, W. H. Catalytic Hydroarylation of Ethylene Using TpRu(L)(NCMe)Ph (L = 2,6,7-Trioxa-1-Phosphabicyclo[2,2,1]Heptane): Comparison to TpRu(L')(NCMe)Ph Systems (L' = CO, PMe₃, P(Pyr)₃, or P(OCH₂)₃CEt). *Organometallics* **2012**, *31*, 6851-6860.

31. Burgess, S. A.; Joslin, E. E.; Gunnoe, T. B.; Cundari, T. R.; Sabat, M.; Myers, W. H. Hydrophenylation of Ethylene Using a Cationic Ru(II) Catalyst: Comparison to a Neutral Ru(II) Catalyst. *Chem. Sci.* **2014**, *5*, 4355-4366.

32. Clement, M. L.; Grice, K. A.; Luedtke, A. T.; Kaminsky, W.; Goldberg, K. I. Platinum(II) Olefin Hydroarylation Catalysts: Tuning Selectivity for the Anti-Markovnikov Product. *Chem. - Eur. J.* **2014**, *20*, 17287-17291.

33. Luedtke, A. T.; Goldberg, K. I. Intermolecular Hydroarylation of Unactivated

-
- Olefins Catalyzed by Homogeneous Platinum Complexes. *Angew. Chem., Int. Ed.* **2008**, *47*, 7694-7696.
34. Suslick, B. A.; Liberman-Martin, A. L.; Wambach, T. C.; Tilley, T. D. Olefin Hydroarylation Catalyzed by (Pyridyl-Indolate)Pt(II) Complexes: Catalytic Efficiencies and Mechanistic Aspects. *ACS Catal.* **2017**, *7*, 4313-4322.
35. McKeown, B. A.; Foley, N. A.; Lee, J. P.; Gunnoe, T. B. Hydroarylation of Unactivated Olefins Catalyzed by Platinum(II) Complexes. *Organometallics* **2008**, *27*, 4031-4033.
36. McKeown, B. A.; Gonzalez, H. E.; Friedfeld, M. R.; Brosnahan, A. M.; Gunnoe, T. B.; Cundari, T. R.; Sabat, M. Platinum(II)-Catalyzed Ethylene Hydrophenylation: Switching Selectivity between Alkyl- and Vinylbenzene Production. *Organometallics* **2013**, *32*, 2857-2865.
37. McKeown, B. A.; Gonzalez, H. E.; Gunnoe, T. B.; Cundari, T. R.; Sabat, M. Pt^{II}-Catalyzed Ethylene Hydrophenylation: Influence of Dipyridyl Chelate Ring Size on Catalyst Activity and Longevity. *ACS Catal.* **2013**, *3*, 1165-1171.
38. McKeown, B. A.; Gonzalez, H. E.; Michaelos, T.; Gunnoe, T. B.; Cundari, T. R.; Crabtree, R. H.; Sabat, M. Control of Olefin Hydroarylation Catalysis Via a Sterically and Electronically Flexible Platinum(II) Catalyst Scaffold. *Organometallics* **2013**, *32*, 3903-3913.
39. McKeown, B. A.; Prince, B. M.; Ramiro, Z.; Gunnoe, T. B.; Cundari, T. R. Pt^{II}-Catalyzed Hydrophenylation of α -Olefins: Variation of Linear/Branched Products as a Function of Ligand Donor Ability. *ACS Catal.* **2014**, *4*, 1607-1615.
40. McKeown, B. A.; Gonzalez, H. E.; Friedfeld, M. R.; Gunnoe, T. B.; Cundari, T. R.; Sabat, M. Mechanistic Studies of Ethylene Hydrophenylation Catalyzed by Bipyridyl Pt(II) Complexes. *J. Am. Chem. Soc.* **2011**, *133*, 19131-19152.
41. She, Z.; Shi, Y.; Huang, Y.; Cheng, Y.; Song, F.; You, J. Versatile Palladium-Catalyzed C–H Olefination of (Hetero)Arenes at Room Temperature. *Chem. Commun.* **2014**, *50*, 13914-13916.
42. Wang, P.; Verma, P.; Xia, G.; Shi, J.; Qiao, J. X.; Tao, S.; Cheng, P. T. W.; Poss, M. A.; Farmer, M. E.; Yeung, K.-S.; Yu, J.-Q. Ligand-Accelerated Non-Directed C–H Functionalization of Arenes. *Nature* **2017**, *551*, 489-493.
43. Vora, H. U.; Silvestri, A. P.; Engelin, C. J.; Yu, J.-Q. Rhodium(II)-Catalyzed Nondirected Oxidative Alkenylation of Arenes: Arene Loading at One Equivalent. *Angew. Chem. Int. Ed.* **2014**, *53*, 2683-2686.
44. Kubota, A.; Emmert, M. H.; Sanford, M. S. Pyridine Ligands as Promoters in PdII/O-Catalyzed C–H Olefination Reactions. *Org. Lett.* **2012**, *14*, 1760-1763.
45. Jia, C.; Lu, W.; Kitamura, T.; Fujiwara, Y. Highly Efficient Pd-Catalyzed Coupling of Arenes with Olefins in the Presence of Tert-Butyl Hydroperoxide as Oxidant. *Org. Lett.* **1999**, *1*, 2097-2100.
46. Agasti, S.; Dey, A.; Maiti, D. Traceless Directing Group Mediated Branched Selective Alkenylation of Unbiased Arenes. *Chem. Commun.* **2016**, *52*, 12191-12194.
47. Ying, C.-H.; Yan, S.-B.; Duan, W.-L. 2-Hydroxy-1,10-Phenanthroline Vs 1,10-Phenanthroline: Significant Ligand Acceleration Effects in the Palladium-Catalyzed Oxidative Heck Reaction of Arenes. *Org. Lett.* **2014**, *16*,

500-503.

48. Liebov, N. S.; Zhu, W.; Chen, J.; Webster-Gardiner, M. S.; Schinski, W. L.; Gunnoe, T. B. Rhodium-Catalyzed Alkenylation of Toluene Using 1-Pentene: Regioselectivity to Generate Precursors for Bicyclic Compounds. *Organometallics* **2019**, *38*, 3860-3870.

49. Ghosh, K.; Mihara, G.; Nishii, Y.; Miura, M. Nondirected C-H Alkenylation of Arenes with Alkenes under Rhodium Catalysis. *Chem. Lett.* **2018**, *48*, 148-151.

50. Patureau, F. W.; Nimphius, C.; Glorius, F. Rh Catalyzed C-H Activation and Oxidative Olefination without Chelate Assistance: On the Reactivity of Bromoarenes. *Org. Lett.* **2011**, *13*, 6346-6349.

51. Jia, X.; Gary, J. B.; Gu, S.; Cundari, T. R.; Gunnoe, T. B. Oxidative Hydrophenylation of Ethylene Using a Cationic Ru (II) Catalyst: Styrene Production with Ethylene as the Oxidant. *Israel Journal of Chemistry* **2017**, *57*, 1037-1046.

52. Hong, P.; Yamazaki, H. Rhodium Carbonyl-Catalyzed Activation of Carbon-Hydrogen Bonds for Application in Organic Synthesis.: V. Phenylation of Olefins with Benzenes. *J. Mol. Catal.* **1984**, *26*, 297-311.

53. Vaughan, B. A.; Webster-Gardiner, M. S.; Cundari, T. R.; Gunnoe, T. B. Organic Chemistry. A Rhodium Catalyst for Single-Step Styrene Production from Benzene and Ethylene. *Science* **2015**, *348*, 421-424.

54. Webster-Gardiner, M. S.; Chen, J.; Vaughan, B. A.; McKeown, B. A.; Schinski, W.; Gunnoe, T. B. Catalytic Synthesis of "Super" Linear Alkenyl Arenes Using an Easily Prepared Rh(I) Catalyst. *J. Am. Chem. Soc.* **2017**, *139*, 5474-5480.

55. Zhu, W.; Gunnoe, T. B. Advances in Rhodium-Catalyzed Oxidative Arene Alkenylation. *Acc. Chem. Res.* **2020**, *53*, 920-936.

56. Matsumoto, T.; Yoshida, H. Oxidative Arylation of Ethylene with Benzene to Produce Styrene. *Chem. Lett.* **2000**, *29*, 1064-1065.

57. Matsumoto, T.; Periana, R. A.; Taube, D. J.; Yoshida, H. Direct Synthesis of Styrene by Rhodium-Catalyzed Oxidative Arylation of Ethylene with Benzene. *J. Catal.* **2002**, *206*, 272-280.

58. Fujiwara, Y.; Moritani, I.; Danno, S.; Asano, R.; Teranishi, S. Aromatic Substitution of Olefins. Vi. Arylation of Olefins with Palladium(II) Acetate. *J. Am. Chem. Soc.* **1969**, *91*, 7166-7169.

59. Keith, J. A.; Henry, P. M. The Mechanism of the Wacker Reaction: A Tale of Two Hydroxypalladations. *Angew. Chem. Int. Ed.* **2009**, *48*, 9038-9049.

60. Babu, B. P.; Meng, X.; Bäckvall, J.-E. Aerobic Oxidative Coupling of Arenes and Olefins through a Biomimetic Approach. *Chem. Eur. J.* **2013**, *19*, 4140-4145.

61. Yamada, T.; Sakakura, A.; Sakaguchi, S.; Obora, Y.; Ishii, Y. Oxidative Arylation of Ethylene with Benzene Catalyzed by Pd(OAc)₂/Heteropoly Acid/O₂ System. *New J. Chem.* **2008**, *32*, 738-742.

62. Obora, Y.; Ishii, Y. Pd(II)/Hpmov-Catalyzed Direct Oxidative Coupling Reaction of Benzenes with Olefins. *Molecules* **2010**, *15*, 1487-1500.

63. Yokota, T.; Tani, M.; Sakaguchi, S.; Ishii, Y. Direct Coupling of Benzene with Olefin Catalyzed by Pd(OAc)₂ Combined with Heteropolyoxometalate under Dioxigen. *J. Am. Chem. Soc.* **2003**, *125*, 1476-1477.

-
64. Jia, X.; Foley, A. M.; Liu, C.; Vaughan, B. A.; McKeown, B. A.; Zhang, S.; Gunnoe, T. B. Styrene Production from Benzene and Ethylene Catalyzed by Palladium(II): Enhancement of Selectivity toward Styrene Via Temperature-Dependent Vinyl Ester Consumption. *Organometallics* **2019**, *38*, 3532-3541.
65. Jia, X.; Frye, L. I.; Zhu, W.; Gu, S.; Gunnoe, T. B. Synthesis of Stilbenes by Rhodium-Catalyzed Aerobic Alkenylation of Arenes Via C–H Activation. *J. Am. Chem. Soc.* **2020**, *142*, 10534-10543.
66. Bechtoldt, A.; Tirlor, C.; Raghuvanshi, K.; Warratz, S.; Kornhaas, C.; Ackermann, L. Ruthenium Oxidase Catalysis for Site-Selective C–H Alkenylations with Ambient O₂ as the Sole Oxidant. *Angew. Chem. Int. Ed.* **2016**, *55*, 264-267.
67. Zhang, Y.-H.; Shi, B.-F.; Yu, J.-Q. Pd(II)-Catalyzed Olefination of Electron-Deficient Arenes Using 2,6-Dialkylpyridine Ligands. *J. Am. Chem. Soc.* **2009**, *131*, 5072-5074.
68. Gandeepan, P.; Cheng, C.-H. Allylic Carbon–Carbon Double Bond Directed Pd-Catalyzed Oxidative Ortho-Olefination of Arenes. *J. Am. Chem. Soc.* **2012**, *134*, 5738-5741.
69. Dams, M.; De Vos, D. E.; Celen, S.; Jacobs, P. A. Toward Waste-Free Production of Heck Products with a Catalytic Palladium System under Oxygen. *Angew. Chem. Int. Ed.* **2003**, *42*, 3512-3515.
70. Shue, R. S. Catalytic Coupling of Aromatics and Olefins by Homogeneous Palladium(II) Compounds under Oxygen. *J. Chem. Soc. D* **1971**, 1510-1511.
71. Weissman, H.; Song, X.; Milstein, D. Ru-Catalyzed Oxidative Coupling of Arenes with Olefins Using O₂. *J. Am. Chem. Soc.* **2001**, *123*, 337-338.
72. Chen, J.; Nielsen, R. J.; Goddard, W. A.; McKeown, B. A.; Dickie, D. A.; Gunnoe, T. B. Catalytic Synthesis of Superlinear Alkenyl Arenes Using a Rh(I) Catalyst Supported by a “Capping Arene” Ligand: Access to Aerobic Catalysis. *J. Am. Chem. Soc.* **2018**, *140*, 17007-17018.
73. Zhu, W.; Luo, Z.; Chen, J.; Liu, C.; Yang, L.; Dickie, D. A.; Liu, N.; Zhang, S.; Davis, R. J.; Gunnoe, T. B. Mechanistic Studies of Single-Step Styrene Production Catalyzed by Rh Complexes with Diimine Ligands: An Evaluation of the Role of Ligands and Induction Period. *ACS Catal.* **2019**, *9*, 7457-7475.
74. Ackermann, L. Carboxylate-Assisted Ruthenium-Catalyzed Alkyne Annulations by C–H/Het–H Bond Functionalizations. *Acc. Chem. Res.* **2014**, *47*, 281-295.
75. Webb, J. R.; Burgess, S. A.; Cundari, T. R.; Gunnoe, T. B. Activation of Carbon–Hydrogen Bonds and Dihydrogen by 1,2-CH-Addition across Metal–Heteroatom Bonds. *Dalton Trans.* **2013**, *42*, 16646-16665.
76. Gunnoe, T. B. Reactivity of Ruthenium(II) and Copper(I) Complexes That Possess Anionic Heteroatomic Ligands: Synthetic Exploitation of Nucleophilicity and Basicity of Amido, Hydroxo, Alkoxo, and Aryloxo Ligands for the Activation of Substrates That Possess Polar Bonds as Well as Nonpolar C–H and H–H Bonds. *Eur. J. Inorg. Chem.* **2007**, *2007*, 1177-1177.
77. Lapointe, D.; Fagnou, K. Overview of the Mechanistic Work on the Concerted Metallation–Deprotonation Pathway. *Chem. Lett.* **2010**, *39*, 1118-1126.

-
78. Ackermann, L. Carboxylate-Assisted Transition-Metal-Catalyzed C–H Bond Functionalizations: Mechanism and Scope. *Chem. Rev.* **2011**, *111*, 1315-1345.
79. Teets, T. S.; Nocera, D. G. Mechanistic Studies of O₂ Reduction Effected by Group 9 Bimetallic Hydride Complexes. *J. Am. Chem. Soc.* **2011**, *133*, 17796-17806.
80. Bakac, A. Kinetics and Thermodynamics of Hydrogen Atom Transfer to Superoxometal Complexes. *J. Am. Chem. Soc.* **1997**, *119*, 10726-10731.
81. Teets, T. S.; Nocera, D. G. Oxygen Reduction Reactions of Monometallic Rhodium Hydride Complexes. *Inorganic Chemistry* **2012**, *51*, 7192-7201.
82. Under the standard set of conditions, substituting 70 psig ethylene with 1000 equivalent of styrene produces 61(13) TOs of Benzaldehyde after 12 hours. A statistically identical amount of benzaldehyde was produced when heating the same amount of styrene without Rh complex and ethylene under the standard set of conditions.
83. Vaughan, B. A.; Khani, S. K.; Gary, J. B.; Kammert, J. D.; Webster-Gardiner, M. S.; McKeown, B. A.; Davis, R. J.; Cundari, T. R.; Gunnoe, T. B. Mechanistic Studies of Single-Step Styrene Production Using a Rhodium(I) Catalyst. *J. Am. Chem. Soc.* **2017**, *139*, 1485-1498.
84. Northcutt, T. O.; Wick, D. D.; Vetter, A. J.; Jones, W. D. Investigation of the Mechanism of Alkane Reductive Elimination and Skeletal Isomerization in Tp'Rh(CNneopentyl)(R)H Complexes: The Role of Alkane Complexes. *J. Am. Chem. Soc.* **2001**, *123*, 7257-7270.
85. Vetter, A. J.; Flaschenriem, C.; Jones, W. D. Alkane Coordination Selectivity in Hydrocarbon Activation by [Tp'Rh(CNneopentyl)]: The Role of Alkane Complexes. *J. Am. Chem. Soc.* **2005**, *127*, 12315-12322.
86. Ellis, S. R. M.; Valteris, R. L.; Harris, G. J. High Pressure Equilibrium Still for Vapor-Phase Extraction Studies. *Chem. Eng. Progr., Symp. Ser.* **1968**, *64*, 16-21.
87. Konnick, M. M.; Guzei, I. A.; Stahl, S. S. Characterization of Peroxo and Hydroperoxo Intermediates in the Aerobic Oxidation of N-Heterocyclic-Carbene-Coordinated Palladium(0). *J. Am. Chem. Soc.* **2004**, *126*, 10212-10213.
88. Keith, J. M.; Nielsen, R. J.; Oxgaard, J.; Goddard, W. A. Pd-Mediated Activation of Molecular Oxygen in a Nonpolar Medium. *J. Am. Chem. Soc.* **2005**, *127*, 13172-13179.
89. Konnick, M. M.; Decharin, N.; Popp, B. V.; Stahl, S. S. O₂insertion into a Palladium(II)-Hydride Bond: Observation of Mechanistic Crossover between H_x-Reductive-Elimination and Hydrogen-Atom-Abstraction Pathways. *Chemical Science* **2011**, *2*, 326-330.
90. Konnick, M. M.; Gandhi, B. A.; Guzei, I. A.; Stahl, S. S. Reaction of Molecular Oxygen with a Pd^{II}-Hydride to Produce a Pd^{II}-Hydroperoxide: Acid Catalysis and Implications for Pd-Catalyzed Aerobic Oxidation Reactions. *Angew. Chem. Int. Ed.* **2006**, *45*, 2904-2907.
91. Denney, M. C.; Smythe, N. A.; Cetto, K. L.; Kemp, R. A.; Goldberg, K. I. Insertion of Molecular Oxygen into a Palladium(II) Hydride Bond. *J. Am. Chem. Soc.* **2006**, *128*, 2508-2509.

-
92. Keith, J. M.; Goddard, W. A.; Oxgaard, J. Pd-Mediated Activation of Molecular Oxygen: Pd(0) Versus Direct Insertion. *J. Am. Chem. Soc.* **2007**, *129*, 10361-10369.
93. Konnick, M. M.; Stahl, S. S. Reaction of Molecular Oxygen with a Pd^{II}-Hydride to Produce a Pd^{II}-Hydroperoxide: Experimental Evidence for an Hx-Reductive-Elimination Pathway. *J. Am. Chem. Soc.* **2008**, *130*, 5753-5762.
94. Konnick, M. M.; Knapp, S. M. M.; Stahl, S. S. Mechanism of the Reaction of an Nhc-Coordinated Palladium(II)-Hydride with O₂ in Acetonitrile. *Polyhedron* **2020**, *182*, 114501.
95. Heiden, Z. M.; Rauchfuss, T. B. Homogeneous Catalytic Reduction of Dioxygen Using Transfer Hydrogenation Catalysts. *J. Am. Chem. Soc.* **2007**, *129*, 14303-14310.
96. Chowdhury, S.; Himo, F.; Russo, N.; Sicilia, E. Mechanistic Investigation of the Hydrogenation of O₂ by a Transfer Hydrogenation Catalyst. *J. Am. Chem. Soc.* **2010**, *132*, 4178-4190.
97. Keith, J. M.; Teets, T. S.; Nocera, D. G. O₂ Insertion into Group 9 Metal-Hydride Bonds: Evidence for Oxygen Activation through the Hydrogen-Atom-Abstraction Mechanism. *Inorganic Chemistry* **2012**, *51*, 9499-9507.
98. Teets, T. S.; Nocera, D. G. Acidolysis and Oxygen Atom Transfer Reactivity of a Diiridium Hydroperoxo Complex. *Dalton Trans.* **2013**, *42*, 3521-3527.
99. Wright, A. M.; Pahls, D. R.; Gary, J. B.; Warner, T.; Williams, J. Z.; M. Knapp, S. M.; Allen, K. E.; Landis, C. R.; Cundari, T. R.; Goldberg, K. I. Experimental and Computational Investigation of the Aerobic Oxidation of a Late Transition Metal-Hydride. *J. Am. Chem. Soc.* **2019**, *141*, 10830-10843.
100. Szajna-Fuller, E.; Bakac, A. Base-Catalyzed Insertion of Dioxygen into Rhodium-Hydrogen Bonds: Kinetics and Mechanism. *Inorganic Chemistry* **2010**, *49*, 781-785.
101. Halbach, R. L.; Teets, T. S.; Nocera, D. G. Oxygen Reduction Mechanism of Monometallic Rhodium Hydride Complexes. *Inorganic Chemistry* **2015**, *54*, 7335-7344.
102. Look, J. L.; Wick, D. D.; Mayer, J. M.; Goldberg, K. I. Autoxidation of Platinum(IV) Hydrocarbyl Hydride Complexes to Form Platinum(IV) Hydrocarbyl Hydroperoxide Complexes. *Inorganic Chemistry* **2009**, *48*, 1356-1369.
103. Keith, J. M.; Ye, Y.; Wei, H.; Buck, M. R. Mechanistic Examination of Aerobic Pt Oxidation: Insertion of Molecular Oxygen into Pt-H Bonds through a Radical Chain Mechanism. *Dalton Trans.* **2016**, *45*, 11650-11656.
104. Yaws, C. L.; Braker, W. Matheson™ Gas Data Book; McGraw-Hill Professional: 2001; pp 443.

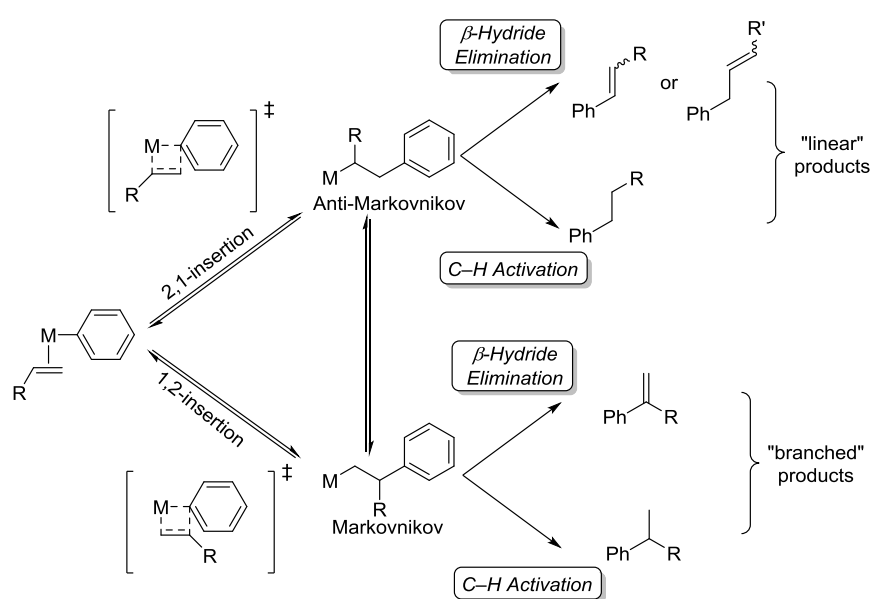
4 Catalytic Synthesis of Super Linear Alkenyl Arenes with a Simple Iridium Salt as Catalyst Precursor

4.1 Introduction

Long chain linear alkyl benzenes (LABs) serve as key starting materials for the detergent and surfactant industries.¹ LABs are usually comprised primarily of 2- and 3-aryl substituted alkanes. Current acid-based catalytic processes for arene alkylation are unable to produce 1-aryl alkanes from arene and α -olefins. As promising starting materials for detergents, 1-aryl alkanes possess potential advantages relative to LABs. For example, it has been reported that 1-aryl alkanes show increased detergents power in low concentrations compared to 2- and 3-aryl alkanes.² Additionally, the less branched nature of 1-aryl alkanes are potentially more biodegradable than 2- and 3-aryl substituted alkanes.³ Traditional acid-mediated catalysis exclusively produces m-aryl alkanes ($m \geq 2$, i.e., Markovnikov addition products or branched products) due to the generation of carbocationic intermediates.⁴ The current route to straight-chain linear 1-aryl alkanes includes Friedel-Crafts acylation and subsequent Clemmensen reduction. However, this method is not economically viable for large-scale synthesis due to the high expense of the substrates. As a result, developing catalytic processes that are capable of producing 1-aryl alkanes or alkenes from basic chemical feedstocks, such as benzene and α -olefins, is of interest.

Arene alkylation/alkenylation catalyzed by transition metal complexes offers opportunities to synthesize 1-aryl alkanes or alkenes (i.e., anti-Markovnikov addition

products or linear products) from α -olefins and arenes. The linear to branched (L:B) ratio of alkyl or alkenyl arene products depends on the relative energetics of olefin insertion (*i.e.*, 2,1- versus 1,2-insertion) and/or the relative activation barriers for product formation following olefin insertion (*i.e.*, Curtin-Hammett kinetic conditions) (Scheme 4.1.1). For example, Scheme 4.1.1 shows the steps for conversion of a metal-phenyl complex and α -olefin to alkenyl arene with pathways to linear (anti-Markovnikov) and branched (Markovnikov) products. If the olefin insertion is irreversible, then the relative rate of 2,1-insertion versus 1,2-insertion will dictate the linear:branched selectivity. However, if the olefin insertion reactions are reversible, and establishment of an equilibrium of the metal-alkyl products that result from insertion occurs on a timescale that is more rapid than subsequent steps, Curtin-Hammett conditions apply. Under these conditions, the product ratio is determined by the K_{eq} between the insertion products *and* the relative rates of the subsequent reactions.

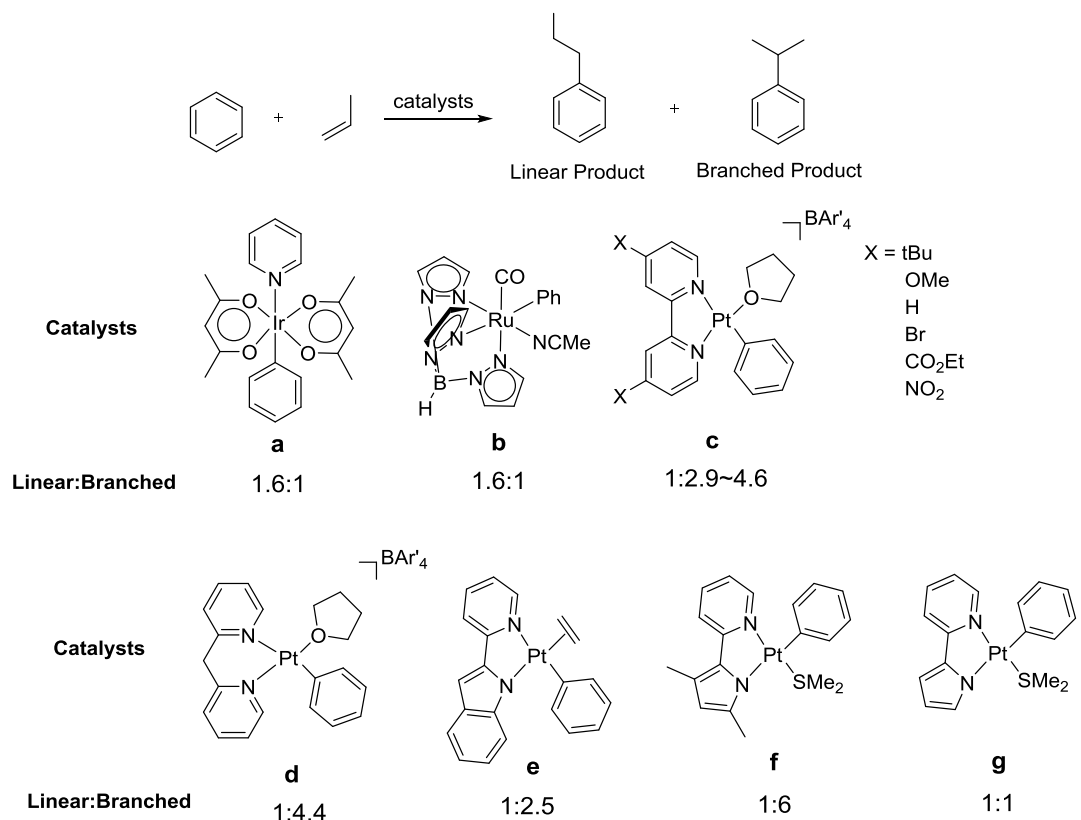


Scheme 4.1.1. Linear/branched product selectivity is controlled by the regioselectivity

of the olefin insertion and/or the relative rates of subsequent reactions following insertion.

Examples of metal-catalyzed arene alkylation/alkenylation to produce 1-aryl alkanes or alkenes have been reported. For olefin hydroarylation using propylene and benzene as reactants to produce phenyl propanes, (L)(Ph)Ir^{III}(acac)₂ (**a**) (L = pyridine or water) and TpRu(CO)(NCMe)Ph (**b**) both show selectivity for the anti-Markovnikov linear product 1-aryl propane with an approximate 1.6:1 ratio of linear to branched products, indicating a non-acid catalyzed mechanism (Scheme 4.1.2).^{5, 6} For our cationic Pt(II) complexes [(^xbpy)Pt(Ph)(THF)][BAr'₄] (**c**) (^xbpy = 4,4'-X-2,2'-bipyridyl, X = OMe, *t*Bu, H, Br, CO₂Et, NO₂; Ar' = 3, 5-bis(trifluoromethyl)phenyl), catalytic propylene (0.1 MPa) hydrophenylation is selective for branched products with L/B ratios ranging from 1:2.9-4.6 (Scheme 4.1.2).⁷ Substituting ^xbpy ligand with dpm (2,2'-dipyridylmethane) ligand does not have a substantial impact on L:B ratio. Catalysis with propylene using [(dpm)Pt(Ph)(THF)][BAr'₄] (**d**) (dpm = di(2-pyridyl)methane) leads to 1:4.4 linear/branched ratios (Scheme 4.1.2).⁸ In addition to cationic bipyridyl Pt(II) catalysts, charge neutral Pt complexes containing pyridyl-indolate ligands [(*t*BuPyInd)PtPh(SMe₂)] (*t*BuPyInd = 2-(4-(*tert*-butyl)pyridin-2-yl)-1*H*-indole) (**e**) reported by Tilley and co-workers yields branched cumene products with approximately 1:2.5 linear/branched ratio under 1 atm propylene pressure at 100 °C after 24 h (Scheme 4.1.2).⁹ This linear/branched selectivity is similar to that observed for our cationic bipyridyl-coordinated Pt complexes. Charge neutral (pyridyl)pyrrolide supported Pt(II) complexes developed by Goldberg and co-workers

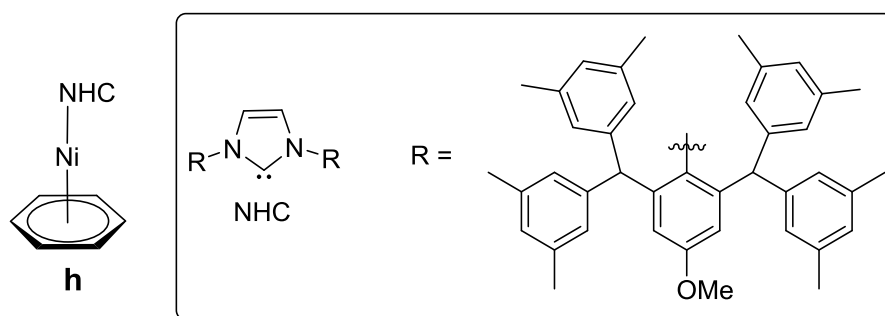
are capable of yielding anti-Markovnikov linear 1-aryl alkane products in arene alkylation with α -olefins, but only for specific olefins. For example, hydrophenylation of propylene using neutral Pt(II) complexes (dmpp)Pt(SMe₂)Ph (dmpp=3,5-dimethyl-2-(2-pyridyl)pyrrolide) (**f**) afford 18 TONs of total propyl benzene products (Scheme 4.1.2).¹⁰ This neutral (pyridyl)pyrrolide supported Pt(II) complexes are selective for cumene over *n*-propylbenzene with ~1:6 L/B ratio (Scheme 4.1.2).¹⁰ Varying the substituents on the (pyridyl)pyrrolide ligands allow effective tuning of the selectivity to anti-Markovnikov alkylarene production. Removing the methyl groups on the pyrrolide portion of the ligand resulted in changes in the linear/branched products selectivity. The complex **f** showed propensity for the Markovnikov product in hydroarylation of different α -olefins (L/B ratio of 15:85 for propylene hydroarylation, 16:83 for 1-hexene, 15:48 for neohexene).¹¹ In contrast, with complex **g**, under the same reaction conditions, the linear and branched products were formed in a 48:52 ratio for propylene hydroarylation (Scheme 4.1.2), 57:43 ratio for 1-hexene hydroarylation, and 85:5 for neohexene hydroarylation.¹¹ Chatani and co-workers reported Rh(I)-catalyzed hydroarylation of 1-hexene with 1-naphthylamide derivatives to selectively afford 1-aryl alkane in 46% yield.¹² Ackermann and co-workers reported Co(III)-catalyzed conversion of indoles and 1-octene to linear alkylated indoles with L/B ratio > 99:1.¹³ These Rh and Co mediated methods require picolinamide or pyridine directing groups.



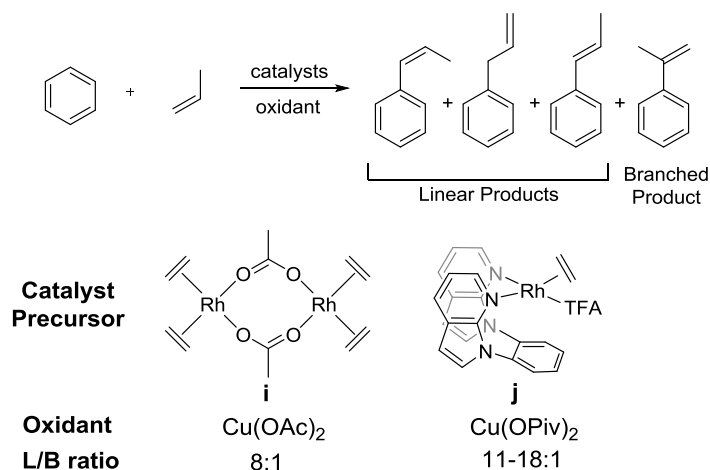
Scheme 4.1.2. Linear/branched selectivity of previously reported catalysts for propylene hydrophenylation.

To our knowledge, catalysts that convert unactivated arenes and α -olefins (propylene, 1-pentene, etc.) to alkyl or alkenyl products with high selectivity for anti-Markovnikov products are relatively rare. For olefin hydroarylation, Hartwig and coworkers demonstrated that using the Ni(0) complex **h** containing a sterically bulky NHC ligand as catalyst (Scheme 4.1.3). Using **h**, unactivated arenes and terminal α -olefins (e.g., 1-decene, *tert*-butylethylene and vinyl siloxanes) can be converted to desired linear alkyl arenes in good yields with linear/branched ratio > 50:1 in most reactions.¹⁴ When the catalyst loading is reduced to 0.3 mol%, 85% yield of 1-alkylarene product is achieved from *tert*-butylethylene and benzene, corresponding to 283 TOs. For benzene alkenylation with propylene to produce phenyl propanes, our

group previously found that $[\text{Rh}(\mu\text{-OAc})(\eta^2\text{-C}_2\text{H}_4)]_2$ (**i**) as catalyst precursor can selectively produce linear 1-aryl propenes with an ~8:1 linear to branched ratio (Scheme 4.1.4) (the linear:branched ratio depends on reaction conditions).¹⁵ Using $(5\text{-FP})\text{Rh}(\text{TFA})(\eta^2\text{-C}_2\text{H}_4)$ (**j**) (TFA = trifluoroacetate, 5-FP = 1,2-bis(*N*-7-azaindolyl)benzene) as catalyst precursor, a linear to branched ratio ranging from 11-18:1 is achieved using $\text{Cu}(\text{OPiv})_2$ as the oxidant (Scheme 4.1.4).¹⁶



Scheme 4.1.3. Structure of Ni complex **h**.



Scheme 4.1.4. Linear/branched selectivity of previously reported Rh(I) catalysts for oxidative propylene hydrophenylation.

With success of anti-Markovnikov selective Rh catalyst for arene alkenylation, we seek to develop catalysts based on Ir. Since Ir-mediated aromatic C–H bond activation, olefin insertion and β -hydride elimination have been demonstrated,¹⁷⁻²⁰ we

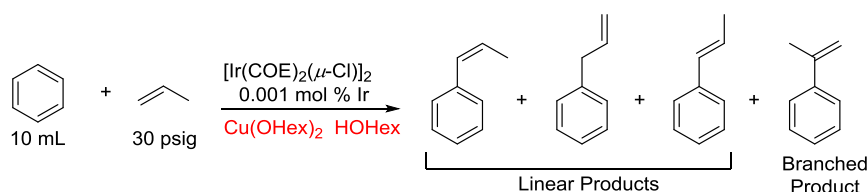
speculate that Ir complexes can combine aromatic C–H activation and olefin insertion into a single catalytic cycle. A previous Ir catalyst is selective for alkyl arene production,²¹⁻²⁵ but we speculated that Ir catalysts similar to our previously reported Rh catalysts^{15, 16, 26} might selectively produce alkenyl arenes. Compared to Rh(I) d⁸ square planar complexes, Ir(I) d⁸ analogs could exhibit different catalytic performance. This chapter outlines preliminary results using Ir(I)_catalyst precursors for the oxidative conversion of arene and olefins to alkenyl arenes.

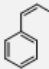
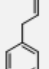
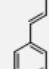
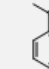
4.2 Results and Discussion

We initially examined [Ir(μ -Cl)(COE)]₂ as a catalyst precursor for the oxidative hydrophenylation of propylene (Table 4.2.1). Heating a 10 mL benzene solution of [Ir(μ -Cl)(COE)]₂ (0.001 mol% Ir relative to benzene) under 30 psig of ethylene at 150 °C in the presence of 240 equivalent of Cu(OHex)₂ (relative to Ir) and 480 equivalents of 2-ethyl hexanoic acid (relative to Ir) affords 24(4) TOs of propenyl benzenes with a L:B ratio of ~33:1 after 100 hours (Table 4.2.1). The formation of 10(2) TOs of biphenyl and 8(2) TOs of *p*henyl 2-ethylhexanoate (PhOHex) were also observed. The production of phenyl ester results from the background reaction that takes place upon heating Cu(OHex)₂ in benzene.¹⁶ To our knowledge, the observed L:B ratio is higher than any previously reported process for oxidative hydrophenylation of propylene. Before the reaction, the color of the reaction mixture is blue, which is the color of soluble copper(II) oxidant. After 100 hours, the solution

color turns bronze, indicating all the Cu(II) oxidant is consumed likely to form Cu(I) species. At this time point, 24 TOs of alkenyl arene products correspond to 20% yield based on Cu(OHex)₂ as limiting reagent (Table 4.2.1). We investigated the influence of temperature on the catalysis. Catalyst activity is increased by raising the temperature from 120 °C to 165 °C. Under the conditions studied, the optimal temperature is 165 °C, which yields 28(3) TOs of propenyl benzenes after 60 hours (the solution color turns bronze at this time point) (Table 4.2.1). Increasing the loading of acid by using 1200 equivalent of Cu(OHex)₂ (relative to Ir) and 4800 equivalents of 2-ethyl hexanoic acid (relative to Ir) results in an increase of L/B selectivity (~42:1) but decreased yield of propenyl benzenes (~11% based on Cu(II) as limiting reagent) when the solution color turns bronze after 84 hours (Table 4.2.1). We observed 12(4) TOs of biphenyl and 43(4) TOs of PhOHex as side products. In all cases, one of the linear products, allylbenzene, accounts for less than 25% of total phenylpropylene products (Table 4.2.1). In contrast, in Rh catalysis, more than 40% of phenylpropylene products are allylbenzene.^{15, 16} Allylbenzene is likely less thermodynamically favored relative to β- and α-methylstyrene.

Table 4.2.1. Results for Ir-catalyzed oxidative hydrophenylation of propylene under different conditions. The TOs are the average of a minimum of three experiments. Values in parentheses represent the standard deviations based on a minimum of three independent experiments. TOs are obtained by GC-FID.

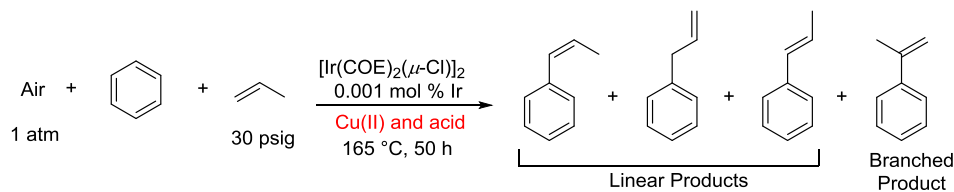


Oxidant	Temperature	Time (h)	Products/TOs				Total TO of propenyl benzene	L:B
								
240 eq. Cu(OHex) ₂ + 480 eq. HOHex	120	231	1.8(4)	0.7(1)	6(1)	0.38(4)	9(2)	23:1
240 eq. Cu(OHex) ₂ + 480 eq. HOHex	150	100	5(1)	1.2(3)	17(2)	0.7(2)	24(4)	33:1
240 eq. Cu(OHex) ₂ + 480 eq. HOHex	165	60	8(1)	0.7(1)	19(4)	1.0(2)	28(3)	27:1
1200 eq. Cu(OHex) ₂ + 4800 eq. HOHex	165	84	17(4)	6(3)	43(9)	1.6(1)	67(9)	42:1

We also studied Ir-catalyzed oxidative propylene hydroarylation under aerobic conditions using air as the in situ terminal oxidant and Cu(OHex)₂ as the co-oxidant. At 165 °C under 30 psig propylene and 1 atm air, 93(13) and 115(24) TOs of propenyl benzenes were formed after 50 hours in the presence of 120 and 240 equivalents of Cu(OHex)₂, respectively, corresponding to 155% yield (relative to 120 equivalent of Cu(OHex)₂) and 96% yield (relative to 240 equivalent of Cu(OHex)₂) (Table 4.2.2). Although the yield was increased under the aerobic conditions, the L/B ratio (L/B ratio < 20:1) is lower than that under anaerobic conditions (L/B ratio = ~30:1) (Table 4.2.2). The difference in L/B selectivity between aerobic and anaerobic catalysis is also observed in benzene propenylation using (5-FP)Rh(TFA)(η^2 -C₂H₄) catalyst.¹⁶ Replacing Cu(OHex)₂ with the same amount of Cu(OPiv)₂ afforded lower TOs and decreased L/B selectivity (Table 4.2.2).

Table 4.2.2. Results for [Ir(μ -Cl)(COE)]₂-catalyzed oxidative hydrophenylation of propylene under aerobic conditions using air as in situ terminal oxidant. The TOs are

the average of a minimum of three experiments. Values in parentheses represent the standard deviations based on a minimum of three independent experiments. TOs are obtained by GC-FID.

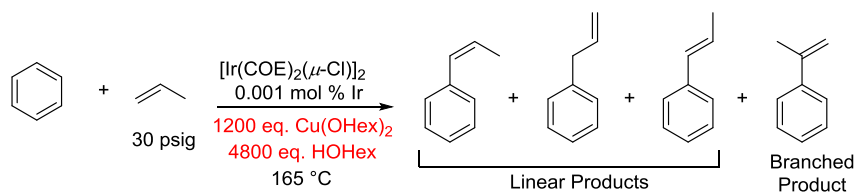


Oxidant	Total TO of propenyl benzene	L:B
120 eq. Cu(OPiv) ₂ + 1200 eq. HOPiv + 1 atm air	65(19)	12:1
240 eq. Cu(OPiv) ₂ + 2400 eq. HOPiv + 1 atm air	90(20)	11:1
120 eq. Cu(OHex) ₂ + 1200 eq. HOHex + 1 atm air	93(19)	16:1
240 eq. Cu(OHex) ₂ + 2400 eq. HOHex + 1 atm air	115(24)	14:1

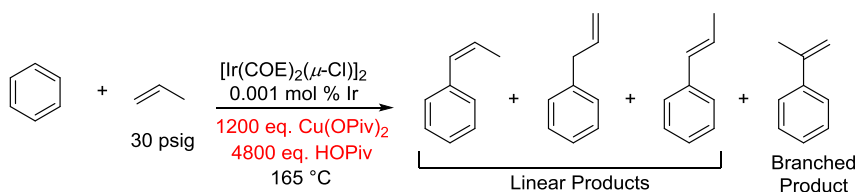
Using 0.0005 mol% of $[\text{Ir}(\mu\text{-Cl})(\text{COE})_2]$, 1200 equivalents of $\text{Cu}(\text{OHex})_2$ (relative to Ir), 4800 equivalents of 2-ethyl hexanoic acid (relative to Ir), 30 psig propylene at 165 °C as a standard set of conditions, the L/B ratio was monitored until the Cu(II) oxidant is consumed at 84 h. The L/B ratio increases from 15 to 42 as the reaction proceeds (Table 4.2.3). A rationalization for this observation will be discussed later. Substituting the $\text{Cu}(\text{OHex})_2$ with $\text{Cu}(\text{OPiv})_2$ under otherwise identical conditions produces afforded less satisfactory results, providing 43 TOs of propenyl benzene products and ~20:1 of L/B ratio when the Cu(II) oxidant is consumed at 50 h (Figure 4.2.1). An increase of L/B ratio as the reaction progresses was also observed.

Table 4.2.3. Results for $[\text{Ir}(\mu\text{-Cl})(\text{COE})_2]$ -catalyzed oxidative hydrophenylation of propylene using 1200 eq. $\text{Cu}(\text{OHex})_2$ (relative to per Ir atom) and 4800 eq. HOHex (relative to per Ir atom). Reaction conditions: 10 mL benzene, 0.0005 mol %

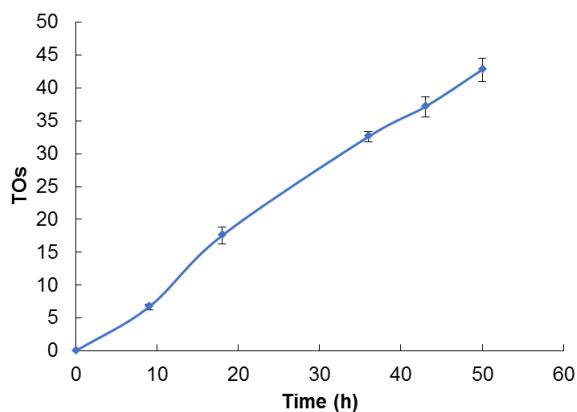
$[\text{Ir}(\mu\text{-Cl})(\text{COE})_2]_2$ (relative to benzene), 30 psig propylene, 165 °C. The TOs are the average of a minimum of three experiments. Values in parentheses represent the standard deviations based on a minimum of three independent experiments. TOs are obtained by GC-FID.



Reaction time	9 h	18 h	36 h	60 h	84 h
Total TOs	13(3)	24(5)	49(12)	65(12)	67(9)
L:B	15	23	35	40	42



TOs of total alkenyl benzene products



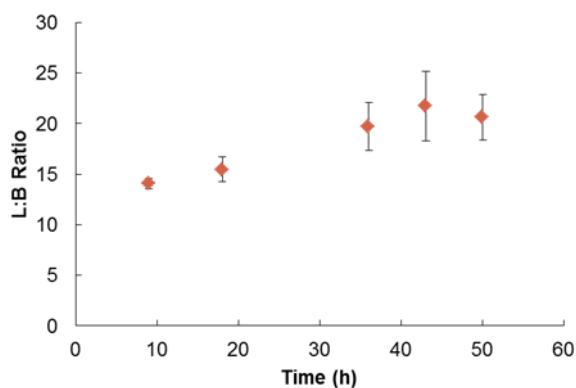
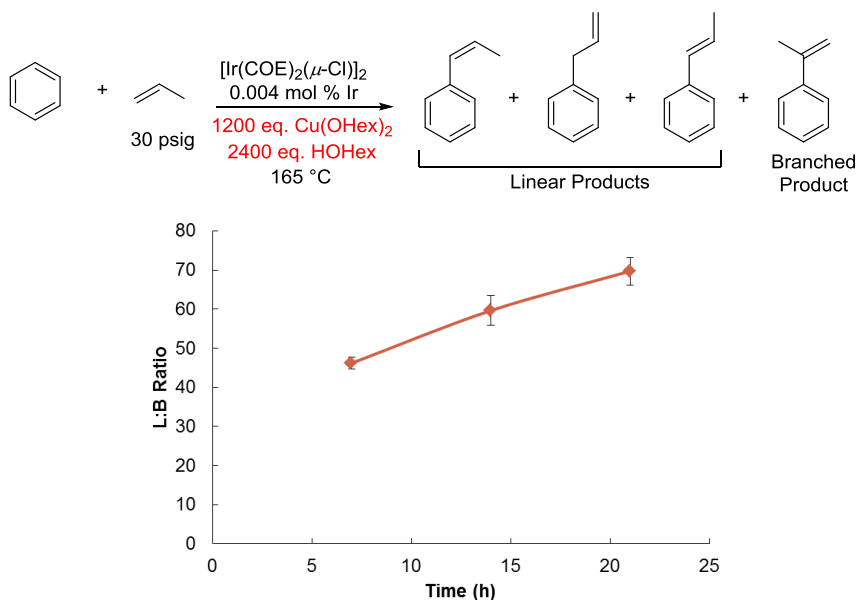


Figure 4.2.1. Results for $[\text{Ir}(\mu\text{-Cl})(\text{COE})_2]_2$ -catalyzed oxidative hydrophenylation of propylene using 1200 eq. $\text{Cu}(\text{OPiv})_2$ (relative to per Ir atom) and 4800 eq. HOPIv (relative to per Ir atom). Reaction conditions: 10 mL benzene, 0.0005 mol % $[\text{Ir}(\mu\text{-Cl})(\text{COE})_2]_2$ (relative to benzene), 30 psig propylene, 165 °C. The TOs are the average of a minimum of three experiments. Each data point represents the average of three separate experiments. Error bars represent the standard deviations based on a minimum of three independent experiments.

When the catalyst loading is increased to 0.002 mol% of $[\text{Ir}(\mu\text{-Cl})(\text{COE})_2]_2$, monitoring the observed L/B selectivity with reaction time reveals that L/B ratio increases from 46 (at 7 h) to 70 (at 21 h) (Figure 4.2.2).



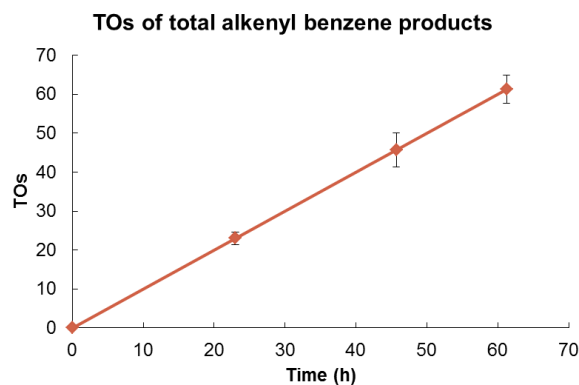


Figure 4.2.2. Results for $[\text{Ir}(\mu\text{-Cl})(\text{COE})]_2$ -catalyzed oxidative hydrophenylation of propylene using 0.004 mol% of Ir (relative to benzene). Reaction conditions: 10 mL benzene, 1200 eq. $\text{Cu}(\text{OHex})_2$ (relative to per Ir atom), 2400 eq. HOHex (relative to per Ir atom), 0.002 mol % $[\text{Ir}(\mu\text{-Cl})(\text{COE})]_2$ (relative to benzene), 30 psig propylene, 165 °C. The TOs are the average of a minimum of three experiments. Each data point represents the average of three separate experiments. Error bars represent the standard deviations based on a minimum of three independent experiments.

To increase the reaction yield without sacrificing L/B selectivity, oxidative propylene hydroarylation with *in situ* aerobic Cu(II) regeneration (two-stage copper recycling method) was performed (Figure 4.2.3). That is, the catalysis is run under anaerobic conditions with 240 equivalent of $\text{Cu}(\text{OHex})_2$ and 1200 equivalents of 2-ethyl hexanoic acid. After all the Cu(II) oxidant is consumed, the solution color turns bronze. $\text{Cu}(\text{OHex})_2$ was regenerated *in situ* by heating the reaction mixture under air at 120 °C until the solution color turns greenish blue. After regeneration of Cu(II), air was removed with a propylene purge and oxidative propylene hydroarylation was continued. Activity of $[\text{Ir}(\mu\text{-Cl})(\text{COE})]_2$ (as catalyst precursor) continues after 10 air cycling procedures and ~60 TOs was achieved after 126 hours, corresponding to 50% yield based on Cu(II) (Figure 4.2.3). A 37:1 L/B ratio was achieved (Figure 4.2.3). The generation of 29(2) TOs of biphenyl and 126(4) TOs of PhOHex side products were also observed.

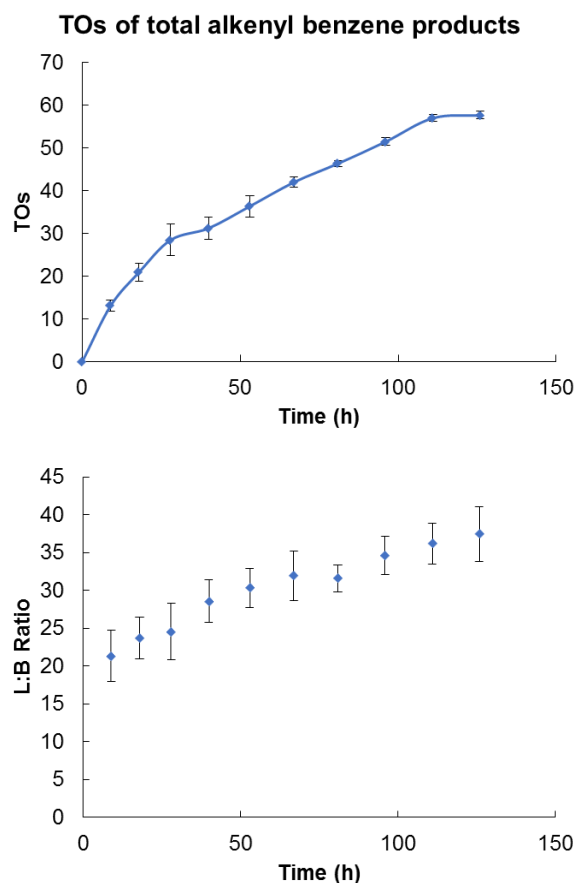
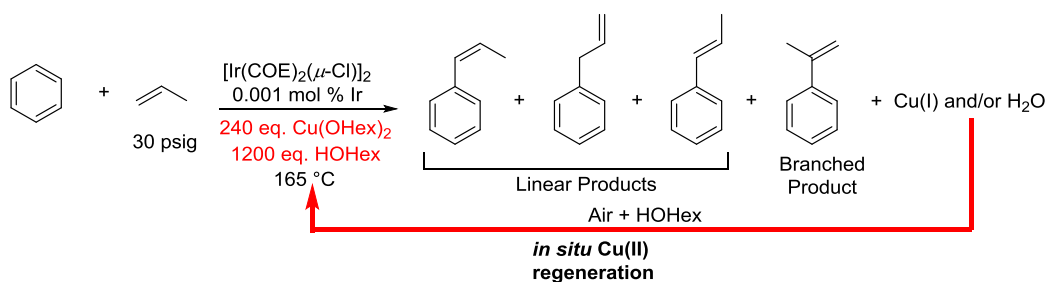
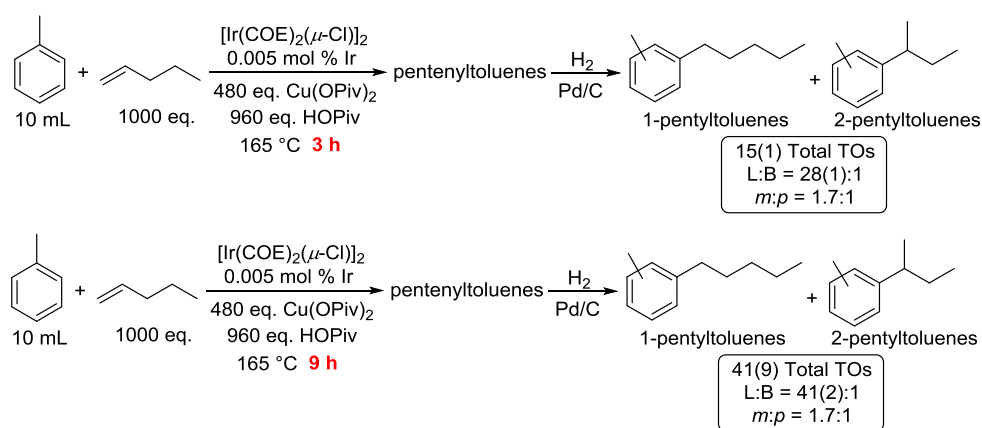


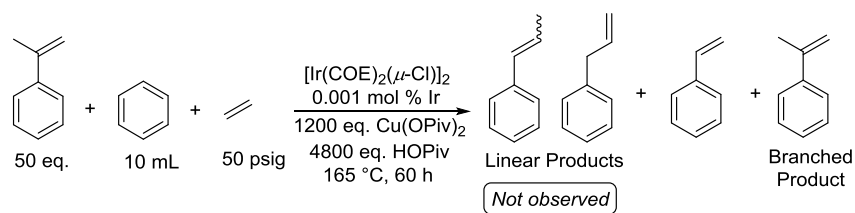
Figure 4.2.3. Results for $[\text{Ir}(\mu\text{-Cl})(\text{COE})_2]_2$ -catalyzed oxidative hydrophenylation of propylene with in situ aerobic Cu(II) regeneration (two-stage copper recycling method). The reactor is charged with 1 atm air and 70 psig of N_2 at every sampling point for regenerating Cu(II) oxidant at 120°C , and then air was removed with a propylene purge and oxidative propylene hydroarylation was continued. Reaction conditions: 10 mL benzene, 240 eq. $\text{Cu}(\text{OHex})_2$ (relative to per Ir atom), 1200 eq. HOHex (relative to per Ir atom), 0.0005 mol % $[\text{Ir}(\mu\text{-Cl})(\text{COE})_2]_2$ (relative to benzene), 30 psig propylene, 165°C . Each data point represents the average of three separate experiments. Error bars represent the standard deviations based on a minimum of three independent experiments.

substituted olefins and arenes. We have reported a Rh-catalyzed alkenylation of toluene with 1-pentene to synthesize meta- and para substituted 1-pentenyltoluenes and 2-pentenyltoluenes, which can serve as potential starting material for bicyclic compounds.²⁷ Using $[\text{Ir}(\mu\text{-Cl})(\text{COE})]_2$ (0.005 mol% Ir) as the catalyst precursor, 1-pentenyltoluenes and 2-pentenyltoluenes can be prepared from toluene and 1-pentene. Upon hydrogenation, 41(9) TOs of pentyltoluenes, and a meta:para ratio of ~1.7:1 were observed after 9 hours (Scheme 4.2.1). The observed meta/para ratio is similar to the meta/para ratio (1.9:1) observed in the catalysis using $[\text{Rh}(\eta^2\text{-C}_2\text{H}_4)_2(\mu\text{-OAc})]_2$ (0.005 mol% Rh) and $\text{Cu}(\text{OHex})_2$ (240 equivalent).²⁷ The ortho products account for < 1% of the total pentyltoluene products. As expected, increase of L/B (1-pentenyltoluenes/2-pentenyltoluenes) ratio from 28(1):1 (at 3 h) to 41(2):1 (at 9 h) was observed (Scheme 4.2.1). The meta/para ratio remains unchanged during the catalysis.



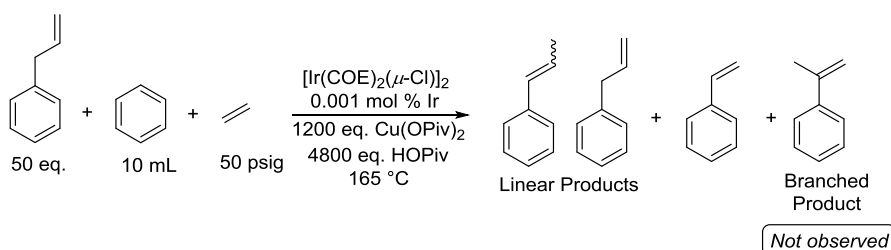
Scheme 4.2.1. $[\text{Ir}(\mu\text{-Cl})(\text{COE})]_2$ -catalyzed alkenylation of toluene with 1-pentene. Reaction conditions: 10 mL toluene, 480 eq. $\text{Cu}(\text{OHex})_2$ (relative to per Ir atom), 960 eq. HOHex (relative to per Ir atom), 0.0025 mol % $[\text{Ir}(\mu\text{-Cl})(\text{COE})]_2$ (relative to toluene), 1000 eq. 1-pentene (relative to per Ir atom), 165 °C. Each data point represents the average of three separate experiments. Error bars represent the standard deviations based on a minimum of three independent experiments.

We speculated that the increase of L/B ratio results from the possible isomerization of branched phenylpropylene products to linear products catalyzed by Ir. To test this hypothesis, we added 50 equivalents of branched phenylpropylene product α -methylstyrene (relative to Ir) at the beginning of a catalytic reaction using benzene and ethylene to produce styrene. After 60 h of the catalytic reaction, linear phenylpropylene products were not observed (Scheme 4.2.2), indicating the isomerization of branched α -methylstyrene to linear phenylpropylene products does not occur under the catalytic conditions. Therefore, we believe that the isomerization of phenylpropylene products does not account for the increase of observed L/B ratio. Adding 50 equivalents of linear phenylpropylene product allyl benzene (relative to Ir) at the beginning of Ir-catalyzed benzene ethylation yields 2(1) equivalents of cis- β -methylstyrene and 18(5) equivalents of trans- β -methylstyrene with 23(3) equivalents of unreacted allyl benzene after 12 hours (Table 4.2.4). This result suggests a facile isomerization of linear allyl benzene to the other two linear products under the catalytic conditions, which provides possible explanations for reduced selectivity for allyl benzene products in Ir-catalyzed benzene propenylation relative to that in Rh catalysis (see above). The conversion of linear allyl benzene to branched α -methylstyrene was not observed under these conditions (Table 4.2.4). Therefore, isomerization of linear phenylpropylene products allyl benzene likely does not impact observed L/B ratios.



Scheme 4.2.2. Isomerization of α -methylstyrene in $[\text{Ir}(\mu\text{-Cl})(\text{COE})]_2$ -catalyzed benzene alkenylation with ethylene. Reaction conditions: 10 mL benzene, 50 eq. α -methylstyrene (relative to per Ir atom), 1200 eq. $\text{Cu}(\text{OHex})_2$ (relative to per Ir atom), 4800 eq. HOHex (relative to per Ir atom), 0.0005 mol % $[\text{Ir}(\mu\text{-Cl})(\text{COE})]_2$ (relative to benzene), 50 psig ethylene, 165 °C, 60 h. Each data point represents the average of three separate experiments. Error bars represent the standard deviations based on a minimum of three independent experiments.

Table 4.2.4. Isomerization of allyl benzene to *cis*- β -methylstyrene and *trans*- β -methylstyrene in $[\text{Ir}(\mu\text{-Cl})(\text{COE})]_2$ -catalyzed benzene alkenylation with ethylene. Reaction conditions: 10 mL benzene, 50 eq. allylbenzene (relative to per Ir atom), 1200 eq. $\text{Cu}(\text{OHex})_2$ (relative to per Ir atom), 4800 eq. HOHex (relative to per Ir atom), 0.0005 mol % $[\text{Ir}(\mu\text{-Cl})(\text{COE})]_2$ (relative to benzene), 50 psig ethylene, 165 °C, 60 h. The equivalents are the average of a minimum of three experiments. Values in parentheses represent the standard deviations based on a minimum of three independent experiments. TOs are obtained by GC-FID.



Reaction time (h)	Products/eq.				Total eq. of propenyl benzenes
0	0	50	0	0	50
12	2(1)	23(3)	18(5)	0	43(6)

Different rates of reaction of the four phenylpropylene products could result in the increase of observed L/B ratio. To study that, we added four phenylpropylene

products (60 equivalent of total products and L/B ratio of 24:1, which is approximately those of phenylpropylene products after 18 h of catalysis under optimal conditions) at the beginning of the catalysis with propylene. If the decay of branched product is substantial while the decay of linear products is not significant under this reaction condition, the increase of L/B ratio with reaction time will be observed. However, in contrast with the trend observed in catalysis under optimal conditions, the L/B ratio decreased from an initial 24:1 to 18:1 after 18 hours (Figure 4.2.4), indicating different rates of reaction of the four phenylpropylene products likely does not account for the increase of observed L/B ratio.

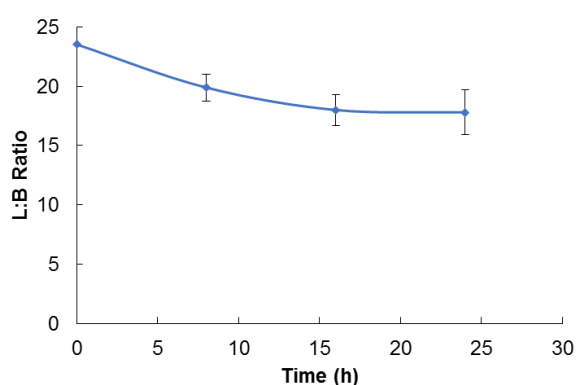
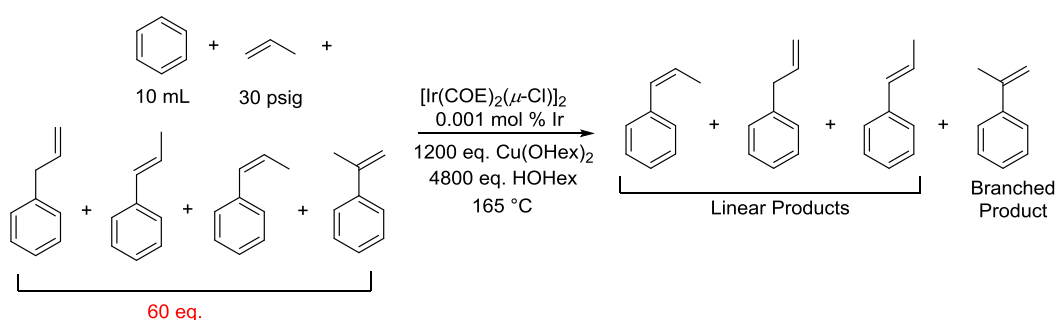


Figure 4.2.4. Plots of L/B ratio of 4 phenylpropylene products versus time under catalytic conditions. Reaction conditions: 10 mL C₆H₆, [Ir(μ-Cl)(COE)]₂ (0.001 mol% of Ir relative to benzene), 1200 equivalent of Cu(OHex)₂ (relative to per Ir atom), 4800 equivalents of 2-ethyl hexanoic acid (relative to per Ir atom), 30 psig propylene, 1.5 eq. of allylbenzene, 2.5 eq. of α-methylstyrene, 15 eq. of cis-β-methylstyrene, 40 eq. of trans-β-methylstyrene, 165 °C. Each data point represents the average of three

separate experiments. Error bars represent the standard deviations based on a minimum of three independent experiments.

Based on aforementioned studies, we hypothesize the intrinsic L/B selectivity of Ir catalyst likely changes as the reaction proceeds. This could be due to the original Ir catalyst evolving to a new Ir catalyst with high L/B selectivity or a change in the reaction conditions that favors higher linear selectivity.

4.3 Conclusions

We have demonstrated Ir-catalyzed arene alkenylation using unactivated α -olefins and unactivated arenes with high selectivity for linear 1-aryl alkene products. Up to 70:1 linear/branched ratio is accomplished under optimized conditions. The L/B ratio increases over the course of the reaction, which is hypothesized to result from the change of the identity of the Ir catalyst or reaction conditions. Compared to previously-reported Rh catalysis for arene alkenylation, the Ir catalyst exhibits higher L/B selectivity but decreased TOs and much lower product yield relative to Cu(II) oxidant. Ir catalyst is less selective for the formation of allyl benzene relative to Rh catalyst, which is potentially due to facile Ir-catalyzed isomerization of allyl benzene to more thermodynamically favorable β -methylstyrene products. The Ir catalysts show similar meta/para product ratio to Rh catalysts for toluene alkenylation with 1-pentene. Another highly anti-Markovnikov catalyst Ni(NHC) **h** developed by the Hartwig group is able to achieve linear/branched ratios > 50:1 in most reactions with

α -alkenes.¹⁴ Different from the Ir catalysis disclosed in this chapter, The Ni catalysis is selective for saturated alkyl arene production. Further study to understand the increase of L/B ratio during the catalysis and optimization of Ir-catalyzed arene alkenylation reactions to enhance catalyst reactivity, longevity and product yield are continuing in our laboratories.

4.4 Experimental Section

General Considerations. Glovebox purity was maintained by periodic nitrogen purges and was monitored by an oxygen analyzer (O_2 concentration was < 15 ppm for all reactions). Benzene was dried by passage through columns of activated alumina. Propylene and hydrogen were purchased in gas cylinders from GTS-Welco and used as received. All other reagents were purchased from commercial sources and used as received. $[Ir(\mu-Cl)(COE)]_2$ was prepared according to a literature procedure.²⁸ GC/FID was performed using a Shimadzu GC-2014 system with a 30 m x 90.25 mm HP5 column with 0.25 μ m film thickness. GC-MS was performed using a Shimadzu GCMS-QP2010 Plus instrument with a 30 m \times 0.25 mm SHRXI-5MS column with a 0.25 μ m thickness using electron impact (EI) ionization was used.

To analyze reaction mixture samples by GC-FID, the reactors were cooled to room temperature, sampled under N_2 , recharged with gases, and reheated. Aliquots of the resulting solution (< 100 μ L) were washed with saturated sodium carbonate solution (0.25 mL). The aqueous and organic layers were separated. The resulting organic

layers were analyzed by GC/FID.

Phenyl 2-ethylhexanoate, biphenyl, allylbenzene, α -methylstyrene, *cis*- β -methylstyrene and *trans*- β -methylstyrene production were quantified using linear regression analysis of gas chromatograms of standard samples of authentic products. A plot of peak area ratios versus molar ratios gave a regression line using hexamethylbenzene as the internal standard. The slopes and correlation coefficients of the regression lines were 1.03 and 0.99 (phenyl 2-ethylhexanoate), 1.07 and 0.99 (biphenyl), 1.40 and 0.99 (allylbenzene), 1.23 and 0.99 (α -methylstyrene), 1.47 and 0.99 (*cis*- β -methylstyrene), 1.38 and 0.99 (*trans*- β -methylstyrene) respectively.

To analyze reaction mixture samples by GC-MS, plots of peak areas versus molar ratios gave regression lines using cyclooctane as the internal standard. 1-tolyl-1-pentane production was quantified using linear regression analysis of gas chromatograms of standard samples of authentic products. The slope and correlation coefficient of the regression lines were 1.34 and 0.998 (1-m-tolyl-1-pentane), 1.85 and 0.997 (1-p-tolyl-1-pentane) and 1.84 and 0.998 (1-o-tolyl-1-pentane), respectively. The production of 2-tolyl-2-pentenenes was quantified using the slope and correlation coefficient for a fit of cumene versus n-propylbenzene, which enabled an approximation of the ratio of 1-tolyl-1-pentenenes to 2-tolyl-2-pentenenes. The slope and correlation coefficient of the regression line were 1.24 and 0.98 for cumene versus n-propylbenzene, respectively.

Anaerobic alkenylation of benzene with propylene using $[\text{Ir}(\mu\text{-Cl})(\text{COE})_2]$ as catalyst precursor and Cu(II) as oxidant. Representative catalytic reactions are

described here. A stock solution containing $[\text{Ir}(\mu\text{-Cl})(\text{COE})_2]$ (0.011 mmol Ir, 0.001 mol % of Ir relative to benzene), hexamethylbenzene (0.073 g, 0.46 mmol), and benzene (200 mL) was prepared in a volumetric flask. Fisher-Porter reactors were charged with stock solution (10 mL), Cu(II) oxidant, acid, and phenylpropylene product (if any). The vessels were sealed, pressurized with propylene (30 psig), and subsequently stirred and heated to 120, 150 or 165 °C. The resulting product mixture was analyzed by GC–FID.

Aerobic alkenylation of benzene with propylene using $[\text{Ir}(\mu\text{-Cl})(\text{COE})_2]$ as catalyst precursor, air as in situ terminal oxidant and $\text{Cu}(\text{OHex})_2$ as the co-oxidant. A stock solution containing $[\text{Ir}(\mu\text{-Cl})(\text{COE})_2]$ (0.011 mmol Ir, 0.001 mol % of Ir relative to benzene), hexamethylbenzene (0.073 g, 0.46 mmol), and benzene (200 mL) was prepared in a volumetric flask. Fisher-Porter reactors were charged with stock solution (10 mL), Cu(II) oxidant and acid. The vessels were sealed, and purged with 1 atm of air, pressurized with propylene (30 psig), and subsequently stirred and heated to 165 °C. The resulting product mixture was analyzed by GC–FID. *The mixture of hydrocarbons and air is flammable and potentially explosive. Taking proper safety precaution (e.g., blast shield, burst valves for pressure relief) and avoiding any possible ignition source was advised.*

Alkenylation of benzene with propylene using $[\text{Ir}(\mu\text{-Cl})(\text{COE})_2]$ as catalyst precursor with *in situ* aerobic Cu(II) regeneration (two-stage copper recycling method) A stock solution containing $[\text{Ir}(\mu\text{-Cl})(\text{COE})_2]$ (0.011 mmol Ir, 0.001 mol % of Ir relative to benzene), hexamethylbenzene (0.073 g, 0.46 mmol), and benzene

(200 mL) was prepared in a volumetric flask. Fisher-Porter reactors were charged with stock solution (10 mL), Cu(II) oxidant and acid. The vessels were sealed, and purged with 1 atm of air, pressurized with propylene (30 psig), and subsequently stirred and heated to 165 °C. At the beginning of the reaction, the color of the reaction mixture is blue, which is the color of soluble copper(II) oxidant. After all the Cu(II) oxidant is consumed to form Cu(I) species for oxidative propylene hydroarylation, the solution color turns bronze. The reaction was sampled when the solution turned bronze. The resulting product mixture was analyzed by GC-FID. After the sampling, Cu(OHex)₂ was regenerated *in situ* by heating the reaction mixture under 1 atm air at 120 °C until the solution color turns greenish blue. After regeneration of Cu(II), the reactors were cooled to room temperature, air was removed with a propylene purge and oxidative propylene hydroarylation was continued. *The mixture of hydrocarbons and air is flammable and potentially explosive. Taking proper safety precaution (e.g., blast shield, burst valves for pressure relief) and avoiding any possible ignition source was advised.*

Catalytic alkenylation of toluene with 1-pentene using [Ir(μ -Cl)(COE)]₂ as catalyst precursor and Cu(OHex)₂ as oxidant. A stock solution containing [Ir(μ -Cl)(COE)]₂ (0.056 mmol Ir, 0.005 mol % of Ir relative to benzene), cyclooctane (252 μ L, 20 equiv relative to Ir), and benzene (200 mL) was prepared in a volumetric flask. Fisher-Porter reactors were charged with stock solution (10 mL), Cu(II) oxidant, acid, and 1-pentene (1000 equivalent relative to Ir). The vessels were sealed, pressurized with N₂ (70 psig), and subsequently stirred and heated to 165 °C. The

reactions were sampled at 3 h and 9 h. Aliquots of the resulting solution (< 200 μ L) were washed with saturated sodium carbonate solution (0.25 mL). The aqueous and organic layers were separated. The resulting organic layers were subject to hydrogenation..

Hydrogenation Procedure. A Fischer–Porter reactor was charged with aliquots of the reaction mixture, 8 mg of 10% Pd/C and 4 mL of ethanol. The vessels were sealed and pressurized with 100 psi of H₂ after the headspace was evacuated. The reactor was stirred at room temperature overnight. The resulting product mixture was analyzed by GC–MS.

4.5 References

1. Marcilly, C. Superacids and Bases of Interest in Catalysis. In *Acido-Basic Catalysis* Editions Technip: Paris; 2006; Vol. 1, pp 57-130.
2. Baumgartner, F. N. Relation of Molecular Structure to Detergency of Some Alkylbenzene Sulfonates. *Ind. Eng. Chem.* **1954**, *46*, 1349-1352.
3. Eckert, M.; Fleischmann, G.; Jira, R.; Bolt, H. M.; Golka, K. Acetaldehyde in *Ullmann's Encyclopedia of Industrial Chemistry*; Wiley-VCH Verlag GmbH & Co. KGaA: 2000.
4. Zhu, W.; Gunnoe, T. B. Advances in Rhodium-Catalyzed Oxidative Arene Alkenylation. *Acc. Chem. Res.* **2020**, *53*, 920-936.
5. Lail, M.; Arrowood, B. N.; Gunnoe, T. B. Addition of Arenes to Ethylene and Propene Catalyzed by Ruthenium. *J. Am. Chem. Soc.* **2003**, *125*, 7506-7507.
6. Matsumoto, T.; Taube, D. J.; Periana, R. A.; Taube, H.; Yoshida, H. Anti-Markovnikov Olefin Arylation Catalyzed by an Iridium Complex. *J. Am. Chem. Soc.* **2000**, *122*, 7414-7415.
7. McKeown, B. A.; Prince, B. M.; Ramiro, Z.; Gunnoe, T. B.; Cundari, T. R. Pti-Catalyzed Hydrophenylation of A-Olefins: Variation of Linear/Branched Products as a Function of Ligand Donor Ability. *ACS Catal.* **2014**, *4*, 1607-1615.
8. McKeown, B. A.; Gonzalez, H. E.; Michaelos, T.; Gunnoe, T. B.; Cundari, T. R.; Crabtree, R. H.; Sabat, M. Control of Olefin Hydroarylation Catalysis Via a

Sterically and Electronically Flexible Platinum(II) Catalyst Scaffold. *Organometallics* **2013**, *32*, 3903-3913.

9. Suslick, B. A.; Liberman-Martin, A. L.; Wambach, T. C.; Tilley, T. D. Olefin Hydroarylation Catalyzed by (Pyridyl-Indolate)Pt(II) Complexes: Catalytic Efficiencies and Mechanistic Aspects. *ACS Catal.* **2017**, *7*, 4313-4322.

10. Luedtke, A. T.; Goldberg, K. I. Intermolecular Hydroarylation of Unactivated Olefins Catalyzed by Homogeneous Platinum Complexes. *Angew. Chem., Int. Ed.* **2008**, *47*, 7694-7696.

11. Clement, M. L.; Grice, K. A.; Luedtke, A. T.; Kaminsky, W.; Goldberg, K. I. Platinum(II) Olefin Hydroarylation Catalysts: Tuning Selectivity for the Anti-Markovnikov Product. *Chem. - Eur. J.* **2014**, *20*, 17287-17291.

12. Rej, S.; Chatani, N. Rhodium(I)-Catalyzed C8-Alkylation of 1-Naphthylamide Derivatives with Alkenes through a Bidentate Picolinamide Chelation System. *ACS Catal.* **2018**, *8*, 6699-6706.

13. Zell, D.; Bursch, M.; Müller, V.; Grimme, S.; Ackermann, L. Full Selectivity Control in Cobalt(III)-Catalyzed C-H Alkylations by Switching of the C-H Activation Mechanism. *Angew. Chem. Int. Ed.* **2017**, *56*, 10378-10382.

14. Saper, N. I.; Ohgi, A.; Small, D. W.; Semba, K.; Nakao, Y.; Hartwig, J. F. Nickel-Catalysed Anti-Markovnikov Hydroarylation of Unactivated Alkenes with Unactivated Arenes Facilitated by Non-Covalent Interactions. *Nature Chemistry* **2020**, *12*, 276-283.

15. Webster-Gardiner, M. S.; Chen, J.; Vaughan, B. A.; McKeown, B. A.; Schinski, W.; Gunnoe, T. B. Catalytic Synthesis of "Super" Linear Alkenyl Arenes Using an Easily Prepared Rh(I) Catalyst. *J. Am. Chem. Soc.* **2017**, *139*, 5474-5480.

16. Chen, J.; Nielsen, R. J.; Goddard, W. A.; McKeown, B. A.; Dickie, D. A.; Gunnoe, T. B. Catalytic Synthesis of Superlinear Alkenyl Arenes Using a Rh(I) Catalyst Supported by a "Capping Arene" Ligand: Access to Aerobic Catalysis. *J. Am. Chem. Soc.* **2018**, *140*, 17007-17018.

17. Gao, Y.; Guan, C.; Zhou, M.; Kumar, A.; Emge, T. J.; Wright, A. M.; Goldberg, K. I.; Krogh-Jespersen, K.; Goldman, A. S. B-Hydride Elimination and C-H Activation by an Iridium Acetate Complex, Catalyzed by Lewis Acids. Alkane Dehydrogenation Cocatalyzed by Lewis Acids and [2,6-Bis(4,4-Dimethyloxazolonyl)-3,5-Dimethylphenyl]Iridium. *J. Am. Chem. Soc.* **2017**, *139*, 6338-6350.

18. Oxgaard, J.; Muller, R. P.; Goddard, W. A.; Periana, R. A. Mechanism of Homogeneous Ir(III) Catalyzed Regioselective Arylation of Olefins. *J. Am. Chem. Soc.* **2004**, *126*, 352-363.

19. Ishiyama, T.; Takagi, J.; Ishida, K.; Miyaura, N.; Anastasi, N. R.; Hartwig, J. F. Mild Iridium-Catalyzed Borylation of Arenes. High Turnover Numbers, Room Temperature Reactions, and Isolation of a Potential Intermediate. *J. Am. Chem. Soc.* **2002**, *124*, 390-391.

20. Oxgaard, J.; Tenn, W. J.; Nielsen, R. J.; Periana, R. A.; Goddard, W. A. Mechanistic Analysis of Iridium Heteroatom C-H Activation: Evidence for an Internal Electrophilic Substitution Mechanism. *Organometallics* **2007**, *26*, 1565-1567.

-
21. Heiden, Z. M.; Rauchfuss, T. B. Homogeneous Catalytic Reduction of Dioxygen Using Transfer Hydrogenation Catalysts. *J. Am. Chem. Soc.* **2007**, *129*, 14303-14310.
22. Chowdhury, S.; Himo, F.; Russo, N.; Sicilia, E. Mechanistic Investigation of the Hydrogenation of O₂ by a Transfer Hydrogenation Catalyst. *J. Am. Chem. Soc.* **2010**, *132*, 4178-4190.
23. Keith, J. M.; Teets, T. S.; Nocera, D. G. O₂ Insertion into Group 9 Metal-Hydride Bonds: Evidence for Oxygen Activation through the Hydrogen-Atom-Abstraction Mechanism. *Inorg. Chem.* **2012**, *51*, 9499-9507.
24. Teets, T. S.; Nocera, D. G. Acidolysis and Oxygen Atom Transfer Reactivity of a Diiridium Hydroperoxo Complex. *Dalton Trans.* **2013**, *42*, 3521-3527.
25. Wright, A. M.; Pahls, D. R.; Gary, J. B.; Warner, T.; Williams, J. Z.; M. Knapp, S. M.; Allen, K. E.; Landis, C. R.; Cundari, T. R.; Goldberg, K. I. Experimental and Computational Investigation of the Aerobic Oxidation of a Late Transition Metal-Hydride. *J. Am. Chem. Soc.* **2019**, *141*, 10830-10843.
26. Vaughan, B. A.; Webster-Gardiner, M. S.; Cundari, T. R.; Gunnoe, T. B. A Rhodium Catalyst for Single-Step Styrene Production from Benzene and Ethylene. *Science* **2015**, *348*, 421-424.
27. Liebov, N. S.; Zhu, W.; Chen, J.; Webster-Gardiner, M. S.; Schinski, W. L.; Gunnoe, T. B. Rhodium-Catalyzed Alkenylation of Toluene Using 1-Pentene: Regioselectivity to Generate Precursors for Bicyclic Compounds. *Organometallics* **2019**, *38*, 3860-3870.
28. Onderdelinden, A. L.; van der Ent, A. Chloro- and Bromo-(Alkene)Iridium(I) Complexes. *Inorg. Chim. Acta* **1972**, *6*, 420-426.

5 Future outlook

5.1 Future Direction of Rh-Catalyzed Arene Alkenylation

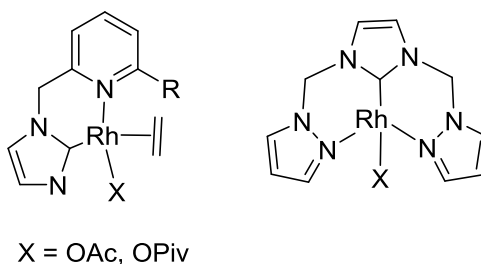
Molecular Rh complexes are successful for arene alkenylation in the presence of oxidants (Cu(II) and/or air). The transformations have been demonstrated to exhibit important features including catalyst longevity (at least for styrene production), high activity, and unique selectivity including both ortho/meta/para selectivity for alkenylation of substituted arenes and anti-Markovnikov selectivity for arene alkenylation using α -olefins. Despite these features, questions and challenges remain for possible extension to large-scale chemical production. For example, for large-scale catalysis, a commonly referred to target is activity in the range of TOFs $\sim 1 \text{ s}^{-1}$. Thus, our most efficient Rh catalyzed styrene formation with TOF $\sim 0.06 \text{ s}^{-1}$ needs further optimization studies to reach the range of this standard. For styrene production the reactions are performed in neat benzene, and the current best yield of styrene (based on benzene) is $\sim 3\%$. Demonstrating high selectivity at conversions $> 10\%$ (and ideally, much higher) is important. This will require that the catalytic process avoid divinylation as well as styrene polymerization at higher concentrations. In addition, high substrate conversion can potentially result in an increased propensity toward formation of other side products such as stilbene and benzaldehyde (when air/O₂ is used as the sole oxidant). Also, at higher benzene conversions, ethylene functionalization could become an issue. Quantification of these various products

under different catalyst conditions and higher conversion is important.

In Chapter 3, Rh-catalyzed aerobic arene alkenylation reactions incorporate large amount of acetic acid (benzene/HOAc ratio (v/v) up to 3:1). Our studies reveal that excess carboxylic acid likely suppresses the decomposition of Rh catalysts, especially under aerobic conditions in the absence of Cu(II) oxidant. Therefore, acetic acid (and other acids, potentially) serves as a promising solvent to enable studies of high benzene conversion. Increasing Rh catalyst loading may also be beneficial for accomplishing high arene conversion. For styrene production, we have demonstrated long-lived Rh catalysis for days with thousands of TOs with no evidence of catalyst decomposition. However, such catalyst longevity has not been demonstrated for other substrates, and some studies have indicated that other olefins might result in reduced catalyst stability.¹ But, catalyst longevity as a function of substrate identity needs better quantification.

In Chapter 2, we demonstrated that diimine Rh complexes readily dissociate diimine ligands and are likely converted into the same catalytically active Rh species under catalytic conditions. Thus, ligand effect on catalysis was not accessible for this and related Rh complexes (not included in this thesis). Studying catalysis using Rh(I) complexes with new ligand motifs that will remain coordinated to Rh during catalysis offers opportunities to enhance catalyst selectivity. The strong donating ability of N-heterocyclic carbene (NHC) ligands enhances the chances that this class of ligand can remain coordinated to Rh during catalysis. Examples of NHC-Rh complexes have been reported.²⁻⁶ NHC ligands are easily tuned to alter steric and electronic properties

via modification of the substituents in NHC ligand. Therefore, the reactivity and selectivity of Rh catalysts could be potentially optimized by screening a series of NHC ligands with various steric and electronic properties. Rh complexes that incorporate known classes of NHC ligand can be prepared and probed for catalytic arene alkenylation (Scheme 5.1.1). In addition, it has been reported that a $(\text{NHC})_2\text{Rh}(\text{I})$ complex can reversibly bind O_2 without being oxidized to Rh(III).⁷ Thus, NHC ligands also provide opportunities to design Rh(I) complexes with increased aerobic stability.

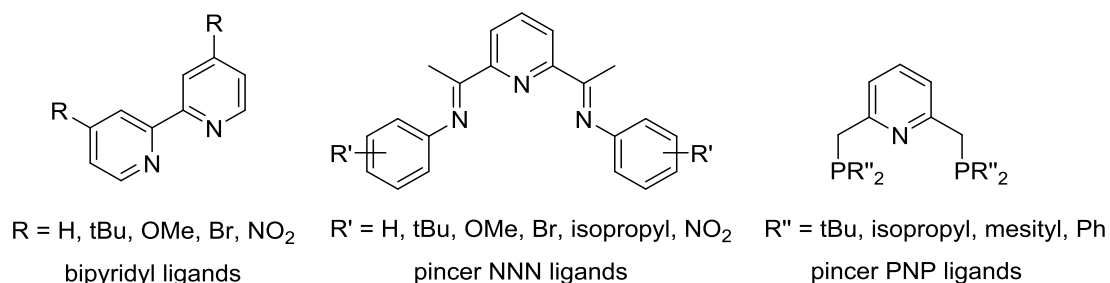


Scheme 5.1.1. Candidates of NHC-Rh complexes that will be prepared and probed for catalytic arene alkenylation.

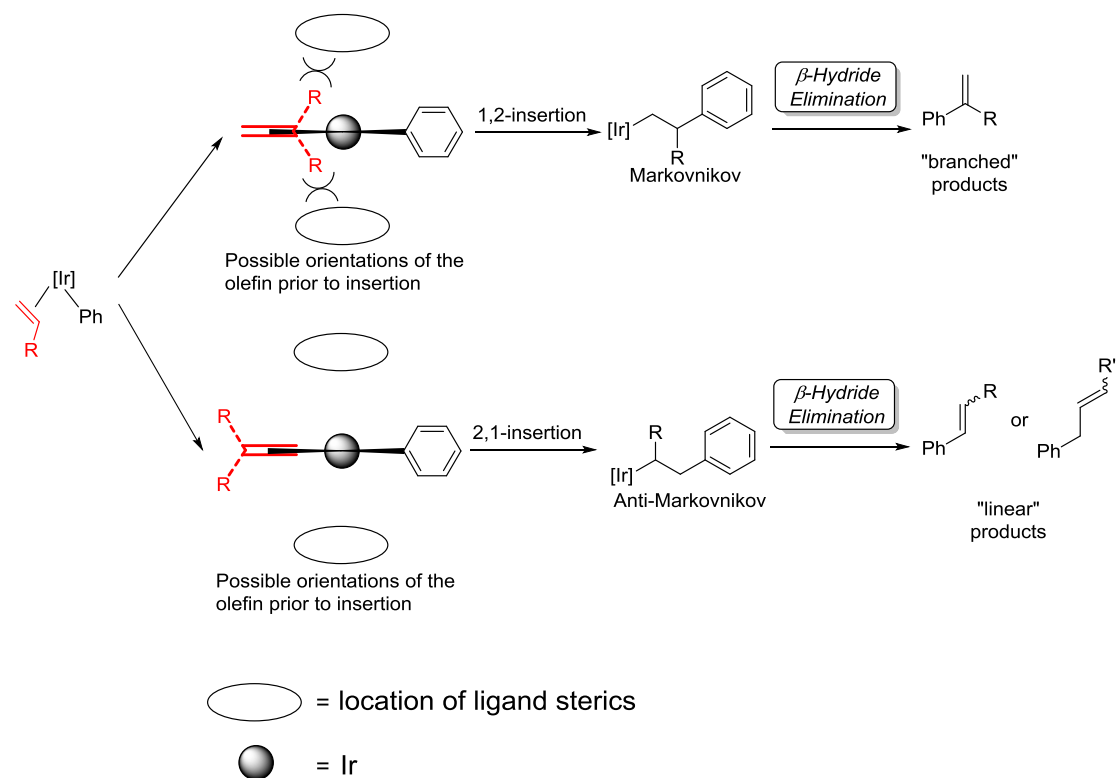
5.2 Future Direction of Ir-Catalyzed Arene Alkenylation

Ir(I) complexes serve as catalyst precursors catalytic arene alkenylation using unactivated hydrocarbons. Compared to other arene alkylation and alkenylation catalysts {Ir(III), Ru(II), Rh(I) and Pt(II)}, Ir(I) precursors exhibit high selectivity toward anti-Markovnikov 1-aryl alkene products. In order to further enhance the selectivity for linear alkenylbenzene products, it is necessary to focus on lowering the activation barrier and the thermodynamic energetics for the pathway that proceeds through 2,1-insertion relative to the 1,2-insertion. Previous studies on our bipyridyl Pt(II) catalyst system showed that olefin insertion step is likely reversible and the

subsequent C–H activation is the rate-determining step, and hence, Curtin–Hammett conditions could be responsible for linear/branched product selectivity. Under Curtin–Hammett conditions, ligand donor ability can also influence linear/branched selectivity by impacting the relative rates of rate-limiting aromatic C–H activation.⁸ The introduction of ancillary ligand sets that can be electronically tuned via substituent modification (such as well-precedent bipyridyl ligands, pincer PNP and NNN ligands in Scheme 5.2.1) can potentially improve the Ir catalyst selectivity toward linear alkenyl benzene by influencing the relative rates of 2,1- versus 1,2-olefin insertion (if olefin insertion is a rate-limiting step) and/or the relative rates for product formation following olefin insertion (if olefin insertion is a reversible step and product formation under Curtin-Hammett conditions). In addition, placing ligand sterics either "above" or "below" the Ir(I) square plane may bias the orientation of the olefin prior to insertion such that the alkyl group orients away from the phenyl ligand, and result in the formation of linear products (Scheme 5.2.2). For example, capping arene ligands⁹⁻¹¹ provide opportunities to install steric bulk and facilitate the formation of the olefin coordination mode that precedes 2,1-insertion.



Scheme 5.2.1. Examples of potential ligands to support Ir(I) metal.



Scheme 5.2.2. Ligand sterics "above" or "below" the Ir square plane bias the orientation of the olefin and facilitate the formation of linear products.

Ir catalyzed arene alkenylation is limited by low yield relative to Cu(II) oxidants (the best yield, based on Cu(II), thus far is < 30% without Cu(II) oxidant regeneration). We hypothesize, without experimental confirmation at this point, that the majority of Cu(II) oxidant is are consumed to produce undesired oxidation products including biphenyl, phenyl esters and vinyl esters. Therefore, it is worthwhile to screen other types of oxidants that have been used for other reported metal-catalyzed arene alkenylation reactions, such as such as $(\text{NH}_4)_2\text{S}_2\text{O}_8$,¹² AgOAc ,¹³ V_2O_5 ,¹⁴ PhCO_3tBu ,¹⁵ tBuOOH ¹⁶ and O_2 .¹⁷⁻²⁰

5.3 Future Research Opportunities for Arene Alkenylation Using Other Metals

Other suitable metal catalyst candidates for the production of alkenyl arenes are Pt and Ru. Oxidative olefin hydroarylation with unactivated arenes and olefins to produce alkenyl arenes using Ru(II) catalysts have been reported.²¹ Unsaturated vinyl arene products are observed in Pt-catalyzed olefin hydroarylation in the absence of oxidant.²² However, these Pt and Ru-mediated vinyl arene production processes are limited by catalyst longevity. For example, our cationic Pt catalysts produce ~1 TO of styrene due to the formation of unstable Pt(II)-H intermediates, which likely decomposes to elemental Pt. To prevent reductive decomposition of metal hydride species and accomplish long-lived catalytic processes, a series of oxidants can be screened as additives to react with metal hydride intermediates to regenerate the catalytically active metal catalyst. In that case, oxidation of metal hydride is more competitive than its reduction and thus the reaction pathway is driven toward alkenyl arene production. Besides classic copper carboxylates and silver salts oxidant, sustainable electricity serves as a green and effective oxidant source for arene alkenylation type reactions.²³

5.4 References

1. Liebov, N. S.; Zhu, W.; Chen, J.; Webster-Gardiner, M. S.; Schinski, W. L.; Gunnoe, T. B. Rhodium-Catalyzed Alkenylation of Toluene Using 1-Pentene: Regioselectivity to Generate Precursors for Bicyclic Compounds. *Organometallics* **2019**, *38*, 3860-3870.
2. Morales-Cerón, J. P.; Lara, P.; López-Serrano, J.; Santos, L. L.; Salazar, V.;

-
- Álvarez, E.; Suárez, A. Rhodium(I) Complexes with Ligands Based on N-Heterocyclic Carbene and Hemilabile Pyridine Donors as Highly E Stereoselective Alkyne Hydrosilylation Catalysts. *Organometallics* **2017**, *36*, 2460-2469.
3. Praetorius, J. M.; Crudden, C. M. N-Heterocyclic Carbene Complexes of Rhodium: Structure, Stability and Reactivity. *Dalton Trans.* **2008**, 4079-4094.
 4. Gyton, M. R.; Leforestier, B.; Chaplin, A. B. Rhodium(III) and Iridium(III) Complexes of a Nhc-Based Macrocyclic: Persistent Weak Agostic Interactions and Reactions with Dihydrogen. *Organometallics* **2018**, *37*, 3963-3971.
 5. Chianese, A. R.; Li, X.; Janzen, M. C.; Faller, J. W.; Crabtree, R. H. Rhodium and Iridium Complexes of N-Heterocyclic Carbenes Via Transmetalation: Structure and Dynamics. *Organometallics* **2003**, *22*, 1663-1667.
 6. Tobisu, M.; Yasui, K.; Aihara, Y.; Chatani, N. C–O Activation by a Rhodium Bis(N-Heterocyclic Carbene) Catalyst: Aryl Carbamates as Arylating Reagents in Directed C–H Arylation. *Angew. Chem. Int. Ed.* **2017**, *56*, 1877-1880.
 7. Praetorius, J. M.; Allen, D. P.; Wang, R.; Webb, J. D.; Grein, F.; Kennepohl, P.; Crudden, C. M. N-Heterocyclic Carbene Complexes of Rh: Reaction with Dioxygen without Oxidation. *J. Am. Chem. Soc.* **2008**, *130*, 3724-3725.
 8. McKeown, B. A.; Prince, B. M.; Ramiro, Z.; Gunnoe, T. B.; Cundari, T. R. Pt^{II}-Catalyzed Hydrophenylation of α -Olefins: Variation of Linear/Branched Products as a Function of Ligand Donor Ability. *ACS Catal.* **2014**, *4*, 1607-1615.
 9. Chen, J.; Nielsen, R. J.; Goddard, W. A.; McKeown, B. A.; Dickie, D. A.; Gunnoe, T. B. Catalytic Synthesis of Superlinear Alkenyl Arenes Using a Rh(I) Catalyst Supported by a “Capping Arene” Ligand: Access to Aerobic Catalysis. *J. Am. Chem. Soc.* **2018**, *140*, 17007-17018.
 10. O'Reilly, M. E.; Fu, R.; Nielsen, R. J.; Sabat, M.; Goddard, W. A.; Gunnoe, T. B. Long-Range C–H Bond Activation by Rh^{III}-Carboxylates. *J. Am. Chem. Soc.* **2014**, *136*, 14690-14693.
 11. Fu, R.; O'Reilly, M. E.; Nielsen, R. J.; Goddard, W. A.; Gunnoe, T. B. Rhodium Bis(Quinolinyl)Benzene Complexes for Methane Activation and Functionalization. *Chem. Eur. J.* **2015**, *21*, 1286-1293.
 12. She, Z.; Shi, Y.; Huang, Y.; Cheng, Y.; Song, F.; You, J. Versatile Palladium-Catalyzed C–H Olefination of (Hetero)Arenes at Room Temperature. *Chem. Commun.* **2014**, *50*, 13914-13916.
 13. Wang, P.; Verma, P.; Xia, G.; Shi, J.; Qiao, J. X.; Tao, S.; Cheng, P. T. W.; Poss, M. A.; Farmer, M. E.; Yeung, K.-S.; Yu, J.-Q. Ligand-Accelerated Non-Directed C–H Functionalization of Arenes. *Nature* **2017**, *551*, 489-493.
 14. Vora, H. U.; Silvestri, A. P.; Engelin, C. J.; Yu, J.-Q. Rhodium(II)-Catalyzed Nondirected Oxidative Alkenylation of Arenes: Arene Loading at One Equivalent. *Angew. Chem. Int. Ed.* **2014**, *53*, 2683-2686.
 15. Kubota, A.; Emmert, M. H.; Sanford, M. S. Pyridine Ligands as Promoters in Pd^{II}/O-Catalyzed C–H Olefination Reactions. *Org. Lett.* **2012**, *14*, 1760-1763.
 16. Jia, C.; Lu, W.; Kitamura, T.; Fujiwara, Y. Highly Efficient Pd-Catalyzed Coupling of Arenes with Olefins in the Presence of Tert-Butyl Hydroperoxide as Oxidant. *Org. Lett.* **1999**, *1*, 2097-2100.

-
17. Matsumoto, T.; Yoshida, H. Oxidative Arylation of Ethylene with Benzene to Produce Styrene. *Chem. Lett.* **2000**, *29*, 1064-1065.
 18. Matsumoto, T.; Periana, R. A.; Taube, D. J.; Yoshida, H. Direct Synthesis of Styrene by Rhodium-Catalyzed Oxidative Arylation of Ethylene with Benzene. *J. Catal.* **2002**, *206*, 272-280.
 19. Weissman, H.; Song, X.; Milstein, D. Ru-Catalyzed Oxidative Coupling of Arenes with Olefins Using O₂. *J. Am. Chem. Soc.* **2001**, *123*, 337-338.
 20. Shue, R. S. Catalytic Coupling of Aromatics and Olefins by Homogeneous Palladium(II) Compounds under Oxygen. *J. Chem. Soc. D* **1971**, 1510-1511.
 21. Jia, X.; Gary, J. B.; Gu, S.; Cundari, T. R.; Gunnoe, T. B. Oxidative Hydrophenylation of Ethylene Using a Cationic Ru (II) Catalyst: Styrene Production with Ethylene as the Oxidant. *Israel Journal of Chemistry* **2017**, *57*, 1037-1046.
 22. McKeown, B. A.; Gonzalez, H. E.; Friedfeld, M. R.; Brosnahan, A. M.; Gunnoe, T. B.; Cundari, T. R.; Sabat, M. Platinum(II)-Catalyzed Ethylene Hydrophenylation: Switching Selectivity between Alkyl- and Vinylbenzene Production. *Organometallics* **2013**, *32*, 2857-2865.
 23. Qiu, Y.; Kong, W.-J.; Struwe, J.; Sauermann, N.; Rogge, T.; Scheremetjew, A.; Ackermann, L. Electrooxidative Rhodium-Catalyzed C–H/C–H Activation: Electricity as Oxidant for Cross-Dehydrogenative Alkenylation. *Angew. Chem. Int. Ed.* **2018**, *57*, 5828-5832.